Process for Improving the Exfoliation and Dispersion of Nanoclay Particles into Polymer Matrices Using Supercritical Carbon Dioxide

Quang Tran Nguyen

Dissertation submitted to the Faculty of
Virginia Polytechnic Institute and State University
in partial fulfillment of the requirements for the degree of

DOCTOR OF PHILOSOPHY

in

Chemical Engineering

Advisory Committee:

Dr. Donald G. Baird, Chairman

Dr. James McGrath

Dr. Richey Davis

Dr. Eva Marand

April 25, 2007

Blacksburg, Va

Keywords: Polypropylene, maleated polypropylene, nanocomposites, nanoclay, supercritical carbon dioxide, extrusion.

Process for Improving the Exfoliation and Dispersion of Nanoclay Particles into Polymer Matrices Using Supercritical Carbon Dioxide

Quang Tran Nguyen

(ABSTRACT)

An environmentally benign process, which uses supercritical carbon dioxide (sc-CO_2) as a processing aid, was developed in this work to help exfoliate and disperse nanoclay into the polymer matrices at high clay content. The process involves the use of a pressurized CO_2 chamber to assist in the exfoliation and delivery of the clay into a stream of polypropylene (PP) melt within the extruder. This CO_2 method was evaluated and compared to other conventional processing techniques.

It was observed that the conventional direct-melt compounding methods, with and without the direct injection of CO_2, did not show much improvement in the mechanical properties due to their inability to adequately exfoliate the nanoparticles into the polymer matrix. The commercial RTP sample prepared using a TSE and a MA compatibilizer showed moderate improvements in the clay dispersion and properties due to high shear forces and mixing capabilities of TSE. The most improvements were seen from the technique of using the pressurized CO_2 chamber, which directly injected pre-mixed sc-CO_2 and nanoclay into the polypropylene melt during extrusion. It was observed that the mechanical properties of the PP nanocomposites prepared using the CO_2 chamber technique, especially when combined with maleic anhydride (MA) compatibilizer,

outperformed those of the commercial RTP samples and those of samples prepared using conventional melt compounding techniques. WAXD and TEM data showed a good degree of exfoliation for clay concentrations as high as 6.8 wt% when the clay was expanded and mixed with CO_2. At this concentration, mechanical properties such as yield strength and modulus increased by as much as 13% and 69%, respectively, relative to the pure PP, and approximately 15% higher than those of samples prepared by direct melt compounding (without the use of CO_2). Furthermore, yield-like behavior in the viscosity and a plateau in the low-frequency behavior of storage modulus, G', was also attributed to polymer-clay interaction due to strong hydrogen bonding between MA groups and the hydroxyl groups on the clay surface, not just solely to the formation of percolation network due to exfoliation between clay platelets that is commonly reported in literature for clay-filled functionalized polypropylene.

Acknowledgments

I would like to express my appreciation to Dr. Donald G. Baird for his guidance and support throughout the completion of this work. His great knowledge and professionalism have facilitated the completion of this project. In addition, I wish to extend special thanks to Dr. Rick Davis, Dr. Eva Marand, and Dr. James McGrath for serving on my research committee. Their advices and suggestions were very helpful and greatly appreciated.

I would also like to acknowledge the following individuals for their additional support during my graduate studies:

- Parents: Ba, Me, for giving up their future for the futures of their children. Your unconditional love, hard work, and support have motivated me to work harder.
- Other family members: Ba Noi, Ba Ngoai, Chi Trang, Anh Thanh, Anh Duy, Thao for their love, support, and encouragement.
- Van, for your love, patience, and understanding. You gave me hopes.
- Roy/Melissa Wagner, without you guys I couldn't be here today. Also your encouragement and support is much appreciated.
- Matt, Heather, Wade, and Vinh for being good friends during my stay here at VTech. Special thanks to Matt and Wade for providing assistance on many occasions.
- Lab Mates he has had the honor to work with: Matt, Wade, Mike, Eric, Desmond, Chris S., Chris M., Dave, Brent, Gregorio, Myoungbae, Jianhua, Dave C., and Joe.
- Department of Chemical Engineering Staff: Chris Moore, Diane Cannaday, Jane Price, Riley Chan, and Mike Vaught for all the assistance needed to facilitate successful completion of this work.

Attribution

Prof. Donald G. Baird - Ph.D. (Department of Chemical Engineering, Virginia Tech) is the primary Advisor and Committee Chair. Prof. Donald G. Baird provided assistance in the writing and research of this dissertation, especially in chapters 4 and 5. Prof. Baird provided useful ideas and aid in the design of the pressurized CO_2 chamber. Prof. Baird also provided advice on the tests needed for characterizing the nanocomposites. Furthermore, Prof. Baird also provided assistance in the writing and proofread these chapters.

Original Contributions

The following are considered to be significant original contributions of this research:

1. An environmentally benign process, which uses supercritical carbon dioxide ($scCO_2$) as a processing aid, is developed to help exfoliate and disperse nano-clay into the polymer matrices at high clay content. Exfoliated structures have been achieved for clay concentrations as high as 6.7 wt% (only limited by physical design of current chamber). Most melt intercalation techniques in literature have achieved exfoliated structures only up to 4 wt% clay (except for Nylon-6 systems).

2. Significant enhancement of mechanical properties such as Young's Modulus has been achieved for non-compatibilized and compatibilized polypropylene (PP)-clay nanocomposites. It has been shown that the mechanical properties of the PP nanocomposites prepared using the CO_2 chamber technique, especially when combined with maleic anhydride (MA) compatibilizer, outperformed those of the commercial RTP nanocomposites and those of nanocomposites prepared using conventional melt compounding techniques.

3. A clearer understanding of the effect of a maleic anhydride compatibilizer on the linear viscoelastic properties of PP-clay nanocomposites. It has been shown that the enhancement in dynamic rheological properties at low frequencies is also attributed to polymer-clay interaction due to strong hydrogen bonding between MA groups and the hydroxyl groups on the clay surface, not just solely to the formation of percolation

network due to exfoliation between clay platelets that is commonly reported in literature for clay-filled functionalized polypropylene.

4. A benign process that can potentially be applied for any polymer-clay system. Conventional melt blending techniques require a compatible polymer/clay system. It has been shown that even for a non-compatible system like hydrophobic PP and hydrophilic clay, significant enhancement in the mechanical properties and degree of dispersion was achieved.

Table of Contents

List of Figures

List of Tables

1.0 Introduction

1.1 Polymer-clay nanocomposite

Much academic as well as industrial research in polymer layered silicate nanocomposites has rapidly been increasing at an unprecedented level due to their potential for enhanced physical, chemical, and mechanical properties compared to conventionally filled composites [1-6]. It is well established that when layered silicates are uniformly dispersed and exfoliated in a polymer matrix, the polymer properties can be improved to a dramatic extent. These improvements may include increased strength [7], higher modulus [8-13], thermal stability [14-16], barrier properties [17, 18], and decreased flammability [19-23].

The main reason for these marked improvements stem from the large aspect ratio of layered silicate, e.g., montmorillonite (MMT). Each individual layer of MMT has a thickness on the order of 1 nanometer (nm) with lengths ranging from 100 nm to 300 nm [24, 25]. The high aspect ratio leads to a high contact surface area and, thus, physical interactions between the polymer and layered silicates with only a small concentration of clay. However, because the layered silicates typically exist as aggregates due to attractive van der Waals forces [26], the contact surface area available and, thus, improvements in physical properties do not reach theoretical expectations. Achieving a nanocomposite with an exfoliated morphology in which each individual layered silicate has been separated from its initial stack and dispersed uniformly throughout a given polymer matrix is the key to reaching the full potential of the nanoclays to enhance mechanical, thermal, and barrier properties of a polymeric matrix.

The attractive interactions between the polymer matrix and the layered silicates determine, in large part, the degree of compatibility between the two separate phases. Layered silicates are naturally hydrophilic while many polymers such as polyolefins are hydrophobic and, thus, the surface energies between the two materials can be vastly different prohibiting any significant degree of dispersion of nanoclay within the polymer [11]. In order to have a successful development of clay-based nanocomposites, it is necessary to chemically modify a natural clay so that it can be compatible with a chosen polymer matrix. Modification of layered silicates via ion exchange reactions through which quaternary alkyl ammonium cations replace the existing cations (Na^+, Ca^+, Li^+ etc.) residing in the interlayer of the silicates help to make the layered silicates more organophilic. Generally, this can be done through ion exchange reactions by replacing interlayer cations with quarternary alkylammonium or alkylphosphonium cations [27-29].

For polymer containing polar functional groups, an alkylammonium surfactant is adequate to promote the nanocomposite formation. For non-polar polypropylene (PP), however, it is not simple because interfacial bonding between the clay surface and PP matrix is unfavorable. To increase the compatibility between the MMT nanoclays and PP matrix, two major methods including melt intercalation [30-35] and in-situ polymerization [36] have recently been introduced. The latter method usually involves in a slurry phase, which requires large volumes of solvents and a need of purification. Thus this method may be impractical because it is environmentally as well as economically unfriendly. The melt intercalation of PP-clay nanocomposites usually involves the use of a compatibilizer, such as maleic anhydride grafted PP (PP-g-MA), to facilitate the intercalation of PP in clay [30-32]. However, in spite of improved homogeneity and

properties, complete exfoliation is practically never reached [33-47]. Usually a mix between intercalated and partially exfoliated structure is frequently observed. Also, in order to achieve a good level of intercalation at high clay concentration, a high ratio of PP-g-MA must be used. However, using a high level of PP-g-MA can be expensive and may reduce the nanocomposite's elongation at break and mechanical properties. Thus, it is also necessary to explore the MA compatibilizer on the final microstructure and properties of the nanocomposites.

1.2 Supercritical Carbon Dioxide

Supercritical fluids have been receiving tremendous attention recently in various applications such as in the food and pharmaceutical industries as well as in the plastics industry. Particularly, supercritical carbon dioxide (sc-CO_2) has been used widely in many applications because it is environmentally friendly, nontoxic, relatively low cost, and nonflammable compared to other supercritical fluids [48]. Furthermore, sc-CO_2 can yield practical benefits such as reductions in the use of toxic organic solvents as well as ease of solvent separation because CO_2 acts as a reversible plasticizer that can easily be removed upon depressurization. In the supercritical state, CO_2 is known to have similar solubilization characteristics to those of organic solvents and is well known to plasticize a number of amorphous polymers [49]. In addition, sc-CO_2 possesses a unique combination of properties from both liquid and gas states, exhibiting liquid like densities combined with low viscosities and high diffusion rates characteristic of a gas phase, which promotes rapid plasticization of amorphous materials [49-57]. For these and many other factors, sc-CO_2 has proven to be a very useful alternative to many solvent based applications [58].

To overcome some of the issues with using melt intercalation and modified PP and other solvent-based techniques, recently, there has been considerable interest in using sc-CO_2 as an alternative route for the preparation of polymer-clay nanocomposites [59-64]. A recent approach to prepare polymer nanocomposites using sc-CO_2 in the melt intercalation process was reported by Lesser et al. [50]. They used a modified hopper in the feed section of the extruder to allow polymer and clay to interact with sc-CO_2 before processing. It was found that the presence of sc-CO_2 promotes significant increase in the basal spacing of the clay, and thereby may enhance the ease of the polymer intercalation into the galleries of the clay. In a different approach, Mielewski et al. [63] proposed a method to directly inject sc-CO_2 to a melt mixture of silicate particles and polymer in an extruder. The silicates are expected to exfoliate when exiting the extruder. No WAXD or TEM evidence of exfoliated morphology was presented. Alternatively, Manke et al. [64] developed a process that allows clay particles to be pre-treated with sc-CO_2 in a pressurized vessel and then rapidly depressurized into another vessel at atmospheric pressure to force the clay platelets apart. The result was exfoliated nanoclay particles as observed by X-Ray diffraction. However, they did not provide any mechanism for assuring that the exfoliated particles remain exfoliated when they are combined with the polymer via conventional melt blending.

In this study, we develop a process to help exfoliate and disperse the nanoclay into PP matrix with the aid of supercritical CO_2. The process involves the use of a pressurized CO_2 chamber to assist in the exfoliation and delivery of the clay into a stream of polymer melt in the extruder. This process is different from the systems previously mentioned above in ways that it allows only the clay to be in direct contact with sc-CO_2,

as opposed to both clay and polymer as described in Lesser's and Mielewski's processes, and that the mixture of exfoliated clay and sc-CO_2 is fed into the extruder in a one-step process instead of a two-step like Manke's process. This CO_2 method is evaluated and compared to other processing methods including the direct melt-blending technique using a single-screw extruder, single-screw extrusion capable of a direct in-line feed of sc-CO_2 to the extruder barrel, and conventional twin screw extrusion with PP-g-MA.

In the second part of this study, the CO_2 chamber technique is extended further by incorporating a MA compatibilizer to prepare PP-clay nanocomposites. We would like to ascertain whether or not further improvements on the mechanical properties of the nanocomposites can be achieved when prepared with the incorporation of a maleic anhydride compatibilizer. The effect of a MA compatibilizer on the microstructure and on the mechanical and linear viscoelastic properties of the nanocomposites prepared using two different processing techniques is also studied.

1.3 References

1. Usuki A, Kojima Y, Kawasumi M, Okada A, Fukushima Y, Kurauchi T, Kamigaito O. J Mater Res 1993; 8: 1185.
2. Kojima Y, Usuki A, Kawasumi M, Okada A, Kurauchi T, Kamigaito O. J Polym Sci Part A 1993; 31: 983.
3. Kojima Y, Usuki A, Kawasumi M, Okada A, Kurauchi T, Kamigaito O. J Polym Sci Part A 1993; 31: 1755.
4. Liu L, Qi Z, Zhu X. J Appl Polym Sci 1999; 71: 1133.
5. Lan T, Kaviratna D, Pinnavaia J. Chem Mater 1994; 6: 573.
6. Gilman W, Morgan A, Giannelis P, Wuthenow M, Manias E. Flame Retardancy 10th Annual BBC Conference Proceedings 1999; 1.
7. Giannelis P. Appl Organomet Chem 1998; 12: 675.
8. Okada A, Kawasumi M, Usuki A, Kojima Y, Kurauchi T, Kamigaito O. In: Schaefer W, Mark E, editors. Polymer based molecular composites MRS Symposium Proceedings. Pittsburgh; 1990; vol. 171:45–50.
9. Giannelis P. Adv Mater 1996; 8: 29.
10. Giannelis EP, Krishnamoorti R, Manias E. Adv Polym Sci 1999; 138: 107.
11. LeBaron PC, Wang Z, Pinnavaia TJ. Appl Clay Sci 1999; 15: 11.
12. Vaia RA, Price G, Ruth PN, Nguyen HT, Lichtenhan J. Appl Clay Sci 1999; 15: 67.
13. Biswas M, Sinha S. Adv Polym Sci 2001; 155: 167.
14. Gilman JW. Appl Clay Sci. 1999; 15: 31.
15. Bins & Associates. Plastics Additives & Compounding 2002; 4(1): 30-33.
16. Lan T, Kaviratna PD, Pinnavaia TJ. Chem Mater 1994; 6: 573.
17. Sall K. European Plastics News March 14, 2002.
18. Messersmith PB, Giannelis EPJ. Polym Sci Part A: Polym Chem 1995; 33: 1047.
19. Gilman JW, Kashiwagi T, Lichtenhan JD. SAMPE J 1997; 33: 40.
20. Gilman JW. Appl Clay Sci 1999; 15: 31.

21. Dabrowski F, Bras L, Bourbigot S, Gilman JW, Kashiwagi T. Proceedings of the Eurofillers. Lyon-Villeurbanne, France 1999; 6:9.

22. Bourbigot S, LeBras M, Dabrowski F, Gilman JW, Kashiwagi T. Fire Mater 2000; 24:201.

23. Gilman JW, Jackson CL, Morgan AB, Harris R, Manias E, Giannelis EP, Wuthenow M, Hilton D, Phillips H. Chem Mater 2000; 12: 1866.

24. Mehrabzadeh M, Kamal MR. Poly. Eng Sci 2004; 44: 152.

25. Pinnavaia TJ, Beall GW. Polymer-Clay Nanocomposites. New York: J. Wiley & Sons; 2000.

26. Zanetti M, Lomakin S, Camino G. Macromol Mater Eng *2000;* 279**:**1.

27. Blumstein A. J Polym Sci A 1965; 3:2665.

28. Theng BKG. Formation and properties of clay–polymer complexes. Elsevier, Amsterdam, 1979.

29. Krishnamoorti, Vaia A, Giannelis P. Chem Mater 1996; 8:1728.

30. Kawasami M, Hasegawa N, Kato M, Usuki A, Okada A. Macromolecules 1997; 30:6333–6338.

31. Nam PH, Maiti P, Okamoto M, Kotaka T, Hasegawa N, Usuki A. Polymer 2001; 42:9633–9640.

32. Kato M, Usuki A, Okada A. J Appl Polym Sci 1997; 66:1781–1785.

33. Modesti M, Lorenzetti A, Bon D, Besco S. Effect of processing conditions on morphology and mechanical properties of compatibilized polypropylene nanocomposites. Polymer 2005; 46: 10237-10245.

34. Kanny K, Moodley VK. Characterization of polypropylene nanocomposite structures. J. Eng. Mater. & Tech. 2007; 129: 105-112.

35. Lee JW, Kim MH, Choi WM, Park OO. Effects of organoclay modification on microstructure and properties of polypropylene-organoclay nanocomposites. J Appl Polym Sci 2006; 99: 1752-1759.

36. Alexandre M, Dubois P. Mater Sci. Eng 2000; 28: 1.

37. Ray SS, Okamoto M. Prog Polym Sci 2003; 28: 1539.

38. Pinnavaia TJ, Beall GW. ‘‘Polymer-Clay Nanocomposites’’, J Wiley & Sons. New York 2000.

39. LeBaron PC, Wang Z, Pinnavaia TJ. Appl Clay Sci 1999; 15:11.

40. Fornes TD, Paul DR. Polymer 2003; 44: 4993.

41. Osman MA, Rupp JEP, Suter UW. Polymer 2005; 46:1653.

42. Wang ZM, Nakajima H, Manias E, Chung TC. Macromolecules 2003; 36:8919.

43. Manias E. Origins of the Materials Properties Enhancements in Polymer/Clay Nanocomposites. In Golovoy A, editor. Nanocomposites 2001, Delivering New Value to Plastics. ECM Inc., Chicago; 2001.

44. Dennis HR, Hunter DL, Chang D, Kim S, White JL, Cho JW, Paul DR. Polymer 2001; 42:9513.

45. Manias E, Touny A, Wu L, Strawhecker K, Lu B, Chung TC. Chem Mater 2001; 13:3516.

46. Svoboda P, Zeng CC, Wang H, Lee LJ, Tomasko DL. J Appl Polym Sci 2002; 85:1562.

47. Ellis TS, D'Angelo JS. J Appl Polym Sci 2003; 90: 1639.

48. D.L. Tomasko, H. Li, D. Liu, X. Han, M.J. Wingert, L.J. Lee, K.W. Koelling. A Review of CO_2 Applications in the Processing of Polymers. *Ind. Eng. Chem. Res*. **42** (2003); p. 6431-56.

49. Y.T. Shieh, J.H. Su, G. Manivannan, P.H.C. Lee, S.P. Sawan, W.D. Spall, Interaction of supercritical carbon dioxide with polymers. II amorphous polymers, *J. Appl. Polym. Sci.*, **59** (1996), p. 707-717.

50. Y.T. Shieh, J.H. Su, G. Manivannan, P.H.C. Lee, S.P. Sawan, W.D. Spall, Interaction of supercritical carbon dioxide with polymers. I crystalline polymers, *J. Appl. Polym. Sci.*, **59** (1996), p. 695-705.

51. A. Garg, E. Gulari, C.W. Manke, *Macromolecules*, **27** (1994), p. 5643.

52. J.F. Brennecke, Solvents: Molecular trees for green chemistry, *Nature* **389** (1997), p. 333-334.

53. L. A. Blanchard; Hancu, D.; Beckman, E. J.; Brennecke, J. F. *Nature*, **399** (1999), p. 28-29.

54. T. Sarbu, Styranec, T., Beckman, E. J., Non-fluorous polymers with very high solubility in supercritical CO2 down to low pressures, *Nature*, **405** (2000), p. 165-168.

55. W. Leitner, Green chemistry: Designed to dissolve, *Nature*, **405** (2000), p. 129-130.

56. D. Adam, News feature: Clean and green...but are they mean?, *Nature*, **407** (2000), p. 938-940.

57. A.I. Cooper, Londono, J. D.; Wignall, G.; McClain, J. B.; Samulski, E. T.; Lin, J. S.; Dobrynin, A.; Rubinstein, M.; Burke, A. L. C.; Fréchet, J. M.; DeSimone, J. M., Extraction of a hydrophilic compound from water into liquid CO2 using dendritic surfactants, *Nature* 1997, 389, 368-371.

58. A. Couper and S. Howdle, *Materials World*, **8(5)** (2000), p. 10.

59. Garcia-Leiner M, Lesser AJ. ANTEC 2004; 1528:32.

60. Zerda AS, Caskey TC, Lesser AJ. Macromolecules 2003; 36:1603.

61. Caskey TC, Lesser AJ. Polym Eng Sci 2001; 84:134.

62. Wingert MJ, Han Z, Zeng C, Li H. ANTEC 2003; 986:990.

63. Mielewski DF, Lee EC, Manke CW, Gulari E. U.S. Patent 6,753,360 (2004).

64. Manke CW, Gulari E, Mielewski DF, Lee EC. U.S. Patent 6,469,073 (2002)

2.0 Literature Review

An overview of the progress in polymer nanocomposites is presented in the following sections with an emphasis on the review of different methods used to prepare PLS nanocomposites and the extent to which properties are enhanced. First, the types of PLS nanocomposites morphologies that are most commonly achieved are discussed. Then a brief summary of various types of polymers used in PLS nanocomposites preparation is presented. Next, the structure and properties of layered silicates are discussed. Some of the most common techniques used for characterization of nanocomposites will be presented in section 2.1.2. In section 2.1.3 and its subsections, different methods used to prepare PLS nanocomposites are discussed including the use of super critical carbon dioxide which is the thrust of this research.

2.1 Background

2.1.1 Types of polymer-clay nanocomposites

In general, the degree of dispersion of the clay platelets into the polymer matrix determines the structure of nanocomposites. Depending on the interaction between the clay and the polymer matrix, two main idealized types of polymer-clay morphologies can be obtained: namely, intercalated and exfoliated (Figure 2.1). The intercalated structure results from penetration of a single polymer chain into the galleries between the silicate layers, resulting in formation of alternate layers of polymer and inorganic layers. Exfoliated structure results when the individual silicate layers are completely separated and dispersed randomly in a polymer matrix. Usually exfoliated nanocomposites are preferred because they provide the best property improvements [1].

Figure 2.1: Schematic illustrations of two types of polymer-layered silicate morphologies: (left) intercalated and (right) exfoliated [2].

2.1.2 Types of polymers used in nanocomposite synthesis

Since the remarkable improvements of the material properties in nylon 6/clay nanocomposite demonstrated by the Toyota research group [3], numerous other polymers have been investigated by many researchers around the world. These include, but are not limited to, polypropylene [4-49], polyethylene [50-59], polystyrene [60-66], poly(ethylene oxide) [67-71], polycaprolactone [72,73], polyimides [74-91], polyamides [92-99], poly(ethylene terephthalate) [100-106], polycarbonate [107,108], polyurethane [109], and epoxy resin [110-114]. There are other polymers that have been reported in literature, and it is not feasible to cite them all here. Additional information can be found in paper by Sur et al. [115] who cited many references regarding other polymers.

2.1.3 Structure and properties of layered silicates

To understand the complex morphologies that occur in polymer-layered silicate nanocomposites, it is important to review the structural details of layered silicates and their properties. The most heavily used filler materials in the fabrication of PLS

nanocomposites are based on the 2:1 layered structure also known as phillosilicates, of which the most common representative is montmorillonite (MMT) [116]. Although, MMT is most commonly used, other layered silicates in the same general family are also used, such as hectorite, saporite, mica, talc, vermiculite, etc. [117,118]. MMT crystal structure is made up of a layer of aluminum hydroxide octahedral sheet sandwiched between two layers of silicon oxide tetrahedral sheets (Figure 2.2) [119]. The nominal composition of MMT is $Na_{1/3}(Al_{5/3}Mg_{1/3})Si_4O_{10}(OH)_2$ [120]. The layer thickness of each platelet is on the order of 1 nm and its lateral dimension is approximately 200 nm [120]. These clay platelets are stacked on each other and held together through van der Waal forces and are separated from each other by 1 nm gaps (galleries) [116]. These galleries are usually occupied by cations, normally alkali and alkaline-earth cations such as Na^+ and K^+, which counterbalance the negative charges generated from isomorphic substitution within the layers (for montmorillonite, Al^{3+} replaced by Mg^{2+}) [116]. It is well established that the key in preparing PLS nanocomposites is to obtain exfoliation of the large stacks of silicate nanoplatelets into individual layers [121,122]. Analogous to polymer blends, the physical mixture of silicate layers and polymer matrix may not form a nanocomposite due to the unmatched chemical affinity between the two. Thus, in order to have a successful development of clay-based nanocomposites, it is necessary to chemically modify a naturally hydrophilic silicate surface to an organophilic one so that it can be compatible with a chosen polymer matrix. Generally, this can be done through ion-exchange reactions by replacing interlayer cations with quarternary alkylammonium or alkylphosphonium cations (Figure 2.3) [123-125]. Ion-exchange reactions with cationic surfactants such as those mentioned above render the normally hydrophilic

silicate surface organophilic, thus making it compatible with non-polar polymers. These cationic surfactants modify interlayer interactions by lowering the surface energy of the inorganic component and improve the wetting characteristics with the polymer [123,124]. Furthermore, they can provide functional groups that can react with the polymer or initiate polymerizations of monomers and thereby improve the strength of the interface between the polymer and inorganic [120,123,124].

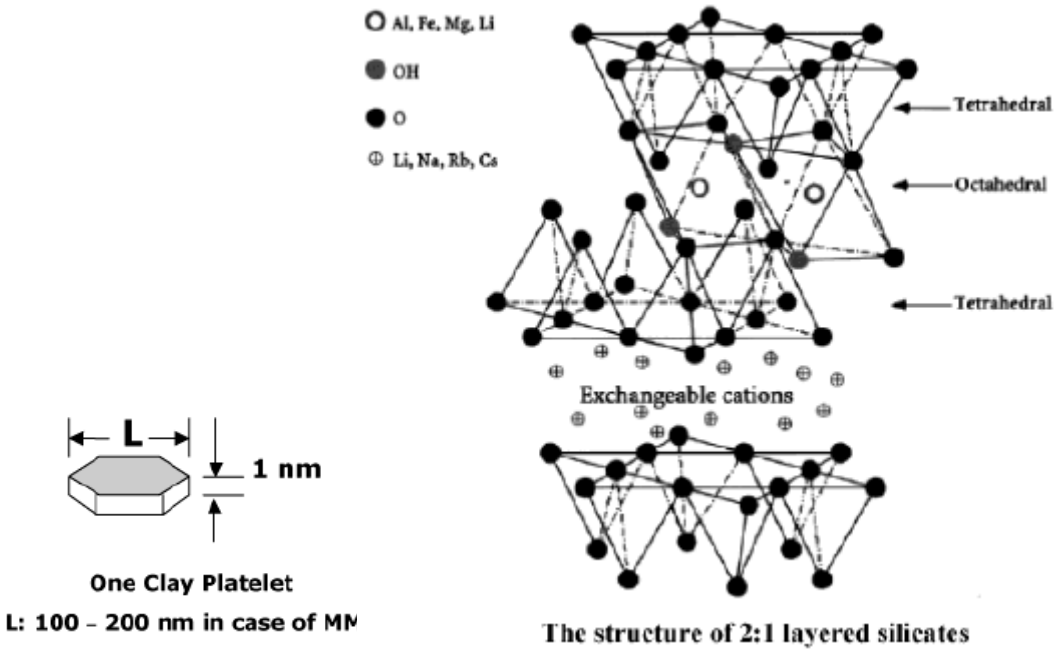

Figure 2.2: Structure of 2:1 layered silicate showing two tetrahedral sheets of silicon oxide fused to an octahedral sheet of aluminum hydroxide [2].

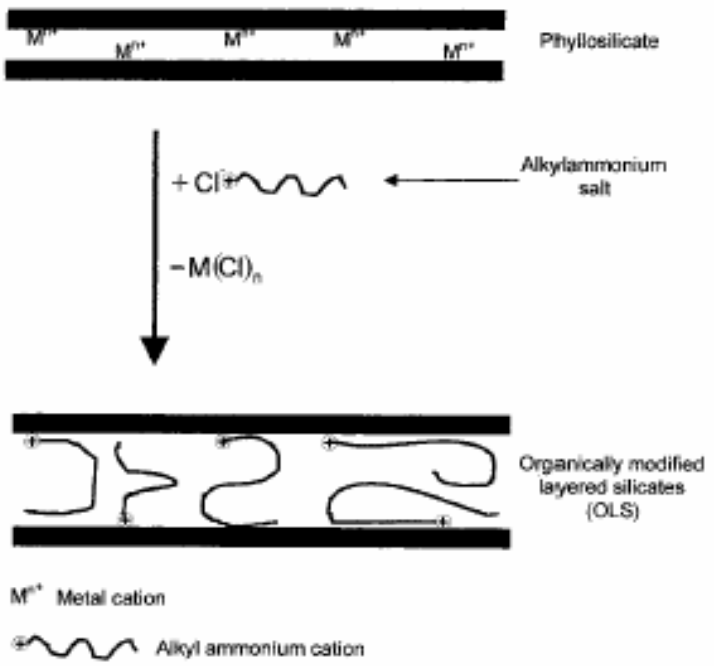

Figure 2.3: Schematic representation of a cation-exchange reaction between the silicate and an alkylammonium salt [116].

2.2 Techniques used for characterization of nanocomposites

In developing and optimizing nanocomposites one needs to know the degree of exfoliation of a particular sample and compare it to other samples. A number of methods have been reported in literature for this purpose [126-139]. Wide angle X-ray diffraction (WAXD) analysis and transmission electron micrographic (TEM) observation are generally the two methods that have been used to typically establish the structure of nanocomposites. Because of its easiness and availability WAXD is most commonly used to probe the nanocomposite structure and occasionally to study the kinetics of the polymer melt intercalation [140]. The nanocomposite structure, namely intercalated or exfoliated, may be identified by monitoring the position, shape, and intensity of the basal reflections from the distributed silicate layers. WAXD can offer a convenient method to determine the interlayer spacing of the silicate layers in the original layered silicates and in the intercalated nanocomposites (1-4 nm), but little can be concluded about the spatial distribution of the silicate layers [119]. Additionally, because some layered silicates initially do not exhibit well-defined basal reflections, peak broadening and intensity decreases are very difficult to study systematically. Thus, conclusions based solely on WAXD patterns are only tentative when concerning the mechanism of nanocomposites formation and their structure. To fill in what WAXD is missing, TEM can be used. TEM allows a qualitative understanding of the internal structure, spatial distribution of the various phases, and views of the defect structure through direct visualization [119]. Together, TEM and WAXD are essential tools for evaluating nanocomposite structure [126]. TEM is time-intensive, and gives qualitative information on the sample as a whole, while low-angle peaks in WAXD allow quantification of changes in layer spacing.

Occasionally, small angle X-ray scattering (SAXS) can also be used to characterize structure of nanocomposites. SAXS is useful when layer spacing exceed 6–7 nm in intercalated nanocomposites or when the layers become relatively disordered in exfoliated nanocomposites. Recent simultaneous SAXS and WAXD studies yielded quantitative characterization of nanostructure and crystallite structure in N6 based nanocomposites [127].

2.3 Methods used for the synthesis of polymer-clay nanocomposites

The key to the successful development of clay-based nanocomposites is to achieve exfoliation of the layered silicate in the polymer matrix. A number of PLS nanocomposite preparation methods have been reported in literature. The three most common methods to synthesize PLS nanocomposites are: intercalation of a suitable monomer and subsequent in situ polymerization, intercalation of polymer from solution, and polymer melt intercalation. In the in situ polymerization method (Figure 2.4), the monomer is used directly as the solubilizing agent for swelling the layered silicate. Subsequent polymerization takes place after combining the silicate layers and monomer, thus allowing formation of polymer chains between the intercalated sheets [116]. The next method involves intercalation of polymer from solution (Figure 2.5). This method requires a suitable solvent that can both solubilize the polymer and swell the silicate layers. When the layered silicate is dispersed within a solution of the polymer, the polymer chains intercalate and displace the solvent within the gallery of the silicate [116]. PLS nanocomposite is obtained upon the removal of the solvent, either by solvent evaporation or polymer precipitation [144-146]. The drawbacks in these two previously mentioned methods are the requirement of suitable monomer/solvent or polymer solvent

pairs and the high costs associated with the solvents, their disposal, and their impact on the environment. The last method, melt intercalation (Figure 2.6), does not require the use of a compatible solvent or suitable monomer. In this method, a polymer and layered silicate mixture is annealed under either static or dynamic shear (in an extruder) above the softening point of the polymer [116]. During the annealing process, polymer chains diffuse from the molten polymer into the silicate galleries to form either intercalated or exfoliated depending on the degree of penetration [147,148]. This method has become the mainstream for the fabrication of PLS nanocomposites in recent years [149,150] because it is simple, economical, and environmentally friendly. However, melt mixing seems to be only partially successful since concentrations of exfoliated silicates greater than about 4 wt% have not been possible.

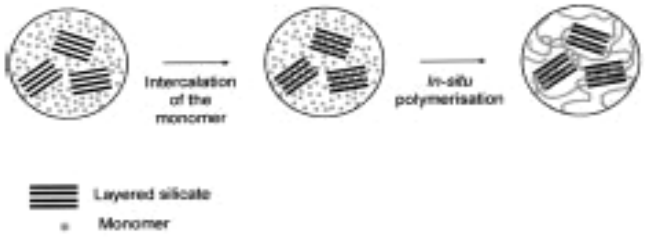

Figure 2.4: Schematic representation of PLS nanocomposite obtained by in situ polymerization [116].

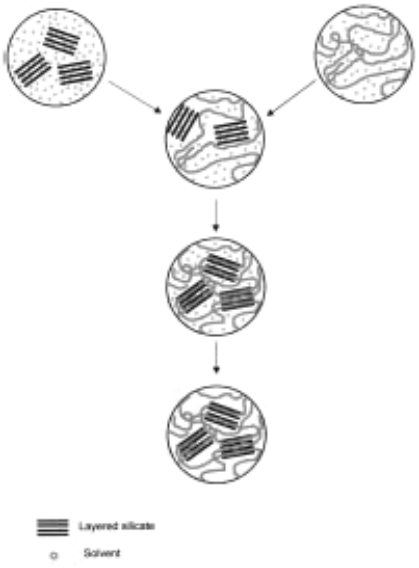

Figure 2.5: Schematic representation of PLS nanocomposite obtained by intercalation of polymer from solution [116].

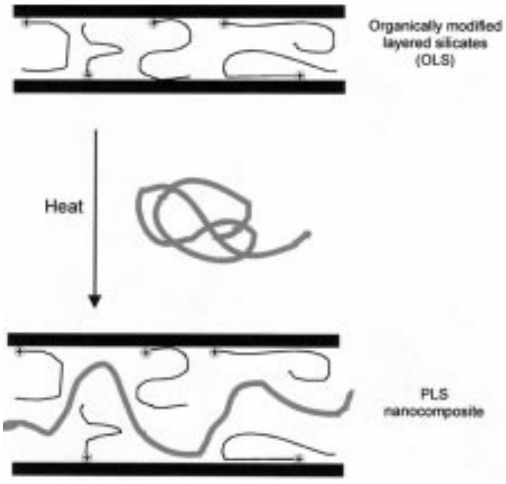

Figure 2.6: Schematic representation of nanocomposite obtained direct melt intercalation [116].

2.3.1 Method of In situ intercalative polymerization

The field of PLS nanocomposites gained tremendous attention recently due to the accomplishments with a N6/MMT nanocomposite from the Toyota research group [50a], even though the method of in situ polymerization has long been known [123,124]. Their findings showed that with only very small amounts of layered silicate loadings, the thermal and mechanical properties had improved remarkably. They first discovered the ability of ε-caprolactam monomer to swell α,ω-amino acids ($COOH–(CH2)_{n-1}–NH_2^+$, with *n*=2,3,4,5,6,8,11,12,18) modified Na^+-MMT at 100°C and subsequently to initiate its ring opening polymerization to obtain N6/MMT nanocomposites [151]. They chose the ammonium cation of ω-amino acids for the intercalation of ε-caprolactam because these acids catalyze ring-opening polymerization of ε-caprolactam. They showed that the swelling behavior of ω-amino acid modified MMT is strongly affected by the number of carbon atoms in the α,ω-amino acids, suggesting that the extent of intercalation of ε-caprolactam monomer is high when the number of carbon atoms in the ω-amino acid is high. A conceptual scheme for the synthesis of Nylon-6/clay nanocomposite is presented in Figure 2.7. A more detailed description of the process can be found in ref. [152]. The authors also demonstrated that intercalative polymerization of ε-caprolactam could be achieved even without the organic modification of MMT. However, it was proven that the degree of intercalation of ε-caprolactam seemed to be sensitive to the nature of the acid used.

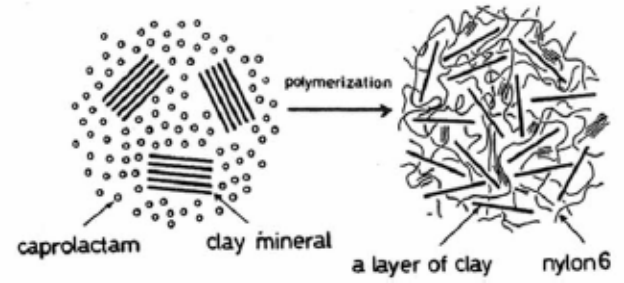

Figure 2.7: Schematic illustration for synthesis of Nylon-6/clay nanocomposite [152].

Messersmith and Giannelis [153] utilized this method for the preparation of poly(ε-caprolactam)-based nanocomposites. They modified MMT using protonated aminolauric acid and dispersed the modified MMT in liquid ε-caprolactone before polymerizing at high temperature. The nanocomposites were prepared by mixing up to 30 wt% of the modified MMT with ε-caprolactone for a few of hours, followed by ring opening polymerization under stirring at 170 ^{o}C for 48 h. Wang and Pinnavaia [154] used this PCL-based nanocomposites synthesis technique for the preparation of polyurethane–MMT nanocomposites. WAXD analyses of these nanocomposites established the formation of intercalated structure.

Polystyrene-based nanocomposites were prepared using this in situ intercalative polymerization technique by Akelah and Moet [155,156]. Modified Na^{+}-MMT and Ca^{2+}-MMT with vinylbenzyltrimethyl ammonium cation were used for the preparation of nanocomposites. First modified clays were dispersed in various solvent and co-solvent mixtures such as acetonitrile, acetonitrile/toluene and acetonitrile/THF by stirring for 1 h under N_2 atmosphere. Then *N*-*N*′-azobis (isobutyronitrile) was added to the stirred solution, and finally, polymerization of styrene was carried out at 80 °C for 5 h. The

resulting nanocomposites were obtained after precipitation of the colloidal suspension in methanol, filtered off, and dried. In this approach, intercalated PS/MMT nanocomposites were produced. Although the PS is well intercalated, one drawback in this procedure is that the macromolecule produced is not a pure PS, but rather a copolymer between styrene and vinylbenzyltrimethylammonium cations.

In a similar approach, Doh and Cho [157] prepared PS-based nanocomposites with several different quaternary alkylammonium cations incorporated in Na^+-MMT. They found the resulting materials, even with MMT loading as low as 0.3 wt%, showed an expansion of interlayer distance. Also, they exhibited higher thermal stability compared with the virgin polystyrene (PS). Additionally, they found that the structural affinity between styrene monomer and the organically modified MMT plays an important role in the final structure and properties of the nanocomposites. Weimer et al. [158] also used this concept in the preparation of PS/MMT nanocomposites. WAXD analyses together with the TEM observations showed exfoliation of the layered silicate in the PS matrix.

Polyethylene/layered silicate nanocomposites have also been prepared by in situ intercalative polymerization of ethylene [56]. WAXD and TEM analyses showed the formation of exfoliated nanocomposites with up to 3.4 wt% MMT. In the absence of a chain transfer agent, the tensile properties of these nanocomposites were poor and essentially independent of the nature and content of the silicate. Upon chain transfer agent addition, the resulting nanocomposites exhibited improvements in mechanical properties. With about 3.4 wt% MMT loading, Young's modulus increased roughly 85%.

Polyethylene terephthalate (PET) has also been studied using this technique. There are many literature reports on the preparation and characterization of PET/clay nanocomposites [100-106], but no reports give a detailed description of the preparative method. For example, one report presents the preparation of a PET nanocomposite by in situ polymerization of a dispersion of organoclay in water. However characterization of the resulting composite was not reported [100]. In this report, the authors claim that water serves as a dispersing aid for the intercalation of monomers into the galleries of the organoclay.

2.3.2 Intercalation of polymer from solution

Aranda and Ruiz-Hitzky [71] reported the first preparation of PEO/MMT nanocomposites by this method. They investigated a series of experiments to intercalate PEO (Mw =10^5 g/mol) into Na^+-MMT using different polar solvents. The nature of solvents is critical in facilitating the insertion of polymers between the silicate layers in this method [124,159]. The high polarity of water causes swelling of Na^+-MMT. Methanol is not suitable as a solvent for high molecular weight (HMW) PEO, whereas water/methanol mixtures appear to be useful for intercalations, although cracking of the resulting materials is frequently observed. Wu et al. [160] reported the intercalation of PEO in Na^+-MMT and Na^+-hectorite using this method in acetonitrile. Diffusion of one or two polymer chains in between the silicate layers was observed and the inter-sheet spacing increased from 0.98 to 1.36 and 1.71 nm, respectively. In another study, Choi et al. [161] prepared PEO/MMT nanocomposites by a solvent casting method using chloroform as a co-solvent. Intercalated structure was observed for the resulting nanocomposites as confirmed by WAXD analyses and TEM observations. Other authors

[162,163] have also used the same method and same solvent for the preparation of PEO/clay nanocomposites.

Jeon et al. applied this technique to the preparation of nanocomposites of nitrile-based copolymer and polyethylene-based polymer with organically modified MMT [50]. A partially exfoliated structure was obtained as revealed by TEM analysis where both stacked intercalated and exfoliated silicate layers coexist. This observation was confirmed by WAXD analysis, which reveals a broad diffraction peak that has been shifted towards a higher d-spacing. The same authors also presented HDPE-based nanocomposites prepared by dissolving HDPE in a mixture of xylene and benzonitrile with dispersed OMLS [50]. Syndiotactic polystyrene (s-PS) organically modified clay nancomposites have also been prepared by the solution intercalation technique by mixing pure s-PS and organophilic clay with adsorbed cetyl pyridinium chloride [165]. The WAXD analyses and TEM observations showed a nearly exfoliated structure of these nanocomposites.

Sur et al. [166] applied this solvent-based technique to the preparation of polysulfone (PSF)-organoclay nanocomposites. PSF/organoclay nanocomposites were obtained by mixing the desired amount of the organoclay with PSF in DMAC at 80 °C for 24 h. WAXD and TEM analyses indicated exfoliation of the organoclay in the nanocomposites. Polylactide (PLA) or poly(ε-caprolactone) (PCL)-based nanocomposites have also been produced [167,168] using this technique, but neither intercalation nor exfoliation was obtained as the clay existed in the form of tactoids, consisting of several stacked silicate monolayers.

In another report [89], polyimide/MMT nanocomposites were prepared using solutions of poly(amic acid) precursors and dodecyl-MMT using *N*-methyl-2-pyrrolidone as a solvent. FTIR, TEM and WAXD showed exfoliated nanocomposite structures at low MMT content (< 2 wt%) and partially exfoliated structures at high MMT content. Polyimide hybrids in thin-film form display a 10-fold decrease in permeability toward water vapor at 2 wt% clay loading.

Zhong and Wang [168a] studied the exfoliation of silicate nanoclays in organic solvents such as xylene and toluene. In particular, they exposed the solutions of clay loadings from 1 to 10 wt % to ultrasound for several hours. When the clay particles were exfoliated the solutions became transparent and extremely viscous. The exfoliation was confirmed by X-ray diffraction measurements where a peak associated with diffraction from the silicate layers disappeared. Furthermore, they observed that solvents such as tetrahydrofuran (THF) did not lead to exfoliation as evidenced by a low viscosity turbid solution. Hence, the importance of the compatibility between the dispersing medium and the modified clay for exfoliation was established. Although they carried out an extensive study of the rheology of the exfoliated clay solutions, they did not consider how this information would be used in generating thermoplastic composites.

In another study, Avella et al. investigated the crystallization behavior and properties of exfoliated isotactic polypropylene (iPP)/organoclay nanocomposites prepared by a solution technique [168b]. From the XRD results, it was shown that the nanocomposite filled with 1 wt% of organoclay possesses exfoliated structure, while the sample with 3 wt% contains both exfoliated and intercalated structures. Above 3 wt%, clay aggregates were observed. Young's moduli increased with increasing clay content

and reached the maximum at 3 wt% filler content. Above 3 wt%, tensile moduli actually decreased due to the agglomeration and collapse of the clay layers. Regarding the crystallization behavior, the authors observed spherulites with positive birefringence in the optical microscope images for the crystallized iPP filled with 1% of organoclay. Also, the nucleation density increased with increasing nanoparticle content, indicating that the nanoparticles behave as nucleating agents. While a lot of interesting observations were presented, this study was only able to achieve exfoliated and stable structures only up to 1 wt% clay content. Also, it would be useful to conduct rheological experiments to determine the nanocomposites' behavior of the exfoliated and non-exfoliated structures. This study, along with other studies using solvent-based technique, requires a suitable polymer/solvent pair, which can be expensive and environmentally unfriendly due to the use of organic solvents.

2.3.3 Melt intercalation

This method was first demonstrated by Vaia et al. [169] in 1993, which stimulated the revival of interest in PLS nanocomposites. In recent years, this method has become the mainstream for the fabrication of PLS nanocomposites [149,150] because it is simple, economical, and environmentally friendly.

Vaia et al. [170,171] applied a mean-field statistical lattice model to study the thermodynamic issue associated with nanocomposite formation. They reported that calculations based on the mean field theory agree well with experimental results. Details regarding this model and explanation are presented in Ref. [170]. The authors claimed that from the theoretical model, entropic and energetic factors primarily determine the outcome of nanocomposite formation via polymer melt intercalation. General guidelines

may be established for selecting potentially compatible polymer/OMLS systems based on the Vaia et al. study [170]. According to the authors, polymers containing polar groups capable of associative interactions, such as Lewis-acid/base interactions or hydrogen bonding, lead to intercalation. The greater the polarizability or hydrophilicity of the polymer, the shorter the functional groups in the OMLS should be in order to minimize unfavorable interactions between the aliphatic chains and the polymer [170].

Vaia et al. [169] were the first to apply the melt intercalation technique in the preparation of Polystyrene (PS)/OMLS based nanocomposites. The resulting hybrid shows a WAXD pattern corresponding to that of the intercalated structure. The same authors also carried out the same experiment under the same experimental conditions using non-modified Na^+-MMT, but WAXD patterns did not show any intercalation of PS into the silicate galleries, emphasizing the importance of polymer/OMLS interactions. Vaia et al. [172] and Shen et al. [173] also applied the same technique to the preparation of PEO/Na^+-MMT and PEO/OMLS nanocomposites, respectively.

Liu et al. [174] first applied melt intercalation technique in the preparation of a commercially available N6 with octadecylammonium-MMT nanocomposites, using a twin-screw extruder. WAXD patterns and TEM observations indicate exfoliated nanocomposite structures with MMT less than 5 wt%. At a loading of 4.2 wt% MMT, yield strength increased from 68.2 to 91.3 MPa, tensile modulus increased from 3.0 to 4.1 GPa, and heat distortion temperature increased from 62 to 112^{o}C.

Fornes et al. [174a] investigated the effect of organoclay structure on nylon-6 (N6) nanocomposite morphology and properties. To study this effect, a series of organic amine salts were ion exchanged with sodium montmorillonite (Na^+-MMT) to form

organoclays varying in amine structure or exchange level relative to the clay. Each organoclay was melt-mixed with a high molecular grade of N6 (Capron B135WP, with M_n = 29,300) using a twin screw extruder. Figure 2.8 summarizes the structure and corresponding nomenclature of various amine compounds for the modification of Na^+-MMT using ion exchange method. Figure 2.9 summarizes WAXD patterns and TEM observations for one representative nanocomposite. From WAXD analysis, the authors observed that the galleries of the organoclays expand in a systematic manner to accommodate the molecular size and the amount of amine surfactant exchanged for the Na^+-MMT. They also identified three distinct surfactant structural effects that led to greater extents of exfoliation, higher stiffness, and increased yield strengths for the nanocomposites: decreasing the number of long alkyl tails from two to one tallow, use of methyl rather than hydroxyl-ethyl groups, and finally, use of an equivalent amount of surfactant on the clay as opposed to an excess amount.

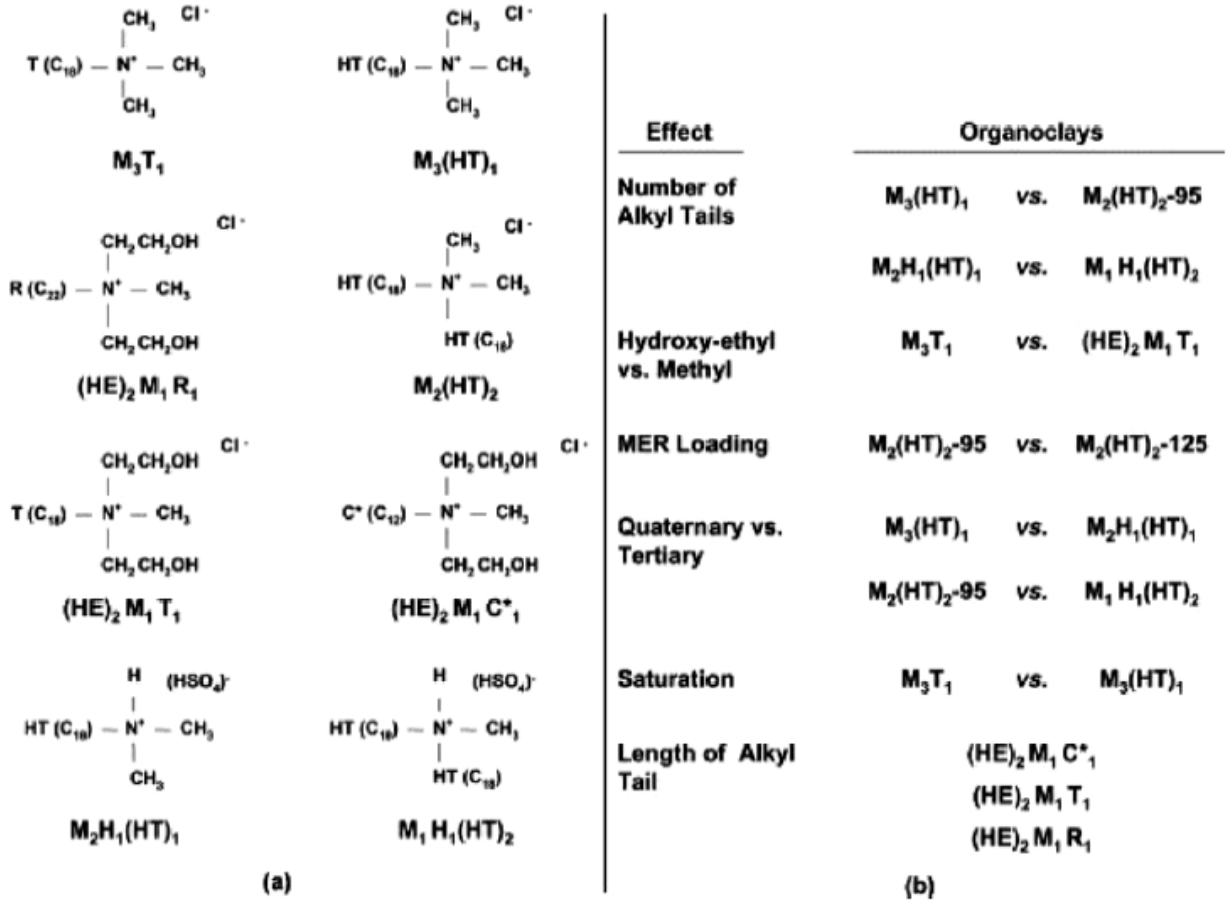

Figure 2.8: (a) Molecular structure and nomenclature of amine salts used to organically modify Naþ-MMT by ion exchange. The symbols M: Methyl, T: Tallow, HT: hydrogenated tallow, HE: 2-hydroxy-ethyl, R: rapeseed, C: coco, and H: hydrogen designate the substitutents on the nitrogen. (b) Organoclays used to evaluate the effect of structural variations of the amine cations on nanocomposite morphology and properties [174a]

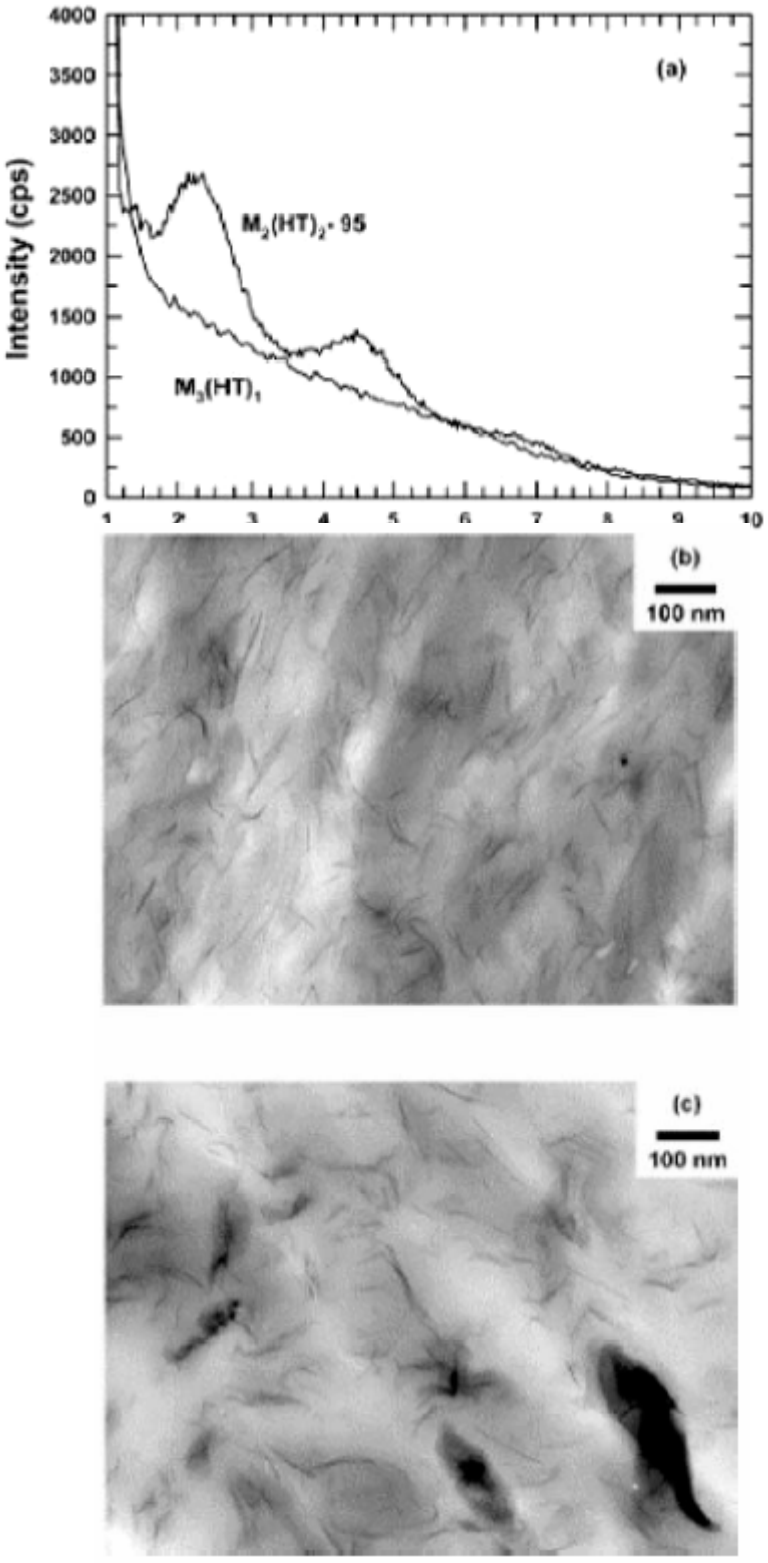

Figure 2.9: Morphological analysis of nanocomposites based on HMW Nylon-6 and the organoclays M3(HT)1 and M2(HT)2-95. (a) WAXD patterns and TEM images of (b) M3(HT)1 and (c) M2(HT)2-95 based nanocomposites. The concentration of MMT in the M3(HT)1 and M2(HT)2-95 nanocomposites are 2.9 and 3 wt% [174a].

Gilman et al. [175] reported the preparation of polyamide-6 (PA6) and PS-based nanocomposites of MMT modified with trialkylimidazolium cations. WAXD analyses and TEM observations showed an exfoliated structure for a PA6-based nanocomposite, whereas for a PS/MMT system, mixed intercalated and exfoliated structures were obtained.

In another study, Huang et al. [107] reported the synthesis of a partially exfoliated bisphenol polycarbonate nanocomposite prepared by using carbonate cyclic oligomers and dimethylditallowammonium-exchanged MMT. WAXD patterns indicated that exfoliation of this OMLS occurred after mixing with the cyclic oligomers in a Brabender mixer for 1 h at 180 ^{o}C. Subsequent ring-opening polymerization of the cyclic oligomers converted the matrix into a linear polymer without disruption of the nanocomposite structure. TEM imaging revealed that partial exfoliation was obtained, although no indication of layer correlation was observed in the WAXD.

Lee and Huang et al. prepared poly(etherimide) (PEI)/MMT nanocomposites by melt blending hexadecylamine modified MMT and PEI at 350^{o}C to obtain thermoplastic poly(etherimide) (PEI) based nanocomposites [176, 177]. The dispersion of the MMT layers within the PEI matrix was verified using WAXD and TEM. From WAXD patterns, it was assumed that exfoliation was achieved because of the lack of diffraction peaks. However, TEM observations revealed stacked silicate layers heterogeneously dispersed in the polymer matrix. According to the authors, the strong interaction between PEI and OMLS caused a substantial increase at the thermal decomposition temperature, and a drastic decrease in solvent uptake as compared to the virgin PEI. However they did not check the stability of the intercalated salts in OMLS at this high mixing temperature.

Finally, in a different study, Liu and coworkers investigated the effects of clay concentration and processing-induced clay dispersion on the structure and properties of PA6/clay nanocomposites [190]. The PA6/clay nanocomposites were prepared via a melt-compounding method using a Brabender twin-screw extruder. The nanostructure and morphology of PA6/clay nanocomposites were examined using XRD, TEM and optical microscopy. By combining XRD and TEM studies, the authors observed mostly exfoliated structure in the nanocomposite at low concentration (< 5 wt%), while above it, intercalated clay aggregates were observed. Young's moduli and tensile strength of the PA6/clay nanocomposites were seen to increase with increasing clay concentration up to 5 wt%. Above 5 wt%, yield strength actually dropped. The authors also made another interesting observation regarding an uneven clay distribution resulting from injection molding, which affected the crystalline structure of PA6. It would be useful to know how these PA6/clay nanocomposites behave rheologically at different clay concentration. Regarding the processing conditions, the processing temperature of PA6/clay nanocomposites was a bit high, it might be interesting to find out whether there were any degradation in the organic modifiers and how it could have affected the final structure and properties of the nanocomposites.

Different processing machinery, conditions, and clay modifiers can significantly affect the resulting nanocomposites. A paper by Dolgovskij et al. shows the effect of different mixer types on the exfoliation of polypropylene (PP) nanocomposites [191]. The mixers examined in this study were DACA Micro Compounder co-rotating twin-screw, Haake internal mixer, DSM co-rotating twin-screw, KWP ZSK30 twin-screw, and a two-step multilayer extrusion using a Prism 16 mm co-rotating twin screw extruder followed

by a Davis-Standard single-screw extruder. The best dispersion of clay, thus the best mechanical and thermal properties, was achieved by using the DACA mixer. This effectiveness could be due to the right balance of shear rate and residence time in the DACA mixer.

Another paper by Dennis et al. also shows the important impact of extruder types on the delamination and dispersion of layered silicate nanocomposites [192]. Although not an exhaustive study of mixer types, they included enough variety to demonstrate the importance of the process for making nanocomposites. The extruders included in the study were a Leistritz 34 mm modular intermeshing, counter-rotating twin screw extruder, a Leistritz 34 mm modular non-intermeshing, counter-rotating twin screw extruder, a Killion 25.4 mm single screw extruder outfitted with a high intensity mixing head, and a Japan Steel Works 30 mm modular self-wiping co-rotating twin screw extruder. The non-intermeshing twin screw extruder was proven to yield the best delamination and dispersion of the clay, hence the most property improvement.

Other processing conditions, such as temperature and screw speed, can also affect the properties of the nanocomposites as demonstrated by Modesti et al. [193]. In this study, the authors demonstrated the influence of varying the processing temperature and screw speed on the enhancement of mechanical properties of polypropylene nanocomposites. Using XRD, SEM, TEM, and a dynamometer as characterization methods, the authors observed the best results at high screw speed (350 rpm) and low barrel profile temperature (170-180^{o}C). At these processing conditions, maximum shear stress exerted on the polymer was achieved, which helped shearing and breaking the clay platelets apart more effectively. Clay types can also have critical effect on the

morphology and physical properties of the nanocomposites. Thus, depending on the polymer matrix, the right surface clay modifier must be selected in order to achieve the best delamination and dispersion.

Lei et al. studied the effect of clay types on the processing and properties of polypropylene nanocomposites and showed that the surface treatment of clay can improve the clay dispersion in the PP matrix [194]. The clays included in the study were Cloisite 15A, Cloisite 20A, Nanocor I30E and Nanocor I31PS. Cloisite 15A and 20A were modified by long alkyl chain with quaternary ammonium group while I30E and I31PS were modified by long alkyl chain with amine group. It was found that nanocomposites with alkyl onium ion treated clays have higher moduli and better thermal stability than the ones with alkyl amine treated clays. Similar study by Dan et al. also shows the effect of clay modifiers on the morphology and properties of thermoplastic polyurethane/clay nanocomposites [195].

This is not an exhaustive list of work that studied the effects of processing machinery, conditions, and clay modifiers on the resulting nanocomposites. However, it includes enough to show the importance of many processing factors have on the melt compounding of the nanocomposites. Therefore, when preparing nanocomposites using the melt compounding technique careful selection of mixer type, clay modifier, and processing conditions must be made in order to have a successful development of good quality nanocomposites.

2.3.4 Nanocomposite synthesis with aid of sc-CO2

Supercritical fluids have been receiving attention recently in various applications such as in the food and pharmaceutical industries as well as in the plastics industry.

Particularly, supercritical carbon dioxide (sc-CO_2) has been used widely in many applications because it is environmentally friendly, nontoxic, relatively low cost, and nonflammable compared to other supercritical fluids [178]. High viscosity is usually a major problem in the processing of high molecular weight polymers or complex mixtures of particles filled polymers. To overcome this problem, sc-CO2 can be used as plasticizing agents to lower the viscosity of various polymer melts [179-181]. Under ambient condition, CO_2 is a gas which makes its removal from the polymeric product easy. At near critical, as Berens and Huvard [182] pointed out, CO_2 behaves like a polar, highly volatile organic solvent, which swells and plasticizes polymers when it interacts with them. Montmorillonite is a typical swellable mineral because it contains alkali metals between the silicate sheets, and therefore, it can be swollen in polar solvents such as water and sc-CO_2 [120]. In polar solvents, the basal distance of the silicate sheets expands and finally the silicate sheets come to exfoliate into individual sheets. These concepts can be utilized in the fabrication of PLS nanocomposites as a few authors have reported [183,184]. However, the extent of success is questionable and further research is needed because most authors did not investigate or report quantitatively the improvements in the materials properties.

To overcome some of the issues with using melt intercalation and modified PP and other solvent-based techniques, recently, there has been considerable interest in using sc-CO_2 as an alternative route for the preparation of polymer-clay nanocomposites [196-201]. To date, there are only a few papers that have reported on the use of supercritical carbon dioxide as an alternative route for the preparation of polymer-clay nanocomposites [183,184]. Zerda et al. [184] used sc-CO_2 for the synthesis of poly

(methyl methacrylate)-layered silicate intercalated nanocomposites. The authors presented a synthetic route to produce nanocomposites with significantly high concentrations of organically modified layered silicate (OMLS). OMLS used in this experiment were Cloisite 15A, 20A, and 25A from Southern Clay Products. At high levels of OMLS (> 20 wt%), the viscosity was apparently high and was overcome by using sc-CO_2 as a reaction medium. Homogeneous dispersion of monomer, initiation, and subsequent polymerization all occur under a significantly reduced viscosity in this medium. The detailed experiment can be found in ref. [185]. The authors reported a homogenous morphology, which was aided by sc-CO2, in the intercalated nanocomposites containing as high as 40 wt% of OMLS. At this loading, only a 50% increase in modulus was observed.

In a different approach, Wingert et al. [186] investigated the effect of nanoclay and sc-CO_2 on polymer melt rheology in an extrusion process. Polystyrene and organophilic montmorillonite (Cloisite 20A) were used in the fabrication of the nanocomposite. An extrusion slit die rheometer with backpressure regulator was used to measure the shear viscosity of polystyrene/CO_2/nanoclay melts. The authors observed that, without the presence of CO_2, the viscosity of the nanocomposite (< 5 wt% OMLS) increased with nanoclay loading. With the presence of CO_2, the nanocomposite melt is swollen, and the nanoclay acts to reduce viscosity compared to the pure polystyrene/CO_2 system. No profound explanation of why the nanoclay lubricates the flow was given by the authors. No information regarding nanocomposite structures nor material properties were reported.

Recently, another approach to prepare polymer nanocomposites using sc-CO_2 in the melt intercalation process was reported by Lesser et al. [187]. Here, a study of the effect of sc-CO_2 on the melt intercalation process and on the final structure and morphology of polymer-clay nanocomposites is presented. sc-CO_2 was absorbed into the nano-clay particles and pellets in a pressurized hopper. Hence, mixing of the nano-clays with sc-CO_2 was done by means of diffusion which may limit the amounts of CO_2 absorbed. High-density polyethylene (HDPE) and unmodified montmorillonite (Cloisite Na^+) and surface modified montmorillonite (Cloisite 15A) were used in the preparation PLS nanocomposites. A detailed processing system can be found in ref. [188,189]. WAXS and TEM were used to analyze the resulting nanocomposites. In summary, the authors found that, regardless of the clay nature (modified or unmodified), the presence of sc-CO_2 promotes significant increase in the basal spacing of the clay, and thereby may enhance the ease of the polymer intercalation into the galleries of the clay. The increases in the clays d-spacings were reported to be as much as 100%. Properties of the nanocomposites were not reported.

In a different approach, Mielewski et al. [200] proposed a method to directly inject sc-CO_2 to a melt mixture of silicate particles and polymer in an extruder. The silicates are expected to exfoliate when exiting the extruder. No WAXD or TEM evidence of exfoliated morphology was presented. Alternatively, Manke et al. [201] developed a process that allows clay particles to be pre-treated with sc-CO_2 in a pressurized vessel and then rapidly depressurized into another vessel at atmospheric pressure to force the clay platelets apart. The result was exfoliated nanoclay particles as observed by X-Ray diffraction. However, they did not provide any mechanism for

assuring that the exfoliated particles remain exfoliated when they are combined with the polymer via conventional melt blending.

2.4 Theoretical Modeling of the Young's Modulus

The observed increase in the Young's modulus with addition of layered silicates into a polymer matrix is of obvious practical benefit to many applications where improved strength and stiffness may be utilized. In order to realize the full potential of mechanical property increase, it is necessary to compare the observed property enhancements, such as modulus, to those predicted by composite theories like that of Halpin-Tsai [202, 203]. Realizing the full potential of mechanical property enhancement remains unclear even when fully exfoliated nanocomposite morphologies are shown by XRD. Evaluation of the expected modulus increase for polymer composites presented here will be based on a composite theory developed by Halpin and Tsai.

The effectiveness of the model to predict actual experimental values of Young's modulus depend on the assumptions it is based upon. Halpin and Tsai's model shown below in Equation 1 assumes fully exfoliated clay platelets, unidirectional, i.e. well oriented filler particles, as well as a high degree of adhesion of the filler particles to the surrounding polymer matrix,

$$E_c = E_m\left[\frac{1+\zeta\eta\phi_f}{1-\eta\phi_f}\right], \tag{1}$$

where E_c = composite modulus, E_m = unfilled matrix modulus, ϕ_f = filler volume fraction,

$$\eta = \frac{E_f/E_m - 1}{E_f/E_m + \zeta}, \tag{2}$$

$$\zeta = 2(l/t), \tag{3}$$

E_f = filler modulus taken to be 178 GPa for MMT [203], and l/t = aspect ratio of the silicate platelets taken here to be approximately 100 for fully exfoliated platelets [203].

It is important to point out that there are numerous complexities arise when comparing experimental data to those of composite theory, especially when dealing with polymer layered silicate nanocomposites. How effectively the model can predict the actual experimental values depend on the assumptions it is based upon. Some issues that limit the ability to model the stiffness properties of polymer-clay nanocomposites are summarized in Figure 2.10.

Issue	Theory	Experimental
Filler shape and size	- Uniform shape - Constant dimensions	- Non-uniform shape - Distribution of lengths and thickness - Imperfect exfoliation of LAS
Filler orientation	- Unidirectional	- Some degree of misalignment
Filler interface	- The filler and matrix are well bonded	- Imperfect bonding between the filler and matrix
Filler modulus	- Assumes filler modulus is the same in all directions	- Filler is anisotropic
Matrix considerations	- Assumes matrix is isotropic	- Polymer chain orientation - Presence of polymer crystallites
Filler Concentration Effects	- No particle-particle interactions - Ignores changes in viscosity - No particle agglomeration	- Particle-particle interactions and agglomeration - Changes in viscosity can alter morphology during injection molding - Changes in crystalline morphology (e.g. type, crystallite size, and amount)

Figure 2.10: Some important issues that limit the ability to model the stiffness properties of polymer-clay nanocomposites [203]

2.5 Research objectives

The previous sections of this chapter have shown encouraging signs that PLS nanocomposites can exhibit significantly better properties than possible with conventional reinforcement systems (i.e. glass) but at lower loading levels. These improved properties are generally attained at lower silicate content (< 5 wt %) compared to that of conventional reinforcing systems. For example, with only a small MMT loading (4-7 wt%) in nylon 6, the modulus doubled, tensile strength increased more than 50%, heat distortion temperature increased by 100^{o}C, and combustion heat release rate was reduced by up to 63% [50a-c]. For the polyethylene/layered silicate nanocomposites prepared by in situ intercalative polymerization, with about 3.4 wt% MMT loading, Young's modulus increased approximately 85%. Polyimide hybrids in thin-film form displayed a 10-fold decrease in permeability of water vapor at 2 wt% clay loading [89]. Wang et al. [190] reported 20% increase in tensile strength and 50% increase in tensile modulus in situ emulsion polymerized PMMA with fully exfoliated 3 wt% layered silicate clay. The same nanocomposite system was prepared via melt intercalation by Park et al. [191], who reported 13% increase in Young's modulus and 12% increase in impact strength with only 2% MMT loading.

There are certain limitations and drawbacks to each of the techniques used to disperse nano-particles in polymer matrices. For the methods of intercalation of polymer from solution and in situ polymerization, the drawback is the requirement of a suitable solvent. It has, in fact, been shown that intercalation only occurs for certain polymer/solvent or monomer/solvent pairs. Application of these methods in the production of industrially significant polymers may, thus, be impracticable, especially in

view of the high costs associated with solvents themselves, their disposal and their environmental impact. Furthermore, the extent of intercalation completely depends upon the nature of solvent used. For the melt intercalation technique, the drawback is its dependent on the processing conditions, and favorable interactions between the polymer and the clay is required. Thus far, most studies can only achieve exfoliated nanocomposite structures with only up to 4 wt% MMT. This leads us to the first objective of this study:

2.5.1 Research objective #1

The first objective of this research is to invent a technique for increasing the exfoliation and dispersion of nano-clay particles into polymeric matrices, preferably greater than 5 wt% MMT, using supercritical carbon dioxide.

The studies presented by Zerda et al. [184], Wingert et al. [186], and Lesser et al. [187] provide evidence that sc-CO_2 can swell the layered silicates, which thereby may enhance the ease of polymer intercalation into the galleries of the clay. Furthermore, sc-CO_2 is highly soluble in a number of polymers which will aid dispersion and at same time lower the viscosity of the melt. Once mixing is complete sc-CO_2 can be extracted from the system leaving the particles dispersed within the thermoplastic.

However, a few questions still remain to be answered which will constitute the thrust of this research. Can higher levels of sc CO_2 be absorbed into the nano-clay galleries and can the clays be exfoliated in sc-CO_2 before injecting into a molten polymer stream by developing mixing methods. Can scCO_2 help disperse higher levels of clay particles in the polymer matrix? Can the exfoliated structure still be achieved at higher

clay loadings? Will a higher degree of property enhancements be obtained? Most studies dealing with PP-clay nanocomposites, even with the incorporation of a MA compatibilizer, are only partially successful because complete exfoliation was practically never reached [33-47]. Can the CO_2 chamber technique be combined with a MA compatibilizer to produce more exfoliated PP-clay nanocomposites? This leads to objective 2:

2.5.2 Research objective #2

Extend the CO_2 chamber technique further by incorporating a MA compatibilizer to prepare PP-clay nanocomposites.

We would like to ascertain whether or not further improvements on the mechanical properties of the nanocomposites can be achieved when prepared with the incorporation of a maleic anhydride compatibilizer. The effect of a MA compatibilizer on the microstructure and on the mechanical and linear viscoelastic properties of the nanocomposites prepared using different processing techniques is also studied.

2.6 References

1. K. Masenelli-Varlot, E. Reynaud, G. Vigier, and J. Varlet, Mechanical properties of clay-reinforced polyamide. *J. Polymer. Sci*., Part B: Polymer. Phys., **40** (2002), pp. 272.

2. S. Sinha Ray, K. Okamoto and M. Okamoto, Structure–property relationship in biodegradable poly(butylene succinate)/layered silicate nanocomposites. *Macromolecules* **36** (2003), pp. 2355–2367.

3. A. Okada, Y. Fukoshima, S. Inagaki, A. Usuki, S. Sugiyama, T. Kurashi, O. Kamigaito., U.S. **4,739,007** (1998).

4. M. Kato, A. Usuki and A. Okada, Synthesis of polypropylene oligomer - clay intercalation compounds. *J Appl Polym Sci* **66** (1997), pp. 1781.

5. M. Kawasumi, N. Hasegawa, M. Kato, A. Usuki and A. Okada Preparation and Mechanical Properties of Polypropylene-Clay Hybrids. *Macromolecules* **30** (1997), pp. 6333.

6. N. Hasegawa, M. Kawasumi, M. Kato, A. Usuki and A. Okada, Preparation and mechanical properties of polypropylene-clay hybrids using a maleic anhydride-modified polypropylene oligomer *J Appl Polym Sci* **67** (1998), p. 87.

7. X. Liu and Q. Wu, PP/clay nanocomposites prepared by grafting-melt intercalation. *Polymer* **42** (2001), p. 10013.

8. P.H. Nam, P. Maiti, M. Okamoto, T. Kotaka, N. Hasegawa and A. Usuki, A hierarchical structure and properties of intercalated polypropylene/clay nanocomposites. *Polymer* **42** (2001), p. 9633.

9. Y. Kurokawa, H. Yasuda and A. Oya, Preparation of nanocomposites of polypropylene and smectite. *J Mater Sci Lett* **15** (1996), pp. 1481–1487.

10. N. Furuichi, Y. Kurokawa, K. Fujita, A. Oya, H. Yasuda and M. Kiso, Preparation and properties of polypropylene reinforced by smectite. *J Mater Sci* **31** (1996), pp. 4307–4310.

11. J. Tudor, L. Willington, D. O'Hare and B. Royan, Intercalation of catalytically active metal complexes in phyllosilicates and their application as propene polymerization catalyst. *Chem Commun* (1996), pp. 2031–2032.

12. Y. Kurokawa, H. Yasuda, M. Kashiwagi and A. Oya, Structure and properties of a montmorillonite/polypropylene nanocomposite. *J Mater Sci Lett* **16** (1997), pp. 1670–1672

13. M.R. Nyden and J.W. Gilman, Molecular dynamics simulations of the thermal degradation of nano-confined polypropylene. *Comput Theor Polym Sci* **7** (1997), pp. 191–198.

14. M. Kato, A. Usuki and A. Okada, Synthesis of polypropylene oligomer–clay intercalation compounds. *J Appl Polym Sci* **66** (1997), pp. 1781–1785

15. A. Usuki, M. Kato, A. Okada and T. Kurauchi, Synthesis of polypropylene–clay hybrid. *J Appl Polym Sci,* **63** (1997), pp. 137–138.

16. M. Kawasumi, N. Hasegawa, M. Kato, A. Usuki and A. Okada, Preparation and mechanical properties of polypropylene–clay hybrids. *Macromolecules* **30** (1997), pp. 6333–6338.

17. N. Hasegawa, M. Kawasumi, M. Kato, A. Usuki and A. Okada, Preparation and mechanical properties of polypropylene–clay hybrids using a maleic anhydride-modified polypropylene oligomer. *J Appl Polym Sci* **67** (1998), pp. 87–92.

18. A. Oya, Polypropylene–clay nanocomposites. In: T.J. Pinnavaia and G.W. Beall, Editors, *Polymer–clay nanocomposites*, Wiley, London (2000), pp. 151–172.

19. N. Hasegawa, H. Okamoto, M. Kato and A. Usuki, Preparation and mechanical properties of polypropylene–clay hybrids based on modified polypropylene and organophilic clay. *J Appl Polym Sci* **78** (2000), pp. 1918–1922.

20. A. Oya, Y. Kurokawa and H. Yasuda, Factors controlling mechanical properties of clay mineral/polypropylene nanocomposites. *J Mater Sci* **35** (2000), pp. 1045–1050.

21. J.W. Lee, Y.T. Lim and O.O. Park, Thermal characteristics of organoclay and their effects upon the formation of polypropylene/organoclay nanocomposites. *Polym Bull* **45** (2000), pp. 191–198.

22. Q. Zhang, Q. Fu, L. Jiang and Y. Lei, Preparation and properties of polypropylene/montmorillonite layered nanocomposites. *Polym Int* **49** (2000), pp. 1561–1564

23. J.M. Garces, D.J. Moll, J. Bicerano, R. Fibiger and D.G. McLeod, Polymeric nanocomposites for automotive applications. *Adv Mater* **12** (2000), pp. 1835–1839

24. N. Hasegawa, H. Okamoto, M. Kawasumi, M. Kato, A. Tsukigase and A. Usuki, Polyolefin–clay hybrids based on modified polyolefins and organoclay. *Macromol Mater Engng* **280/281** (2000), pp. 76–79.

25. S. Hambir, N. Bulakh, P. Kodgire, R. Kalgaonkar and J.P. Jog, PP/clay nanocomposites: a study of crystallization and dynamic mechanical behavior. *J Polym Sci, Part B: Polym Phys* **39** (2001), pp. 446–450.

26. M. Zanetti, G. Camino, P. Reichert and R. Mulhaupt, Thermal behaviour of poly(propylene) layered silicate nanocomposites. *Macromol Rapid Commun* **22** (2001), pp. 176–180.

27. G. Galgali, C. Ramesh and A. Lele, A rheological study on the kinetics of hybrid formation in propylene nanocomposites. *Macromolecules* **34** (2001), pp. 852–858.

28. M.J. Solomon, A.S. Almusallam, K.F. Seefeldt, A. Somwangthanaroj and P. Varadan, Rheology of polypropylene/clay hybrid materials. *Macromolecules* **34** (2001), pp. 1864–1872.

29. J.M. Gloaguen and J.M. Lefebvre, Plastic deformation behavior of thermoplastic/clay nanocomposites. *Polymer* **42** (2001), pp. 5841–5847.

30. J.M. Garcia-Martinez, O. Laguna, S. Areso and E.P. Collar, Polypropylene/mica composites modified by succinic anhydride-grafted atactic polypropylene: a thermal and mechanical study under dynamic conditions. *J Appl Polym Sci* **81** (2001), pp. 625–636.

31. D. Schmidt, D. Shah and E.P. Giannelis, New advances in polymer/layered silicate nanocomposites. *Curr Opin Solid State Mater Sci,* **6** (2002), pp. 205–212.

32. P. Reichert, B. Hoffman, T. Bock, R. Thomann, R. Mulhaupt and C. Friedrich, Morphological stability of polypropylene nanocomposites. *Macromol Rapid Commun* **22** (2001), pp. 519–523.

33. P.H. Nam, P. Maiti, M. Okamoto, T. Kotaka, N. Hasegawa and A. Usuki, A hierarchical structure and properties of intercalated polypropylene/clay nanocomposites. *Polymer* **42** (2001), pp. 9633–9640.

34. X. Liu and Q. Wu, PP/clay nanocomposites prepared by grafting-melt intercalation. *Polymer* **42** (2001), pp. 10013–10019.

35. P.H. Nam, P. Maiti, M. Okamaoto, T. Kotaka, Foam processing and cellular structure of polypropylene/clay nanocomposites. Proceeding Nanocomposites, June 25–27, 2001, Chicago, Illinois, USA: ECM Publication; 2001.

36. E. Manias, A direct-blending approach for polypropylene/clay nanocomposites enhances properties. *Mater Res Soc Bull* **26** (2001), pp. 862–863.

37. M. Okamoto, P.H. Nam, P. Maiti, T. Kotaka, N. Hasegawa and A. Usuki, A house-of-cards structure in polypropylene/clay nanocomposites under elongational flow. *Nano Lett* **1** (2001), pp. 295–298.

38. M. Okamoto, P.H. Nam, M. Maiti, T. Kotaka, T. Nakayama, M. Takada, M. Ohshima, A. Usuki, N. Hasegawa and H. Okamoto, Biaxial flow-induced alignment of silicate layers in polypropylene/clay nanocomposite foam. *Nano Lett* **1** (2001), pp. 503–505

39. S. Hambir, N. Bulakh, P. Kodgire, R. Kalgaonkar and J.P. Jog, PP/clay nanocomposites: a study of crystallization and dynamic mechanical behavior. *J Polym Sci, Part B: Polym Phys* **39** (2001), pp. 446–450.

40. T. Sun and J.M. Garces, High-performance polypropylene–clay nanocomposites by in-situ polymerization with metallocene/clay catalysts. *Adv Mater* **14** (2002), pp. 128–130.

41. P. Maiti, P.H. Nam, M. Okamoto, T. Kotaka, N. Hasegawa and A. Usuki, Influence of crystallization on intercalation, morphology, and mechanical properties of propylene/clay nanocomposites. *Macromolecules* **35** (2002), pp. 2042–2049.

42. P. Maiti, P.H. Nam, M. Okamoto, T. Kotaka, N. Hasegawa and A. Usuki, The effect of crystallization on the structure and morphology of polypropylene/clay nanocomposites. *Polym Engng Sci* **42** (2002), pp. 1864–1871.

43. P.H. Nam, P. Maiti, M. Okamoto, T. Kotaka, T. Nakayama, M. Takada, M. Ohshima, A. Usuki, N. Hasegawa and H. Okamoto, Foam processing and cellular structure of polypropylene/clay nanocomposites. *Polym Engng Sci* **42** (2002), pp. 1907–1918

44. S. Hambir, N. Bulakh and J.P. Jog, Propylene/clay nanocomposites: effect of compatibilizer on the thermal, crystallization and dynamic mechanical behavior. *Polym Engng Sci* **42** (2002), pp. 1800–1807.

45. D. Kaempfer, R. Thomann and R. Mulhaupt, Melt compounding of syndiotactic polypropylene nanocomposites containing organophilic layered silicates and in situ formed core/shell nanoparticles. *Polymer* **43** (2002), pp. 2909–2916.

46. A. Lele, M. Mackley, G. Galgali and C. Ramesh, In situ rheo-X-ray investigation of flow-induced orientation in layered silicate-syndiotactic polypropylene nanocomposite melt. *J Rheol* **46** (2002), pp. 1091–1110.

47. Q. Zhang, Y. Wang and Q. Fu, Shear-induced change of exfoliation and orientation in polypropylene/montmorillonite nanocomposites. *J Polym Sci, Part B: Polym Phys* **41** (2003), pp. 1–10.

48. A. Somwangthanaroj, E.C. Lee and M.J. Solomon, Early stage quiescent and flow-induced crystallization of intercalated polypropylene nanocomposites by time-resolved light scattering. *Macromolecules* **36** (2003), pp. 2333–2342

49. A.B. Morgan and J.D. Harris, Effects of organoclay soxhlet extraction on mechanical properties, flammability properties and organoclay dispersion of polypropylene nanocomposites. *Polymer* **44** (2003), pp. 2113–2320.

50. H.G. Jeon, H.T. Jung, S.W. Lee and S.D. Hudson, Morphology of polymer silicate nanocomposites. High density polyethylene and a nitrile. *Polym Bull* **41** (1998), pp. 107–113.

a) A. Okada, M. Kawasumi, A. Usuki, Y. Kojima, T. Kurauchi and O. Kamigaito, Synthesis and properties of nylon-6/clay hybrids. In: D.W. Schaefer and J.E. Mark, Editors, *Polymer based molecular compositesMRS Symposium Proceedings, Pittsburgh, vol.* ***171*** (1990), pp. 45–50.

b) A. Usuki, M. Kawasumi, Y. Kojima, A. Okada, T. Kurauchi, and O. Kamigaito, Swelling behavior of montmorillonite cation exchanged for v-amino acids by e-caprolactam. *J. Mater. Res.*, **8** (1993), p. 1174.

c) T.D. Fornes, P.J. Yoon, H. Keskkula, D.R. Paul, Nylon 6 nanocomposites: the effect of matrix molecular weight. *Polymer* **42** (2001) 9929-9940.

51. J. Heinemann, P. Reichert, R. Thomson and R. Mulhaupt, Polyolefin nanocomposites formed by melt compounding and transition metal catalyzed ethane homo- and copolymerization in the presence of layered silicates. *Macromol Rapid Commun* **20** (1999), pp. 423–430.

52. V.P. Privalko, F.J.B. Calleja, D.I. Sukhorukov, E.G. Privalko, R. Walter and K. Friedrich, Composition-dependent properties of polyethylene/Kaolin composites. Part II. Thermoelastic behavior of blow-molded samples. *J Mater Sci* **34** (1999), pp. 497–508.

53. J.S. Bergman, H. Chen, E.P. Giannelis, M.G. Thomas and G.W. Coates, Synthesis and characterization of polyolefin-silicate nanocomposites: a catalyst intercalation and in situ polymerization approach. *J Chem Soc Chem Commun* **21** (1999), pp. 2179–2180.

54. J. Rong, J. Jing, H. Li and M. Sheng, A polyethylene nanocomposite prepared via in-situ polymerization. *Macromol Rapid Commun* **22** (2001), pp. 329–334.

55. K.H. Wang, M.H. Choi, C.M. Koo, Y.S. Choi and I.J. Chung, Synthesis and characterization of maleated polyethylene/clay nanocomposites. *Polymer* **42** (2001), pp. 9819–9826.

56. M. Alexandre, P. Dubois, T. Sun, J.M. Graces and R. Jerome, Polyethylene-layered silicate nanocomposites prepared by the polymerization-filling technique: synthesis and mechanical properties. *Polymer* **43** (2002), pp. 2123–2132.

57. T.G. Gopakumar, J.A. Lee, M. Kontopoulou and J.S. Parent, Influence of clay exfoliation on the physical properties of montmorillonite/polyethylene composites. *Polymer* **43** (2002), pp. 5483–5491.

58. Y.-H. Jin, H.-J. Park, S.-S. Im, S.-Y. Kwak and S. Kwak, Polyethylene/clay nanocomposite by in situ exfoliation of montmorillonite during Ziegler–Natta polymerization of ethylene. *Macromol Rapid Commun* **23** (2002), pp. 135–140.

59. A. Bafna, G. Beaucage, F. Mirabella and S. Mehta, 3D hierarchical orientation in polymer–clay nanocomposite films. *Polymer* **44** (2003), pp. 1103–1115.

60. R. A Vaia, H. Isii, and E. P. Giannelis, Synthesis and properties of two-dimensional nanostructures by direct intercalation of polymer melts in layered silicates. *Chem Mater* **5** (1993), pp 1694.

61. R. A. Vaia, K. D. Jandt, J. K. Edward, and E. P. Giannelis, Kinetics of Polymer Melt Intercalation. *Macromolecules* **28** (1995), pp. 8080.

62. M. W. Weiner, H. Chen, E. P. Giannelis, and D. Y. Sogah, *J. Am. Chem. Soc*. **122** (1999), pp. 1615.

63. A. Moet and A. Akelah, Polymer-clay nanocomposites: polystyrene grafted onto montmorillonite interlayers. *Mater Lett*. **18** (1993), pp. 97.

64. N. Hasegawa, H. Okamoto, M. Kawasumi, and A. Usuki, Preparation and mechanical properties of polystyrene-clay hybrids. *J. Appl. Polym. Sci*., **74** (1999), pp. 3359.

65. M. Alexandre and P. Dubois, Polymer-layered silicate nanocomposites: preparation, properties and uses of a new class of materials. *Mater. Sci, and Eng*., **28** (2000), pp. 1-63.

66. D. M. Lincoln, R. A. Vaia, Z. G. Wang, and B. S. Hsiao, Secondary structure and elevated temperature crystallite morphology of nylon-6/layered silicate nanocomposites. *Polymer* **42** (2001), pp. 1621-31.

67. K. Sall, European Plastics News, March 14, 2002.

68. P. B. Messersmith and E. P. Giannelis, Synthesis and barrier properties of poly(ε-caprolactone)-layered silicate nanocomposites. *J. Polym. Sci. Part A: Polym. Chem*., **33** (1995), pp. 1047.

69. E. Hackett, E. Manias and E.P. Giannelis, Computer simulation studies of PEO/layered silicate nanocomposites. *Chem Mater* **12** (2000), pp. 2161–2167.

70. V. Kuppa and E. Manias, Computer simulation of PEO/layered-silicate nanocomposites: 2. Lithium dynamics in PEO/Li^+ montmorillonite intercalates. *Chem Mater* **14** (2002), pp. 2171–2175.

71. P. Aranda and E. Ruiz-Hitzky, Poly(ethylene oxide)-silicate intercalation materials. *Chem Mater* **4** (1992), pp. 1395–1403.

72. T. Lan, P. D. Kaviratna, and T. J. Pinnavaia, On the Nature of Polyimide-Clay Hybrid Composites. *Chem. Mater*., **6** (1994), pp 573.

73. P. B. Messersmith and E. P. Giannelis, Synthesis and barrier properties of poly(ε-caprolactone)-layered silicate nanocomposites. J. Polym. Sci. Part A: Polym. Chem. Ed., **33** (1995), pp. 1407.

74. K. Yano, A. Usuki, A. Okada, T. Kurauchi and O. Kamigaito, Synthesis and properties of polyimide–clay hybrid. *Polym Prepr (Jpn)* **32** 1 (1991), pp. 65–67.

75. T. Lan, P.D. Kaviratna and T.J. Pinnavaia, On the nature of polyimide–clay hybrid composites. *Chem Mater* **6** (1994), pp. 573–575.

76. K. Yano, A. Usuki and A. Okada. Synthesis and properties of polyimide–clay hybrid films. *J Polym Sci, Part A: Polym Chem* **35** (1997), pp. 2289–2294.

77. Z.-K. Zhu, Y. Yang, J. Yin, X.Y. Wang, Y.C. Ke and Z.N. Qi. Preparation and properties of organosoluble montmorillonite/polyimide hybrid materials. *J Appl Polym Sci* **73** (1999), p. 2063.

78. Y. Yang, Z.K. Zhu, J. Yin, X.Y. Wang and Z.E. Qi, Preparation and properties of hybrids of organo-soluble polyimide and montmorillonite with various chemical surface modification methods. *Polymer* **40** (1999), pp. 4407–4414.

79. H.L. Tyan, K.H. Wei and T.E. Hsieh, Mechanical properties of clay–polyimide (BTDA-ODA) nanocomposites via ODA-modified organoclay. *J Polym Sci, Part B: Polym Phys* **38** (2000), p. 2873.

80. K. Yano, A. Usuki and A. Okada, Polyimide/montmorillonite hybrid. *Polym Prepr (201 ACS)* **32** (1991), pp. 65–66.

81. A. Gu and F.C. Chang, A novel preparation of polyimide/clay hybrid films with low coefficient of thermal expansion. *J Appl Polym Sci* **79** (2001), pp. 289–294.

82. A. Gu, S.W. Kuo and F.C. Chang, Syntheses and properties of PI/clay hybrids. *J Appl Polym Sci* **79** (2001), pp. 1902–1910.

83. S.H. Hsiao, G.S. Liou and L.M. Chang, Synthesis and properties of organosoluble polyimide/clay hybrids. *J Appl Polym Sci* **80** (2001), pp. 2067–2072.

84. H.L. Tyan, C.M. Leu and K.H. Wei, Effect of reactivity of organics-modified montmorillonite on the thermal and mechanical properties of montmorillonite/polyimide nanocomposites. *Chem Mater* **13** (2001), pp. 222–226.

85. J.C. Huang, Z.K. Zhu, X.D. Ma, X.F. Qian and J. Yin, Preparation and properties of montmorillonite/organo-soluble polyimide hybrid materials prepared by a one-step approach. *J Mater Sci* **36** (2001), p. 871.

86. T. Agag, T. Koga and T. Takeichi, Studies on thermal and mechanical properties of polyimide–clay nanocomposites. *Polymer* **42** (2001), pp. 3399–3408.

87. A.B. Morgan, J.W. Gilman and C.L. Jackson, Characterization of the dispersion of clay in a polyetherimide nanocomposite. *Macromolecules* **34** (2001), pp. 2735–2738.

88. C.M. Leu, Z.W. Wu and K.H. Wei, Synthesis and properties of covalently bonded layered silicates/polyimide (BTDA-ODA) nanocomposites. *Chem Mater* **14** (2002), pp. 3016–3021.

89. R. Magaraphan, W. Lilayuthalert, A. Sirivat and J.W. Schwank, Preparation, structure, properties and thermal behavior of rigid-rod polyimide/montmorillonite nanocomposites. *Compos Sci Technol* **61** (2001), pp. 1253–1264.

90. D.M. Delozier, R.A. Orwoll, J.F. Cahoon, J.S. Ladislaw, J.G. Smith, Jr and J.W. Connell, Polyimide nanocomposites prepared from high-temperature reduced charge organoclays. *Polymer* **44** (2003), pp. 2231–2241.

91. Z.-M. Liang, J. Yin and H.-J. Xu, Polyimide/montmorillonite nanocomposites based on thermally stable, rigid-rod aromatic amine modifiers. *Polymer* **44** (2003), pp. 1391–1399.

92. F. Dabrowski, S. Bourbigot, R. Delbel and M.L. Bras, Kinetic molding of the thermal degradation of polyamide-6 nanocomposite. *Eur Polym J* **36** (2000), pp. 273–284.

93. Y. Ding, D.J. Jones, P. Maireles-Torres and J. Roziere, Two-dimensional nanocomposites: alternating inorganic–organic polymer layers in zirconium phosphate. *Chem Mater* **7** (1995), pp. 562–571.

94. P. Reichert, J. Kressler, R. Thomann, R. Mulhaupt and G. Stoppelmann, Nanocomposites based on a synthetic layer silicate and polyamide-12. *Acta Polym* **49** (1998), pp. 116–123.

95. B. Hoffman, J. Kressler, G. Stoppelmann, C. Friedrich and G.M. Kim, Rheology of nanocomposites based on layered silicate and polyamide-12. *Colloid Polym Sci* **278** (2000), pp. 629–636.

96. E. Giza, H. Ito, T. Kikutani and N. Okui, Structural control of polyamide 6/clay nanocomposites fibers in-line drawing process. *J Polym Engng* **20** (2000), pp. 403–425.

97. G.M. Kim, D.H. Lee, B. Hoffmann, J. Kresler and G. Stoppelmann, Influence of nanofillers on the deformation process in layered silicate/polyamide-12 nanocomposites. *Polymer* **42** (2001), pp. 1095–1100.

98. S.V. Nair, L.A. Goettler and B.A. Lysek, Toughness of nanoscale and multiscale polyamide-6,6 composites. *Polym Engng Sci* **42** (2002), pp. 1872–1882

99. X. Liu, Q. Wu, Q. Zhang and Z. Mo, Phase transition in polyamide-66/montmorillonite nanocomposites on annealing. *J Polym Sci, Part B: Polym Phys* **44** (2003), p. 6367.

100. Y.C. Ke, C. Long and Z. Qi, Crystallization, properties, and crystal and nanoscale morphology of PET–clay nanocomposites. *J Appl Polym Sci* **71** (1999), pp. 1139–1146.

101. D.J. Sekelik, S. Stepanov Enazarenko, D. Schiraldi, A. Hiltner and E. Baer, Oxygen barrier properties of crystallized and talc-filled poly(ethylene terephthalate). *J Polym Sci, Part B: Polym Phys* **37** (1999), pp. 847–857.

102. J.C. Jr Matayabas, S.R. Turner, B.J. Sublett, G.W. Connell, R.B. Barbee, Nanocomposite technology for enhancing the gas barrier of polyethylene terephthalate. PCT Int Appl Wo 98/29499; July 9, 1998.

103. T. Takekoshi, F.F. Khouri, J.R. Campbell, T.C. Jordan, K.H. Dai, PET nanocomposites prepared by in situ incorporation of varying amounts of four different organoclays. US Pat 5,530.052 (General Electric Co.); June 25, 1996.

104. T.Y. Tsai, Polyethylene terephthalate–clay nanocomposites. In: T.J. Pinnavaia and G.W. Beall, Editors, *Polymer–clay nanocomposites*, Wiley, England (2000), pp. 173–189.

105. C.H. Davis, L.J. Mathias, J.W. Gilman, D.A. Schiraldi, J.R. Shields, P. Trulove, T.E. Sutto and H.C. Delong, Effects of melt-processing conditions on the quality of poly(ethylene terephthalate) montmorillonite clay nanocomposites. *J Polym Sci, Part B: Polym Phys* **40** (2002), pp. 2661–2666.

106. Y. Imai, S. Nishimura, E. Abe, H. Tateyama, A. Abiko, A. Yamaguchi, T. Aoyama and H. Taguchi, High-modulus poly(ethylene terephthalate)/expandable fluorine mica nanocomposites with a novel reactive compatibilizer. *Chem Mater* **14** (2002), pp. 477–479.

107. X. Huang, S. Lewis, W.J. Brittain and R.A. Vaia, Synthesis of polycarbonate-layered silicate nanocomposites via cyclic oligomers. *Macromolecules* **33** (2000), pp. 2000–2004.

108. M. Mitsunaga, Y. Ito, S. Sinha Ray, M. Okamoto and K. Hironaka, Polycarbonate/clay nanocomposites: nanostructure control and foam processing. *Macromol Mater Engng* **288** (2003), pp. 543–548.

109. C. Zilg, R. Thomann, R. Mulhaupt, and J. Finter, Polyurethane Nanocomposites Containing Laminated Anisotropic Nanoparticles Derived from Organophilic Layered Silicates. *Adv. Mater*., **11** (1999); pp. 49.

110. A. Usuki, T. Mizutani, Y. Fukushima, M. Fujimoto, K. Fukumori, Y. Kojima, N. Sato, T. Kurauchi, and O. Kamigaito, U.S. Patent **4,889,885** (1989).

111. M. S. Wang and T. J. Pinnavaia, Clay-Polymer Nanocomposites Formed from Acidic Derivatives of Montmorillonite and an Epoxy Resin. *Chem Mater*. **6** (1994); pp 468.

112. T. Lan and T. J. Pinnavaia, Clay-Reinforced Epoxy Nanocomposites. *Chem. Mater*. **6** (1994); pp 2216.

113. T. Lan, P. J. Kaviratna, and T. J. Pinnavaia, Mechanism of Clay Tactoid Exfoliation in Epoxy-Clay Nanocomposites. *Chem. Mater*., **7** (1995), pp.2214

114. P. Kelly, A. Akelah, S. Qutubuddin, and A. Moet, Synthesis and characterization of "epoxyphilic" montmorillonites. *J. Mater Sci*., **29** (1994), pp. 2274

115. G.S. Sur, H.L. Sun, S.G. Lyu and J.E. Mark, Synthesis, structure, mechanical properties, and thermal stability of some polysulfone/organoclay nanocomposites. *Polymer* **42** (2001), p. 9783.

116. M. Zanetti, S. Lomakin, G. Camino, Polymer layered silicate nanocomposites. *Macromol. Mater. Eng.* **279** (2000), p. 1-9

117. S. Bridley, G. Brown, "Crystal Structure of Clay Minerals and Their X-ray Diffraction", Mineralogical Society, London 1980

118. T. Pinnavaia, Intercalated clay catalysts. *Science* **220**, 365 (1983)

119. B. Yalcin and M. Cakmak, *Polymer* (2004), p. 1-16

120. T. Pinnavaia and G. Beall, "Polymer-Clay Nanocomposites", John Wiley & Sons, Ltd., New York 2000.

121. E.P. Giannelis, Polymer Layered Silicate Nanocomposites. *Adv Mater* **8** (1996); pp. 29.

122. T.D. Fornes, P.J. Yoon, H. Keskkula, D.R. Paul, Nylon 6 nanocomposites: the effect of matrix molecular weight. *Polymer* **42** (2001); pp.9929.

123. A. Blumstein, Polymerization of adsorbed monolayers: II. Thermal degradation of the inserted polymers. *J Polym Sci A* **3** (1965), pp. 2665–2673.

124. B.K.G. Theng. *Formation and properties of clay–polymer complexes*, Elsevier, Amsterdam (1979).

125. R.A. Vaia, Krishnamoorti and E.P. Giannelis, Structure and dynamics of polymer-layered silicate nanocomposites. *Chem Mater* **8** (1996), pp. 1728–1734.

126. A.B. Morgan and J.W. Gilman, Characterization of poly-layered silicate (clay) nanocomposites by transmission electron microscopy and X-ray diffraction: a comparative study. *J Appl Polym Sci* **87** (2003), pp. 1329–1338

127. L.J. Mathias, R.D. Davis and W.L. Jarrett, Observation of α- and γ-crystal forms and amorphous regions of nylon 6-clay nanocomposites using solid-state ^{15}N nuclear magnetic resonance. *Macromolecules* **32** (1999), pp. 7958–7960.

128. R. Roe, Methods of X-ray and neutron scattering in polymer science, Oxford University Press, New York (2000), p. 199.

129. A. Bafna, G. Beaucage, F. Mirabella, G. Skillas and S. Sukumaran, Optical properties and orientation in polyethylene blown films. *J Polym Sci, Part B: Polym Phys* **39** (2001), pp. 2923–2936.

130. A. Bafna, G. Beaucage, F. Mirabella and S. Mehata. Shear induced orientation and associated property enhancement in polymer/clay nanocompositesProceedings Nanocomposites, Sept. *23–25, 2002*, ECM Publication, San Diego, CA, USA (2002).

131. L. Alexander. X-ray diffraction methods in polymer science, R.E. Krieger Publications, Florida (1985) p. 245.

132. D.L. VanderHart, A. Asano and J.W. Gilman, NMR measurements related to clay dispersion quality and organic-modifier stability in nylon 6/clay nanocomposites. *Macromolecules* **34** (2001), pp. 3819–3822.

133. Y. Bensimon, B. Deroide and J.V. Zanchetta, Comparison between the electron paramagnetic resonance spectra obtained in X- and W-bands on a fired clay: a preliminary study. *J Phys Chem Solid* **60** (1999), pp. 813–818.

134. D.K. Yang and D.B. Zax, Li^+ dynamics in a polymer nanocomposite: an analysis of dynamic line shapes in nuclear magnetic resonance. *J Chem Phys* **110** (1991), pp. 5325–5336.

135. W.E. Blumberg, Nuclear spin–lattice relaxation caused by paramagnetic impurities. *Phys Rev* **119** (1960), pp. 79–84.

136. A. Abragam, Editor, *The principles of nuclear magnetism*, Oxford University Press, New York (1961) [chapter V].

137. D.L. VanderHart, A. Asano and J.W. Gilman, Solid-state NMR investigation of paramagnetic nylon 6 clay nanocomposites. 2. Measurement of clay dispersion, crystal stratification, and stability of organic modifiers. *Chem Mater* **13** (2001), pp. 3796–3809.

138. S.K. Sahoo, D.W. Kim, J. Kumar, A. Blumstein and A.L. Cholli, Nanocomposites from in-situ polymerization substituted polyacetylene within lamellar surface of the montmorillonite: a solid-state NMR study. *Macromolecules* **36** (2003), pp. 2777–2784.

139. S.S. Hou, T.J. Bonagamba, F.L. Beyer, P.H. Madison and K. Schmidt-Rohr, Clay intercalation of poly(styrene-ethylene oxide) block copolymers studied by two-dimensional solid-state NMR. *Mocromolecules* **36** (2003), pp. 2769–2776.

140. C.I. Park, O.O. Park, J.G. Lim and H.J. Kim, The fabrication of syndiotactic polystyrene/organophilic clay nanocomposites and their properties. *Polymer* **42** (2001), pp. 7465–7475.

141. H.D. Wu, C.R. Tseng and F.C. Chang, Chain conformation and crystallization behavior of the syndiotactic polystyrene nanocomposites studied using Fourier transform infrared analysis. *Macromolecules* **34** (2001), pp. 2992–2999.

142. L.S. Loo and K.K. Gleason, Fourier transforms infrared investigation of the deformation behavior of montmorillonite in nylon 6/nanoclay nanocomposite. *Macromolecules* **36** (2003), pp. 2587–2590

143. G.M. Nascimento, V.R.L. Constantino and M.L.A. Temperini, Spectroscopic characterization of a new type of conducting polymer–clay nanocomposite. *Macromolecules* **35** (2002), pp. 7535–7537.

144. G. Jimenez, N. Ogata, H. Kawai, T. Ogihara, Structure and thermal/mechanical properties of poly(*l*-lactide)-clay blend. *J Polym Sci*: Part B: polym Phys 1997; **35**:389-96.

145. N. Ogata, S. Kawakage, T. Ogihara, Poly(vinyl alcohol)-clay and poly(ethylene oxide)-clay blends prepared using water as solvent. *J Appl Polym Sci* 1997; **66**:573-81.

146. N. Ogata, G. Jimenez, H. Kawai, T. Ogihara, Structure and thermal/mechanical properties of poly(*l*-lactide)-clay blend. J Polym Sci: Part B: polym Phys 1997;35:389-96.

147. R.A. Vaia, E.P. Giannelis, Polymer Melt Intercalation in Organically-Modified Layered Silicates: Model Predictions and Experiment. Macromol. **30** (1997); pp. 8000-09.

148. R.A. Vaia, E.P. Giannelis, Liquid crystal polymer nanocomposites: direct intercalation of thermotropic liquid crystalline polymers into layered silicates. *Polymer* **42** (2001); pp. 1281-85.

149. R.A. Vaia, H. Ishii, E.P. Giannelis, Synthesis and properties of two-dimensional nanostructures by direct intercalation of polymer melts in layered silicates. *Chem. Mater*. **5** (1993); pp. 1694-96.

150. P.H. Nam, P. Maiti, M. Okamoto, T. Kotaka, N. Hasegawa, A. Usuki, A hierarchical structure and properties of intercalated polypropylene/clay nanocomposites. *Polymer* **42** (2001); pp. 9633-40

151. A. Usuki, M. Kawasumi, Y. Kojima, A. Okada, T. Kurauchi and O. Kamigaito, Swelling behavior of montmorillonite cation exchanged for ω-amine acid by ε-caprolactam. *J Mater Res* **8** (1993), pp. 1174–1178.

152. A. Usuki, Y. Kojima, M. Kawasumi, A. Okada, Y. Fukushima, T. Kurauchi and O. Kamigaito, Synthesis of nylon-6–clay hybrid. *J Mater Res* **8** (1993), pp. 1179–1183.

153. P.B. Messersmith and E.P. Giannelis, Polymer-layered silicate nanocomposites: in-situ intercalative polymerization of ε-caprolactone in layered silicates. *Chem Mater* **5** (1993), pp. 1064–1066.

154. Z. Wang and T.J. Pinnavaia, Nanolayer reinforcement of elastomeric polyurethane. *Chem Mater* **10** (1998), pp. 3769–3771.

155. A. Akelah, Polystyrene/clay nanocomposites. In: P.N. Prasad, J.E. Mark and F.J. Ting, Editors, *Polymers and other advanced materials. Emerging technologies and business opportunities*, Plenum Press, New York (1995), pp. 625–630.

156. A. Akelah and M. Moet, Polymer–clay nanocomposites: free-radical grafting of polystyrene on to organophilic montmorillonite interlayers. *J Mater Sci* **31** (1996), pp. 3589–3596.

157. J.G. Doh and I. Cho, Synthesis and properties of polystyrene–organoammonium montmorillonite hybrid. *Polym Bull* **41** (1998), pp. 511–518.

158. M.W. Weimer, H. Chen, E.P. Giannelis and D.Y. Sogah, Direct synthesis of dispersed nanocomposites by in situ living free radical polymerization using a silicate-anchored initiator. *J Am Chem Soc* **121** (1999), pp. 1615–1616.

159. J.A. Rausell-Colom and J.M. Serratosa, Reactions of clays with organic substances. In: A.C.D. Newman, Editor, *Chemistry of clays and clay minerals* (1987), p. 371.

160. J. Wu and M.M. Lerner, Structural, thermal, and electrical characterization of layered nanocomposites derived from sodium-montmorillonite and polyethers. *Chem Mater* **5** (1993), pp. 835–838.

161. H.J. Choi, S.G. Kim, Y.H. Hyun and M.S. Jhon, Preparation and rheological characteristics of solvent-cast poly(ethylene oxide)/montmorillonite nanocomposites. *Macromol Rapid Commun* **22** (2001), pp. 320–325.

162. Y.H. Hyun, S.T. Lim, H.J. Choi and M.S. Jhon, Rheology of poly(ethylene oxide)/organoclay nanocomposites. *Macromolecules* **34** (2001), pp. 8084–8093.

163. S.K. Lim, J.W. Kim, I. Chin, Y.K. Kwon and H.J. Choi, Preparation and interaction characteristics of organically modified montmorillonite nanocomposite with miscible polymer blend of poly(ethylene oxide) and poly(methyl methacrylate). *Chem Mater* **14** (2002), pp. 1989–1994

164. B. Liao, M. Song, H. Liang and Y. Pang, Polymer-layered silicate nanocomposites. 1. A study of poly(ethylene oxide)/Na^+-montmorillonite nanocomposites as polyelectrolytes and polyethylene-*block*-poly(ethylene glycol) copolymer/Na^+-

montmorillonite nanocomposites as fillers for reinforcement of polyethylene. *Polymer* **42** (2001), pp. 10007–10011.

165. C.-R. Tseng, J.-Y. Wu, H.-Y. Lee and F.-C. Chang, Preparation and crystallization behavior of syndiotactic polystyrene–clay nanocomposites. *Polymer* **42** (2001), pp. 10063–10070.

166. G.S. Sur, H.L. Sun, S.G. Lyu and J.E. Mark, Synthesis, structure, mechanical properties, and thermal stability of some polysulfone/organoclay nanocomposites. *Polymer* **42** (2001), pp. 9783–9789.

167. N. Ogata, G. Jimenez, H. Kawai and T. Ogihara, Structure and thermal/mechanical properties of poly(L-lactide)–clay blend. *J Polym Sci Part B: Polym Phys* **35** (1997), pp. 389–396.

168. G. Jimenez, N. Ogata, H. Kawai and T. Ogihara, Structure and thermal/mechanical properties of poly(ε-caprolactone)–clay blend. *J Appl Polym Sci* **64** (1997), pp. 2211–2220.

a) Y. Zhong and S.Q. Wang, Exfoliation and yield behavior in nanodispersions of organically modified montmorillonite clay, *J. Rheol*. **47**(2) (2003), p. 483-95.

b) Y. Zhong and S.Q. Wang, Exfoliation and yield behavior in nanodispersions of organically modified montmorillonite clay, *J. Rheol*. **47**(2) (2003), p. 483-95.

169. R.A. Vaia, H. Ishii and E.P. Giannelis, Synthesis and properties of two-dimensional nanostructures by direct intercalation of polymer melts in layered silicates. *Chem Mater* **5** (1993), pp. 1694–1696.

170. R.A. Vaia and E.P. Giannelis, Lattice of polymer melt intercalation in organically-modified layered silicates. *Macromolecules* **30** (1997), pp. 7990–7999.

171. R.A. Vaia and E.P. Giannelis, Polymer melts intercalation in organically-modified layered silicates: model predictions and experiment. *Macromolecules* **30** (1997), pp. 8000–8009.

172. R.A. Vaia, S. Vasudevan, W. Krawiec, L.G. Scanlon and E.P. Giannelis, New polymer electrolyte nanocomposites: melt intercalation of poly(ethylene oxide) in mica-type silicates. *Adv Mater* **7** (1995), pp. 154–156.

173. Z. Shen, G.P. Simon and Y.B. Cheng, Comparison of solution intercalation and melt intercalation of polymer–clay nanocomposites. *Polymer* **43** (2002), pp. 4251–4260.

174. L.M. Liu, Z.N. Qi and X.G. Zhu, Studies on nylon 6/clay nanocomposites by melt-intercalation process. *J Appl Polym Sci* **71** (1999), pp. 1133–1138.

a) T.D. Fornes, P.J. Yoon, D.L. Hunter, H. Keskkula, D.D. Paul, Effect of organoclay structure on nylon-6 nanocomposite morphology and properties. *Polymer*, **43** (2002), p. 5915-33.

175. J.W. Gilman, W.H. Awad, R.D. Davis, J. Shields, R.H. Harris, Jr, C. Davis, A.B. Morgan, T.E. Sutto, J. Callahan, P.C. Trulove and H.C. DeLong, Polymer/layered silicate nanocomposites from thermally stable trialkylimidazolium-treated montmorillonite. *Chem Mater* **14** (2002), pp. 3776–3785.

176. J. Lee, T. Takekkoshi and E.P. Giannelis, Fire retardant polyetherimide nanocomposites. *Mater Res Soc Symp Proc* **457** (1997), pp. 513–518.

177. J.C. Huang, Z.K. Zhu, X.F. Qian and Y.Y. Sun, Poly(etherimide)/montmorillonite nanocomposites prepared by melt intercalation: morphology, solvent resistance properties and thermal properties. *Polymer* **42** (2001), pp. 873–877.

178. Tomasko DL, Li H, Liu D, han X, Wingert MJ, Lee LJ, Koelling KW. A Review of CO2 Applications in the Processing of Polymers. *Ind. Eng. Chem. Res*. **42** (2003), pp. 6431-56.

179. J.S. Chiou, J.W. Barlow, D.R. Paul, Plasticization of glassy polymers by CO_2. *J. of App. Polym. Sci.* **30** (1985), pp.2633.

180. A. Garg, E. Gulari, C.W. Manke, Thermodynamics of Polymer Melts Swollen with Supercritical Gases. *Macromolecules* **27** (1994); pp. 5643-53.

181. M.H. Lee, C. Tzoganakis, C.B. Par. Effects of supercritical CO2 on the viscosity and morphology of polymer blends. *Advances in Polymer Technology* 2000; 19(4):300.

182. A.R. Berens, G.S. Huvard. Interaction of Polymers with Near-Critical Carbon Dioxide. In Supercritical Fluid Science and Technology; Johnston KP, Penninger JML eds 1989. American Chemical Society: Washington, DC, 1989; pp 208.

183. M. Garcia-Leiner, A.J. Lesser, Polymer-clay Nanocomposites Prepared in Supercritical Carbon Dioxide. ANTEC 2004, pp. 1528-32.

184. A.S. Zerda, T.C. Caskey, A.J. Lesser. Highly Concentrated, Intercalated Silicate Nanocomposites: Synthesis and Characterization. *Macromolecules* **36** (2003); pp 1603-08.

185. T.C. Caskey, A.J. Lesser. Interface studies on supercritical CO2 welded semi-crystalline polymers *Polym. Eng. Sci*. **84** (2001), pp. 134.

186. M.J. Wingert, Z. Han, C. Zeng, H. Li, Rheological Changes in CO_2 Impregnated Polystryrene Reinforced with Nanoclays. ANTEC 2003; 986-990.

187. A.J. Lesser, GL. Manuel, Polymer-Clay Nanocomposites Prepared in Supercritical Carbon Dioxide. ANTEC 2004; pp. 1528-1532.

188. M. Garcia-Leiner, A.J Lesser, 225th ACS National Meeting PMSE Proceedings, New Orleans, LA, (2003).

189. M. Garcia-Leiner, A.J Lesser. 226th ACS National Meeting PMSE Proceedings, New York, NY, (2003).

190. T. Liu, W.C Tjiu, C. He, S.S Na, T.S Chung, A processing-induced clay dispersion and its effect on the structure and properties of polyamide 6. *Polym. Int*., **53** (2004), pp. 392.

191. Dolgovskij, M.K.; Fasulo, P.D.; Lortie, F.; Macosko, C.W.; Ottaviani R.A.; Rodgers, W.R. ANTEC 2003, 2255.

192. H.R Dennis, D.L Hunter, D Chang, S. Kim, J.L White, J.W Cho, D.R Paul, Effect of melt processing conditions on the extent of exfoliation in organoclay-based nanocomposites. *Polymer* **42** (2001), pp. 9513.

193. M. Modesti, A. Lorenzetti, D. Bon, S. Besco, Effect of processing conditions on morphology and mechanical properties of compatibilized polypropylene nanocomposites. *Polymer* **46** (2005), pp. 10237.

194. S.G. Lei, S.V. Hoa, M.-T Ton-That, Effect of clay types on the processing and properties of polypropylene nanocomposites. *Composites Science and Technology* **66** (2006), pp. 1274.

195. C.H. Dan, M.H. Lee, Y.D. Kim, B.H. Min, J.H Kim, Effect of clay modifiers on the morphology and physical properties of thermoplastic polyurethane/clay nanocomposites. *Polymer* **47** (2006), pp. 6718-6730.

196. M. Garcia-Leiner, A.J Lesser, Polymer-clay nanocomposites prepared in supercritical carbon dioxide. ANTEC 2004; pp.1528-32.

197. A.S. Zerda, T.C Caskey, A.J Lesser, Highly Concentrated, Intercalated Silicate Nanocomposites: Synthesis and Characterization. *Macromolecules* **36** (2003) pp.1603.

198. Caskey TC, Lesser AJ. Polym Eng Sci 2001; 84:134.

199. M.J Wingert, Z. Han, C, Zeng, H. Li, Rheological changes in CO2 impregnated polystyrene reinforced with nanoclays. ANTEC 2003; pp. 986-990.

200. Mielewski DF, Lee EC, Manke CW, Gulari E. U.S. Patent 6,753,360 (2004).

201. C.W Manke, E. Gulari, D.F Mielewski, E.C Lee, System and method of delaminating a layered silicate material by supercritical fluid treatment. U.S. Patent 6,469,073 (2002).

202. J.C Halpin, J.L Kardos, The Halpin-Tsai equations: a review . *Polym Eng Sci* **16** (1976), pp. 344.

203. T.D Fornes, D.R Paul, Modeling properties of nylon 6/clay nanocomposites using composite theories. *Polymer* **44** (2003), pp. 4993.

3.0 Materials and Experimental Methods

3.1 Materials and Experimental Methods for objective #1

3.1.1 Materials

Polypropylene (Pro-fax 6523, MFI = 4, Density = 0.90 g/cm^3) was obtained from Basell (Elkton, MD) and was used as received. Commercial RTP (Winona, MN) PP/PP-g-MA/clay nanocomposite sample prepared using a twin-screw extruder (TSE) was received in pellet forms. The clay concentration of the RTP sample determined from the burn-off method is 10 wt%. For the same level of comparison, it was diluted down to 4 and 6.5 wt%. Surface modified montmorillonite (Cloisite 20A) was obtained from Southern Clay Products, Inc. (Gonzalez, TX) and was used as-is. Cloisite 20A is a surface modified montmorillonite obtained through a cation exchange reaction, where the sodium cation is replaced by dimethyl, dihydrogenatedtallow, quaternary ammonium cation. Preliminary experiments using conventional single-screw extrusion technique in our laboratory showed Cloisite 20A to be a preferred candidate over Cloisite Na+, 93A, and 30B in terms of better miscibility and property improvements. The same observation can also be found in other studies [1, 2]. The effect of clay types is important, but it is not a major concern of this study because we are only interested in looking at the effectiveness of the new CO_2 technique in dispersing the nanoclay.

3.1.2 Sample preparation

3.1.2.1 Extrusion experiments

Polypropylene-clay nanocomposites were prepared by direct-melt compounding and by using a modified pressurized chamber. Samples were extruded at a melt temperature of around 190 ^oC and a screw speed of 15 rpm using a single, two-stage

screw Killion KL-100 extruder with a 25.4 mm (1 inch) diameter 30:1 L/D. A capillary die of 1/16 inch diameter and 20:1 L/D was attached at the end of the extruder. The chamber is inserted between the CO_2 pump and the injection port at the beginning of the second stage of the screw. The overall system is shown schematically in Figure 3.1. When using the pressurized chamber, the clays were allowed to be in direct contact with sc-CO_2 at 3000 psi and 80^{o}C for a period of time (12-24hrs) and then the pressure was rapidly released. The mixture of the nano-particles and sc-CO_2 was then injected into the molten polymer stream in a single-screw extruder. This is referred to as Mehod #3.

In addition to the method just described, two other methods were used to prepare the nanocomposites:

METH #1 **(direct melt blending):** Conventional single-screw melt compounding. The clay and PP were dry blended in a Kitchen Aid type mixer, and then the mixture was fed to an extruder and re-pelletized.

METH #2**:** Conventional single-screw melt compounding with in-line sc-CO_2 supply at the second stage of the screw. The clay and PP were dry mixed and fed to the extruder, as in method 1, but sc-CO_2 was added to the barrel during extrusion.

METH #3**:** Described in detail above.

3.1.2.2 Injection Molding

The nanocomposite pellets were dried at 100°C in an oven overnight and then injection molded using an Arburg Allrounder Model 221-55-250 injection molder. The Arburg Allrounder has a 22 mm diameter barrel, L/D = 24, screw with variable root diameter from approximately 14.25 mm at the feed to 19.3 mm at the exit, a check ring non-return valve, and an insulated nozzle that is 2 mm in diameter. The composites were

injection molded, using a melt temperature of 200°C, a mold temperature of 80°C, a holding pressure of 5 bars, and a screw speed of 200 rpm, and a rectangular end-gated mold with dimensions of 80 mm by 76 mm by 1.5 mm.

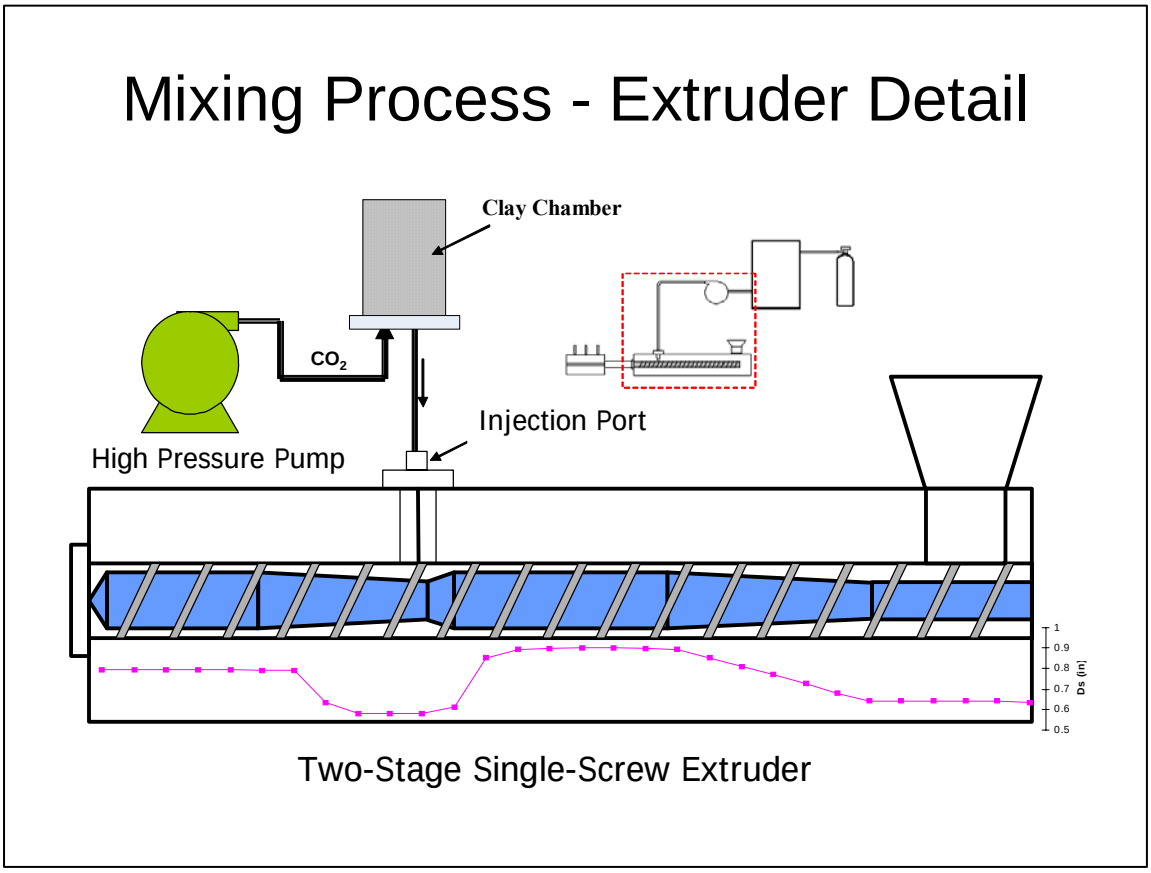

Figure 3.1: Schematic diagram of the overall process showing the CO2 chamber and the two-stage single screw extruder

3.1.3 Characterization

3.1.3.1 Dynamic Mechanical Thermal Analysis (DMTA)

DMTA tests were done on injection molded plaques. Rectangular bars of dimensions 60mm x 8.5mm x 1.5 mm were cut from the plaques parallel to the flow direction. These bars were analyzed in the torsional mode of a Rheometrics Mechanical Spectrometer (RMS-800) at a strain of 0.2%, angular frequency of 1.0 rad/s, and heating rate of 5^{o}C/min. The dynamic temperature ramp was performed from 60 ^{o}C to 180 ^{o}C.

3.1.3.2 Rheological Properties

Rheological studies of the nanocomposites were performed using a Rheometrics Mechanical Spectrometer Model 800 (RMS-800). Samples were prepared by compression molding of the extruded pellets 25 mm diameter disks. Dynamic frequency sweep experiments were performed under a continuous nitrogen atmosphere using 25-mm parallel-plate fixture at 200^{o}C in the linear viscoelastic region of the materials. To determine the limits of linear viscoelastic properties of the materials, dynamic strain sweeps were performed at 200^{o}C and a frequency of 10 rad/s for a filled system with 6.7 wt% of 20A. From this result, it can be safe to perform dynamic frequency sweep experiments at a fixed strain of 5%, which is well within the linear viscoelastic range of the materials investigated. The elastic moduli (G'), loss moduli (G"), and complex viscosities (η^*) of the materials as functions of angular frequency (ω) (ranging from 0.1 to 100 rad/s) are obtained.

3.1.3.3 Tensile Properties

The injection molded plaques were cut into rectangular bars, typically along the machine direction, having dimensions of approximately 8.5 mm wide, 1.5 mm thick, and

80 mm in length. Tensile tests on these bars were performed at room temperature using an Instron model 4204 testing machine. An extensiometer was used to accurately determine the elongation of the sample and, hence, Young's modulus and yield strength. The load was measured with a 5 kN load cell while the cross-head speed was kept at 1.27 mm/min during all tensile tests. For all tests, the average and the standard deviation were calculated from at least four samples, and data points greater than 2 standard deviations from the mean were omitted.

3.1.3.4 Structure and Morphological characterization

The structure of the nanoclay and the morphology of the nanocomposites were analyzed by wide angle X-ray diffraction (WAXD) and transmission electron microscopy (TEM). WAXD patterns were conducted using a Scintag XDS 2000 diffractometer with CuKalpha radiation (wavelength = 1.542Å) at a step size of 0.02^{o} and a scan rate of 0.5 deg/min from 1.5^{o} to 10^{o}.

TEM micrographs were generated using a Philips EM420T with an accelerating voltage of 100kV. The TEM samples, around 95 nm thick, were cut using a cryo-microtom equipped with a diamond knife at -100 ^{o}C.

3.1.3.5 Clay concentration

Clay concentrations were determined by the burn-off technique in an ashing oven at 500^{o}C for 30 minutes. The reported concentrations are an average of three burn-off samples. The clay concentrations reported here include the organic modifiers.

3.2 Materials and Experimental Methods for objective #2

3.2.1 Materials

Polypropylene (Pro-fax 6523, MFI = 4 g/10 min at 230^{o}C and 2.16 kg load, Density = 0.90 g/cm^{3}) was obtained from Basell (Elkton, MD) and was used as received. Polypropylene-graft-maleic anhydride (PP-g-MA) (PB3150, MFI = 52.2 g/10 min at 230^{o}C and 2.16 kg load, MA content = 0.5 wt%) was supplied from Chemtura Corporation (Middlebury, CT). Surface modified montmorillonite (Cloisite 20A) was obtained from Southern Clay Products, Inc. (Gonzalez, TX) and was used as-is. Cloisite 20A is a surface modified montmorillonite obtained through a cation exchange reaction, where the sodium cation is replaced by dimethyl, dihydrogenatedtallow, quaternary ammonium cation.

3.2.2 Sample preparation

3.2.2.1 Extrusion experiments

Compatibilized polypropylene-clay nanocomposites were prepared by direct-melt compounding and by using a modified pressurized CO_2 chamber. Samples were extruded at a melt temperature of around 190 ^{o}C and a screw speed of 15 rpm using a Killion KL-100 extruder with a single, two-stage screw, 25.4 mm (1 inch) diameter and 30:1 L/D. A capillary die of 1/16 inch diameter and 20:1 L/D was attached at the end of the extruder. The chamber was inserted between the CO_2 pump and the injection port at the beginning of the second stage of the screw. A schematic diagram of the overall process is shown in Figure 3.1.

The two processing methods explored in this study are described below. For each blending technique, an approximate 3 to 1 ratio of MA compatibilizer to clay was employed.

***METH #1* + *MA* (direct melt blending):** Conventional single-screw melt compounding. The clay, PP, and PP-g-MA were dry blended in a Kitchen Aid type mixer, and then the mixture was fed to an extruder and re-pelletized.

***METH #3* + *MA*: (CO_2 chamber):** The clays were allowed to be in direct contact with sc-CO_2 at 3000 psi and 80^{o}C for a period of time (12-24hrs) and then the pressure was rapidly released. The mixture of the nano-particles and sc-CO_2 was then injected into the molten polymer stream in a single-screw extruder.

3.2.2.2 Injection Molding

The nanocomposite pellets were dried at 100°C in an oven overnight and then injection molded using an Arburg Allrounder Model 221-55-250 injection molder. The Arburg Allrounder has a 22 mm diameter barrel, L/D = 24, screw with variable root diameter from approximately 14.25 mm at the feed to 19.3 mm at the exit, a check ring non-return valve, and an insulated nozzle that is 2 mm in diameter. The composites were injection molded, using a melt temperature of 200°C, a mold temperature of 80°C, a holding pressure of 5 bars, and a screw speed of 200 rpm, and a rectangular end-gated mold with dimensions of 80 mm by 76 mm by 1.5 mm.

3.2.3 Characterization

Same characterization methods described above will be carried out for this objective.

3.3 References:

1. Lopez-Quintanilla ML, Sanchez-Valdes S, Ramos de Valle LF, Medellin-Rodriguez FJ. Effect of some compatibilizing agents on clay dispersion of polypropylene-clay nanocomposites. J Appl Polym Sci; 100: 4748-4756 (2006).

2. Zhu L, Xanthos M., Effects of process conditions and mixing protocols on structure of extruded polypropylene nanocomposites. J Appl Polym Sci, 93, 1891-1899 (2004).

4.0 Process for Improving the Exfoliation and Dispersion of Nanoclay Particles into Polymer Matrices Using Supercritical Carbon Dioxide

Quang T. Nguyen and Donald G. Baird*

Department of Chemical Engineering
Virginia Polytechnic Institute and State University
Blacksburg, VA 24061-0211
*Email: dbaird@vt.edu

ABSTRACT

An environmentally benign process, which uses supercritical carbon dioxide (sc-CO_2) as a processing aid, is developed in this work to help exfoliate and disperse nanoclay into the polymer matrices. This new process is compared to the conventional direct melt blending techniques. Results from the mechanical properties, rheological studies, and X-ray diffraction (XRD) show a direct effect of the sc-CO_2, suggesting that the presence of sc-CO_2 in the melt blending process can enhance the degree of mixing and dispersion of the nanoclay into the polymer matrices. The greatest mechanical property response was a result of directly injecting pre-mixed sc-CO_2 and nanoclay into the polypropylene melt during extrusion. It was observed that for concentrations as high as 6.6 wt% (limited only by present process capabilities), XRD peaks were eliminated, suggesting a high degree of exfoliation. Mechanical properties such as modulus increased by as much as 54%. The terminal region of the dynamic mechanical spectrum was similar to that of the base polymer, contrary to what is frequently reported in the literature.

Keywords: Polypropylene, nanocomposites, nanoclay, supercritical carbon dioxide, extrusion, WAXD

4.1 Introduction

4.1.1 Polymer-clay nanocomposites

During the last decade, interest in polymer layered silicate nanocomposites has rapidly been increasing at an unprecedented level, both in industry and in academia, due to their potential for enhanced physical, chemical, and mechanical properties compared to conventionally filled composites [1-6]. They have the potential of being a low-cost alternative to high-performance composites for commercial applications in both the automotive and packaging industries. It is well established that when layered silicates are uniformly dispersed and exfoliated in a polymer matrix, the polymer properties can be improved to a dramatic extent. These improvements may include increased strength [7], higher modulus [8-13], thermal stability [14-16], barrier properties [17, 18], and decreased flammability [19-23]. Hence, in order to capitalize on the potential offered by nano-particles in areas such as reinforcement, barrier, and electrical conductivity, higher levels of fully dispersed nano-particles must be obtained.

Polymer-clay nanocomposites (PCNs) are two-phase materials in which the polymers are reinforced by nanoscale fillers. The most heavily used filler material is based on the smectite class of aluminum silicate clays, of which the most common representative is montmorillonite (MMT). MMT has been employed in many polymer-clay nanocomposite systems because it has a potentially high aspect ratio and high surface area that could potentially lead to materials with significantly improved properties. Additionally, it is environmentally friendly, naturally occurring, and readily available in large quantities.

Layered silicates in their pristine state are hydrophilic. Most of the engineering polymers are hydrophobic. Therefore, dispersion of native clays in most polymers is not easily achieved due to the intrinsic incompatibility of hydrophilic layered silicates and hydrophobic engineering polymers [24]. In order to successfully develop clay-based nanocomposites, it is necessary to chemically modify a natural clay so that it can be compatible with a chosen polymer matrix. Generally, this can be done through ion exchange reactions by replacing interlayer cations with quarternary alkylammonium or alkylphosphonium cations [25-27].

One polymer of significant interest to industries such as the automotive sector is polypropylene (PP), but PP is one of the most nonpolar polymers and has no polar groups in its backbone. Thus, interfacial bonding between the clay surface and PP matrix is unfavorable. Recent attempts to increase the compatibility between the nanoclays and PP matrix introduced two major methods including melt intercalation [28-33] and in-situ polymerization [34]. The latter method usually involves in a slurry phase, which requires large volumes of solvents and a need of purification. Thus this method may be impractical due to the high costs associated with the solvents, their disposal, and their impact on the environment. The method of melt intercalation does not require a solvent, but usually involves the use of a compatibilizer, such as maleic anhydride grafted PP (PP-g-MA), to facilitate the intercalation of PP in clay [28-30]. However, in spite of improved homogeneity and properties, complete exfoliation is practically never reached [31-46]. Usually a mix between intercalated and partially exfoliated structure is frequently observed. Also, in order to achieve a good level of intercalation at high clay concentration, a high ratio of PP-g-MA must be used. However, using a high level of PP-

g-MA can be expensive and may reduce the nanocomposite's elongation at break and mechanical properties.

4.1.2 Supercritical Carbon Dioxide

To overcome some of the issues with using melt intercalation and modified PP and other solvent-based techniques, recently, there has been considerable interest in using sc-CO_2 as an alternative route for the preparation of polymer-clay nanocomposites [47-52]. A recent approach to prepare polymer nanocomposites using sc-CO_2 in the melt intercalation process was reported by Lesser et al. [48]. They used a modified hopper in the feed section of the extruder to allow polymer and clay to interact with sc-CO_2 before processing. It was found that the presence of sc-CO_2 promotes significant increase in the basal spacing of the clay, and thereby may enhance the ease of the polymer intercalation into the galleries of the clay. In a different approach, Mielewski et al. [51] proposed a method to directly inject sc-CO_2 to a melt mixture of silicate particles and polymer in an extruder. The silicates are expected to exfoliate when exiting the extruder. No WAXD or TEM evidence of exfoliated morphology was presented. Alternatively, Manke et al. [52] developed a process that allows clay particles to be pre-treated with sc-CO_2 in a pressurized vessel and then rapidly depressurized into another vessel at atmospheric pressure to force the clay platelets apart. The result was exfoliated nanoclay particles as observed by X-Ray diffraction. However, they did not provide any mechanism for assuring that the exfoliated particles remain exfoliated when they are combined with the polymer via conventional melt blending.

In this study, we develop a process to help exfoliate and disperse the nanoclay into PP matrix with the aid of supercritical CO_2. The process involves the use of a

pressurized CO_2 chamber to assist in the exfoliation and delivery of the clay into a stream of polymer melt in the extruder. This process is different from the systems previously mentioned above in ways that it allows only the clay to be in direct contact with sc-CO_2, as opposed to both clay and polymer as described in Lesser's and Mielewski's processes, and that the mixture of exfoliated clay and sc-CO_2 is fed into the extruder in a one-step process instead of a two-step like Manke's process. This CO_2 method is evaluated and compared to other processing methods including the direct melt-blending technique using a single-screw extruder, single-screw extrusion capable of a direct in-line feed of sc-CO_2 to the extruder barrel, and conventional twin screw extrusion with PP-g-MA.

4.2 Experimental

4.2.1 Materials

Polypropylene (Pro-fax 6523, MFI = 4, Density = 0.90 g/cm^3) was obtained from Basell (Elkton, MD) and was used as received. Commercial RTP (Winona, MN) PP/PP-g-MA/clay nanocomposite sample prepared using a twin-screw extruder (TSE) was received in pellet forms. The clay concentration of the RTP sample determined from the burn-off method is 10 wt%. For the same level of comparison, it was diluted down to 4 and 6.5 wt%. Surface modified montmorillonite (Cloisite 20A) was obtained from Southern Clay Products, Inc. (Gonzalez, TX) and was used as-is. Cloisite 20A is a surface modified montmorillonite obtained through a cation exchange reaction, where the sodium cation is replaced by dimethyl, dihydrogenatedtallow, quaternary ammonium cation. Preliminary experiments using conventional single-screw extrusion technique in our laboratory showed Cloisite 20A to be a preferred candidate over Cloisite Na+, 93A, and 30B in terms of better miscibility and property improvements [53]. The same

observation can also be found in other studies [54, 55]. The effect of clay types is important, but it is not a major concern of this study because we are only interested in looking at the effectiveness of the new CO_2 technique in dispersing the nanoclay.

4.2.2 Clay Concentration

Clay concentrations were determined by the burn-off technique in an ashing oven at 500^{o}C for 30 minutes. The reported concentrations are an average of three burn-off samples. The clay concentrations reported here include the intercalants or the organic modifiers.

4.2.3 Extrusion experiments

Polypropylene-clay nanocomposites were prepared by direct-melt compounding and by using a modified pressurized chamber. Samples were extruded at a melt temperature of around 190 ^{o}C and a screw speed of 15 rpm using a single, two-stage screw Killion KL-100 extruder with a 25.4 mm (1 inch) diameter 30:1 L/D. A capillary die of 1/16 inch diameter and 20:1 L/D was attached at the end of the extruder. The chamber is inserted between the CO_2 pump and the injection port at the beginning of the second stage of the screw. The overall system is shown schematically in Figure 4.1. When using the pressurized chamber, the clays were allowed to be in direct contact with sc-CO_2 at 3000 psi and 80^{o}C for a period of time (12-24hrs) and then the pressure was rapidly released. The mixture of the nano-particles and sc-CO_2 was then injected into the molten polymer stream in a single-screw extruder. This is referred to as Mehod #3.

In addition to the method just described, two other methods were used to prepare the nanocomposites:

***METH #1* (direct melt blending):** Conventional single-screw melt compounding. The clay and PP were dry blended in a Kitchen Aid type mixer, and then the mixture was fed to an extruder and re-pelletized.

***METH #2*:** Conventional single-screw melt compounding with in-line sc-CO_2 supply at the second stage of the screw. The clay and PP were dry mixed and fed to the extruder, as in method 1, but sc-CO_2 was added to the barrel during extrusion.

***METH #3*:** Described in detail above.

4.2.4 Injection Molding

The nanocomposite pellets were dried at 100°C in an oven overnight and then injection molded using an Arburg Allrounder Model 221-55-250 injection molder. The Arburg Allrounder has a 22 mm diameter barrel, L/D = 24, screw with variable root diameter from approximately 14.25 mm at the feed to 19.3 mm at the exit, a check ring non-return valve, and an insulated nozzle that is 2 mm in diameter. The composites were injection molded, using a melt temperature of 200°C, a mold temperature of 80°C, a holding pressure of 5 bars, and a screw speed of 200 rpm, and a rectangular end-gated mold with dimensions of 80 mm by 76 mm by 1.5 mm.

4.2.5 Dynamic Mechanical Thermal Analysis (DMTA)

DMTA tests were done on injection molded plaques. Rectangular bars of dimensions 60mm x 8.5mm x 1.5 mm were cut from the plaques parallel to the flow direction. These bars were analyzed in the torsional mode of a Rheometrics Mechanical Spectrometer (RMS-800) at a strain of 0.2%, angular frequency of 1.0 rad/s, and heating rate of 5^{o}C/min. The dynamic temperature ramp was performed from 60 ^{o}C to 180 ^{o}C.

4.2.6 Rheological Properties

Rheological studies of the nanocomposites were performed using a Rheometrics Mechanical Spectrometer Model 800 (RMS-800). Samples were prepared by compression molding of the extruded pellets 25 mm diameter disks. Dynamic frequency sweep experiments were performed under a continuous nitrogen atmosphere using 25-mm parallel-plate fixture at 200^{o}C in the linear viscoelastic region of the materials. To determine the limits of linear viscoelastic properties of the materials, dynamic strain sweeps were performed at 200^{o}C and a frequency of 10 rad/s for a filled system with 6.7 wt% of 20A. From this result, it can be safe to perform dynamic frequency sweep experiments at a fixed strain of 5%, which is well within the linear viscoelastic range of the materials investigated. The elastic moduli (G'), loss moduli (G"), and complex viscosities (η^*) of the materials as functions of angular frequency (ω) (ranging from 0.1 to 100 rad/s) are obtained.

4.2.7 Tensile Properties

The injection molded plaques were cut into rectangular bars, typically along the machine direction, having dimensions of approximately 8.5 mm wide, 1.5 mm thick, and 80 mm in length. Tensile tests on these bars were performed at room temperature using an Instron model 4204 testing machine. An extensiometer was used to accurately determine the elongation of the sample and, hence, Young's modulus and yield strength. The load was measured with a 5 kN load cell while the cross-head speed was kept at 1.27 mm/min during all tensile tests. For all tests, the average and the standard deviation were calculated from at least four samples, and data points greater than 2 standard deviations from the mean were omitted.

4.2.8 Structure and Morphological characterization

The structure of the nanoclay and the morphology of the nanocomposites were analyzed by wide angle X-ray diffraction (WAXD) and transmission electron microscopy (TEM). WAXD patterns were conducted using a Scintag XDS 2000 diffractometer with CuKalpha radiation (wavelength = 1.542Å) at a step size of 0.02^o and a scan rate of 0.5 deg/min from 1.5^o to 10^o.

TEM micrographs were generated using a Philips EM420T with an accelerating voltage of 100kV. The TEM samples, around 95 nm thick, were cut using a cryo-microtom equipped with a diamond knife at -100 ^oC.

4.3 Results and Discussion

4.3.1 X-Ray Diffraction

WAXD patterns for pristine organoclay 20A, commercial RTP PP/PP-g-MA/clay nanocomposite, and PP/clay nanocomposites prepared via methods 1, 2, and 3 are illustrated in Figure 4.3 and 4.4, where Figure 4.3 corresponds to WAXD patterns of extruded samples before injection molding and Figure 4.4 represents WAXD patterns of injection molded samples. As shown in Figure 4.3, the RTP extruded sample prepared via twin-screw extrusion with the incorporation of a compatibilizer shows a diffraction peak, which means that the nanocomposite is not fully exfoliated. This is a typical observation that is often seen in literature when dealing with PP-clay nanocomposites [56-66]. Similarly, the extruded sample prepared via method #2 also shows a diffraction peak, which suggests intercalated morphology. From the diffraction pattern, we can see that the peak is shifted to a lower angle compared to the pristine organoclay, which indicates some expansion of the clay gallery when exiting the extruder. This expansion could be due to both the CO_2 and the diffusion of polymer chains into the clay galleries.

Comparing the diffraction patterns of the extruded samples prepared via method #1 and #2, we see that the peak of sample prepared using method #2 is shifted not much lower than that of sample prepared using method #1, which leads us to believe that the expansion at the die due to CO_2 is not significant. On the other hand, WAXD patterns of extruded samples prepared via method #3 for 4 wt% and 6.6 wt% of 20A show no peaks, which may indicate fully exfoliated nanostructures. From this observation, we can conclude that the exfoliation of the layered silicate resulted from method #3 did not cause by the foaming of the CO_2 when exiting the extruder. Due to the limitation of the current technique, i.e. chamber design, we were not able to get exfoliated structure for clay concentration at 9.5 wt%. WAXD pattern for the nanocomposite at this concentration clearly indicates no expansion of the d-spacing. Therefore, no further analyses were done on concentrations higher than 6.6 wt%.

As the extruded product is melt processed further into other desired forms depending on the type of applications, the effect of additional processing on exfoliation must be examined. The nanocomposite structures upon subsequent melt processing, in this case injection molding, were examined by means of WAXD patterns which for various nanocomposites are shown in Figure 4.4. The resulting d-spacings determined from WAXD patterns are calculated from Bragg's Law and are summarized in Table 4.1. We can see that commercial RTP sample and samples prepared via method 1 and method 2 all show peaks, but shifted to lower angles relative to pristine 20A, indicating expansion of the d-spacing due to intercalation of polymer between the galleries of the clay. The RTP sample shows a slight shift of the peak towards a lower angle, i.e. bigger d-spacing, compared to samples prepared via method 1 and 2 due to the use of a

compatibilizer and high shear processing. As observed in Figure 4.3, WAXD patterns for the nanocomposite samples prepared using method 3 before the injection molding process show no peaks, but the peaks reappear after the injection molding process (Figure 4.4), suggesting partial collapse and re-aggregation of the clay platelets during this process. This phenomenon was also observed by Alexandre et al. [67], who studied the thermodynamic stability of melt processed PE nanocomposites. The collapse observed here could suggest that the exfoliated nanocomposite structure is thermodynamically unfavorable for a highly non-polar polymer, such as PP, which has little to no attractive interactions with the clay itself. Looking at the WAXD pattern illustrated in Figure 4.4 for the 4wt% nanocomposite prepared via method 3, we see that the peak, however, is shifted to a lower angle, even lower than the ones shown by the RTP sample and samples prepared via methods 1 and 2, which indicates that the most expansion of the clay galleries still occurs in samples prepared by method #3. The WAXD patterns suggest that the method of using the pressurized CO_2 chamber is more effective in swelling and expanding, if not exfoliating, the clays and helps facilitate the intercalation of polymer into the clay galleries.

Although WAXD can offer a convenient method to determine the nanocomposite structure, not much can be concluded about the spatial distribution of the silicate layers. The nanocomposite structure, namely intercalated or exfoliated, may be identified by monitoring the position, shape, and intensity of the basal reflections from the distributed silicate layers. In fact, this has been studied by Kojima et al. [68] who used the peak intensity together with the peak position to characterize the relative proportion of exfoliated and intercalated species with the nanofiller content. However, peak broadening

and intensity decreases are very difficult to study systematically, and thus, conclusions based solely on WAXD patterns are only tentative when concerning the mechanism of nanocomposite formation and their structure. To supplement the deficiencies of WAXD, TEM can be used. TEM allows a qualitative understanding of the internal structure, spatial distribution of the various phases, and views of the defect structure through direct visualization. TEM also has limitations. TEM is time consuming, and only gives qualitative information on a very small area, which may not entirely represent the microstructure of the nanocomposite as a whole. Regardless of their limitations, together, TEM and WAXD are essential tools for evaluating nanocomposite structure [69].

4.3.2 Transmission Electron Microscopy

To further confirm the degree of dispersion of the clay in the matrix, TEM analysis was carried out. TEM micrographs of various nanocomposites prepared using different processing techniques are presented in Figures 4.5-4.9. Two different magnifications at 17,000x and 34,000x are shown for each micrograph. As can be seen from Figure 4.5, the 4 wt% nanocomposite prepared via method #1 is composed mostly of intercalated structure with very large aggregates or tactoids in the order of several tens of silicate layers. Similarly, the extruded sample of the 4 wt% nanocomposite prepared using method #2 also contains many large tactoids (Figure 4.6), which again proves that the foaming due to CO_2 at the die exit does not cause exfoliation of the clay platelets. TEM for the 4 wt% RTP sample is shown in Figure 4.7. We can see better dispersion in the RTP nanocomposite compared to the other two methods due to the use of a twin-screw extrusion and a MAH compatibilizer. The best exfoliation can be seen in the nanocomposites prepared using method #3 for concentration as high as 6.6 wt% clay

(Figures 4.8 and 4.9). Although, there are still some areas that show little aggregates, most show fairly well dispersed clay platelets even at high magnification. This observation is similar for the extruded sample and the injection molded sample. However, more little aggregates, but not as much as those observed in the other processing methods, were observed for the injection molded sample. This TEM observation confirms with the WAXD patterns discussed in previous section.

4.3.3 Tensile Properties

The tensile properties of various nanocomposites prepared via different processing techniques are summarized in Table 4.2 and Figure 4.10. Pure polypropylene used in this study has a Young's modulus of 1.374 ± 0.133 GPa. With the addition of approximately 4 wt% Cloisite 20A, prepared via method 1, the nanocomposite was found to have a Young's modulus of 1.611 ± 0.059 GPa, an increase of about 17% compared to that of pure PP. Using the same technique, at concentration of 6.7 wt%, 10 wt%, and 14 wt% of 20A, the nanocomposites were found to have Young's moduli of 1.753 ± 0.045 GPa, 1.725 ± 0.130 GPa, and 1.787 ± 0.037 GPa, respectively. In order words, the modulus shows little increase beyond the addition of 4.0 wt% (when direct blended) which is a frequent observation [70-72]. It is important to note that using the direct melt blending technique via single-screw extrusion, i.e. method 1, the properties leveled out at a clay level of 6.7 wt%. At clay concentration higher than 6.7 wt%, there was not much improvement in Young's modulus. This could be due to formation of big agglomerates in the nanocomposite as shown by TEM. Aggregation of clay particles has been shown to reduce the amount of reinforcement that can be provided by the clays resulting in less enhancement of the Young's modulus [73]. For the nanocomposites prepared via method

2, moderate improvement in Young's moduli was observed when compared to those processed using method 1. This indicates a positive effect of the addition of sc-CO_2 during melt processing. For the RTP sample prepared via TSE with a compatibilizer, the highest Young's modulus was found to be around 1.861 ± 0.068 GPa at 6.5 wt% of clay, an increase of about 35% compared to pure PP. Similar to the properties observed for samples prepared using methods 1 and 2, the properties for the RTP nanocomposite also leveled off at around 6.5 wt% of clay. At the same level of clay concentration, the RTP nanocomposite possesses higher properties than those prepared via methods 1 and 2. This is due to the compatibilizer that was used in preparing the nanocomposite, which increased the bonding between the nanoparticles and the polymer matrix and helped with dispersion. Also, the RTP nanocomposite was prepared using a twin-screw extruder, which exerted high shear forces to break the clay platelets apart and helped better mix and disperse the clays into the polymer matrix. The biggest improvement was seen when the nanocomposites were prepared using the pressurized CO_2 chamber. This agrees with the TEM and WAXD data that was discussed earlier. At 4 wt% of 20A, the nanocomposite was determined to have a Young's modulus of 1.848 ± 0.107 GPa, an increase of about 34% compared to pure PP, which is also a little higher than that of the RTP sample. At 4 wt% the nanocomposites prepared via method 3 possesses slightly higher Young's modulus (1.848 GPa vs. 1.769 GPa), higher yield strength (16.10 MPa vs. 14.3 MPa), and higher elongation at break (80% vs. 40%) than those of the RTP nanocomposite prepared using TSE with a compatibilizer. This means that method 3 can potentially replace the need for high shear processing and a compatibilizer and can still perform well in terms of tensile properties. At 6.6 wt%, an even bigger improvement in

properties was observed. Young's modulus was increased to 2.118 ± 0.077 GPa, a 54% improvement compared to the base matrix. This indicates an essential contribution of the CO_2 chamber to the melt intercalation process in terms of expanding and exfoliating the nanoparticles into the polymer matrix. Also, the addition of sc-CO_2 during melt processing can enhance the mixing and the degree of intercalation/exfoliation of the clay in the polymer matrix. Although collapse and re-aggregation of the nanoparticles upon subsequent melt processing were observed, it is believed that the relative portion of the exfoliated structure remains in the nanocomposites is still higher when the nanocomposite is prepared via method 3 than method 1, 2, and TSE with PP-g-MA and hence, better improvements in tensile properties occur.

It is interesting to point out that the injection molded plagues of the nanocomposites processed using method 1 and 2 appear to be opaque, whereas the ones prepared using method 3 appear to be a little shinier and more transparent. Presumably, higher degree of exfoliation of the clay into finer particles could be the reason why the scCO_2-treated samples appear more transparent than the non-treated samples. Nevertheless, the property enhancement observed here is not optimum, as will be shown by the composite theory, which is most probably ascribed to the combined effect of poor particle alignment in the test direction and the collapse of clay particles during the injection molding process. For optimum performance, the silicate must be fully exfoliated into individual layers and the platelets must orient parallel to the applied load direction.

In order to realize the full potential of mechanical property increase, it is necessary to compare the observed property enhancements, such as modulus, to those predicted by composite theories like that of Halpin-Tsai [74, 75]. Realizing the full

potential of mechanical property enhancement remains unclear even when fully exfoliated nanocomposite morphologies are shown by XRD. Evaluation of the expected modulus increase for polymer composites presented here will be based on a composite theory developed by Halpin and Tsai.

The effectiveness of the model to predict actual experimental values of Young's modulus depend on the assumptions it is based upon. Halpin and Tsai's model shown below in Equation 4.1 assumes fully exfoliated clay platelets, unidirectional, i.e. well oriented filler particles, as well as a high degree of adhesion of the filler particles to the surrounding polymer matrix,

$$E_c = E_m \left[\frac{1 + \zeta \eta \phi_f}{1 - \eta \phi_f} \right], \tag{4.1}$$

where E_c = composite modulus, E_m = unfilled matrix modulus, ϕ_f = filler volume fraction,

$$\eta = \frac{E_f / E_m - 1}{E_f / E_m + \zeta}, \tag{4.2}$$

$$\zeta = 2(l/t), \tag{4.3}$$

E_f = filler modulus taken to be 178 GPa for MMT [75], and l/t = aspect ratio of the silicate platelets taken here to be approximately 100 for fully exfoliated platelets [75].

The theoretical and experimentally measured modulus of the composites versus wt% MMT is shown in Figure 4.10. As can be seen, the experimental Young's moduli presented are below those predicted by the Halpin-Tsai model. All values are lower than those predicted by the theory. This may be due to some important issues such as the lack of significant bonding between MMT and polypropylene because of the differences in the surface energies of hydrophilic MMT and hydrophobic PP, lack of complete orientation

of the filler particles the flow direction, and the aspect ratio may be less than the assumed value of 100.

4.3.4 Dynamic Mechanical Thermal Analysis

Dynamic Mechanical Thermal Analysis (DMTA) was performed on various nanocomposites to assess the effect of clay on the heat distortion temperature (HDT) as described by Scobbo [76]. The dynamic storage moduli of the nanocomposites versus temperature as a function of different processing methods is illustrated in Figure 4.11. All the nanocomposites exhibit similar relative moduli curves versus temperature and possess a higher storage modulus than pure PP throughout the entire temperature range tested. The nanocomposite prepared via method #3 at 6.6 wt% of clay exhibits the greatest increase in the storage modulus. The vertical lines in Figure 4.11 represent the HDT values for a stress of 0.45 MPa. The results are reported in Figure 4.12. As can be seen, the heat distortion temperature increases with the addition of clay for all the nanocomposites. As much as 20 degrees increase in the HDT at 6.6 wt% clay loading was observed for the nanocomposite prepared using method #3.

4.3.5 Rheology

In this section we look at the effect of the degree of exfoliation on the dynamic mechanical properties of melts containing various levels of nano-clay. In general it has been reported that when the nano-clays are exfoliated, a "tail" in the storage modulus, G', versus angular frequency is observed [77, 78] at low frequencies. The tail is also reflected in the low frequency behavior of the magnitude of complex viscosity ($|\eta^*|$) as yield-like behavior. However, sufficient evidence for exfoliation is usually not supplied to confirm the degree of exfoliation.

The storage moduli, G', loss moduli, G", and the complex viscosities, η*, resulting from the dynamic frequency scan measurements are compared in Figures 4.13, 4.14, and 4.15, respectively. As can be seen in Figure 4.13, big tactoids or agglomerates of clay can also exhibit the plateau or tailing effect at low frequencies as shown in Figure 4.13. Larger aggregates can occlude and confine more polymer chains between the platelet layers. Thus, the increase of G', G", and η* might arise from the confinement of the polymer chains within the silicate layers. In fact, it has been shown that the viscosities of confined polymer melts are greater than those of bulk chains [79]. The RTP nanocomposite, which was confirmed by X-ray diffraction to be non-exfoliated, also shows a tail in G' at low frequencies. Also, the RTP nanocomposite possesses much higher values of G', G", and η* than the other nanocomposites prepared using the two described in this study. The reason for the increasing of G', G", and η* could be attributed to the use of a maleic anhydride compatibilizer that increases interaction and hydrogen bonding between filler and polymer matrix, which probably leads to a lower polymeric chain mobility, making the material more rigid and solid-like. The nanocomposites synthesized by methods 1 and 3 do not show solid-like behavior at low frequencies and do not indicate the presence of a network structures. In fact, the two composites show process behavior similar to the neat unfilled PP resin. The extruded sample, prepared by method 3, as shown by XRD and TEM data contains nano-clay that appears to be fairly exfoliated and dispersed, shows no tail in the G'. Here, the lack of a tail in the G' could be due to the absence of a network formed by the strong hydrogen bonding between the polar functional group of PP-g-MAH group and the oxygen group of the silicate. In addition, the confinement effect is largely reduced due to a fairly

dispersed structure of the silicate. Therefore, regardless of the fine dispersion of the clay tactoids, the increase in G', G", and η*, is less pronounced for the nanocomposites prepared using method 3.

Using rheology to determine the degree of exfoliation of the nanocomposites is still ambiguous. Therefore, conclusions regarding the morphology based on the rheological data presented here cannot be made. What can be concluded from this rheological study is the processability of the nanocomposites. The shear viscosities of the nanocomposites prepared via method 3 (Figure 4.15) are much lower than that of RTP sample prepared using TSE. Therefore, it can be concluded that PCNs prepared via method 3 should have better processability than the ones synthesized by TSE with a compatibilizer.

4.4 Conclusions

Evidence from WAXD, TEM data, and improvements of the material properties, such as Young's modulus, yield strength, and HDT, leads us to believe that the technique of using the pressurized CO_2 chamber has significant potential as a benign and efficient process for exfoliating and dispersing nanoclays in polymer melts. Having sc-CO_2 contact directly with the clays before injecting them into the polymer melt improves the dispersion of the clays in the polymer matrix. In the supercritical state, CO_2 behaves as a polar organic solvent. It is believed that CO_2 readily enters the galleries of the nano-clay (treated with alkyl quarternary ammonium salts) and swells the alkyl chains. When the pressure is partially released, CO_2 expands the galleries and, thereby, further exfoliates the clay particles. Furthermore, CO_2 is partially soluble in a number of polymers and further facilitates the mixing process. As observed, the conventional direct-melt

compounding methods, with and without the direct injection of CO_2, did not show much improvement in the mechanical properties due to their inability to adequately exfoliate the nanoparticles into the polymer matrix. The commercial RTP sample prepared using a TSE and a MAH compatibilizer showed moderate improvements over methods 1 and 2. However, most improvements were seen from the technique of using the pressurized CO_2 chamber. WAXD and TEM data showed a good degree of exfoliation for concentrations as high as 6.6 wt% and mechanical properties such as modulus increased by as much as 54%.

4.5 Acknowledgements

This work was supported by the Environmental Protection Agency (grant #: R-82955501-0) and the National Science Foundation (grant #: CTS-0507995). We express gratitude to the VPI&SU Materials Science & Engineering colleagues for their aid in conducting the XRD studies.

4.6 References

[1] Usuki A, Kojima Y, Kawasumi M, Okada A, Fukushima Y, Kurauchi T, Kamigaito O. J Mater Res 1993; 8: 1185.

[2] Kojima Y, Usuki A, Kawasumi M, Okada A, Kurauchi T, Kamigaito O. J Polym Sci Part A 1993; 31: 983.

[3] Kojima Y, Usuki A, Kawasumi M, Okada A, Kurauchi T, Kamigaito O. J Polym Sci Part A 1993; 31: 1755.

[4] Liu L, Qi Z, Zhu X. J Appl Polym Sci 1999; 71: 1133.

[5] Lan T, Kaviratna D, Pinnavaia J. Chem Mater 1994; 6: 573.

[6] Gilman W, Morgan A, Giannelis P, Wuthenow M, Manias E. Flame Retardancy 10th Annual BBC Conference Proceedings 1999; 1.

[7] Giannelis P. Appl Organomet Chem 1998; 12: 675.

[8] Okada A, Kawasumi M, Usuki A, Kojima Y, Kurauchi T, Kamigaito O. In: Schaefer W, Mark E, editors. Polymer based molecular composites MRS Symposium Proceedings. Pittsburgh; 1990; vol. 171:45–50.

[9] Giannelis P. Adv Mater 1996; 8: 29.

[10] Giannelis EP, Krishnamoorti R, Manias E. Adv Polym Sci 1999; 138: 107.

[11] LeBaron PC, Wang Z, Pinnavaia TJ. Appl Clay Sci 1999; 15: 11.

[12] Vaia RA, Price G, Ruth PN, Nguyen HT, Lichtenhan J. Appl Clay Sci 1999; 15: 67.

[13] Biswas M, Sinha S. Adv Polym Sci 2001; 155: 167.

[14] Gilman JW. Appl Clay Sci. 1999; 15: 31.

[15] Bins & Associates. Plastics Additives & Compounding 2002; 4(1): 30-33.

[16] Lan T, Kaviratna PD, Pinnavaia TJ. Chem Mater 1994; 6: 573.

[17] Sall K. European Plastics News March 14, 2002.

[18] Messersmith PB, Giannelis EPJ. Polym Sci Part A: Polym Chem 1995; 33: 1047.

[19] Gilman JW, Kashiwagi T, Lichtenhan JD. SAMPE J 1997; 33: 40.

[20] Gilman JW. Appl Clay Sci 1999; 15: 31.

[21] Dabrowski F, Bras L, Bourbigot S, Gilman JW, Kashiwagi T. Proceedings of the Eurofillers. Lyon-Villeurbanne, France 1999; 6:9.

[22] Bourbigot S, LeBras M, Dabrowski F, Gilman JW, Kashiwagi T. Fire Mater 2000; 24:201.

[23] Gilman JW, Jackson CL, Morgan AB, Harris R, Manias E, Giannelis EP, Wuthenow M, Hilton D, Phillips H. Chem Mater 2000; 12: 1866.

[24] LeBaron P, Wang Z, Pinnavaia TJ. Applied Clay Science 1999; 15: 11.

[25] Blumstein A. J Polym Sci A 1965; 3: 2665.

[26] Theng BKG. Formation and properties of clay–polymer complexes. Elsevier Amsterdam 1979.

[27] Krishnamoorti, Vaia A, Giannelis P. Chem Mater 1996; 8: 1728.

[28] Kawasami M, Hasegawa N, Kato M, Usuki A, Okada A. Macromolecules 30 1997; 6333:6338.

[29] Nam PH, Maiti P, Okamoto M, Kotaka T, Hasegawa N, Usuki A. Polymer 42 2001; 9633:9640.

[30] Kato M, Usuki A, Okada A. J Appl Polym Sci 66 1997; 1781:1785.

[31] Modesti M, Lorenzetti A, Bon D, Besco S. Polymer 2005; 46: 10237-10245.

[32] Kanny K, Moodley VK. J Eng Mater & Tech 2007; 129: 105-112.

[33] Lee JW, Kim MH, Choi WM, Park OO. J Appl Polym Sci 2006; 99: 1752-1759.

[34] Alexandre M, Dubois P. Mater Sci. Eng 2000; 28: 1.

[35] Ray SS, Okamoto M. Prog Polym Sci 2003; 28: 1539.

[36] Pinnavaia TJ, Beall GW. ‘‘Polymer-Clay Nanocomposites’’, J Wiley & Sons. New York 2000.

[37] LeBaron PC, Wang Z, Pinnavaia TJ. Appl Clay Sci 1999; 15:11.

[38] Fornes TD, Paul DR. Polymer 2003; 44: 4993.

[39] Osman MA, Rupp JEP, Suter UW. Polymer 2005; 46:1653.

[40] Wang ZM, Nakajima H, Manias E, Chung TC. Macromolecules 2003; 36:8919.

[41] Manias E. Origins of the Materials Properties Enhancements in Polymer/Clay Nanocomposites. In Golovoy A, editor. Nanocomposites 2001, Delivering New Value to Plastics. ECM Inc., Chicago; 2001.

[42] Koo CM, Kim JH, Wang KH, Chung IJ. Melt-Extensional Properties and Orientation Behaviors of Polypropylene-layered silicate nanocomposites. J Polym Sci: PartB: Polym Phys 2005; 43:158-167.

[43] Dennis HR, Hunter DL, Chang D, Kim S, White JL, Cho JW, Paul DR. Polymer 2001; 42:9513.

[44] Manias E, Touny A, Wu L, Strawhecker K, Lu B, Chung TC. Chem Mater 2001; 13:3516.

[45] Svoboda P, Zeng CC, Wang H, Lee LJ, Tomasko DL. J Appl Polym Sci 2002; 85:1562.

[46] Ellis TS, D'Angelo JS. J Appl Polym Sci 2003; 90: 1639.

[47] Garcia-Leiner M, Lesser AJ. ANTEC 2004; 1528:32.

[48] Zerda AS, Caskey TC, Lesser AJ. Macromolecules 2003; 36:1603.

[49] Caskey TC, Lesser AJ. Polym Eng Sci 2001; 84:134.

[50] Wingert MJ, Han Z, Zeng C, Li H. ANTEC 2003; 986:990.

[51] Mielewski DF, Lee EC, Manke CW, Gulari E. U.S. Patent 6,753,360 (2004).

[52] Manke CW, Gulari E, Mielewski DF, Lee EC. U.S. Patent 6,469,073 (2002).

[53] Nguyen QT, Baird DG. Process for increasing the exfoliation and dispersion of nanoclay particles into polymer matrices using supercritical carbon dioxide, PhD Dissertation, Virginia Polytechnic Institute and State University (2007).

[54] Lopez-Quintanilla ML, Sanchez-Valdes S, Ramos de Valle LF, Medellin-Rodriguez FJ. Effect of some compatibilizing agents on clay dispersion of polypropylene-clay nanocomposites. J Appl Polym Sci; 100: 4748-4756 (2006).

[55] Zhu L, Xanthos M., Effects of process conditions and mixing protocols on structure of extruded polypropylene nanocomposites. J Appl Polym Sci, 93, 1891-1899 (2004).

[56] Alexandre M, Dubois P. Mater Sci Eng 2000; 28:1.

[57] Ray SS, Okamoto M. Prog Polym Sci 2003; 28:1539.

[58] Pinnavaia TJ, Beall GW. ''Polymer-Clay Nanocomposites'', J Wiley & Sons, New York 2000.

[59] LeBaron PC, Wang Z, Pinnavaia TJ. Appl Clay Sci 1999; 15:11.

[60] T D Fornes, D R Paul, Polymer 2003, 44: 4993.

[61] Osman MA, Rupp JEP, Suter UW. Polymer 2005; 46:1653.

[62] Wang ZM, Nakajima H, Manias E, Chung TC. Macromolecules 2003; 36: 8919.

[63] Dennis HR, Hunter DL, Chang D, Kim S, White JL, Cho JW, Paul DR. Polymer 2001, 42: 9513.

[64] Manias E, Touny A, Wu L, Strawhecker K, Lu B, Chung TC. Chem Mater 2001; 13: 3516.

[65] Svoboda P, Zeng CC, Wang H, Lee LJ, Tomasko DL, J Appl Polym Sci 2002; 85: 1562.

[66] Ellis TS, D'Angelo JS. J Appl Polym Sci 2003; 90:1639.

[67] Alexandre M, Dubois P, Sun T, Garces JM, Jerome R. Polymer; 43: 2123 (2002).

[68] Kojima Y, Usuki A, Kawasumi M, Okada A, Kurauchi T, Kamigaito, O. J Polym Sci Polym Chem Ed 2001; 39:1360.

[69] Morgan AB, Gilman JW. Characterization of poly-layered silicate (clay) nanocomposites by transmission electron microscopy and X-ray diffraction: a comparative study. *J Appl Polym Sci* 2003; 83:1329–1338.

[70] Hasegawa N, Okamoto H, Kawasumi M, Kato M, Tsukigase A, Usuki A. Macromol Mater Eng 2000; 280: 76.

[71] Reichert P, Nitz H, Klinke S, Brandsch R, Thomann R, Mu¨lhaupt R. Macromol Mater Eng 2000; 275: 8.

[72] Kim KN, Kim H, Lee JW. Polym Eng Sci 2001; 41: 1963.

[73] Fornes TD, Yoon PJ, Keskkula H, Paul DR. Polymer 2001; 42**:** 9929.

[74] Halpin JC, Kardos JL. Polym Eng Sci 1976; 16: 344 (1976).

[75] Fornes TD, Paul DR. Polymer 2003; 44: 4993.

[76] Scobbo JJ Jr. Polymer Blends, Volume 2: Performance, Wiley, New York 2000; 335.

[77] Litchfield DW, Baird DG. The rheology of high aspect ratio nano-particle filled liquids. Rheology Reviews 2006; 1-60.

[78] Wagener R, Reisinger TLG. Polymer 2003; 44: 7513.

[79] Leungo G, Schmitt FJ, Hill R, Israelachvili J. Macromolecules 1997; 30: 2482.

Table 4.1: d-spacings for various nanocomposites calculated from Bragg's Law.

Sample Description	2Θ (°)	d_{001} (Å)	% Increase
20A powder	3.58	24.66	-
METH#1: 4wt%	2.86	30.87	25.17
METH#2: 4wt%	2.64	33.44	35.60
RTP: 10wt%	2.60	33.95	37.68
METH#3: 4wt%	2.50	35.31	43.19
METH#3: 6.6wt%	2.65	33.31	35.08

Table 4.2: Tensile properties of various nanocomposites prepared using different processing methods.

Materials	Young's Modulus (GPa)	S.D.	% Increase	Yield Strength (MPa)	S.D.	% Elongation	S.D.
PP - Pure	1.374	0.133	-	15.16	0.47	115.30	19.79
METH#1: 4wt%	1.611	0.059	17	13.68	0.32	32.00	28.71
METH#1: 6.7wt%	1.753	0.045	28	14.61	0.35	26.89	15.41
METH#1: 10wt%	1.726	0.130	26	12.13	0.77	16.59	2.42
METH#1: 14wt%	1.787	0.037	30	12.29	0.34	10.16	0.77
METH#2: 4wt%	1.716	0.136	25	14.28	0.39	34.59	6.92
METH#2: 6.7wt%	1.810	0.122	32	14.50	0.33	24.09	13.92
RTP_TSE: 4wt%	1.769	0.167	29	14.30	0.56	48.85	33.77
RTP_TSE: 6.5wt%	1.861	0.068	35	14.00	0.42	17.67	5.57
RTP_TSE: 10wt%	1.850	0.185	35	11.58	0.48	4.11	2.45
METH#3: 4wt%	1.848	0.107	34	16.10	0.32	80.40	0.10
METH#3: 6.6wt%	2.118	0.077	54	13.00	0.89	14.82	5.90

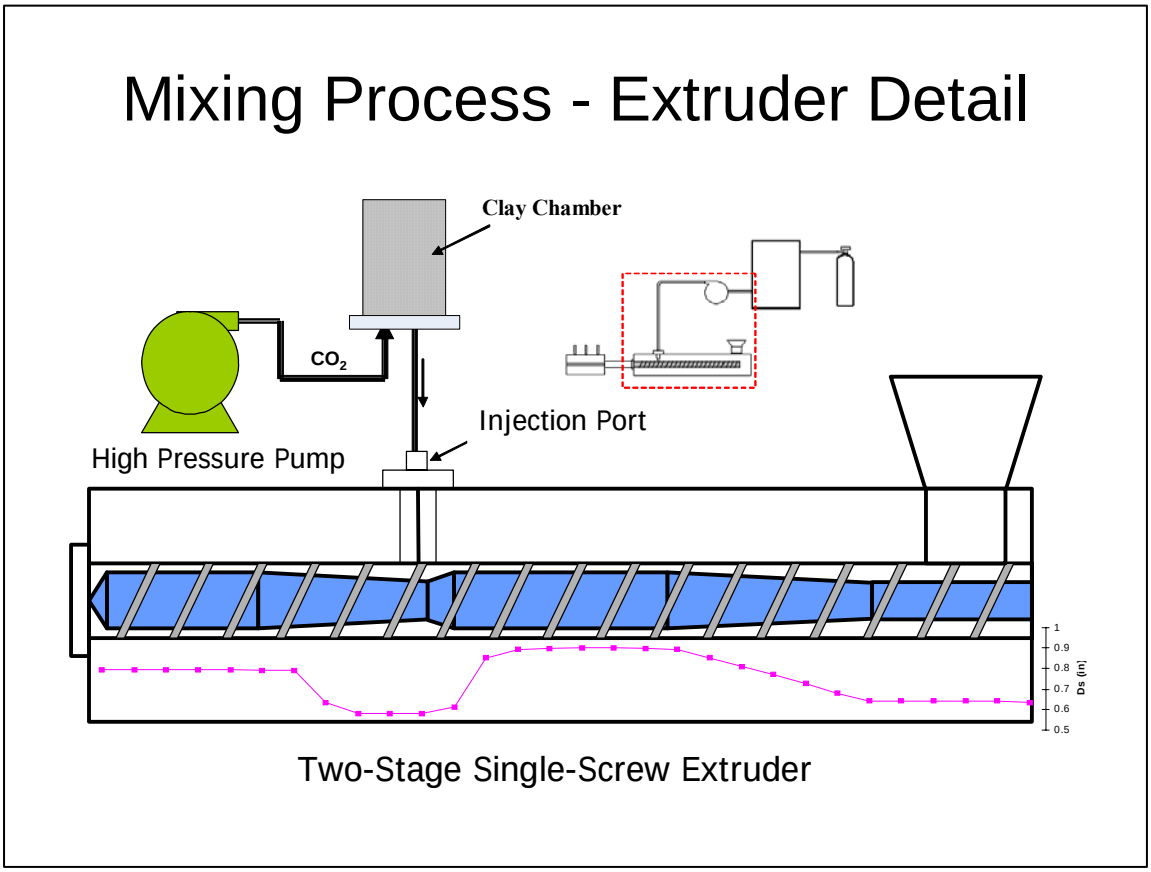

Figure 4.1: Schematic diagram of the overall process showing the CO2 chamber and the two-stage single screw extruder

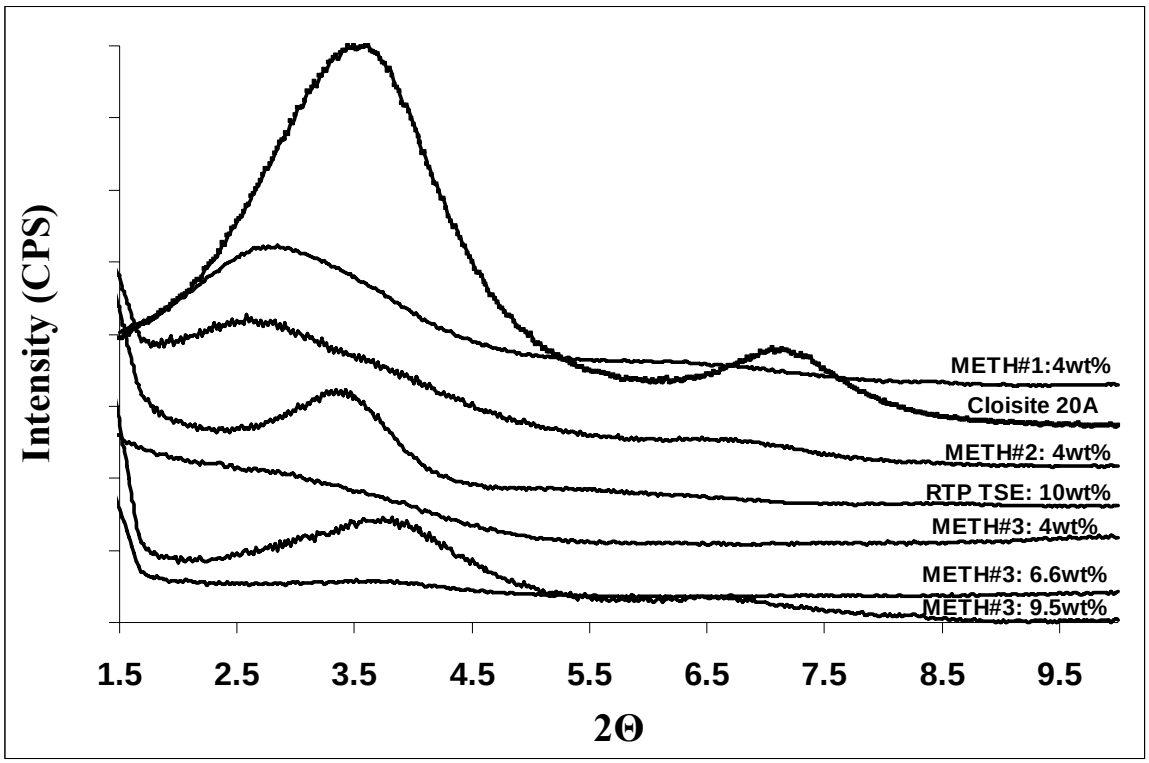

Figure 4.3: WAXD patterns of extruded pellets before the injection molding step

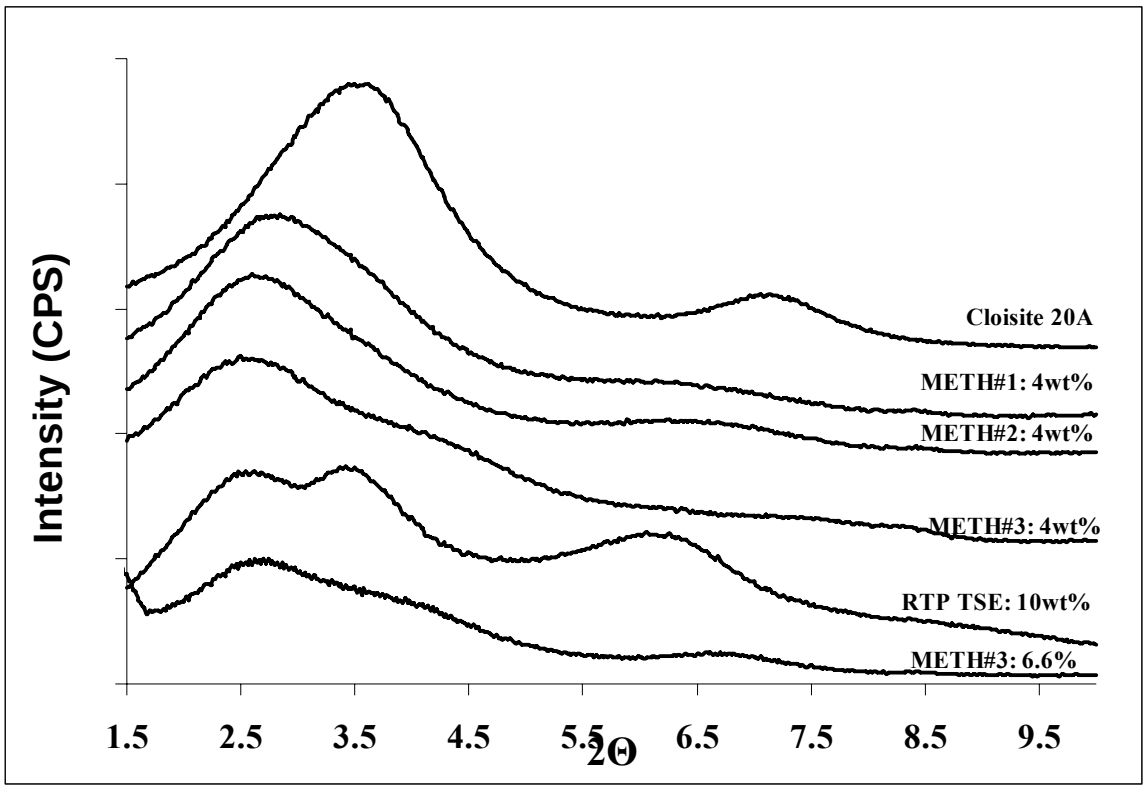

Figure 4.4: WAXD patterns of different nanocomposites prepared using different methods. Tests were done on injection molded samples.

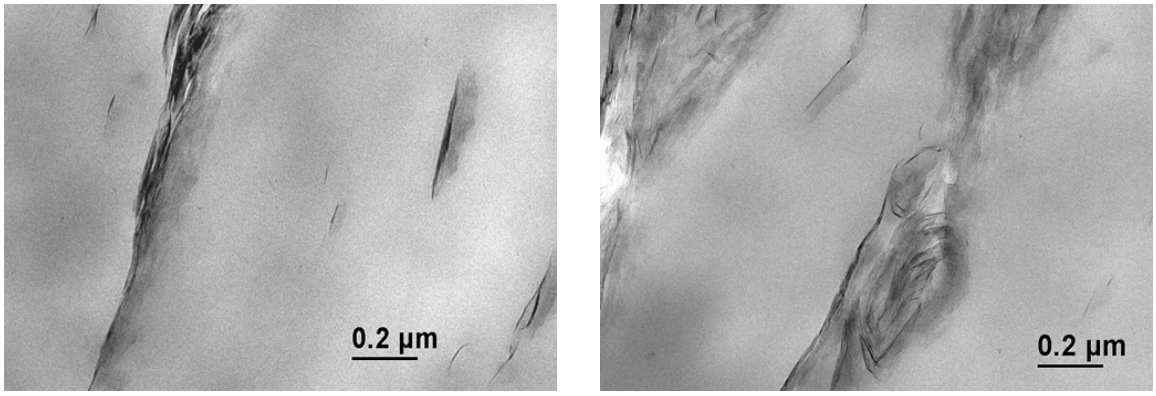

Figure 4.5: METH#1:4wt% (Left = 17,000x Right = 17,000x)

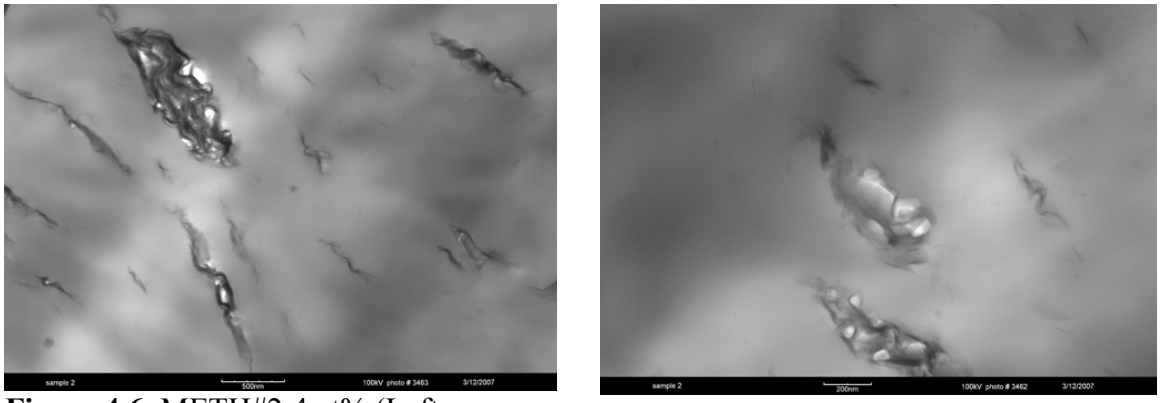

Figure 4.6: METH#2:4wt% (Left = 17,000x Right = 34,000x). Extruded pellets

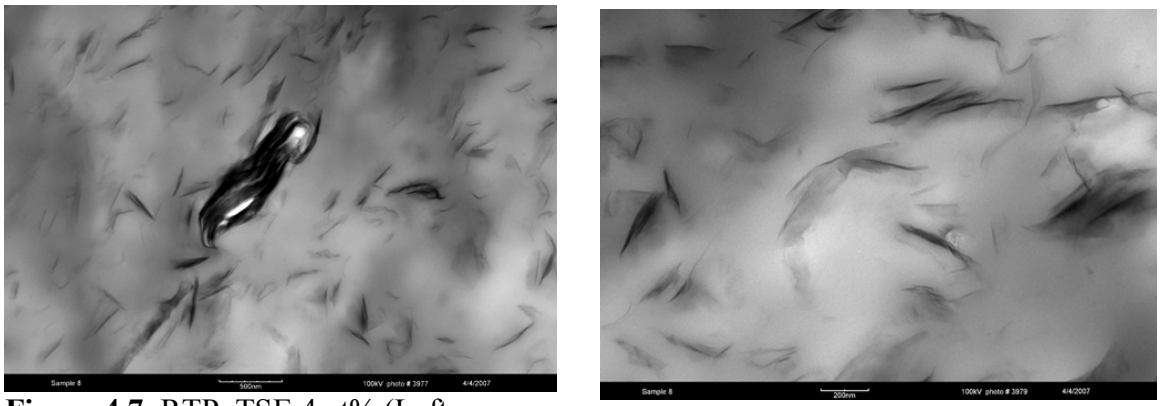

Figure 4.7: RTP_TSE:4wt% (Left = 17,000x Right = 34,000x)

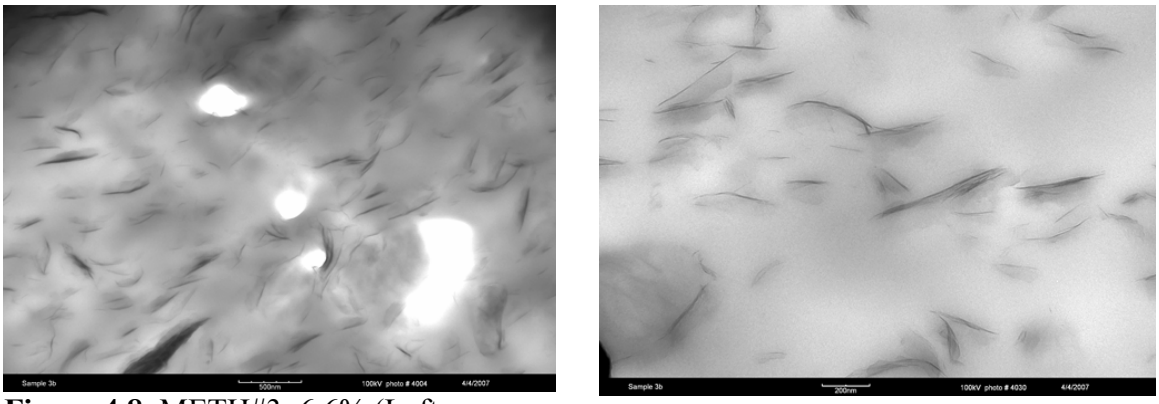

Figure 4.8: METH#3: 6.6% (Left = 17,000x Right = 34,000x). Extruded pellets

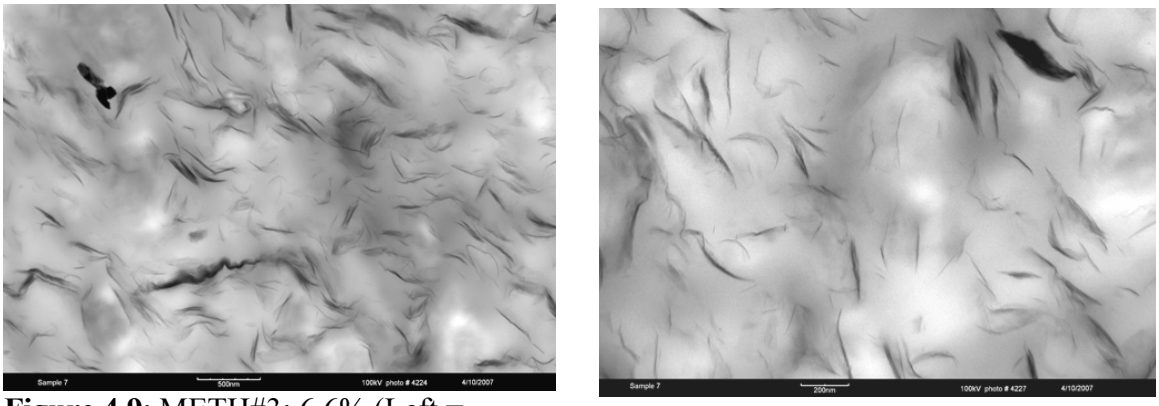

Figure 4.9: METH#3: 6.6% (Left = 17,000x Right = 34,000x). Injection molded sample

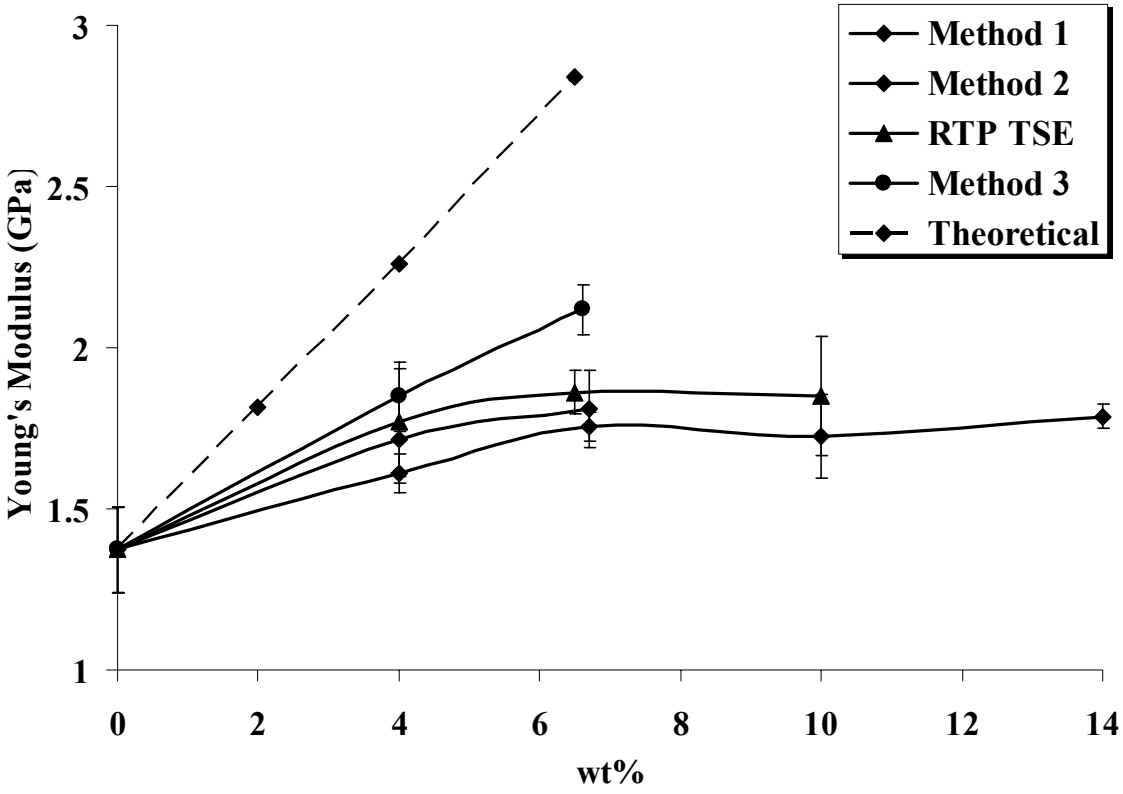

Figure 4.10: Young's modulus of different nanocomposites versus clay weight percent as a function of different processing techniques

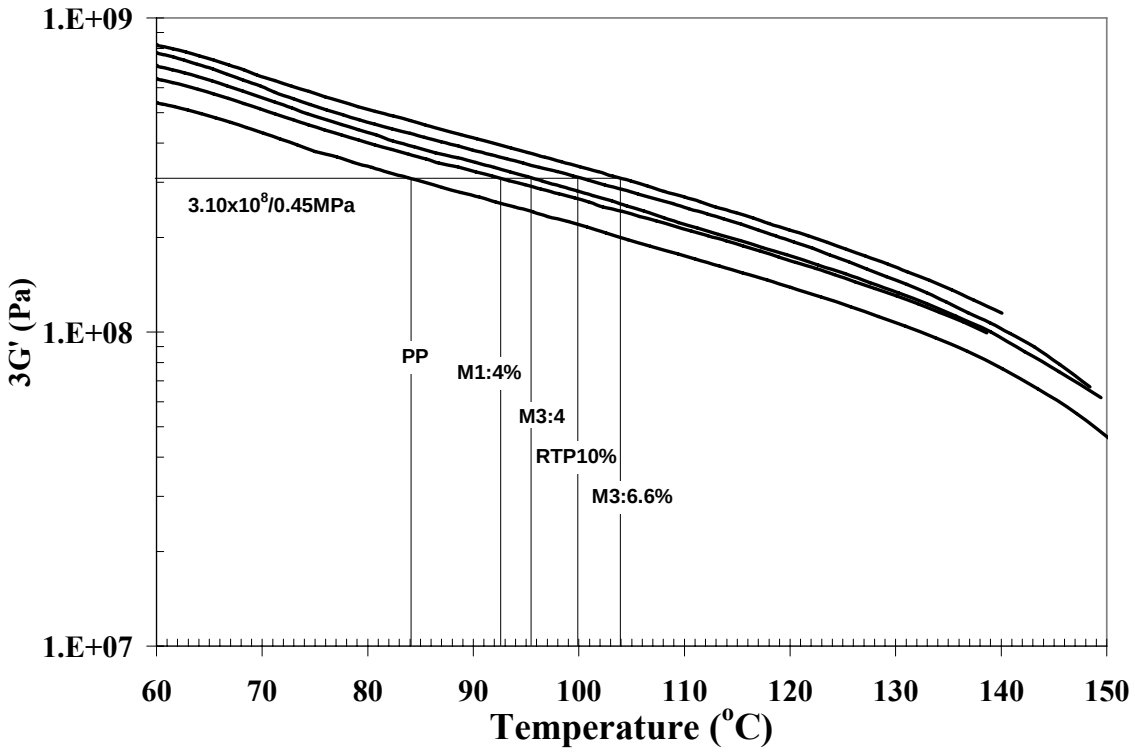

Figure 4.11: 3G' as a function of temperature from DMTA. Vertical lines correspond to estimated HDTs.

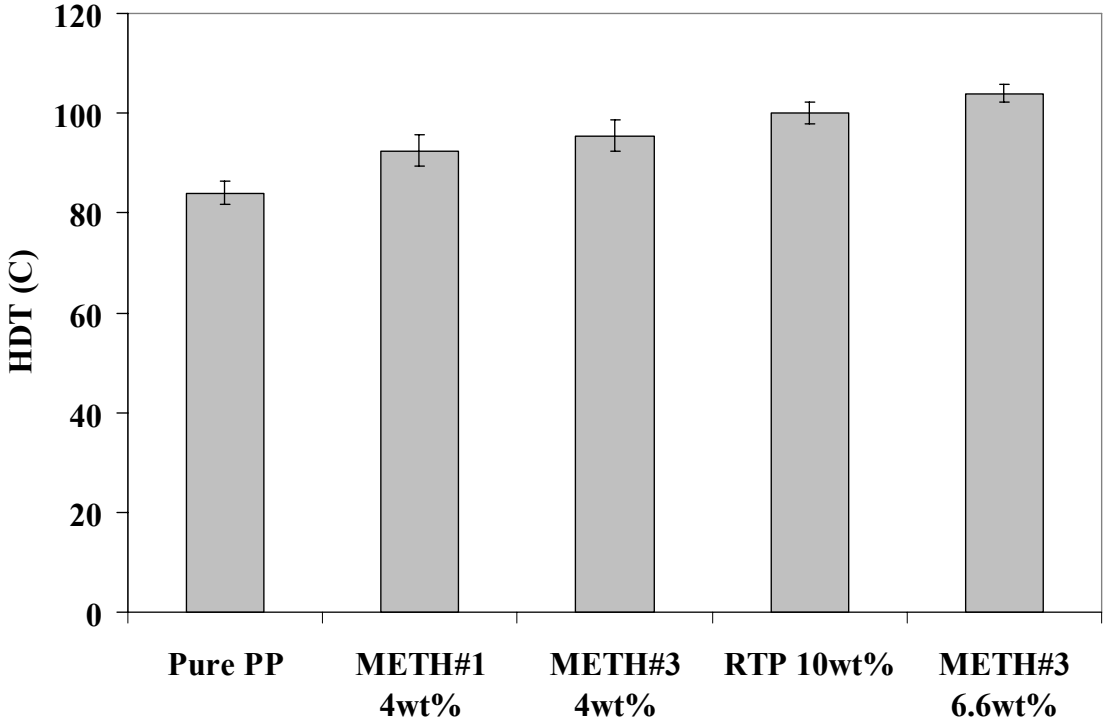

Figure 4.12: HDT of different nanocomposites estimated from DMTA

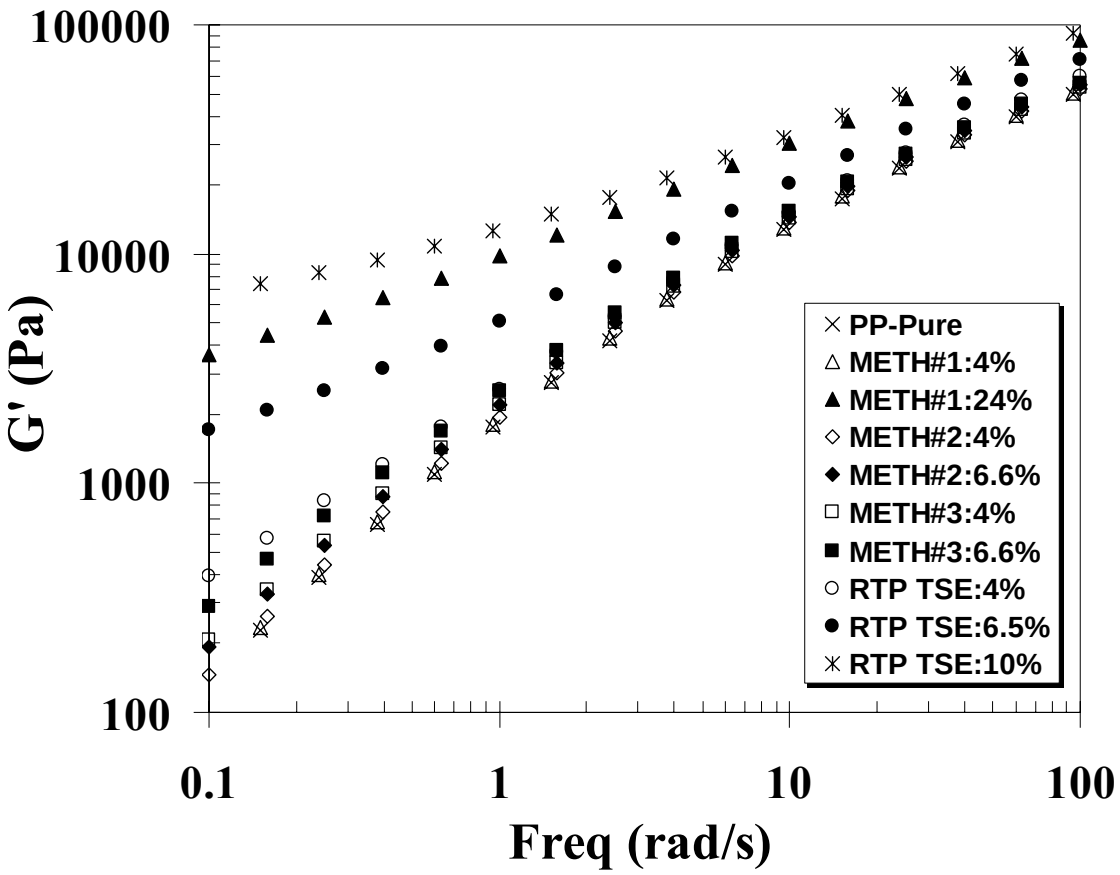

Figure 4.13: Storage modulus versus frequency of different nanocomposites at 200^{o}C

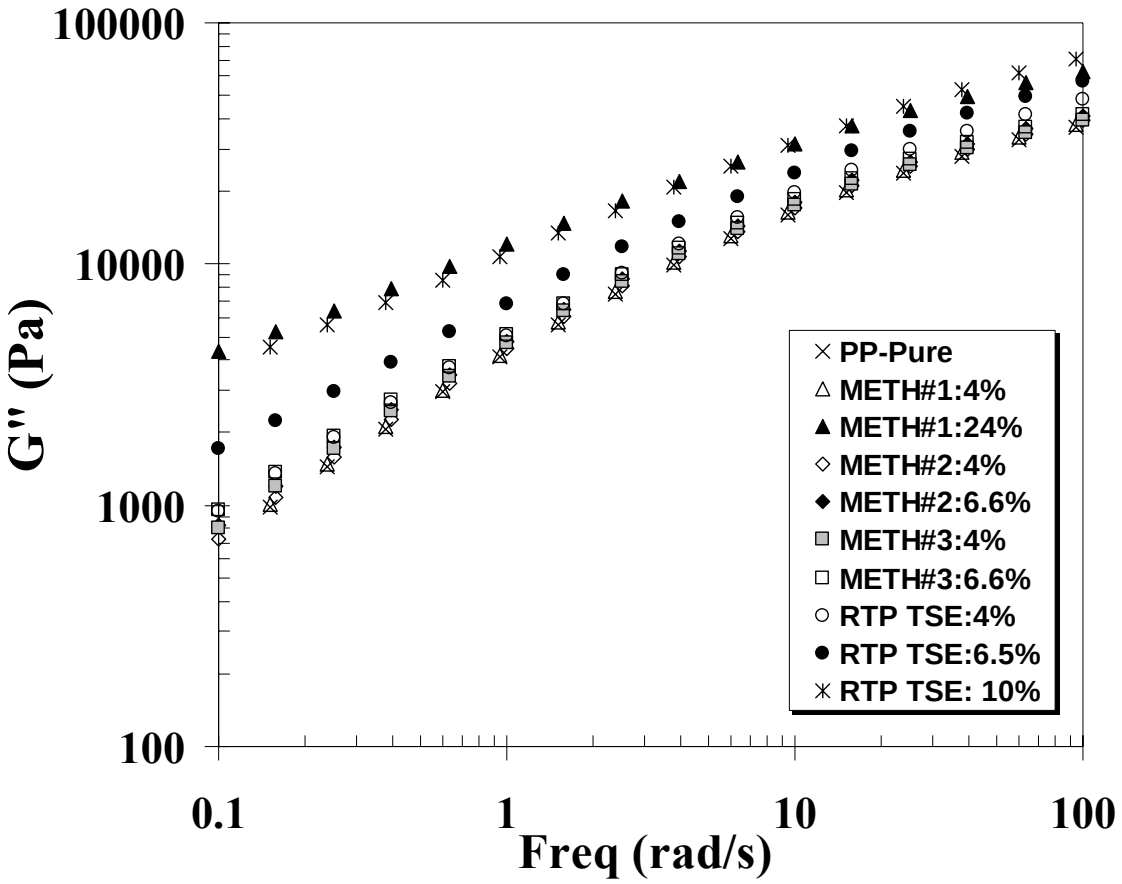

Figure 4.14: Loss modulus versus frequency of different nanocomposites at 200^{o}C

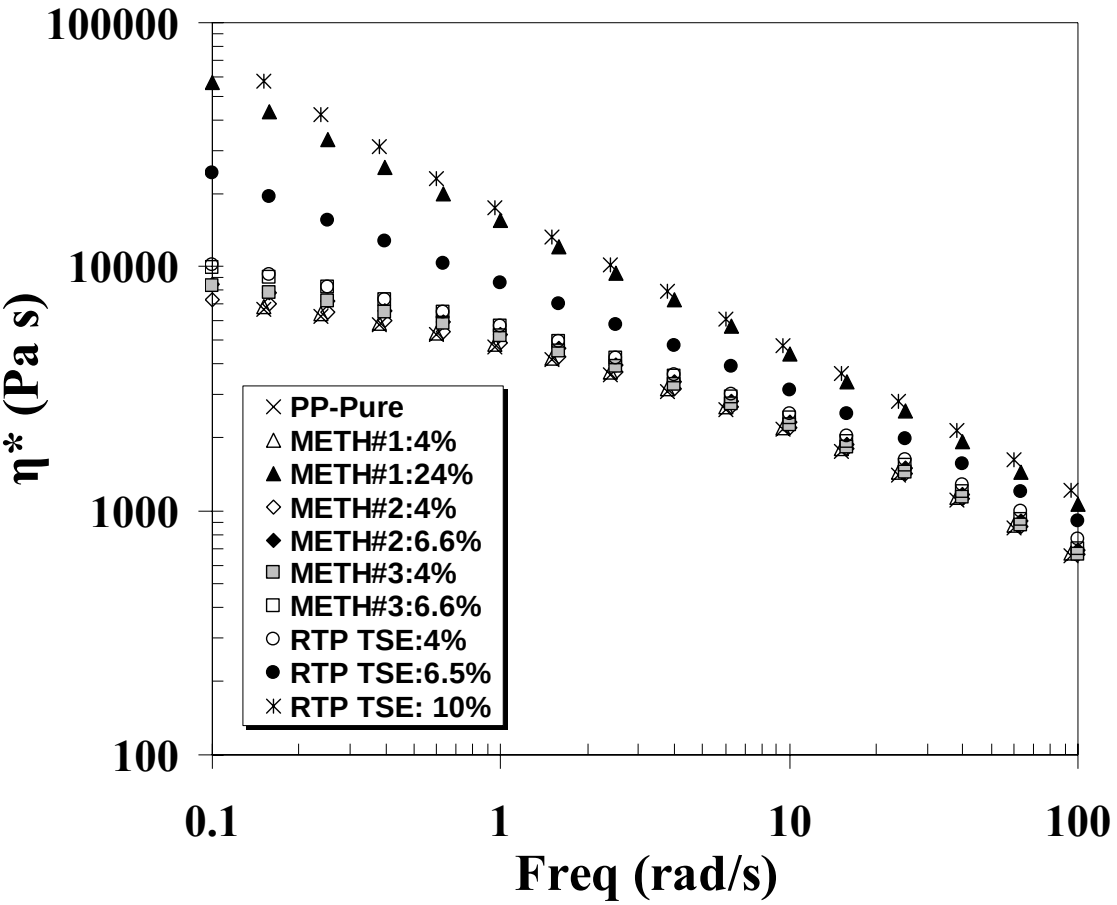

Figure 4.15: Complex viscosity versus frequency of different nanocomposites at 200^{o}C

5.0 Effect of PP-g-MA on the Mixing of Nano-Clay into Polypropylene Using Carbon Dioxide

Quang T. Nguyen and Donald G. Baird*

Department of Chemical Engineering, Virginia Polytechnic Institute and State University
Blacksburg, VA 24061-0211
*Email: dbaird@vt.edu

ABSTRACT

The effect of maleic anhydride compatibilizer (MA) on the mechanical and rheological properties of polypropylene (PP)-clay nanocomposites prepared using CO_2 and direct melt blending was studied. Results from the mechanical properties, rheological studies, and transmission electron microscopy (TEM) showed that when MA compatibilizer was combined with the technique employing CO_2, greater enhancement in the mechanical properties and degree of dispersion was observed. Furthermore, yield-like behavior in the viscosity and a tail in the low-frequency behavior of G' was attributed to the reaction of MA group with the nano-clay surface and not exfoliation alone. A fairly well dispersed morphology was observed for concentrations as high 6.8 wt% clay when the clay was expanded and mixed with CO_2. At this concentration, mechanical properties such as yield strength and modulus increased by as much as 13% and 69%, respectively, relative to the pure PP. Furthermore, the modulus of the composite samples prepared using PP-g-MA and CO_2 was some 15% higher than that of samples prepared by direct melt compounding (without the use of CO2).

Keywords: Polypropylene, maleated polypropylene, nanocomposites, nanoclay, supercritical carbon dioxide, extrusion.

5.1 Introduction

Much academic as well as industrial research in polymer layered silicate nanocomposites has rapidly been increasing at an unprecedented level due to their potential for enhanced physical, chemical, and mechanical properties compared to conventionally filled composites [1-6]. It is well established that when layered silicates are uniformly dispersed and exfoliated in a polymer matrix, the polymer properties can be improved to a dramatic extent. These improvements may include increased strength [7], higher modulus [8-13], thermal stability [14-16], barrier properties [17, 18], and decreased flammability [19-23].

The main reason for these marked improvements stem from the large aspect ratio of layered silicate, e.g., montmorillonite (MMT). Each individual layer of MMT has a thickness on the order of 1 nanometer (nm) with lengths ranging from 100 nm to 300 nm [24, 25]. The high aspect ratio leads to a high contact surface area and, thus, physical interactions between the polymer and layered silicates with only a small concentration of clay. However, because the layered silicates typically exist as aggregates due to attractive van der Waals forces [26], the contact surface area available and, thus, improvements in physical properties do not reach theoretical expectations. Achieving a nanocomposite with an exfoliated morphology in which each individual layered silicate has been separated from its initial stack and dispersed uniformly throughout a given polymer matrix is the key to reaching the full potential of the nanoclays to enhance mechanical, thermal, and barrier properties of a polymeric matrix.

The attractive interactions between the polymer matrix and the layered silicates determine, in large part, the degree of compatibility between the two separate phases.

Layered silicates are naturally hydrophilic while many polymers such as polyolefins are hydrophobic and, thus, the surface energies between the two materials can be vastly different prohibiting any significant degree of dispersion of nanoclay within the polymer [11]. In order to have a successful development of clay-based nanocomposites, it is necessary to chemically modify a natural clay so that it can be compatible with a chosen polymer matrix. Modification of layered silicates via ion exchange reactions through which quaternary alkyl ammonium cations replace the existing cations (Na^+, Ca^+, Li^+ etc.) residing in the interlayer of the silicates help to make the layered silicates more organophilic. Generally, this can be done through ion exchange reactions by replacing interlayer cations with quarternary alkylammonium or alkylphosphonium cations [27-29].

For polymer containing polar functional groups, an alkylammonium surfactant is adequate to promote the nanocomposite formation. For non-polar polypropylene (PP), however, it is not simple because interfacial bonding between the clay surface and PP matrix is unfavorable. To increase the compatibility between the MMT nanoclays and PP matrix, two major methods including melt intercalation [30-35] and in-situ polymerization [36] have recently been introduced. The latter method usually involves in a slurry phase, which requires large volumes of solvents and a need of purification. Thus this method may be impractical because it is environmentally as well as economically unfriendly. The melt intercalation of PP-clay nanocomposites usually involves the use of a compatibilizer, such as maleic anhydride grafted PP (PP-g-MA), to facilitate the intercalation of PP in clay [30-32]. The MA compatibilizer has mechanical properties lower than those of the native polypropylene and, hence, adding MA compatibilizer can

harm the final properties of the composites. Thus, it is necessary to explore the MA compatibilizer on the final microstructure and properties of the nanocomposites.

In the previous study, we developed a process to help exfoliate and disperse the nanoclay into PP matrix with the aid of supercritical CO_2 [37]. The process involves the use of a pressurized CO_2 chamber to assist in the exfoliation and delivery of the clay into a stream of polymer melt in the extruder. It was observed that for concentrations as high as 6.6 wt% (only limited by the physical design of the chamber), fairly exfoliated nanocomposites were observed with as much as 54% increase in Young's modulus was achieved. Most studies dealing with PP-clay nanocomposites, even with the incorporation of a MA compatibilizer, are only partially successful because complete exfoliation was practically never reached [51-65]. In this study, the CO_2 chamber technique is extended further by incorporating a MA compatibilizer to prepare PP-clay nanocomposites. We would like to ascertain whether or not further improvements on the mechanical properties of the nanocomposites can be achieved when prepared with the incorporation of a maleic anhydride compatibilizer. The effect of a MA compatibilizer on the microstructure and on the mechanical and linear viscoelastic properties of the nanocomposites prepared using two different processing techniques is also studied.

5.2 Experimental

5.2.1 Materials

Polypropylene (Pro-fax 6523, MFI = 4 g/10 min at 230^{o}C and 2.16 kg load, Density = 0.90 g/cm^{3}) was obtained from Basell (Elkton, MD) and was used as received. Polypropylene-graft-maleic anhydride (PP-g-MA) (PB3150, MFI = 52.2 g/10 min at 230^{o}C and 2.16 kg load, MA content = 0.5 wt%) was supplied from Chemtura

Corporation (Middlebury, CT). Surface modified montmorillonite (Cloisite 20A) was obtained from Southern Clay Products, Inc. (Gonzalez, TX) and was used as-is. Cloisite 20A is a surface modified montmorillonite obtained through a cation exchange reaction, where the sodium cation is replaced by dimethyl, dihydrogenatedtallow, quaternary ammonium cation.

5.2.2 Clay Concentration

Clay concentrations were determined by the burn-off technique in an ashing oven at 500^{o}C for 30 minutes. The reported concentrations are an average of three burn-off samples. The clay concentrations reported here include the organic modifiers.

5.2.3 Extrusion experiments

Compatibilized polypropylene-clay nanocomposites were prepared by direct-melt compounding and by using a modified pressurized CO_2 chamber [37]. Samples were extruded at a melt temperature of around 190 ^{o}C and a screw speed of 15 rpm using a Killion KL-100 extruder with a single, two-stage screw, 25.4 mm (1 inch) diameter and 30:1 L/D. A capillary die of 1/16 inch diameter and 20:1 L/D was attached at the end of the extruder. The chamber was inserted between the CO_2 pump and the injection port at the beginning of the second stage of the screw. A schematic diagram of the overall process is shown in Figure 5.1.

It was shown in the previous study [37] that the method of direct injection of $scCO_2$ into the barrel during extrusion (METH #2) did not show much property improvements over the conventional direct-melt compounding technique (METH #1) due to its inability to adequately exfoliate and disperse the nanoclay into the polymer matrix. For this reason, METH #2 was not examined again in this study. The two processing

methods explored in this study are described below. For each blending technique, an approximate 3 to 1 ratio of MA compatibilizer to clay was employed.

***METH #1* + *MA* (direct melt blending):** Conventional single-screw melt compounding. The clay, PP, and PP-g-MA were dry blended in a Kitchen Aid type mixer, and then the mixture was fed to an extruder and re-pelletized.

***METH #3* + *MA*: (CO_2 chamber):** The clays were allowed to be in direct contact with sc-CO_2 at 3000 psi and 80^{o}C for a period of time (12-24hrs) and then the pressure was rapidly released. The mixture of the nano-particles and sc-CO_2 was then injected into the molten polymer stream in a single-screw extruder.

5.2.4 Injection Molding

The nanocomposite pellets were dried at 100°C in an oven overnight and then injection molded using an Arburg Allrounder Model 221-55-250 injection molder. The Arburg Allrounder has a 22 mm diameter barrel, L/D = 24, screw with variable root diameter from approximately 14.25 mm at the feed to 19.3 mm at the exit, a check ring non-return valve, and an insulated nozzle that is 2 mm in diameter. The composites were injection molded, using a melt temperature of 200°C, a mold temperature of 80°C, a holding pressure of 5 bars, and a screw speed of 200 rpm, and a rectangular end-gated mold with dimensions of 80 mm by 76 mm by 1.5 mm.

5.2.5 Rheological Properties

Rheological studies of the nanocomposites were performed using a Rheometrics Mechanical Spectrometer Model 800 (RMS-800). Samples were prepared by compression molding of the extruded pellets 25 mm diameter disks. Dynamic frequency sweep experiments were performed under a continuous nitrogen atmosphere using 25-

mm parallel-plate fixture at 200°C in the linear viscoelastic region of the materials. To determine the limits of linear viscoelastic properties of the materials, dynamic strain sweeps were performed at 200°C and a frequency of 10 rad/s for a filled system with 6.7 wt% of Cloisite 20A. The samples were observed to exhibit linear viscoelastic behavior for strains less than about 8%. The elastic moduli (G'), loss moduli (G"), and complex viscosities (η*) of the materials as functions of angular frequency (ω) (ranging from 0.1 to 100 rad/s) are obtained.

5.2.6 Tensile Properties

The injection molded plaques were cut into rectangular bars, typically along the machine direction, having dimensions of approximately 8.5 mm wide, 1.5 mm thick, and 80 mm in length. Tensile tests on these bars were performed at room temperature using an Instron model 4204 testing machine. An extensiometer was used to accurately determine the elongation of the sample and, hence, Young's modulus and yield strength. The load was measured with a 5 kN load cell while the cross-head speed was kept at 1.27 mm/min during all tensile tests. For all tests, the average and the standard deviation were calculated from at least four samples, and data points greater than 2 standard deviations from the mean were omitted.

5.2.7 Structure and Morphological characterization

WAXD scans were not conducted in this study due to limited access to an XRD machine. The processing techniques and conditions were kept the same for this study as they were for the previous study [37]. Therefore, we are assuming that the relative trend of the WAXD patterns for the nanocomposites generated in this study are the same as those of the previous. Transmission electron microscopy (TEM) was used to confirm the

morphology of the composites. TEM micrographs were generated using a Philips EM420T with an accelerating voltage of 100kV. The TEM samples, around 95 nm thick, were cut using a cryo-microtom equipped with a diamond knife at -100 ^{o}C. Injection molded samples were used for TEM.

5.3 Results and Discussion

5.3.1 Transmission Electron Microscopy

To qualitatively understand the internal structure of the composites and to examine the degree of dispersion of the clay in the matrix, TEM analysis was carried out. TEM micrographs (at magnification of 17,000 and 34,000) of various nanocomposites prepared using different processing techniques are presented in Figures 5.2-5.5. As can be seen from Figure 5.2, the 4 wt% nanocomposite prepared via method #1 without the MA compatibilizer shows very poor dispersion. Mostly an intercalated structure with very large aggregates or tactoids in the order of several tens to hundreds of silicate layers can be observed. This observation is common because of the lack of the affinity between the polar clay and the highly nonpolar polymer matrix. Using the same processing method with the incorporation of PP-g-MA, better dispersion was observed (Figure 5.3). Clearly, the size of the aggregates is greatly reduced, although some aggregates still exist. It is apparent from this observation that the MA compatibilizer has a positive effect on the dispersion of the clay into the polypropylene matrix. The ability of the polar functional groups to hydrogen bond and interact with the silicate surface helps promote diffusion of the polymer chains into the clay galleries. Further improvement in the exfoliation of the clay particles in the PP matrix is observed when using PP-g-MA in the preparation method #3 (Figures 5.4 & 5.5). From the TEM micrographs shown in Figures

5.4 and 5.5, we can see that the nanocomposite is fairly well dispersed and the clay is evenly distributed throughout the polymer matrix. Although, there are still some areas that show thick silicate layers, most show fairly well dispersed clay platelets even at high magnification. This observation is consistent with that of the previous study, which further confirms the effectiveness of method #3 in dispersing the silicate into the polymer matrix.

5.3.2 Tensile Properties

In the previous study, we have reported the mechanical properties for various PP-clay nanocomposites prepared without the incorporation of a MA compatibilizer using different processing techniques [37]. In general, we found that the conventional direct-melt compounding methods (METH #1 and METH #2) using a single-screw extrusion, with and without the direct injection of $scCO_2$, did not lead to much improvement in the mechanical properties of injection molded samples due to their inability to adequately exfoliate the nanoparticles into the polymer matrix. However, most improvements were seen from the technique of using the pressurized CO_2 chamber (METH #3). As much as 54% increase in Young's modulus was obtained for 6.6 wt% clay.

In this section, the effect of a maleic anhydride compatibilizer on the mechanical performance of the nanocomposites prepared using the two different processing techniques described above (METH #1 and #3) is examined. The tensile properties presented in the following discussion are summarized in Tables 5.1 and Figure 5.6. In Figure 5.6, the mechanical properties of non-compatibilized PP-clay nanocomposites obtained from the previous study for methods 1 and 3 are also plotted for comparison. Analyzing the trends on the mechanical properties could give useful information about

the effect of MA compatibilizer and processing methods on the nanocomposites' performance. Comparing the mechanical properties of the compatibilized and non-compatibilized nanocomposites prepared via method #1, we can see that the mechanical properties of the compatibilized nanocomposites are much more enhanced than those of the non-compatibilized ones at all clay levels. As much as 20% additional increase in Young's moduli and 15-20% additional increase in the yield strengths were observed for the compatibilized composites. It is important to point out, however, that the mechanical properties of the compatibilized composites prepared via method #1 also showed little increase beyond the addition of 4.0 wt%, which is a common observation [38-40]. When using method #3 with the incorporation of MA compatibilizer, further improvements in the mechanical properties were achieved at all clay levels. At clay loading of 6.8 wt%, as much as 69% increase in Young's modulus and 13% increase in yield strength were observed. In both processing methods, we can see that the addition of MA compatibilizer greatly enhanced the mechanical performance of the nanocomposites. This is due to the compatibilizer that was used in preparing the nanocomposite, which increased the bonding between the nanoparticles and the polypropylene matrix and helped with dispersion. Despite the improvements in the yield strength and Young's modulus, we observed a decrease in the elongation at break values with increasing clay content for the compatibilized PP-clay nanocomposites. In this kind of systems, this behavior is common because the clay could act as a defect affecting the deformation capability [41].

Comparing the tensile properties of the compatibilized nanocomposites prepared using method 1 to those of non-compatibilized nanocomposites prepared using method 3, we can see that those prepared using method 3, even without a MA compatibilizer, could

still perform as well as those prepared using method 1 with a MA compatibilizer. Also, the non-compatibilized composites prepared via method 3 possessed much higher elongation at break values than those of compatibilized composites prepared via method 1 at all clay levels. This, again, proves that method 3 is much more effective than method 1 in terms of its ability to better disperse the nanoclay into the polymer matrix to achieve better mechanical properties. Additionally, from the mechanical response curves in Figure 5.6, it can be seen that the nanocomposites prepared via method 3 could potentially exhibit higher mechanical properties beyond a clay level of 6.7 wt% (if not limited by present process capabilities), whereas in method 1, even with the incorporation of a MA compatibilizer, the mechanical properties leveled out beyond a clay level of 4 wt%.

In order to realize the full potential of mechanical property increase, it is necessary to compare the observed property enhancements, such as modulus, to those predicted by composite theories like that of Halpin-Tsai [42, 43]. Halpin-Tsai's model shown below in Equation 5.1 assumes fully exfoliated clay platelets, unidirectional, i.e. well oriented filler particles, as well as a high degree of adhesion of the filler particles to the surrounding polymer matrix,

$$E_c = E_m \left[\frac{1 + \zeta \eta \phi_f}{1 - \eta \phi_f} \right], \tag{5.1}$$

where E_c = composite modulus, E_m = unfilled matrix modulus, ϕ_f = filler volume fraction,

$$\eta = \frac{E_f / E_m - 1}{E_f / E_m + \zeta}, \tag{5.2}$$

$$\zeta = 2(l/t), \tag{5.3}$$

E_f = filler modulus taken to be 178 GPa for MMT [43], and l/t = aspect ratio of the silicate platelets taken here to be approximately 100 for fully exfoliated platelets [43].

The theoretical and experimentally measured modulus of the composites versus wt% MMT is shown in Figure 5.6. As can be seen, the experimental Young's moduli presented are below those predicted by the Halpin-Tsai model. Although the values approach closer for the compatibilized nanocomposites, they are still below those of the theory prediction. The difference must be attributed to the assumptions made in the Halpin-Tsai theory. It is important to point out that there are numerous complexities arise when comparing experimental data to those of composite theory, especially when dealing with polymer layered silicate nanocomposites. The main reasons for the difference may be due to lack of complete orientation of the filler particles in the flow direction, imperfect bonding between the filler and the matrix, and the aspect ratio of the platelets may be much less than the assumed value of 100.

5.3.3 Linear viscoelastic properties

In this section we look at the effect of the MA compatibilizer on the rheological behavior of the nanocomposite melts prepared using different processing techniques at various levels of nanoclay. The storage moduli, G', loss moduli, G", and the complex viscosities, η*, resulting from the dynamic frequency scan measurements are compared in Figures 5.7, 5.8, and 5.9, respectively. Results from the previous study [37] for processing method #3 without the incorporation of MA compatibilizer are also shown in those figures for comparison.

According to the previous study [37], the nanocomposites prepared by method #3 did not exhibit a tail or plateau in the G' at low frequencies, even though a good degree

of clay dispersion was observed by XRD and TEM. However, moderate enhancement in the G' at low frequencies was noticed, which we hypothesized arose from the interactions between the exfoliated clay platelets. Here, the lack of a tail in G', as we mentioned in the previous study, could be due to the absence of a network formed by the strong hydrogen bonding between the polar functional groups of PP-g-MA and the hydroxyl groups of the silicate.

In this study, we can clearly observe the onset plateau of the storage and loss moduli (Figures 5.7 & 5.8) and the diverging of the complex viscosity (Figure 5.9) at low frequencies for all the nanocomposites prepared with the incorporation of MA compatibilizer using methods 1 and 3. A direct comparison of the rheological response of the nanocomposites prepared with and without the use of PP-g-MA showed a direct effect of the MA compatibilizer on the enhancement of low-frequency G', G", and η*. The reason for the increasing of G', G", and η* could be attributed to the use of a maleic anhydride compatibilizer that increases interaction and hydrogen bonding between filler and polymer matrix, which probably leads to a lower polymeric chain mobility, making the material more rigid and solid-like. Many studies believe that the pseudo-solid-like behavior at low frequencies might be ascribed to the formation of the percolated network structure of the clay platelets or the frictional interactions between the anisotropic clay tactoids [44-48]. Comparing the low-frequency storage moduli, G', of the compatibilized PP-clay nanocomposites prepared via method 1 and 3, we can see that the low-frequency G' of the composites prepared using method 3 is more enhanced at both clay levels of 4.3 wt% and 6.7 wt%. Assuming everything else was constant except for the processing technique, the increase in the low-frequency G' must be attributed to the increased

particle-particle interactions due to better dispersion resulted from the pressurized CO_2 chamber technique. Also, when the layered silicate particles are more exfoliated, there would be more surface area available for the MA groups to hydrogen bond with the hydroxyl groups on the clay surface to form network. This increase in network formation can contribute to the increase in G' at low frequencies.

Using rheology to determine the degree of exfoliation of the nanocomposites is still ambiguous and the information obtained from it can only be used to probe the structure of the layered silicate indirectly. It still remains unclear in literature whether the changes in dynamic rheological properties in the low frequency region were due to the interactions of exfoliated clay platelets within the maleated PP matrix or whether network occurred between the maleic anhydride groups and the hydroxylated surfaces of the silicate layers [49, 50]. The results presented in this paper led us to believe that the enhancement of the low-frequency G' is a contribution of both the inter-particle interaction and the polymer-clay interaction. Thus, the rheological properties commonly reported for clay-filled functionalized polypropylene cannot be attributed solely to the formation of percolation network between clay platelets, but the contribution and the properties of the functionalized matrix must be considered.

5.4 Conclusions

Compatibilized polypropylene-clay nanocomposites were prepared in this study via direct melt intercalation and by using the pressurized CO_2 chamber technique. It was observed that the degree of dispersion and the mechanical and rheological properties of the nanocomposites were greatly affected by the incorporation of a maleic anhydride compatibilizer. The polarity and reactivity of the functional groups of the MA helped

improve the interaction between the filler and polymer, which led to better dispersion of the silicate platelets, enhanced storage modulus at low frequencies, and improved mechanical performance. The most improvements were seen from the technique of using the pressurized CO_2 chamber with the incorporation of PP-g-MA. TEM data showed a fairly good degree of exfoliation for concentrations as high as 6.6 wt%, and the mechanical properties such as modulus increased by as much as 69%.

5.5 Acknowledgements

We express gratitude to the Environmental Protection Agency (grant #: R-82955501-0) and the National Science Foundation (grant #: CTS-0507995) for supporting this work. We would like to thank Chemtura Corp. for providing PP-g-MA and Steve McCartney at the VPI&SU Materials Research Institute for aid in conducting the TEM study.

5.6 References

[1] Usuki A, Kojima Y, Kawasumi M, Okada A, Fukushima Y, Kurauchi T, Kamigaito O. J Mater Res 1993; 8: 1185.

[2] Kojima Y, Usuki A, Kawasumi M, Okada A, Kurauchi T, Kamigaito O. J Polym Sci Part A 1993; 31: 983.

[3] Kojima Y, Usuki A, Kawasumi M, Okada A, Kurauchi T, Kamigaito O. J Polym Sci Part A 1993; 31: 1755.

[4] Liu L, Qi Z, Zhu X. J Appl Polym Sci 1999; 71: 1133.

[5] Lan T, Kaviratna D, Pinnavaia J. Chem Mater 1994; 6: 573.

[6] Gilman W, Morgan A, Giannelis P, Wuthenow M, Manias E. Flame Retardancy 10th Annual BBC Conference Proceedings 1999; 1.

[7] Giannelis P. Appl Organomet Chem 1998; 12: 675.

[8] Okada A, Kawasumi M, Usuki A, Kojima Y, Kurauchi T, Kamigaito O. In: Schaefer W, Mark E, editors. Polymer based molecular composites MRS Symposium Proceedings. Pittsburgh; 1990; vol. 171:45–50.

[9] Giannelis P. Adv Mater 1996; 8: 29.

[10] Giannelis EP, Krishnamoorti R, Manias E. Adv Polym Sci 1999; 138: 107.

[11] LeBaron PC, Wang Z, Pinnavaia TJ. Appl Clay Sci 1999; 15: 11.

[12] Vaia RA, Price G, Ruth PN, Nguyen HT, Lichtenhan J. Appl Clay Sci 1999; 15: 67.

[13] Biswas M, Sinha S. Adv Polym Sci 2001; 155: 167.

[14] Gilman JW. Appl Clay Sci. 1999; 15: 31.

[15] Bins & Associates. Plastics Additives & Compounding 2002; 4(1): 30-33.

[16] Lan T, Kaviratna PD, Pinnavaia TJ. Chem Mater 1994; 6: 573.

[17] Sall K. European Plastics News March 14, 2002.

[18] Messersmith PB, Giannelis EPJ. Polym Sci Part A: Polym Chem 1995; 33: 1047.

[19] Gilman JW, Kashiwagi T, Lichtenhan JD. SAMPE J 1997; 33: 40.

[20] Gilman JW. Appl Clay Sci 1999; 15: 31.

[21] Dabrowski F, Bras L, Bourbigot S, Gilman JW, Kashiwagi T. Proceedings of the Eurofillers. Lyon-Villeurbanne, France 1999; 6:9.

[22] Bourbigot S, LeBras M, Dabrowski F, Gilman JW, Kashiwagi T. Fire Mater 2000; 24:201.

[23] Gilman JW, Jackson CL, Morgan AB, Harris R, Manias E, Giannelis EP, Wuthenow M, Hilton D, Phillips H. Chem Mater 2000; 12: 1866.

[24] Mehrabzadeh M, Kamal MR. Poly. Eng Sci 2004; 44: 152.

[25] Pinnavaia TJ, Beall GW. Polymer-Clay Nanocomposites. New York: J. Wiley & Sons; 2000.

[26] Zanetti M, Lomakin S, Camino G. Macromol Mater Eng *2000;* 279**:**1.

[27] Blumstein A. J Polym Sci A 1965; 3:2665.

[28] Theng BKG. Formation and properties of clay–polymer complexes. Elsevier, Amsterdam, 1979.

[29] Krishnamoorti, Vaia A, Giannelis P. Chem Mater 1996; 8:1728.

[30] Kawasami M, Hasegawa N, Kato M, Usuki A, Okada A. Macromolecules 1997; 30:6333–6338.

[31] Nam PH, Maiti P, Okamoto M, Kotaka T, Hasegawa N, Usuki A. Polymer 2001; 42:9633–9640.

[32] Kato M, Usuki A, Okada A. J Appl Polym Sci 1997; 66:1781–1785.

[33] Modesti M, Lorenzetti A, Bon D, Besco S. Effect of processing conditions on morphology and mechanical properties of compatibilized polypropylene nanocomposites. Polymer 46 2005; 10237-10245.

[34] Kanny K, Moodley VK. Characterization of polypropylene nanocomposite structures. J Eng Mater & Tech 2007; 129:105-112.

[35] Lee JW, Kim MH, Choi WM, Park OO. Effects of organoclay modification on microstructure and properties of polypropylene-organoclay nanocomposites. J Appl Polym Sci 2006; 99:1752-1759.

[36] Alexandre M, Dubois P. Mater Sci Eng 2000; 28:1.

[37] Nguyen QT, Baird DG. Process for increasing the exfoliation and dispersion of nanoclay particles into polymer matrices using supercritical carbon dioxide. PhD Dissertation. Department of Chemical Engineering, Virginia Polytechnic Institute and State University; 2007.

[38] Hasegawa N, Okamoto H, Kawasumi M, Kato M, Tsukigase A, Usuki A. Macromol Mater Eng 2000; 280:76.

[39] Reichert P, Nitz H, Klinke S, Brandsch R, Thomann R, Mu¨lhaupt R. Macromol Mater Eng 2000; 275:8.

[40] Kim KN, Kim H, Lee JW. Polym Eng Sci 2001; 41:1963.

[41] Lopez-Quintanilla ML, Sanchez-Valdes S, Ramos de Valle LF, Medellin-Rodriguez FJ. J Appl Polym Sci 100 2006; 4748-4756.

[42] Halpin JC, Kardos JL. Polym Eng Sci 1976; 16:344.

[43] Fornes TD, Paul DR. Polymer 2003; 44:4993.

[44] Ren J, Casanueva BF, Mitchell CA, Krishamoorti R. Macromolecules 2003; 36:4188.

[45] Krishnamoorti R, Yurekli K. Curr Opin Colloid Interface Sci 2001; 6:464.

[46] Galgali G, Ramesh C, Lele A. Macromolecules 2001; 34:852.

[47] Solomon MJ, Almuallam AS, Seefeldt KF, Somwangth-anaroj A, Varadan P. Macromolecules 2001; 34:1864.

[48] Litchfield DW, Baird DG. The rheology of high aspect ratio nano-particle filled liquids. Rheology Reviews 2006; 1-60.

[49] Gilman JW, Jackson CL, Morgan AB, Harris Jr R. Chem. Mater 2000; 12**:**1866.

[50] Lee JA, Kontopoulou M, Parent JS. Time and shear dependent rheology of maleated polyethylene and its nanocomposites. Polymer 45 2004; 6595-6600.

[51] Modesti M, Lorenzetti A, Bon D, Besco S. Effect of processing conditions on morphology and mechanical properties of compatibilized polypropylene nanocomposites. Polymer 2005; 46: 10237-10245.

[52] Kanny K, Moodley VK. Characterization of polypropylene nanocomposite structures. J. Eng. Mater. & Tech. 2007; 129: 105-112.

[53] Lee JW, Kim MH, Choi WM, Park OO. Effects of organoclay modification on microstructure and properties of polypropylene-organoclay nanocomposites. J Appl Polym Sci 2006; 99: 1752-1759.

[54] Alexandre M, Dubois P. Mater Sci. Eng 2000; 28: 1.

[55] Ray SS, Okamoto M. Prog Polym Sci 2003; 28: 1539.

[56] Pinnavaia TJ, Beall GW. ‘‘Polymer-Clay Nanocomposites’’, J Wiley & Sons. New York 2000.

[57] LeBaron PC, Wang Z, Pinnavaia TJ. Appl Clay Sci 1999; 15:11.

[58] Fornes TD, Paul DR. Polymer 2003; 44: 4993.

[59] Osman MA, Rupp JEP, Suter UW. Polymer 2005; 46:1653.

[60] Wang ZM, Nakajima H, Manias E, Chung TC. Macromolecules 2003; 36:8919.

[61] Manias E. Origins of the Materials Properties Enhancements in Polymer/Clay Nanocomposites. In Golovoy A, editor. Nanocomposites 2001, Delivering New Value to Plastics. ECM Inc., Chicago; 2001.

[62] Dennis HR, Hunter DL, Chang D, Kim S, White JL, Cho JW, Paul DR. Polymer 2001; 42:9513.

[63] Manias E, Touny A, Wu L, Strawhecker K, Lu B, Chung TC. Chem Mater 2001; 13:3516.

[64] Svoboda P, Zeng CC, Wang H, Lee LJ, Tomasko DL. J Appl Polym Sci 2002; 85:1562.

[65] Ellis TS, D’Angelo JS. J Appl Polym Sci 2003; 90: 1639.

Table 5.1: Tensile properties of various nanocomposites prepared using different processing methods.

Materials	Young's Modulus (GPa)	S.D.	% Increase	Yield Strength (MPa)	S.D.	% Elongation	S.D.
PP - Pure	1.374	0.133	-	15.16	0.47	115.3	19.79
METH#1+MA: 4.3wt%	1.916	0.023	39	16.68	0.38	17.06	13.21
METH#1+MA: 6.7wt%	2.073	0.076	51	18.21	0.64	11.62	4.75
METH#1+MA: 12wt%	2.158	0.195	57	15.84	0.84	17.78	10.31
METH#3+MA: 4.2wt%	2.020	0.134	47	17.15	0.47	16.23	4.92
METH#3+MA: 6.8wt%	2.326	0.093	69	17.03	0.24	7.13	2.30

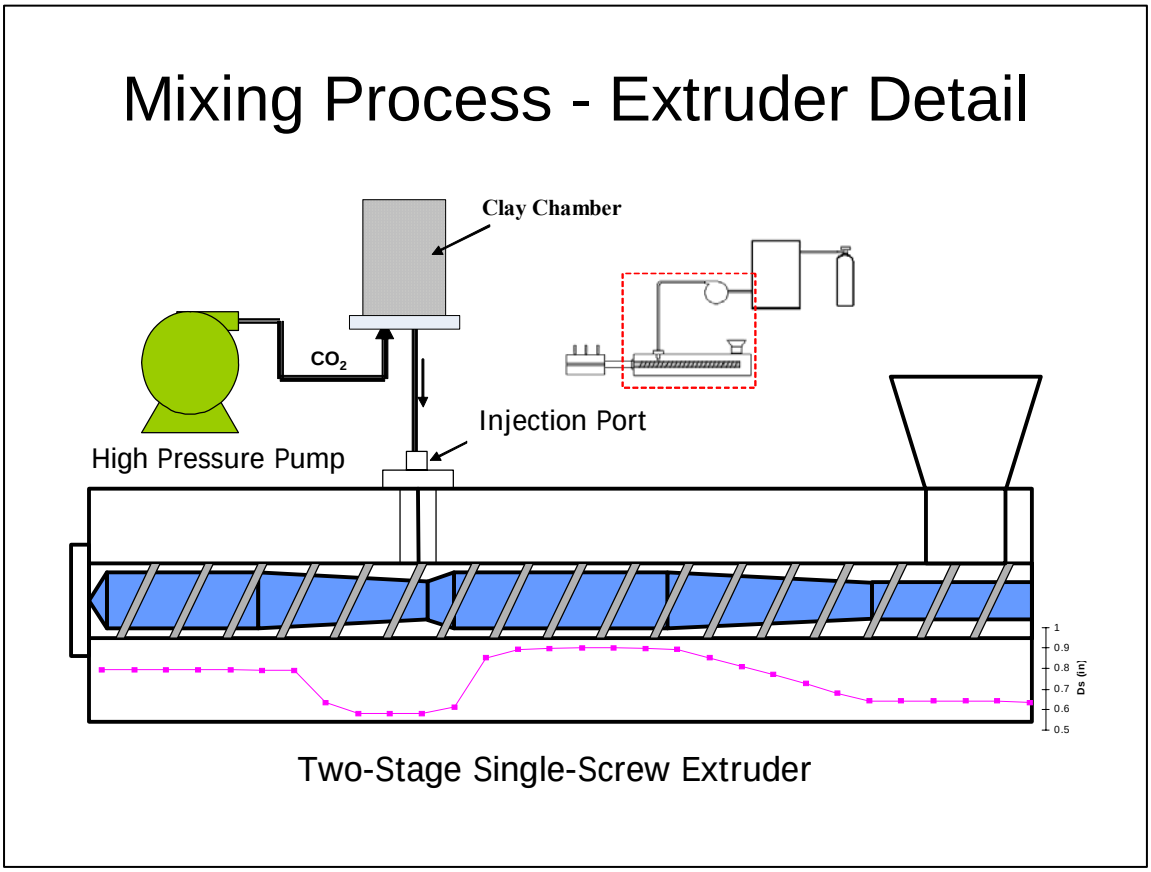

Figure 5.1: Schematic diagram of the overall process showing the CO2 chamber and the two-stage single screw extruder

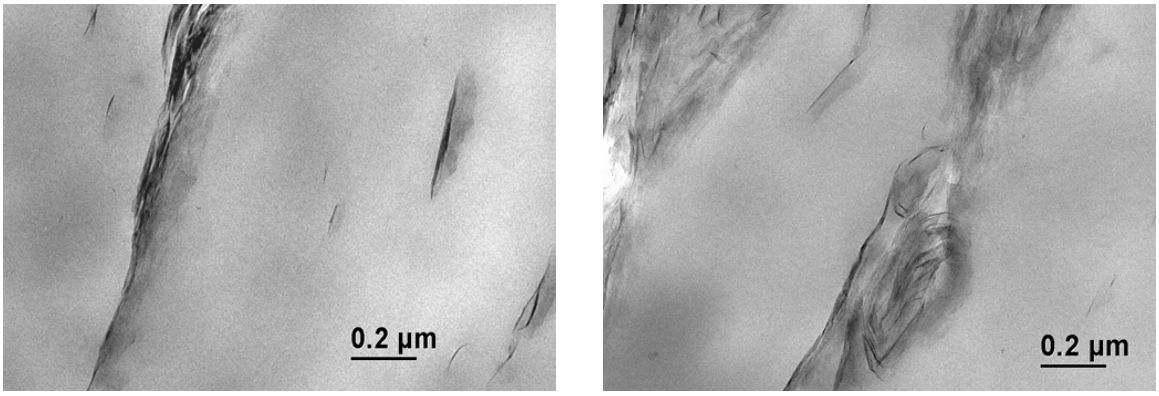

Figure 5.2: METH#1:4wt% (Left = 17,000x Right = 17,000x)

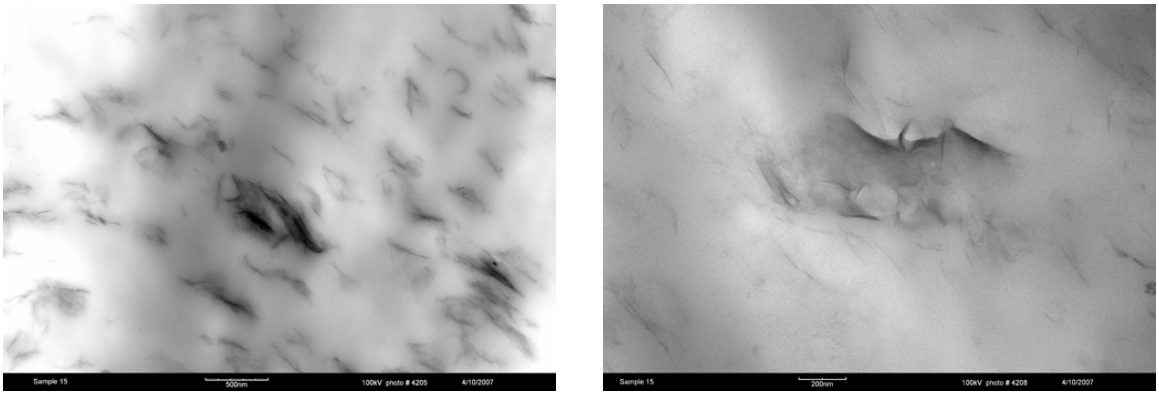

Figure 5.3: METH#1+MA: 4.3 wt% (Left = 17,000x, Right = 34,000x)

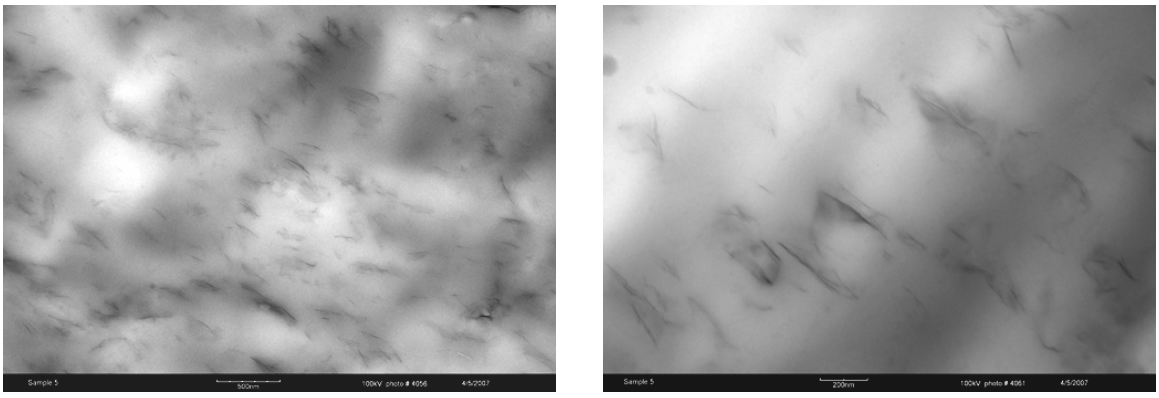

Figure 5.4: METH#3+MA: 4.2 wt% (Left = 17,000x, Right = 34,000x)

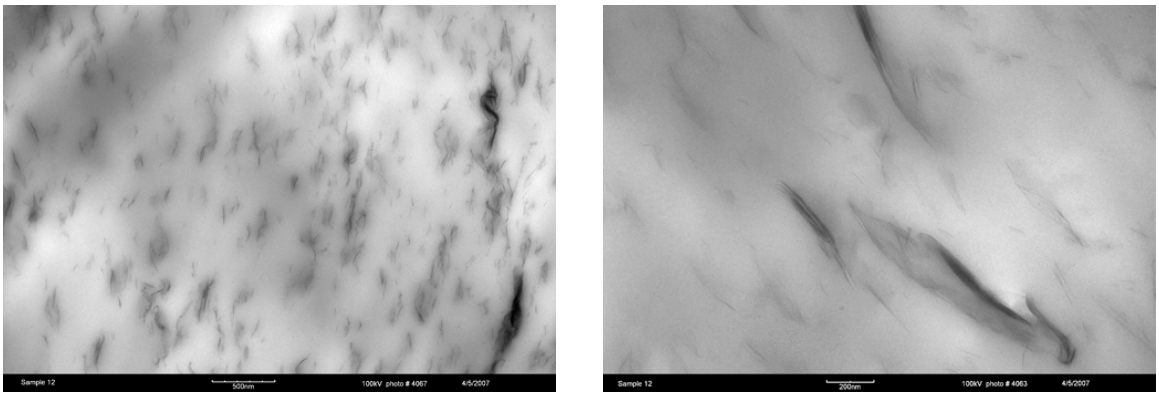

Figure 5.5: METH#3+MA: 6.8 wt% (Left = 17,000x, Right = 34,000x)

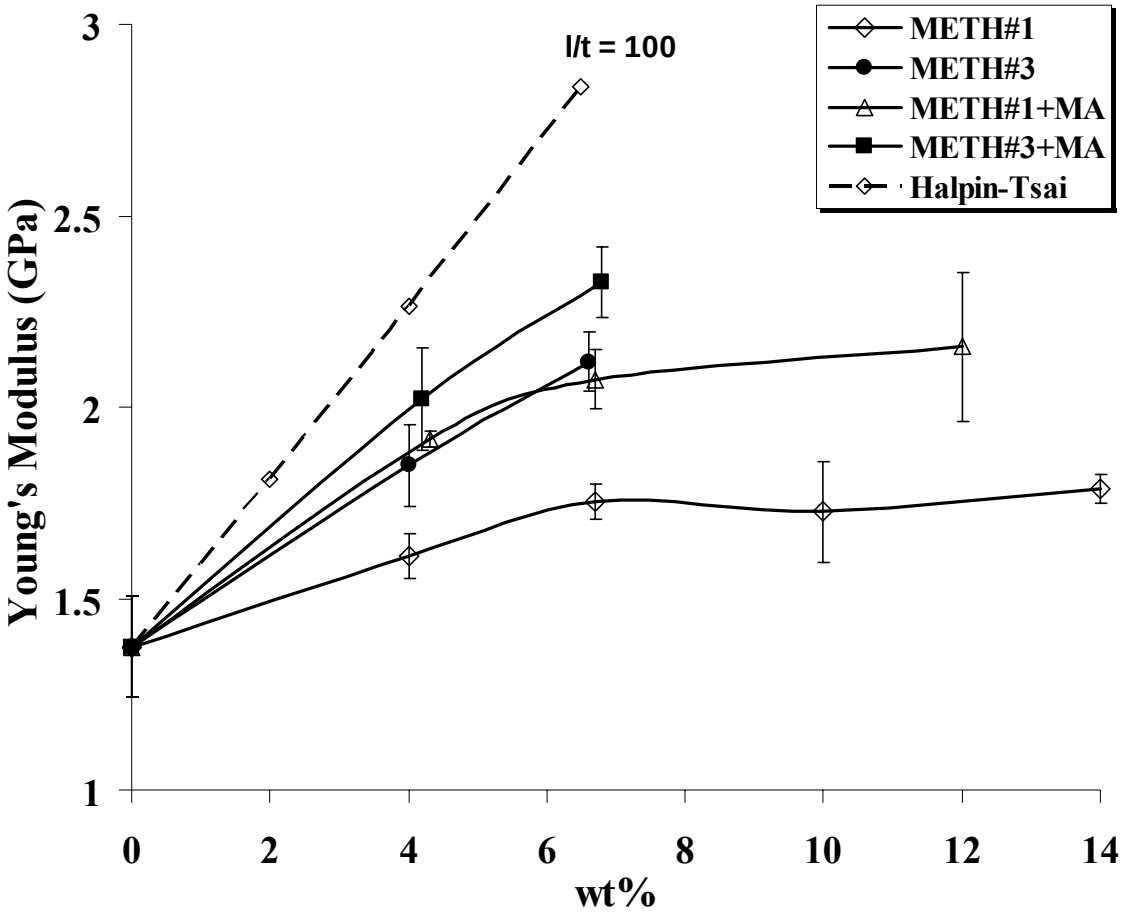

Figure 5.6: Young's modulus of different nanocomposites prepared using different processing techniques.

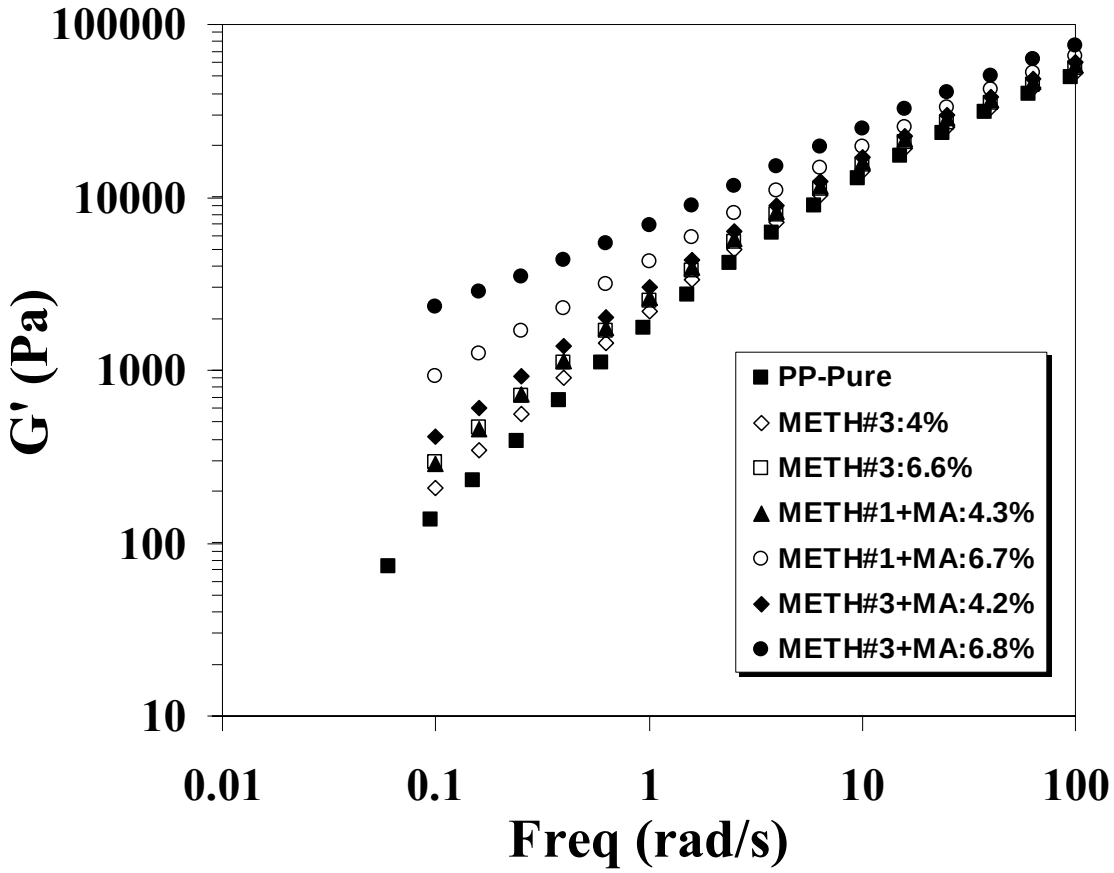

Figure 5.7: Storage modulus versus frequency of different nanocomposites at 200^{o}C

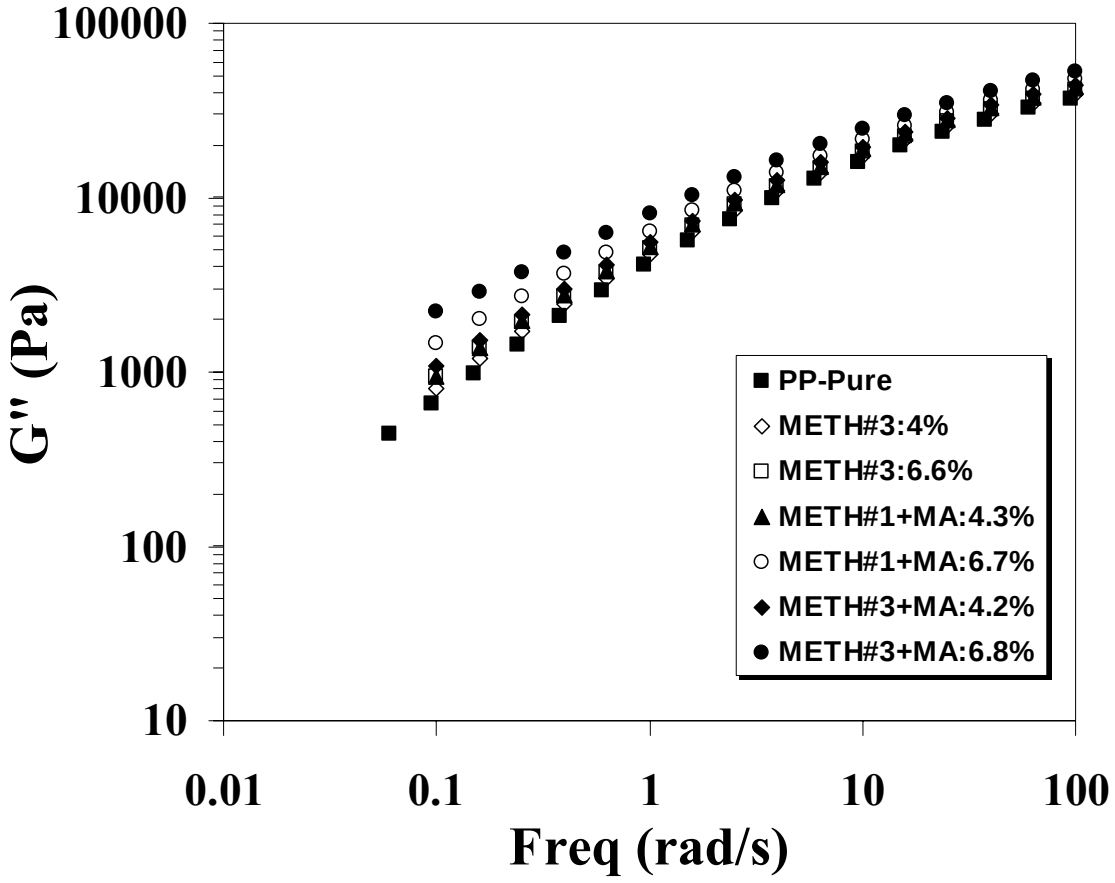

Figure 5.8: Loss modulus versus frequency of different nanocomposites at 200^{o}C

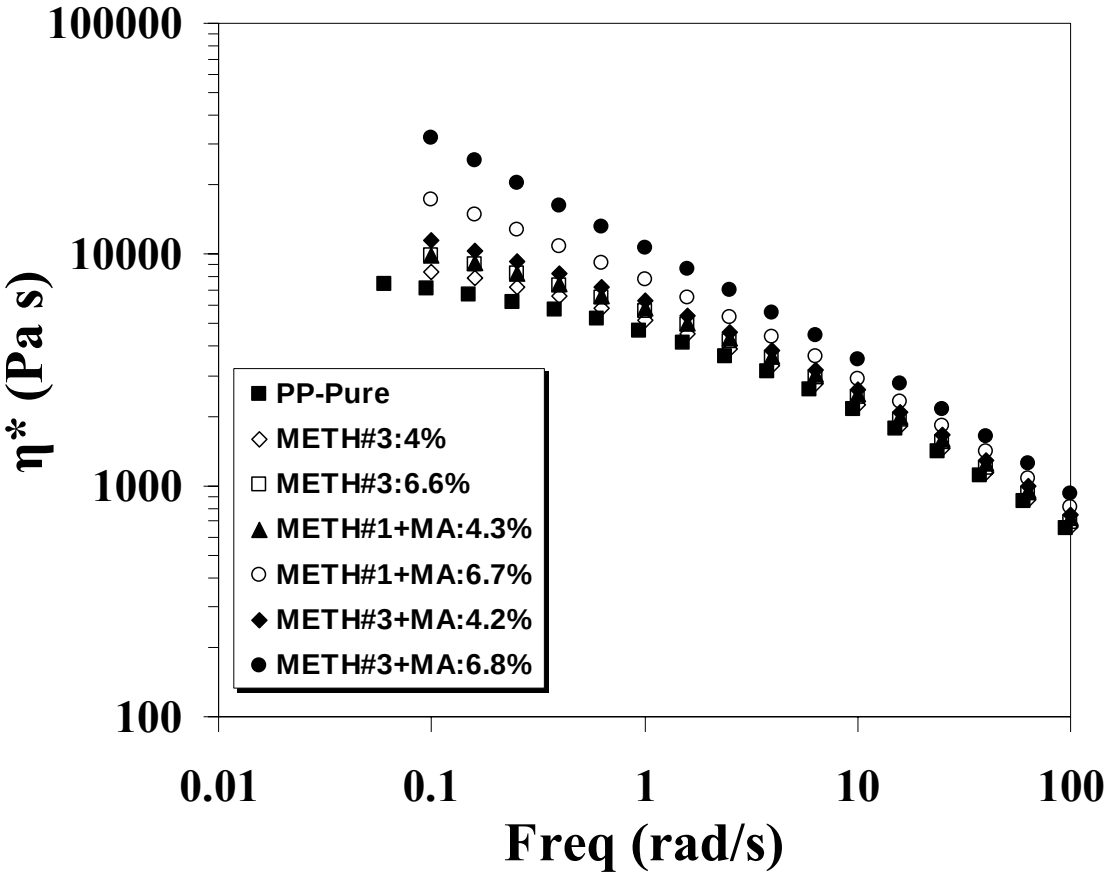

Figure 5.9: Complex viscosity versus frequency of different nanocomposites at 200^{o}C

6.0 Crystallization Behavior of the Nanocomposites

The crystallization behavior of the virgin polypropylene and nanocomposites was evaluated employing differential scanning calorimetry (DSC). The melting temperature (T_m), crystallization temperature (T_c), and the degree of crystallinity (X_c) of PP and the nanocomposites are shown in Table 6.1. The characteristic melting behavior is graphically illustrated in Figure 6.1, which shows peaks corresponding to melting temperatures of PP and the nanocomposites prepared using different processing methods. As can be seen from this figure, incorporating approximately 6.5 wt% nanoclays (exfoliated or non-exfoliated) into PP did not affect the melting temperature significantly. Overall, T_m of the nanocomposites decreased slightly compared to pure PP, which could be due to the low molecular weight surface modifier of the clay. Similar behavior has also been observed by Koo et al. and Lei et al. for PP [1, 2] and by Mohanty et al. and Liu et al. for polyamide-6 [3, 4].

Crystallization temperature was investigated by employing DSC cooling scans as illustrated in Figure 6.2. It was observed that incorporation of nanoclay in PP significantly increased the T_c, from 109 ^oC to about 116 ^oC. This indicates that the nanoclay acts as a nucleating agent in the crystallization of PP and contributes to rise of the crystallization temperature. The extent of increase of T_c varied slightly with the methods used to prepare the nanocomposites. In general, the most increase in the T_c was exhibited from samples prepared using method 3 and the RTP sample, which suggests that the degree of clay dispersion has some effect on the crystallization temperature.

The degree of crystallinity (X_c) was calculated from the heat of fusion (ΔH_f) on the second heating as follows:

$$X_c = \frac{\Delta H_f}{\Delta H_o\left(1 - \Phi_{clay}\right)}, \tag{6.1}$$

where ΔH_o, taken as 208 J/g [5], represents the heat of fusion of 100% crystalline PP and Φ_{clay} is the volume fraction of organoclay in the nanocomposite. It is evident from Table 6.1 that the degree of crystallinity of the matrix polymer decreased with incorporation of organoclay. X_c of the RTP nanocomposite and the compatibilized composite prepared using method 3 decreased the most. The decrease may be attributed to the reduction in the mobility of crystallizable polymer chain segments resulted from higher interfacial area and adhesion between the exfoliated clay and the PP-g-MA matrix. This decrease in X_c may counteract the reinforcement potential of exfoliated clay in the matrix which may have deleterious effect on the mechanical properties of the composites. The degree of the negative effect is yet to be determined and needs further investigation.

6.1 References

[1] Koo CM, Kim JH, Wang KH, Chung IJ. J Polym Sci: Part B: Polym Phys 2005; 43: 158-167.

[2] Lei SG, Hoa SV, Ton-That MT. Composites Sci & Tech 2006; 66: 1274-1279.

[3] Mohanty S, Nayak SK. Polymer Composites 2007; 28: 153-162.

[4] Liu X, Wu Q, Berglund LA, Lindberg H, Fan J, Qi Z. J Appl Polym Sci 2003; 88: 953.

[5] Moore EP, editor. Polypropylene Handbook: Polymerization, Characterization, Properties, Processing, Applications. Hanser/Gardner: Munich; 1996.

Table 6.1: Crystallization and melting behavior of the composites prepared via different processing techniques

Materials	T_c (^oC)	T_m (^oC)	X_c (%)
PP - Pure	108.9	163.0	39.2
METH#1: 6.7wt%	114.2	161.5	39.8
METH#3: 6.6wt%	114.7	163.1	37.5
METH#1+MA: 6.7wt%	112.5	162.4	37.8
METH#3+MA: 6.8wt%	116.3	162.0	35.5
RTP: 6.5wt%	116.1	163.0	33.5

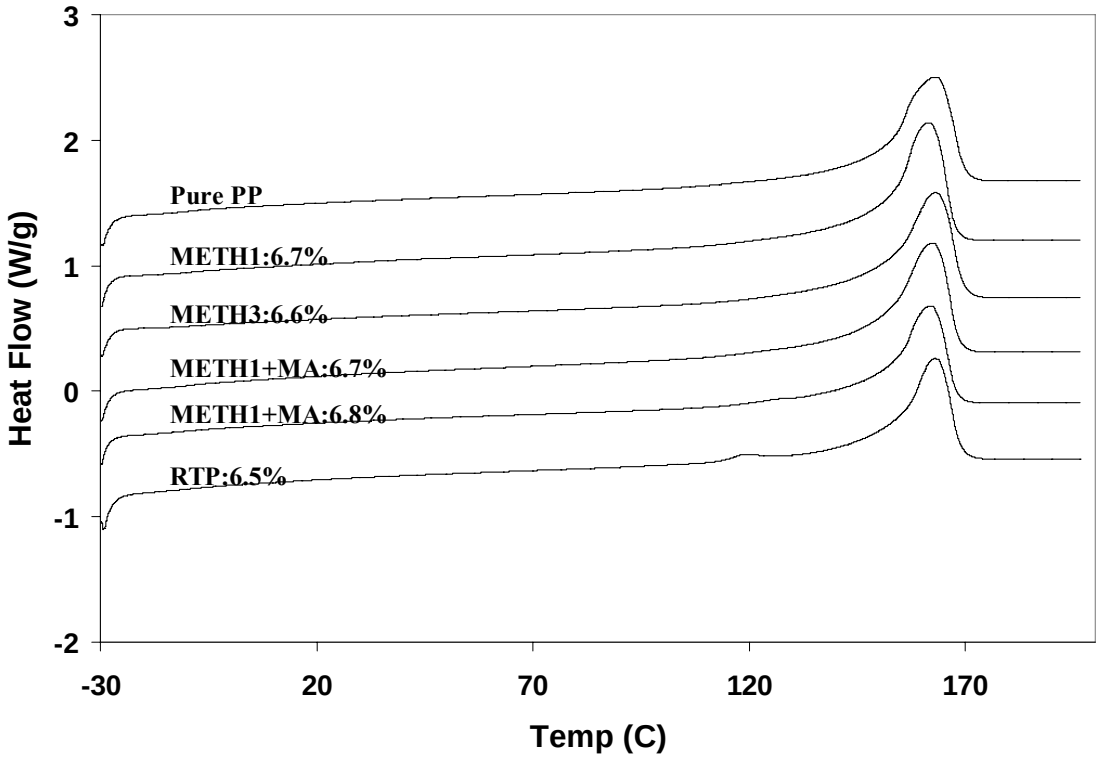

Figure 6.1: DSC heating scans of pure PP and different composites prepared using different processing techniques.

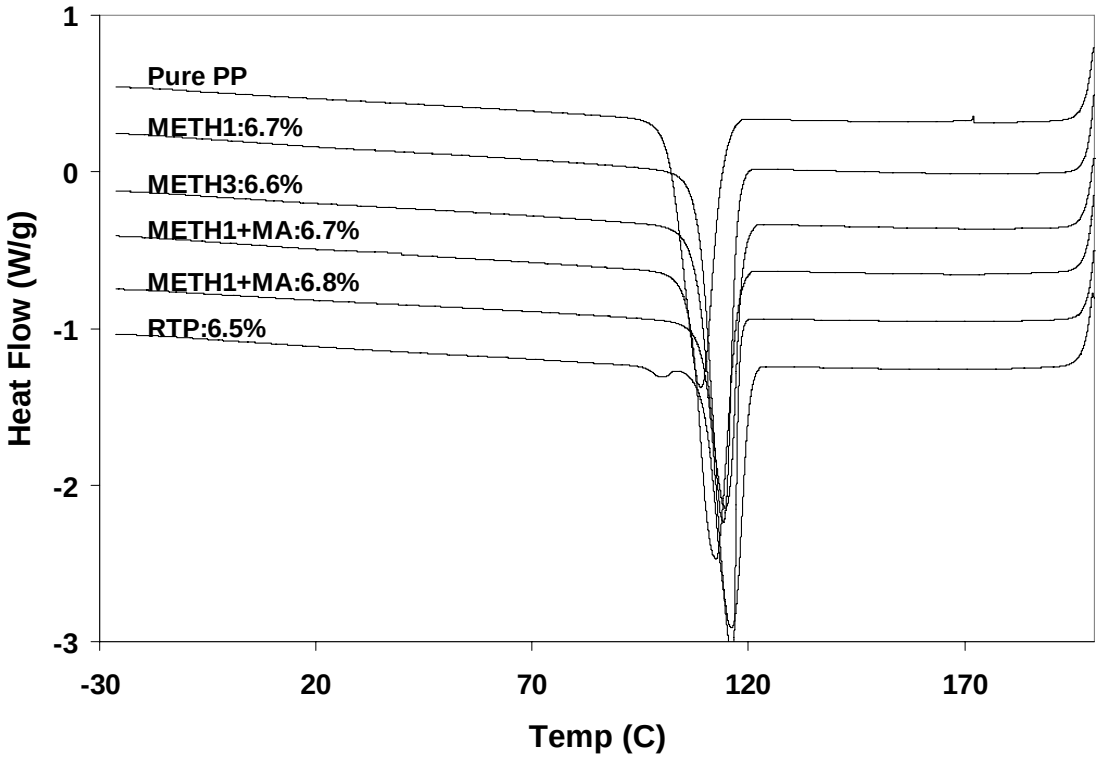

Figure 6.2: DSC cooling scans of pure PP and different composites prepared using different processing techniques.

7.0 Overall Conclusions

In this work, an environmentally benign process was developed to help exfoliate and disperse nano-clay into the polymer matrices at high clay content. The process involved the use of a pressurized CO_2 chamber to assist in the exfoliation and delivery of the clay into a stream of polymer melt in the extruder. By allowing the clay to be in direct contact with sc-CO_2, expanding via quick pressure release, and injecting the mixture into the polymer melt, great improvement in the exfoliation of the clay in the polymer matrix was observed. The presence of exfoliated clay greatly enhanced the mechanical and rheological properties of the nanocomposites. Exfoliated clay structures were achieved for clay concentrations as high as 6.7 wt% when the CO_2 chamber technique was employed, while most melt intercalation techniques in literature have achieved exfoliated structures only up to 4 wt% clay (except for Nylon-6 systems). Significant enhancement of mechanical properties such as Young's Modulus has been achieved for non-compatibilized and compatibilized polypropylene (PP)-clay nanocomposites. It was shown that the mechanical properties of the PP nanocomposites prepared using the CO_2 chamber technique, especially when combined with maleic anhydride (MA) compatibilizer, outperformed those of the commercial RTP nanocomposites and those of nanocomposites prepared using conventional melt compounding techniques. For concentrations as high as 6.7 wt% clay, Young's moduli of non-compatibilized and compatibilized polypropylene nanocomposites prepared using CO_2 chamber technique increased as much as 54% and 69%, respectively. Also, increase in the crystallization temperature, enhanced polymer crystallization rate, and reduction in the degree of crystallinity were also observed. Furthermore, it was shown that the enhancement in

dynamic rheological properties at low frequencies was attributed to polymer-clay interaction due to strong hydrogen bonding between polar anhydride functional group and the hydroxyl groups on the clay surface, not just solely to the formation of percolation network due to exfoliation between clay platelets that is commonly reported in literature for clay-filled functionalized polypropylene.

8.0 Recommendations for Future Work

1. Limited to the current physical design of the CO_2/clay chamber, it was not possible to deliver exfoliated clay content higher than 6.7 wt% into the polymer melt within the extruder. Thus, it is recommended that the chamber be designed bigger so that it can hold more clay and have larger volume to expand the clay.

2. Another limitation of the technique at present is maintaining a uniform concentration of the nano-particles and metering the clays into the extruder. To meter the clay flow rate, it is recommended to add a constant displacement pump into the current setup. To precisely meter the flow of carbon dioxide and exfoliated nanoparticles into the extruder, a Teledyne Isco syringe pump has been selected. Pump model 500D has a 507 ml capacity, and a maximum pressure of 3,750 psi. It has a minimum and maximum flow of 0.001 and 204 ml/min, respectively. It can be operated in constant flow or constant pressure modes, and it is designed to handle supercritical fluids and mixtures. The syringe pump would be placed downstream of the saturation chamber. Once the nanoparticles have been exposed to supercritical carbon dioxide in the saturation chamber, the mixture would be rapidly expanded into the pump's cylinder and then precisely dispensed into the melt within the extruder at the desired rate with some additional expansion.

3. Also, in order to maintain the homogeneity of the nanoparticles/supercritical fluid mixture within the pump and to maintain constant mass flow rates of nanoparticles

and carbon dioxide into the extruder, it is recommended to use a mixing mechanism within or about the pump to prevent the settling of nanoparticles within the solid/fluid mixture. A magnetically driven fan or stir bar could be used within the pump's cylinder, or the entire pump could be set on its side and gently rocked on a motor-driven platform. Employing one of these methods should effectively distribute the particles in suspension.

4. The current process has only one injection port of clay/CO_2 into the extruder. Trying to inject a large amount of clay into a small area can result in physical jam that may lead to poor dispersion of the clay. Therefore, it is recommended that the process have multiple injection ports along the extruder so that higher clay content can be delivered and distributed evenly into the polymer melt.

5. The current process uses a single-screw extruder for preparing the nanocomposites. Most studies have used a twin-screw extruder (TSE) and reported some success due to higher shear forces and better mixing capability. Thus, it could be useful to employ a TSE into this process. While a greater shear force is encountered in a twin screw extruder, it is unclear whether the increased shear leads to greater separation and thus exfoliation of the high aspect ratio clay platelets or whether the twin screw extruder simply beats the clay so much that the aspect ratio of MMT is lost. Thus, it would be beneficial to compare the degree of dispersion as well as mechanical property enhancements of the nanocomposites compounded in a twin-screw extruder to those of the nanocomposites generated in by a single screw extruder.

Appendix A: Preliminary Experiments

A.1 Effects of clay types on the mechanical properties

Four different types of clays were initially examined in this study to determine their effect on the mechanical properties of polypropylene matrix. Better compatibility between the clay and the polymer would presumably give better dispersion and, hence, better property improvements. Because of the availability and the quick results that can be obtained an Instron machine, mechanical testings were used to determine the compatibility between the clay and polypropylene. The clay that gave the most property enhancement was used in the subsequent experiments through out this work. The examined clays were Cloisite Na^+, 20A, 93A, and 30B. The properties of these clays are summarized in Table A.1 and Figure A.1. Conventional direct melt compounding using a single-screw extruder was used to prepare the nanocomposites. A concentration of 4 wt% was used for all clays. The extruded pellets were dried at 100°C in an oven overnight and then were injection molded using an Arburg Allrounder Model 221-55-250 injection molder for mechanical testings.

The properties of the resulting nanocomposites prepared using different clays are illustrated in Table A.2 and Figure A.2. As can be seen, the nanocomposite prepared using Cloisite 20A were preferred over Cloisite Na+, 93A, and 30B because it yielded the most property improvements. Similar observations can also be found in other studies [1, 2]. The effect of clay types is important, but it is not a major concern of this study because we are only interested in looking at the effectiveness of the new CO_2 technique in dispersing the nanoclay. However, future work should investigate other clay types and surface treatments in order to obtain optimized property improvements.

Table A.1: Properties of different clay types (from Southern clay products)

Treatment/Properties:	Organic Modifier (1)	Modifier Concentration	% Moisture	% Weight Loss on Ignition
Cloisite® Na+	None	None	4-9%	7%
Cloisite® 20A	2M2HT	95 meq/100g clay	< 2%	38%
Cloisite® 93A	M2HT	90 meq/100g clay	< 2%	38%
Cloisite® 30B	MT2EtOT	90 meq/100g clay	< 2%	30%

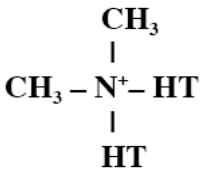

a) T is Tallow (~65% C18; ~30% C16; ~5% C14)
Anion: Chloride
(1) 2M2HT: dimethyl, dehydrogenated tallow, quaternary ammonium

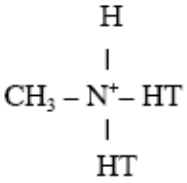

b) T is Tallow (~65% C18; ~30% C16; ~5% C14)
Anion: HSO4
(1) M2HT: methyl, dehydrogenated tallow ammonium

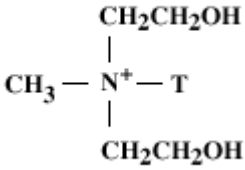

c) Where T is Tallow (~65% C18; ~30% C16; ~5% C14)
Anion: Chloride
(1) MT2EtOH: methyl, tallow, bis-2-hydroxyethyl, quaternary ammonium

Figure A.1: a) Cloisite 20A, b) Cloisite 93A, c) Cloisite 30B

Table A.2: Properties of different nanocomposites prepared using different clay types.

Materials	Young's Modulus (GPa)	S.D.	% Increase	Yield Strength (MPa)	S.D.	% Elongation	S.D.
PP - Pure	1.374	0.133	-	15.16	0.47	115.30	19.79
PP-20A: 4wt%	1.611	0.059	17	13.68	0.32	32.00	28.71
PP-Na+: 4wt%	1.439	0.086	5	11.70	0.30	62.98	12.07
PP-93A: 4wt%	1.540	0.069	12	15.10	0.50	6.91	2.56
PP-30B: 4wt%	1.534	0.119	12	15.30	0.72	8.33	2.71

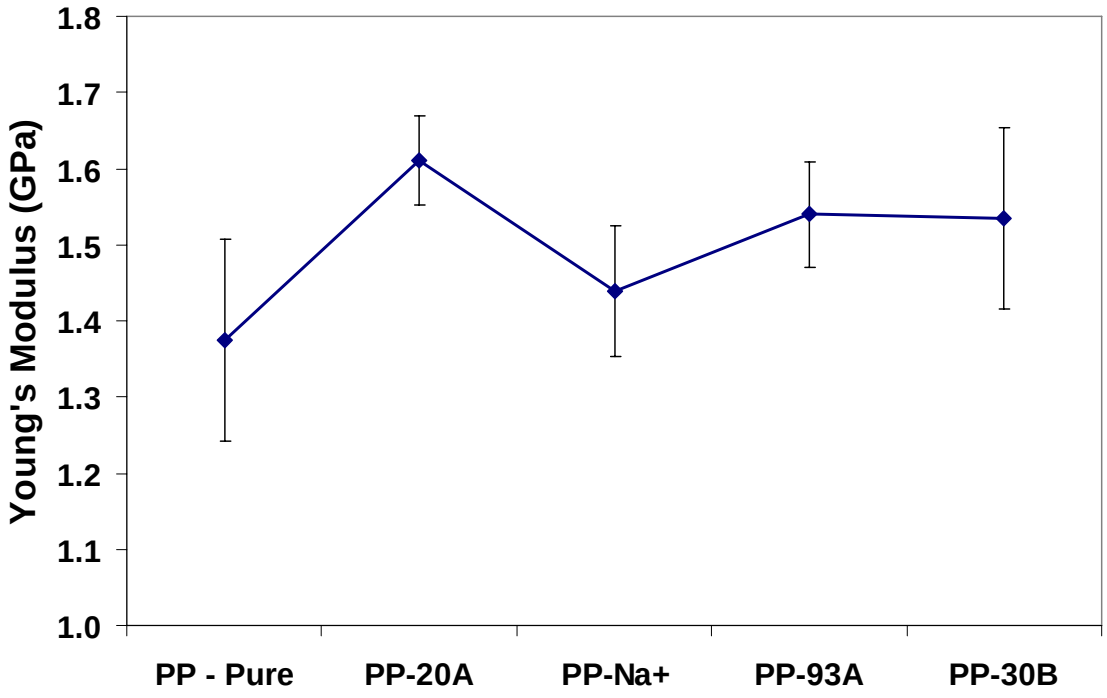

Figure A.2: Young's moduli of different nanocomposites prepared using different clay types at 4wt%.

A.2 References

[1] Lopez-Quintanilla ML, Sanchez-Valdes S, Ramos de Valle LF, Medellin-Rodriguez FJ. Effect of some compatibilizing agents on clay dispersion of polypropylene-clay nanocomposites. J Appl Polym Sci; 100: 4748-4756 (2006).

[2] Zhu L, Xanthos M., Effects of process conditions and mixing protocols on structure of extruded polypropylene nanocomposites. J Appl Polym Sci, 93, 1891-1899 (2004).

Appendix B: Mechanical Properties

Table B.1: Tensile properties of various nanocomposites prepared using different processing methods.

Materials	Young's Modulus (GPa)	S.D.	% Increase	Yield Strength (MPa)	S.D.	% Elongation	S.D.
PP - Pure	1.374	0.133	-	15.16	0.47	115.30	19.79
METH#1: 4wt%	1.611	0.059	17	13.68	0.32	32.00	28.71
METH#1: 6.7wt%	1.753	0.045	28	14.61	0.35	26.89	15.41
METH#1: 10wt%	1.726	0.130	26	12.13	0.77	16.59	2.42
METH#1: 14wt%	1.787	0.037	30	12.29	0.34	10.16	0.77
METH#2: 4wt%	1.716	0.136	25	14.28	0.39	34.59	6.92
METH#2: 6.7wt%	1.810	0.122	32	14.50	0.33	24.09	13.92
RTP_TSE: 4wt%	1.769	0.167	29	14.30	0.56	48.85	33.77
RTP_TSE: 6.5wt%	1.861	0.068	35	14.00	0.42	17.67	5.57
RTP_TSE: 10wt%	1.850	0.185	35	11.58	0.48	4.11	2.45
METH#3: 4wt%	1.848	0.107	34	16.10	0.32	80.40	0.10
METH#3: 6.6wt%	2.118	0.077	54	13.00	0.89	14.82	5.90

Table B.2: Tensile properties of various nanocomposites prepared with the incorporation of MA compatibilizer using different processing methods.

Materials	Young's Modulus (GPa)	S.D.	% Increase	Yield Strength (MPa)	S.D.	% Elongation	S.D.
PP - Pure	1.374	0.133	-	15.16	0.47	115.3	19.79
METH#1+MA: 4.3wt%	1.916	0.023	39	16.68	0.38	17.06	13.21
METH#1+MA: 6.7wt%	2.073	0.076	51	18.21	0.64	11.62	4.75
METH#1+MA: 12wt%	2.158	0.195	57	15.84	0.84	17.78	10.31
METH#3+MA: 4.2wt%	2.020	0.134	47	17.15	0.47	16.23	4.92
METH#3+MA: 6.8wt%	2.326	0.093	69	17.03	0.24	7.13	2.30

Appendix C: Dynamic Mechanical Thermal Analysis Data

Table C.1: Raw DMTA Data for pure PP

time s	G' Pa	3G' Pa	G" Pa	tan_delta	Temp °C
7	1.79E+08	5.38E+08	2.01E+07	0.11201	60.02
23	1.79E+08	5.37E+08	1.99E+07	0.11126	60.09
38	1.77E+08	5.31E+08	1.97E+07	0.11117	60.58
54	1.74E+08	5.22E+08	1.94E+07	0.11167	61.69
71	1.70E+08	5.10E+08	1.91E+07	0.11239	62.93
88	1.65E+08	4.96E+08	1.88E+07	0.11377	64.22
107	1.60E+08	4.81E+08	1.84E+07	0.115	65.58
124	1.55E+08	4.65E+08	1.80E+07	0.11649	67.04
143	1.49E+08	4.48E+08	1.77E+07	0.11847	68.52
161	1.43E+08	4.30E+08	1.72E+07	0.12028	70.14
180	1.37E+08	4.12E+08	1.67E+07	0.12165	71.72
201	1.32E+08	3.95E+08	1.62E+07	0.1233	73.32
221	1.25E+08	3.75E+08	1.58E+07	0.1259	75
245	1.20E+08	3.61E+08	1.51E+07	0.12553	77.09
265	1.16E+08	3.47E+08	1.46E+07	0.12578	78.64
285	1.11E+08	3.34E+08	1.40E+07	0.12603	80.41
306	1.07E+08	3.22E+08	1.35E+07	0.12552	81.95
326	1.03E+08	3.10E+08	1.29E+07	0.12479	83.8
346	9.98E+07	2.99E+08	1.24E+07	0.12427	85.39
366	9.63E+07	2.89E+08	1.19E+07	0.12355	87.02
387	9.27E+07	2.78E+08	1.14E+07	0.12305	88.83
408	8.96E+07	2.69E+08	1.09E+07	0.12215	90.62
428	8.66E+07	2.60E+08	1.05E+07	0.12082	92.1
448	8.36E+07	2.51E+08	1.00E+07	0.12008	93.81
469	8.06E+07	2.42E+08	9.66E+06	0.11977	95.64
489	7.79E+07	2.34E+08	9.23E+06	0.11851	97.02
511	7.49E+07	2.25E+08	8.84E+06	0.11805	98.98
533	7.20E+07	2.16E+08	8.43E+06	0.117	100.75
554	6.89E+07	2.07E+08	8.14E+06	0.11804	102.57
579	6.56E+07	1.97E+08	7.72E+06	0.11767	104.63
605	6.25E+07	1.88E+08	7.33E+06	0.11723	106.79
639	5.92E+07	1.77E+08	6.89E+06	0.11655	109.39
659	5.69E+07	1.71E+08	6.68E+06	0.11729	111.03
685	5.41E+07	1.62E+08	6.30E+06	0.11637	113.34
712	5.15E+07	1.54E+08	5.97E+06	0.11599	115.52
740	4.88E+07	1.46E+08	5.63E+06	0.1155	117.86
767	4.62E+07	1.39E+08	5.34E+06	0.1155	120.07
801	4.32E+07	1.30E+08	4.97E+06	0.11519	122.96
835	4.01E+07	1.20E+08	4.73E+06	0.11785	125.72
867	3.74E+07	1.12E+08	4.42E+06	0.1181	128.35
899	3.48E+07	1.04E+08	4.14E+06	0.11921	130.96
932	3.19E+07	9.58E+07	3.88E+06	0.1215	133.76
970	2.89E+07	8.68E+07	3.59E+06	0.12411	136.8
1010	2.55E+07	7.65E+07	3.28E+06	0.12863	140.12
1052	2.20E+07	6.59E+07	2.92E+06	0.13273	143.46
1097	1.83E+07	5.50E+07	2.53E+06	0.13795	147.15
1143	1.46E+07	4.38E+07	2.03E+06	0.13901	150.98

Table C.2: Raw DMTA Data for METH#1: 4%

time s	G' Pa	3G' Pa	G" Pa	tan_delta	Temp °C
7	2.14E+08	6.41E+08	2.59E+07	0.12107	60.03
22	2.13E+08	6.39E+08	2.57E+07	0.12063	60.07
37	2.11E+08	6.33E+08	2.55E+07	0.1207	60.52
52	2.08E+08	6.23E+08	2.52E+07	0.12144	61.52
69	2.03E+08	6.09E+08	2.49E+07	0.12243	62.68
86	1.98E+08	5.93E+08	2.46E+07	0.12442	63.93
104	1.91E+08	5.74E+08	2.42E+07	0.12665	65.38
121	1.85E+08	5.54E+08	2.39E+07	0.12963	66.81
139	1.78E+08	5.34E+08	2.35E+07	0.13222	68.27
157	1.71E+08	5.14E+08	2.32E+07	0.13522	69.75
175	1.65E+08	4.94E+08	2.27E+07	0.13758	71.25
194	1.58E+08	4.75E+08	2.21E+07	0.13994	72.92
213	1.52E+08	4.57E+08	2.16E+07	0.14187	74.39
232	1.47E+08	4.40E+08	2.10E+07	0.14302	75.91
251	1.41E+08	4.24E+08	2.03E+07	0.14405	77.51
270	1.36E+08	4.09E+08	1.97E+07	0.14435	79.16
288	1.32E+08	3.95E+08	1.90E+07	0.14432	80.64
308	1.27E+08	3.82E+08	1.83E+07	0.14399	82.28
327	1.23E+08	3.69E+08	1.77E+07	0.14418	83.87
347	1.19E+08	3.56E+08	1.71E+07	0.14405	85.52
361	1.15E+08	3.45E+08	1.67E+07	0.14517	86.72
384	1.12E+08	3.35E+08	1.61E+07	0.14383	88.59
404	1.08E+08	3.24E+08	1.54E+07	0.1428	90.23
423	1.05E+08	3.14E+08	1.49E+07	0.14218	91.76
442	1.01E+08	3.04E+08	1.45E+07	0.1427	93.37
461	9.81E+07	2.94E+08	1.39E+07	0.14143	94.91
480	9.50E+07	2.85E+08	1.34E+07	0.14154	96.4
499	9.19E+07	2.76E+08	1.29E+07	0.14084	98.09
518	8.91E+07	2.67E+08	1.25E+07	0.14013	99.57
537	8.63E+07	2.59E+08	1.20E+07	0.13969	101.02
551	8.35E+07	2.50E+08	1.18E+07	0.14134	102.3
574	8.07E+07	2.42E+08	1.12E+07	0.13895	104.12
594	7.79E+07	2.34E+08	1.09E+07	0.13944	105.75
613	7.53E+07	2.26E+08	1.04E+07	0.13858	107.33
632	7.26E+07	2.18E+08	1.01E+07	0.1387	108.99
652	7.00E+07	2.10E+08	9.64E+06	0.1377	110.66
671	6.76E+07	2.03E+08	9.34E+06	0.13819	112.21
692	6.50E+07	1.95E+08	8.96E+06	0.13779	113.95
712	6.27E+07	1.88E+08	8.59E+06	0.13717	115.56
732	6.03E+07	1.81E+08	8.23E+06	0.13639	117.23
753	5.78E+07	1.74E+08	7.97E+06	0.13783	118.91
774	5.55E+07	1.66E+08	7.64E+06	0.13766	120.56
796	5.31E+07	1.59E+08	7.28E+06	0.13706	122.47
818	5.08E+07	1.52E+08	6.99E+06	0.13758	124.18
840	4.82E+07	1.45E+08	6.66E+06	0.13809	126.16
863	4.59E+07	1.38E+08	6.31E+06	0.13745	128.05
888	4.35E+07	1.31E+08	6.08E+06	0.13982	130.07
913	4.10E+07	1.23E+08	5.73E+06	0.13969	132.1
937	3.85E+07	1.16E+08	5.47E+06	0.14203	134.18

Table C.3: Raw DMTA Data for METH#3: 4%

time s	G' Pa	3G' Pa	G" Pa	tan_delta	Temp °C
6	2.35E+08	7.06E+08	2.79E+07	0.11847	60.02
21	2.35E+08	7.04E+08	2.77E+07	0.11822	60.07
36	2.32E+08	6.97E+08	2.75E+07	0.11851	60.5
52	2.28E+08	6.85E+08	2.72E+07	0.11909	61.46
68	2.23E+08	6.70E+08	2.69E+07	0.12057	62.63
85	2.17E+08	6.52E+08	2.65E+07	0.12218	63.89
103	2.10E+08	6.31E+08	2.63E+07	0.12491	65.24
121	2.03E+08	6.08E+08	2.59E+07	0.12762	66.68
138	1.95E+08	5.85E+08	2.55E+07	0.13066	68.18
156	1.87E+08	5.62E+08	2.50E+07	0.13358	69.66
174	1.80E+08	5.39E+08	2.45E+07	0.13656	71.22
193	1.72E+08	5.17E+08	2.39E+07	0.13854	72.82
213	1.65E+08	4.96E+08	2.33E+07	0.14056	74.26
232	1.59E+08	4.77E+08	2.26E+07	0.14217	75.89
251	1.53E+08	4.58E+08	2.18E+07	0.14293	77.5
270	1.47E+08	4.41E+08	2.11E+07	0.14323	79.08
289	1.41E+08	4.24E+08	2.02E+07	0.14326	80.8
310	1.35E+08	4.06E+08	1.97E+07	0.14517	82.37
334	1.30E+08	3.89E+08	1.87E+07	0.14418	84.41
358	1.24E+08	3.72E+08	1.78E+07	0.14368	86.42
383	1.20E+08	3.60E+08	1.71E+07	0.1426	88.47
404	1.16E+08	3.47E+08	1.64E+07	0.14199	90.22
425	1.12E+08	3.35E+08	1.57E+07	0.14081	91.98
444	1.08E+08	3.24E+08	1.52E+07	0.14069	93.5
463	1.04E+08	3.13E+08	1.46E+07	0.14019	95.09
482	1.01E+08	3.02E+08	1.41E+07	0.14024	96.59
503	9.71E+07	2.91E+08	1.36E+07	0.13982	98.32
521	9.39E+07	2.82E+08	1.31E+07	0.13936	99.81
540	9.07E+07	2.72E+08	1.26E+07	0.13879	101.29
560	8.72E+07	2.62E+08	1.21E+07	0.13885	103.13
579	8.41E+07	2.52E+08	1.16E+07	0.13845	104.52
598	8.09E+07	2.43E+08	1.12E+07	0.13795	106.18
622	7.71E+07	2.31E+08	1.08E+07	0.13982	108.06
640	7.44E+07	2.23E+08	1.04E+07	0.14038	109.45
660	7.15E+07	2.14E+08	1.01E+07	0.14112	111.24
684	6.83E+07	2.05E+08	9.55E+06	0.13982	113.2
709	6.53E+07	1.96E+08	9.13E+06	0.13982	115.27
734	6.20E+07	1.86E+08	8.64E+06	0.13938	117.38
763	5.88E+07	1.76E+08	8.15E+06	0.13851	119.66
797	5.44E+07	1.63E+08	7.55E+06	0.13882	122.69
829	5.11E+07	1.53E+08	7.06E+06	0.1382	125.21
858	4.78E+07	1.43E+08	6.65E+06	0.13913	127.59
890	4.44E+07	1.33E+08	6.20E+06	0.13982	130.34
923	4.11E+07	1.23E+08	5.72E+06	0.13919	132.98
957	3.74E+07	1.12E+08	5.34E+06	0.1428	135.73
995	3.34E+07	1.00E+08	4.99E+06	0.14935	139
1035	2.89E+07	8.66E+07	4.43E+06	0.15353	142.21
1076	2.50E+07	7.49E+07	3.95E+06	0.15807	145.48
1122	2.06E+07	6.18E+07	3.21E+06	0.15597	149.45

Table C.4: Raw DMTA Data for METH#3: 6.6%

time s	G' Pa	3G' Pa	G" Pa	tan_delta	Temp °C
6	2.74E+08	8.22E+08	3.40E+07	0.12402	60.05
21	2.73E+08	8.18E+08	3.39E+07	0.12437	60.08
37	2.70E+08	8.11E+08	3.36E+07	0.1242	60.52
53	2.66E+08	7.97E+08	3.31E+07	0.12472	61.53
69	2.60E+08	7.80E+08	3.27E+07	0.1259	62.75
86	2.53E+08	7.58E+08	3.23E+07	0.12789	64.04
104	2.45E+08	7.34E+08	3.20E+07	0.13087	65.45
121	2.36E+08	7.08E+08	3.17E+07	0.1341	66.84
139	2.27E+08	6.82E+08	3.13E+07	0.13782	68.32
153	2.19E+08	6.58E+08	3.09E+07	0.14101	69.52
175	2.11E+08	6.32E+08	3.04E+07	0.14443	71.17
193	2.02E+08	6.07E+08	2.98E+07	0.14711	72.81
213	1.94E+08	5.83E+08	2.90E+07	0.14929	74.45
232	1.87E+08	5.62E+08	2.82E+07	0.15065	75.96
251	1.81E+08	5.42E+08	2.74E+07	0.15166	77.48
270	1.74E+08	5.22E+08	2.66E+07	0.15277	79.06
289	1.68E+08	5.04E+08	2.58E+07	0.15339	80.7
309	1.62E+08	4.87E+08	2.49E+07	0.15366	82.44
328	1.57E+08	4.71E+08	2.42E+07	0.15403	84.02
347	1.52E+08	4.56E+08	2.34E+07	0.1538	85.49
367	1.47E+08	4.41E+08	2.26E+07	0.15402	87.14
386	1.42E+08	4.26E+08	2.19E+07	0.1542	88.81
406	1.37E+08	4.12E+08	2.11E+07	0.15378	90.33
426	1.33E+08	3.98E+08	2.04E+07	0.15348	92
445	1.28E+08	3.85E+08	1.97E+07	0.15328	93.62
465	1.24E+08	3.73E+08	1.91E+07	0.15366	95.17
484	1.20E+08	3.61E+08	1.85E+07	0.15353	96.82
504	1.16E+08	3.49E+08	1.78E+07	0.1533	98.31
524	1.12E+08	3.36E+08	1.72E+07	0.15368	100.1
543	1.08E+08	3.25E+08	1.66E+07	0.15303	101.79
563	1.05E+08	3.14E+08	1.60E+07	0.15307	103.21
582	1.01E+08	3.03E+08	1.55E+07	0.15316	104.91
603	9.72E+07	2.92E+08	1.49E+07	0.15366	106.51
622	9.36E+07	2.81E+08	1.44E+07	0.15353	108.07
642	8.98E+07	2.70E+08	1.38E+07	0.15378	109.99
662	8.67E+07	2.60E+08	1.33E+07	0.15328	111.44
682	8.34E+07	2.50E+08	1.28E+07	0.1537	112.96
703	8.00E+07	2.40E+08	1.23E+07	0.15398	114.89
723	7.69E+07	2.31E+08	1.18E+07	0.15404	116.54
743	7.39E+07	2.22E+08	1.14E+07	0.15389	118.03
764	7.05E+07	2.12E+08	1.09E+07	0.15515	119.93
785	6.75E+07	2.03E+08	1.04E+07	0.15428	121.69
808	6.43E+07	1.93E+08	1.00E+07	0.15583	123.54
830	6.12E+07	1.84E+08	9.55E+06	0.15589	125.34
852	5.82E+07	1.75E+08	9.05E+06	0.15541	127.15
876	5.49E+07	1.65E+08	8.79E+06	0.16029	129.28
901	5.18E+07	1.55E+08	8.29E+06	0.16004	131.11
925	4.88E+07	1.46E+08	7.81E+06	0.16011	133.21
951	4.54E+07	1.36E+08	7.44E+06	0.1638	135.32

Table C.5: Raw DMTA Data for RTP 10%

time s	G' Pa	3G' Pa	G" Pa	tan_delta	Temp °C
6	2.58E+08	7.75E+08	3.83E+07	0.14841	60.05
22	2.57E+08	7.72E+08	3.82E+07	0.14854	60.07
38	2.55E+08	7.64E+08	3.78E+07	0.14841	60.62
54	2.50E+08	7.51E+08	3.74E+07	0.14941	61.58
70	2.45E+08	7.34E+08	3.69E+07	0.15091	62.64
87	2.37E+08	7.12E+08	3.65E+07	0.15366	63.89
106	2.29E+08	6.88E+08	3.63E+07	0.15805	65.34
123	2.21E+08	6.62E+08	3.58E+07	0.16243	66.73
141	2.11E+08	6.34E+08	3.53E+07	0.16718	68.23
159	2.02E+08	6.06E+08	3.47E+07	0.1717	69.88
177	1.93E+08	5.79E+08	3.39E+07	0.17535	71.22
196	1.85E+08	5.54E+08	3.29E+07	0.1785	72.96
215	1.77E+08	5.30E+08	3.19E+07	0.18067	74.52
234	1.70E+08	5.10E+08	3.08E+07	0.18126	76.09
253	1.64E+08	4.92E+08	2.97E+07	0.18132	77.63
271	1.58E+08	4.75E+08	2.87E+07	0.18139	79.18
290	1.53E+08	4.59E+08	2.77E+07	0.18114	80.69
309	1.48E+08	4.44E+08	2.67E+07	0.18082	82.29
328	1.43E+08	4.30E+08	2.58E+07	0.18026	84.02
347	1.39E+08	4.17E+08	2.49E+07	0.17933	85.37
365	1.34E+08	4.03E+08	2.41E+07	0.17887	86.96
384	1.30E+08	3.91E+08	2.33E+07	0.17856	88.63
403	1.26E+08	3.79E+08	2.25E+07	0.17761	89.97
422	1.23E+08	3.68E+08	2.16E+07	0.17661	91.63
441	1.19E+08	3.56E+08	2.08E+07	0.17552	93.12
459	1.15E+08	3.45E+08	2.01E+07	0.17472	94.75
478	1.11E+08	3.34E+08	1.94E+07	0.17384	96.26
497	1.08E+08	3.24E+08	1.88E+07	0.17359	97.93
517	1.05E+08	3.14E+08	1.81E+07	0.17305	99.4
536	1.01E+08	3.04E+08	1.75E+07	0.17229	100.96
555	9.81E+07	2.94E+08	1.68E+07	0.1717	102.47
574	9.48E+07	2.84E+08	1.62E+07	0.17125	104.13
592	9.16E+07	2.75E+08	1.56E+07	0.17077	105.61
612	8.84E+07	2.65E+08	1.50E+07	0.17019	107.27
631	8.54E+07	2.56E+08	1.45E+07	0.16994	108.88
650	8.24E+07	2.47E+08	1.40E+07	0.16929	110.38
670	7.94E+07	2.38E+08	1.35E+07	0.16957	112.12
689	7.65E+07	2.30E+08	1.30E+07	0.1696	113.69
709	7.35E+07	2.21E+08	1.25E+07	0.16944	115.38
729	7.03E+07	2.11E+08	1.20E+07	0.17107	117.07
750	6.76E+07	2.03E+08	1.16E+07	0.17137	118.62
770	6.44E+07	1.93E+08	1.11E+07	0.1722	120.4
791	6.16E+07	1.85E+08	1.06E+07	0.17162	122.16
812	5.87E+07	1.76E+08	1.01E+07	0.17187	123.77
833	5.58E+07	1.67E+08	9.65E+06	0.17306	125.58
855	5.29E+07	1.59E+08	9.12E+06	0.17245	127.29
876	5.01E+07	1.50E+08	8.64E+06	0.17246	129.11
900	4.73E+07	1.42E+08	8.23E+06	0.17416	131.05
922	4.44E+07	1.33E+08	7.80E+06	0.17585	132.98

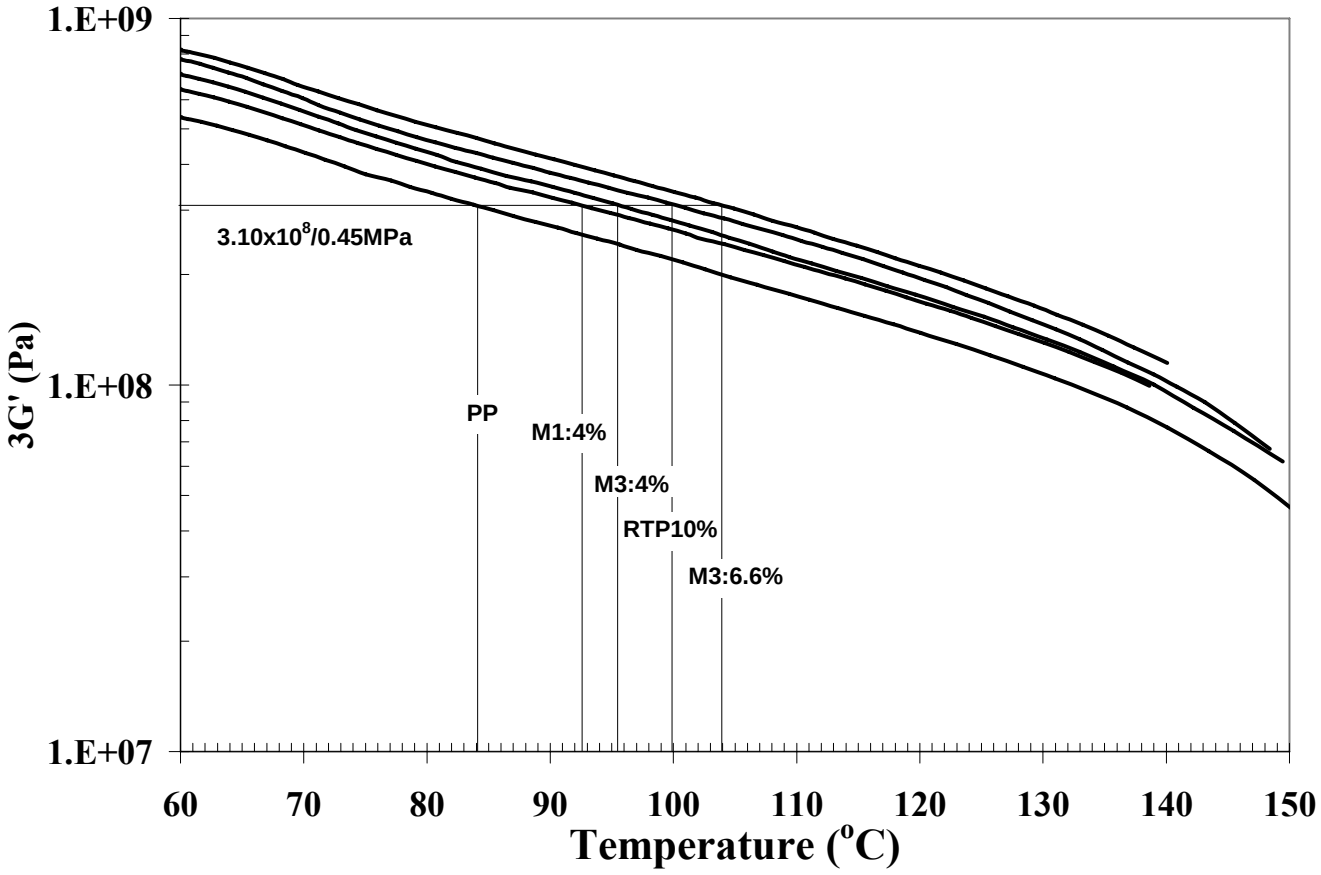

Figure C.1: 3G' as a function of temperature from DMTA. Vertical lines correspond to estimated HDTs.

Table C.6: Heat Distortion Temp for different nanocomposites

	Pure PP	METH#1 4wt%	METH#3 4wt%	RTP 10wt%	METH#3 6.6wt%
Heat distortion temp (C)	84	92.5	95.5	100	104
SD	2.3	3.1	3.2	2.1	1.9
% increase	0.0	10.1	13.7	19.0	23.8

Appendix D: Dynamic Oscillatory Rheometry Data

Table D.1: Dynamic Frequency Sweep Data at 200 C-Pure PP

Freq rad/s	G' Pa	G" Pa	tan_delta	Torque g-cm	Strain %	PhaseAngle °	Eta* Pa-s
0.06	73.4296	439.02	5.97879	0.69722	5.00685	80.505	7418.59
0.09509	137.262	663.375	4.83289	1.06118	5.00722	78.31	7123.71
0.15071	228.079	981.488	4.30329	1.57822	5.00649	76.918	6685.74
0.23887	390.49	1438.14	3.68291	2.33392	5.00621	74.809	6238.62
0.37859	665.061	2080.15	3.12776	3.41999	5.00571	72.27	5768.53
0.60002	1096.2	2951.21	2.69221	4.92988	5.00543	69.623	5246.85
0.95097	1760.99	4115.1	2.33681	7.00848	5.00493	66.832	4706.82
1.5072	2749.78	5628.38	2.04685	9.80551	5.00353	63.962	4156.17
2.38879	4183.72	7541.09	1.80248	13.4989	5.00341	60.979	3610.15
3.78601	6240.81	9920.74	1.58966	18.3424	5.00245	57.827	3095.72
6.00049	9032.07	12732.1	1.40966	24.4279	5.00199	54.648	2601.52
9.51025	12737.2	16025.6	1.25817	32.0382	5.00268	51.522	2152.5
15.0728	17534.6	19748.5	1.12626	41.3364	5.00314	48.398	1752.14
23.8887	23544.2	23810.4	1.01131	52.3855	5.00066	45.322	1401.72
37.8613	30919.6	28119.8	0.90945	65.135	4.98162	42.285	1103.87
60.0068	39635.8	32580.2	0.82199	78.7475	4.90598	39.42	855.028
95.1055	49671.1	36882.6	0.74254	90.9858	4.70094	36.595	650.511

Table D.2: Dynamic Frequency Sweep Data at 200 C-METH#1:4%

Freq rad/s	G' Pa	G" Pa	tan_delta	Torque g-cm	Strain %	PhaseAngle °	Eta* Pa-s
0.06	77.9066	444.659	5.70759	0.70692	5.0055	80.062	7523.82
0.09509	129.777	676.811	5.21517	1.07888	5.00422	79.145	7246.89
0.15071	236.263	1004.46	4.25147	1.61564	5.00481	76.764	6846.55
0.23887	401.759	1474.66	3.6705	2.39281	5.00425	74.76	6398.52
0.37859	682.742	2124.61	3.11188	3.49388	5.00449	72.185	5894.6
0.60002	1118.57	3017.07	2.69726	5.03773	5.00441	69.658	5362.73
0.95097	1795.17	4206.33	2.34313	7.15827	5.00312	66.888	4809.16
1.5072	2801.06	5757.61	2.05551	10.0192	5.00188	64.057	4248.15
2.38879	4277.94	7724.24	1.8056	13.8156	5.00138	61.021	3696.33
3.78601	6341.28	10146.3	1.60004	18.7196	5.00101	57.995	3160.29
6.00049	9188	13059	1.42131	24.9753	4.99977	54.871	2661.01
9.51025	12962.8	16449.1	1.26895	32.7584	4.99984	51.76	2202.14
15.0728	17843	20275.9	1.13635	42.2485	5.00003	48.652	1791.91
23.8887	23984	24505.3	1.02173	53.6039	4.99702	45.616	1435.37
37.8613	31488.4	28999.3	0.92095	66.6558	4.97724	42.644	1130.64
60.0068	40439.1	33610.1	0.83113	80.6338	4.90166	39.731	876.282
95.1055	50718.6	38123.4	0.75166	93.2317	4.69689	36.931	667.143

Table D.3: Dynamic Frequency Sweep Data at 200 C-METH#1:6.7%

Freq rad/s	G' Pa	G" Pa	tan_delta	Torque g-cm	Strain %	PhaseAngle °	Eta* Pa-s
0.1	162.025	717.31	4.42715	1.15174	5.00623	77.272	7353.79
0.15849	277.478	1074.26	3.87151	1.7374	5.00538	75.517	7000.57
0.25119	462.124	1556.03	3.36713	2.54184	5.00549	73.459	6462.05
0.39811	756.304	2247.78	2.97206	3.71386	5.00557	71.404	5957.16
0.63097	1222.51	3179.96	2.60118	5.33455	5.00513	68.971	5399.42
1.00003	1935.03	4420	2.2842	7.55289	5.00364	66.357	4824.86
1.58496	2991.08	6033.14	2.01705	10.5365	5.00151	63.629	4248.62
2.51202	4514.9	8052.08	1.78345	14.4454	5.00181	60.72	3674.92
3.98132	6663.18	10574.4	1.58699	19.5558	5.00132	57.784	3139.31
6.31006	9586.59	13584	1.41698	26.0119	5.00094	54.788	2634.86
10.0007	13484	17073.4	1.2662	34.036	5.00073	51.7	2175.43
15.8501	18482.3	21032.9	1.138	43.8044	5.00076	48.693	1766.53
25.1206	24776.1	25395	1.02498	55.4541	4.99611	45.707	1412.35
39.8135	32479.3	30047.7	0.92514	68.8154	4.97137	42.773	1111.35
63.1006	41600.4	34820.9	0.83703	82.8878	4.88382	39.93	859.743
100	52125.4	39495.4	0.7577	95.311	4.65851	37.151	653.983

Table D.4: Dynamic Frequency Sweep Data at 200 C-METH#1:24%

Freq rad/s	G' Pa	G" Pa	tan_delta	Torque g-cm	Strain %	PhaseAngle °	Eta* Pa-s
0.1	3637.82	4376.98	1.20319	8.89698	4.99686	50.269	56913.5
0.15849	4400.91	5260.73	1.19537	10.7168	4.99445	50.086	43276.2
0.25119	5305.91	6416.04	1.20923	13.004	4.99255	50.41	33145.3
0.39811	6431.13	7902.56	1.2288	15.9046	4.98969	50.861	25592.7
0.63097	7882.5	9764.83	1.2388	19.5749	4.98596	51.088	19889.1
1.00003	9781.04	12062.8	1.23328	24.2039	4.9818	50.963	15529.5
1.58496	12159.3	14841.1	1.22056	29.8706	4.97655	50.672	12105.1
2.51202	15264.7	18147.3	1.18884	36.8947	4.97321	49.931	9440.05
3.98132	19289.7	22086	1.14497	45.5632	4.96667	48.866	7365.34
6.31006	24254.3	26557.2	1.09495	55.8187	4.96087	47.595	5699.8
10.0007	30459.7	31603.8	1.03756	68.0319	4.95437	46.056	4388.97
15.8501	38152.4	37241.5	0.97612	82.5162	4.94717	44.308	3363.73
25.1206	47375.2	43315.5	0.91431	99.1158	4.9355	42.437	2555.36
39.8135	58449.7	49753.9	0.85123	117.765	4.90412	40.405	1927.94
63.1006	71363	56473.1	0.79135	137.044	4.81356	38.356	1442.22
100	8.62E+04	63067.6	0.7315	153.32	4.58786	36.185	1068.22

Table D.5: Dynamic Frequency Sweep Data at 200 C-METH#2:4%

Freq rad/s	G' Pa	G" Pa	tan_delta	Torque g-cm	Strain %	PhaseAngle °	Eta* Pa-s
0.1	145.96	720.173	4.93405	1.14922	4.99917	78.543	7348.13
0.15849	260.705	1081.6	4.14875	1.74013	4.99946	76.448	7019.88
0.25119	440.127	1580.07	3.59003	2.56545	4.99955	74.435	6529.81
0.39811	746.318	2274.36	3.04744	3.7433	4.99872	71.833	6012.62
0.63097	1220.93	3210.37	2.62944	5.37071	4.9982	69.178	5443.56
1.00003	1950.04	4471.42	2.29299	7.62659	4.99743	66.437	4877.99
1.58496	3032.35	6093	2.00934	10.6382	4.99639	63.542	4294.03
2.51202	4601.58	8129.49	1.76667	14.6043	4.99731	60.489	3718.7
3.98132	6796.13	10678.7	1.5713	19.7858	4.99646	57.527	3179.32
6.31006	9802.97	13672.4	1.39472	26.2952	4.99607	54.36	2666.16
10.0007	13765.1	17191.4	1.24891	34.4278	4.99687	51.316	2202.17
15.8501	18861.7	21128.5	1.12018	44.2795	4.99733	48.244	1786.91
25.1206	25274.4	25447.6	1.00685	56.0377	4.99421	45.196	1427.76
39.8135	33088.4	30013.4	0.90707	69.4944	4.97254	42.21	1122.05
63.1006	42312.4	34690	0.81985	83.7477	4.89257	39.347	867.108
100	52917.4	39210.4	0.74097	96.5444	4.68563	36.537	658.613

Table D.6: Dynamic Frequency Sweep Data at 200 C-METH#2:6.7%

Freq rad/s	G' Pa	G" Pa	tan_delta	Torque g-cm	Strain %	PhaseAngle °	Eta* Pa-s
0.1	194.113	822.384	4.23663	1.32295	76.719	5.00456	8449.79
0.15849	327.816	1201.62	3.66553	1.9502	74.74	5.00488	7858.8
0.25119	538.153	1744.29	3.24125	2.85782	72.854	5.00431	7267.07
0.39811	878.394	2477.72	2.82073	4.11471	70.48	5.00323	6603.24
0.63097	1402.35	3476	2.4787	5.86622	68.029	5.0027	5940.44
1.00003	2188.35	4797.21	2.19216	8.25	65.479	5.00133	5272.61
1.58496	3343.27	6498.51	1.94376	11.4295	62.776	4.99914	4610.89
2.51202	4996.13	8644.68	1.73027	15.6169	59.975	4.99961	3974.71
3.98132	7292.63	11265.1	1.54473	20.9825	57.082	4.9979	3370.64
6.31006	10424.1	14407.5	1.38213	27.8003	54.113	4.99703	2818.22
10.0007	14531.5	18037.7	1.24129	36.2081	51.145	4.9967	2316.13
15.8501	19798.2	22149.1	1.11874	46.4309	48.208	4.99583	1874.3
25.1206	26402.1	26637	1.0089	58.5628	45.254	4.99123	1492.98
39.8135	34418.1	31442.1	0.91353	72.4464	42.413	4.96748	1170.9
63.1006	43941.3	36398.7	0.82835	87.1621	39.637	4.88289	904.25
100	54887.6	41257.2	0.75167	100.195	36.931	4.66431	686.645

Table D.7: Dynamic Frequency Sweep Data at 200 C-METH#3: 4%

Freq rad/s	G' Pa	G" Pa	tan_delta	Torque g-cm	Strain %	PhaseAngle °	Eta* Pa-s
0.1	208.285	807.741	3.87806	1.3047	4.99953	75.541	8341.6
0.15849	342.688	1197.63	3.49482	1.94843	4.99968	74.032	7859.83
0.25119	560.894	1720.81	3.06797	2.83113	5.00003	71.947	7205.34
0.39811	897.618	2449.97	2.72941	4.08042	4.99878	69.878	6554.04
0.63097	1422.59	3422.76	2.40601	5.79647	4.99869	67.431	5874.51
1.00003	2199.7	4707.73	2.14017	8.12418	4.99755	64.956	5196.12
1.58496	3335.26	6357.48	1.90614	11.22	4.99559	62.318	4529.6
2.51202	4982.81	8428.17	1.69145	15.3032	4.99606	59.408	3897.63
3.98132	7210.97	10962.2	1.52021	20.5065	4.99559	56.663	3295.7
6.31006	10248.8	13974.8	1.36355	27.0822	4.99519	53.744	2746.43
10.0007	14235.2	17474.2	1.22753	35.2253	4.99573	50.832	2253.7
15.8501	19323.3	21400.6	1.1075	45.073	4.99676	47.92	1819.14
25.1206	25675.1	25685.6	1.00041	56.7438	4.99428	45.012	1445.73
39.8135	33419.4	30280.2	0.90607	70.1493	4.97217	42.179	1132.71
63.1006	42545.8	34963.9	0.82179	84.2921	4.8927	39.413	872.721
100	53045	39529.8	0.74521	96.9824	4.68604	36.694	661.542

Table D.8: Dynamic Frequency Sweep Data at 200 C-METH#3: 6.6%

Freq rad/s	G' Pa	G" Pa	tan_delta	Torque g-cm	Strain %	PhaseAngle °	Eta* Pa-s
0.1	291.262	951.326	3.26623	1.55752	72.977	5.00403	9949.11
0.15849	462.373	1365.73	2.95374	2.25705	71.296	5.00362	9097.62
0.25119	717.402	1939.74	2.70384	3.23707	69.703	5.00312	8233.4
0.39811	1106.74	2717.79	2.45568	4.59189	67.843	5.00183	7371.08
0.63097	1690.26	3758.48	2.22361	6.44842	65.786	5.00167	6531.36
1.00003	2541.67	5123.12	2.01565	8.94538	63.613	4.9998	5718.78
1.58496	3781.66	6862.5	1.81468	12.2509	61.143	4.99773	4943.65
2.51202	5525.96	9051.8	1.63805	16.5793	58.597	4.99707	4221.8
3.98132	7901.27	11696.8	1.48037	22.0606	55.961	4.99567	3545.4
6.31006	11103.8	14856.4	1.33796	28.9778	53.225	4.99404	2939.34
10.0007	15291.6	18527.7	1.21163	37.5271	50.466	4.99329	2402.13
15.8501	20637.7	22630.6	1.09656	47.8302	47.637	4.9918	1932.34
25.1206	27271.3	27158.7	0.99587	60.0434	44.881	4.98668	1532.13
39.8135	35345.4	31958.3	0.90417	73.9762	42.119	4.96238	1196.86
63.1006	44874.4	36928.4	0.82293	88.6839	39.452	4.87779	920.999
100	55841.1	41803.4	0.74861	101.683	36.819	4.65955	697.55

Table D.9: Dynamic Frequency Sweep Data at 200 C-RTP 4%

Freq rad/s	G' Pa	G" Pa	tan_delta	Torque g-cm	Strain %	PhaseAngle °	Eta* Pa-s
0.1	393.67	939.721	2.38708	1.59488	67.27	5.00369	10188.4
0.15849	574.376	1344.7	2.34115	2.28911	66.871	5.00403	9226.08
0.25119	834.679	1896.48	2.27211	3.24322	66.245	5.00323	8248.87
0.39811	1211.03	2664.23	2.19998	4.5801	65.556	5.00252	7351.13
0.63097	1762.31	3692.52	2.09527	6.40237	64.486	5.00183	6484.51
1.00003	2563.1	5066.89	1.97686	8.88314	63.167	5.00059	5678.1
1.58496	3734.12	6863.19	1.83797	12.2183	61.45	4.9986	4929.63
2.51202	5391.91	9187.2	1.70389	16.6596	59.592	4.99897	4240.63
3.98132	7734.75	12023.6	1.55449	22.3532	57.247	4.99778	3590.91
6.31006	10937.2	15527.4	1.41969	29.6854	54.84	4.99605	3009.92
10.0007	15195.6	19663.1	1.294	38.8371	52.303	4.99555	2484.86
15.8501	20755	24419.2	1.17655	50.0696	49.637	4.99397	2021.94
25.1206	27807	29765.4	1.07043	63.5788	46.948	4.98922	1621.51
39.8135	36560.5	35587.9	0.9734	79.2401	44.228	4.96438	1281.51
63.1006	47100.3	41758.7	0.88659	96.0658	41.56	4.87832	997.553
100	59402.6	47942.8	0.80708	111.193	38.906	4.65607	763.36

Table D.10: Dynamic Frequency Sweep Data at 200 C-RTP 6.5%

Freq rad/s	G' Pa	G" Pa	tan_delta	Torque g-cm	Strain %	PhaseAngle °	Eta* Pa-s
0.1	1698.29	1714.23	1.00938	3.77524	45.268	5.00092	24130.3
0.15849	2071.84	2249.06	1.08554	4.78261	47.349	4.99933	19294.1
0.25119	2533.16	2971.18	1.17291	6.10537	49.55	4.9983	15543.8
0.39811	3148.24	3934.83	1.24985	7.87884	51.337	4.99764	12658
0.63097	3968.93	5206.13	1.31172	10.2323	52.68	4.99615	10375.3
1.00003	5104.27	6868.28	1.3456	13.3686	53.382	4.9937	8557.01
1.58496	6639.01	9005.89	1.35651	17.4702	53.603	4.9911	7059.16
2.51202	8758.39	11703.4	1.33625	22.8189	53.19	4.98982	5819.12
3.98132	11637.4	15046.9	1.29298	29.6804	52.281	4.98749	4777.83
6.31006	15411.5	19106.1	1.23973	38.282	51.11	4.98501	3890.14
10.0007	20380.3	23863.7	1.17092	48.9183	49.502	4.98265	3137.97
15.8501	26772.8	29390.2	1.09777	61.9366	47.668	4.9798	2508.27
25.1206	34824.3	35604.9	1.02242	77.4815	45.635	4.97284	1982.59
39.8135	44765.3	42434.4	0.94793	95.4254	43.469	4.94515	1549.26
63.1006	56820.5	49705.1	0.87477	114.662	41.179	4.85496	1196.39
100	70874.8	57123	0.80597	131.675	38.868	4.62374	910.289

Table D.11: Dynamic Frequency Sweep Data at 200 C-RTP 10%

Freq rad/s	G' Pa	G" Pa	tan_delta	Torque g-cm	Strain %	PhaseAngle °	Eta* Pa-s
0.06	5815.85	3195.68	0.54948	10.3612	4.99086	28.788	1.11E+05
0.09509	6629.27	3763.91	0.56777	11.8963	4.98817	29.587	80165.1
0.15071	7431.41	4533.68	0.61007	13.5808	4.98675	31.386	57759.3
0.23887	8337.81	5565.28	0.66747	15.6311	4.98421	33.722	41966.7
0.37859	9443.67	6896.19	0.73024	18.2259	4.98208	36.139	30887.6
0.60002	10843.5	8593.15	0.79247	21.5521	4.97924	38.396	23058.5
0.95097	12586.1	10745.4	0.85375	25.7573	4.97504	40.489	17402.3
1.5072	14856.4	13427.2	0.9038	31.1377	4.9703	42.107	13286.3
2.38879	17771.1	16742.3	0.94211	37.9464	4.96793	43.293	10220.9
3.78601	21569.8	20773.8	0.9631	46.4933	4.96262	43.923	7909.85
6.00049	26373.1	25571	0.96959	56.9718	4.95744	44.115	6121.91
9.51025	32429.2	31168.9	0.96114	69.6933	4.95276	43.865	4729.58
15.0728	40064.9	37661.3	0.94001	85.0916	4.9465	43.229	3648.1
23.8887	49461.8	44952.4	0.90883	103.246	4.93773	42.266	2797.85
37.8613	61015.9	52981	0.86831	124.131	4.91017	40.968	2134.31
60.0068	74977.3	61689.5	0.82278	146.486	4.82254	39.447	1618.04
95.1055	91564	70847.4	0.77375	166.338	4.59258	37.731	1217.31

Table D.12: Dynamic Frequency Sweep Data at 200 C-METH1+MA: 4.3%

Freq rad/s	G' Pa	G" Pa	tan_delta	Torque g-cm	Strain %	PhaseAngle °	Eta* Pa-s
0.1	288.823	941.616	3.26018	1.54187	72.948	5.00403	9849.12
0.15849	456.503	1371.36	3.00405	2.26251	71.588	5.00367	9119.53
0.25119	723.515	1960.68	2.70993	3.27152	69.745	5.00371	8320.04
0.39811	1127.84	2754.78	2.44253	4.65952	67.735	5.00351	7477.13
0.63097	1740.29	3815.75	2.19259	6.56223	65.483	5.00158	6646.74
1.00003	2629.45	5211.08	1.98182	9.13184	63.225	5.00088	5836.72
1.58496	3925.04	6993.89	1.78186	12.5402	60.698	4.99807	5060.07
2.51202	5729.45	9237.53	1.61229	16.9949	58.191	4.99754	4327.22
3.98132	8244.53	11948.9	1.44931	22.6874	55.395	4.99544	3646.32
6.31006	11588.7	15180.1	1.3099	29.834	52.641	4.99338	3026.59
10.0007	15953.9	18926.8	1.18634	38.6584	49.872	4.99198	2475.2
15.8501	21531.3	23149.3	1.07515	49.3559	47.074	4.99024	1994.6
25.1206	28466.8	27777	0.97577	62.0189	44.297	4.98428	1583.3
39.8135	36862.2	32746.6	0.88835	76.4937	41.616	4.95895	1238.44
63.1006	46784.5	37894.9	0.80999	91.8017	39.007	4.87392	954.134
100	58179.2	42969	0.73856	105.299	36.448	4.65367	723.267

Table D.13: Dynamic Frequency Sweep Data at 200 C-METH#1+MA: 6.7%

Freq rad/s	G' Pa	G" Pa	tan_delta	Torque g-cm	Strain %	PhaseAngle °	Eta* Pa-s
0.1	924.06	1469.28	1.59002	2.71641	57.833	5.00255	17356.9
0.15849	1255.19	1997.21	1.59115	3.69073	57.852	5.00122	14883.6
0.25119	1692.14	2706.01	1.59917	4.99379	57.981	5.00152	12705.6
0.39811	2292.29	3648.39	1.59159	6.73927	57.859	4.99957	10823
0.63097	3129.44	4869.89	1.55615	9.05128	57.275	4.99803	9174.37
1.00003	4285.74	6444.04	1.5036	12.0971	56.373	4.99645	7738.84
1.58496	5872.41	8428.74	1.43531	16.0463	55.135	4.99298	6481.37
2.51202	8040.44	10872.1	1.35218	21.116	53.515	4.99152	5383.01
3.98132	10939.3	13841.4	1.26529	27.5343	51.68	4.9887	4431.29
6.31006	14727.5	17325.4	1.1764	35.4723	49.634	4.98639	3603.63
10.0007	19587.9	21351.9	1.09006	45.1761	47.467	4.98364	2897.35
15.8501	25681.3	25897.1	1.0084	56.8343	45.24	4.98109	2301.04
25.1206	33177.4	30896.8	0.93126	70.5512	42.962	4.97431	1804.73
39.8135	42274.2	36266.3	0.85788	86.1804	40.626	4.94577	1398.99
63.1006	52945.7	41893.7	0.79126	102.601	38.353	4.85756	1069.96
100	65205.6	47509.4	0.72861	116.941	36.077	4.63322	806.778

Table D.14: Dynamic Frequency Sweep Data at 200 C-METH3+MA: 4.2%

Freq rad/s	G' Pa	G" Pa	tan_delta	Torque g-cm	Strain %	PhaseAngle °	Eta* Pa-s
0.1	410.396	1073.19	2.61502	1.79862	69.073	5.00376	11489.8
0.15849	609.263	1527.29	2.50678	2.57412	68.252	5.00393	10375
0.25119	919.536	2150.96	2.33917	3.66174	66.853	5.00356	9312.73
0.39811	1368.48	2985.05	2.18129	5.13896	65.371	5.00232	8248.44
0.63097	2036.92	4105.54	2.01556	7.17116	63.612	5.00154	7263.57
1.00003	2998.43	5551.3	1.8514	9.86938	61.625	5.00009	6309.13
1.58496	4380.94	7400.85	1.68933	13.4469	59.377	4.99781	5426.19
2.51202	6303.25	9693.9	1.53792	18.077	56.967	4.99719	4603.06
3.98132	8905.03	12513.7	1.40524	24.0044	54.564	4.99579	3857.71
6.31006	12389.7	15830.9	1.27775	31.4075	51.952	4.994	3185.82
10.0007	16943.5	19658.4	1.16023	40.5365	49.242	4.99272	2595.06
15.8501	22689.2	23994.7	1.05754	51.5633	46.602	4.99102	2083.48
25.1206	29813.9	28719	0.96327	64.5595	43.928	4.98506	1647.9
39.8135	38457.7	33799.2	0.87887	79.463	41.311	4.96102	1285.98
63.1006	48640.1	39062.2	0.80309	95.1423	38.768	4.875	988.637
100	60325.8	44253.5	0.73357	108.826	36.263	4.64948	748.17

Table D.15: Dynamic Frequency Sweep Data at 200 C-METH3+MA: 6.8%

Freq rad/s	G' Pa	G" Pa	tan_delta	Torque g-cm	Strain %	PhaseAngle °	Eta* Pa-s
0.1	2322.72	2211.31	0.95203	5.01587	43.592	4.99939	32069.9
0.15849	2830.87	2856.82	1.00917	6.28781	45.261	4.99741	25376.2
0.25119	3474.78	3714.02	1.06885	7.94911	46.906	4.99583	20247.9
0.39811	4312.36	4837.35	1.12174	10.1259	48.284	4.99455	16278.1
0.63097	5432.8	6273.06	1.15466	12.9606	49.106	4.99219	13152.2
1.00003	6933.79	8099.84	1.16817	16.641	49.435	4.98884	10662
1.58496	8930.07	10367.3	1.16095	21.3383	49.26	4.98478	8633.1
2.51202	11587.2	13118.2	1.13213	27.2803	48.546	4.98208	6967.64
3.98132	15062.8	16436.5	1.0912	34.7225	47.497	4.97832	5599.79
6.31006	19505.7	20304.6	1.04096	43.8159	46.15	4.97435	4462.04
10.0007	25127.4	24729.6	0.98417	54.8156	44.543	4.96993	3525.27
15.8501	32104.3	29678.4	0.92444	67.9072	42.751	4.96479	2758.38
25.1206	40577.5	35090.8	0.86479	83.179	40.853	4.95618	2135.54
39.8135	50725	40922	0.80674	100.452	38.895	4.92672	1636.98
63.1006	62609.1	46993.1	0.75058	118.41	36.891	4.83496	1240.61
100	76139.4	53092.1	0.6973	133.682	34.888	4.60354	928.223

Appendix E: X-ray Diffraction Data

Table E.1: X-ray diffraction data for Cloisite 20A - poweder

Deg.	CPS	Deg.	CPS	Deg.	CPS	Deg.	CPS	Deg.	CPS	Deg.	CPS	Deg.	CPS	Deg.	CPS
1.5	2878	2.64	6879	3.78	10298	4.92	3106	6.06	1669	7.2	2534	8.34	795	9.48	480
1.52	2868	2.66	7023	3.8	10383	4.94	3103	6.08	1695	7.22	2463	8.36	790	9.5	507
1.54	2977	2.68	7126	3.82	10160	4.96	3051	6.1	1747	7.24	2501	8.38	768	9.52	477
1.56	3096	2.7	7273	3.84	9900	4.98	2959	6.12	1668	7.26	2377	8.4	774	9.54	487
1.58	2981	2.72	7406	3.86	9830	5	3012	6.14	1741	7.28	2375	8.42	758	9.56	500
1.6	3110	2.74	7575	3.88	9754	5.02	2834	6.16	1778	7.3	2467	8.44	734	9.58	490
1.62	3165	2.76	7590	3.9	9419	5.04	2729	6.18	1642	7.32	2351	8.46	755	9.6	482
1.64	3191	2.78	7733	3.92	9347	5.06	2743	6.2	1690	7.34	2395	8.48	691	9.62	476
1.66	3204	2.8	7847	3.94	9337	5.08	2712	6.22	1686	7.36	2349	8.5	700	9.64	490
1.68	3270	2.82	8010	3.96	9163	5.1	2590	6.24	1743	7.38	2343	8.52	685	9.66	516
1.7	3293	2.84	8158	3.98	8970	5.12	2622	6.26	1716	7.4	2222	8.54	708	9.68	475
1.72	3364	2.86	8318	4	8805	5.14	2512	6.28	1685	7.42	2183	8.56	674	9.7	468
1.74	3310	2.88	8379	4.02	8648	5.16	2508	6.3	1724	7.44	2158	8.58	668	9.72	444
1.76	3393	2.9	8427	4.04	8498	5.18	2504	6.32	1743	7.46	2170	8.6	670	9.74	477
1.78	3416	2.92	8568	4.06	8313	5.2	2425	6.34	1778	7.48	2029	8.62	695	9.76	474
1.8	3459	2.94	8563	4.08	8033	5.22	2416	6.36	1793	7.5	2050	8.64	657	9.78	444
1.82	3481	2.96	8900	4.1	8046	5.24	2437	6.38	1788	7.52	1964	8.66	637	9.8	470
1.84	3590	2.98	8856	4.12	7735	5.26	2339	6.4	1756	7.54	1944	8.68	646	9.82	464
1.86	3639	3	9094	4.14	7620	5.28	2285	6.42	1819	7.56	1917	8.7	621	9.84	465
1.88	3650	3.02	9280	4.16	7437	5.3	2285	6.44	1803	7.58	1878	8.72	654	9.86	458
1.9	3723	3.04	9267	4.18	7181	5.32	2241	6.46	1823	7.6	1813	8.74	609	9.88	470
1.92	3680	3.06	9322	4.2	7160	5.34	2175	6.48	1822	7.62	1772	8.76	596	9.9	468
1.94	3818	3.08	9488	4.22	6956	5.36	2166	6.5	1884	7.64	1736	8.78	601	9.92	478
1.96	3900	3.1	9736	4.24	6767	5.38	2144	6.52	1905	7.66	1724	8.8	593	9.94	490
1.98	3922	3.12	9711	4.26	6756	5.4	2087	6.54	1869	7.68	1656	8.82	596	9.96	454
2	3990	3.14	9824	4.28	6507	5.42	2086	6.56	1956	7.7	1637	8.84	600	9.98	448
2.02	4051	3.16	10000	4.3	6271	5.44	2088	6.58	1938	7.72	1545	8.86	596	10	463
2.04	4081	3.18	9885	4.32	6145	5.46	2004	6.6	1930	7.74	1522	8.88	587		
2.06	4112	3.2	10188	4.34	5976	5.48	2033	6.62	2021	7.76	1478	8.9	575		
2.08	4192	3.22	10185	4.36	5982	5.5	1990	6.64	2028	7.78	1470	8.92	605		
2.1	4202	3.24	10350	4.38	5764	5.52	1961	6.66	2056	7.8	1403	8.94	571		
2.12	4389	3.26	10309	4.4	5670	5.54	1942	6.68	2115	7.82	1407	8.96	541		
2.14	4443	3.28	10536	4.42	5479	5.56	1967	6.7	2110	7.84	1379	8.98	574		
2.16	4503	3.3	10576	4.44	5445	5.58	1951	6.72	2118	7.86	1313	9	570		
2.18	4523	3.32	10674	4.46	5226	5.6	1930	6.74	2158	7.88	1308	9.02	550		
2.2	4583	3.34	10722	4.48	5139	5.62	1922	6.76	2204	7.9	1265	9.04	539		
2.22	4814	3.36	10642	4.5	5016	5.64	1903	6.78	2244	7.92	1254	9.06	516		
2.24	4834	3.38	10812	4.52	4810	5.66	1883	6.8	2210	7.94	1215	9.08	568		
2.26	4941	3.4	10861	4.54	4711	5.68	1825	6.82	2239	7.96	1181	9.1	550		
2.28	5012	3.42	10864	4.56	4710	5.7	1851	6.84	2345	7.98	1125	9.12	522		
2.3	5080	3.44	11007	4.58	4601	5.72	1798	6.86	2303	8	1102	9.14	540		
2.32	5150	3.46	10938	4.6	4445	5.74	1827	6.88	2385	8.02	1156	9.16	538		
2.34	5312	3.48	10937	4.62	4369	5.76	1805	6.9	2366	8.04	1068	9.18	536		
2.36	5277	3.5	10987	4.64	4223	5.78	1728	6.92	2399	8.06	1060	9.2	541		
2.38	5535	3.52	10899	4.66	4085	5.8	1711	6.94	2393	8.08	1014	9.22	507		
2.4	5479	3.54	10924	4.68	4076	5.82	1803	6.96	2518	8.1	1041	9.24	517		
2.42	5749	3.56	10954	4.7	3989	5.84	1751	6.98	2471	8.12	1020	9.26	540		
2.44	5751	3.58	10957	4.72	3875	5.86	1726	7	2489	8.14	968	9.28	498		
2.46	5923	3.6	10993	4.74	3740	5.88	1758	7.02	2528	8.16	978	9.3	516		
2.48	5951	3.62	11007	4.76	3724	5.9	1763	7.04	2542	8.18	946	9.32	492		
2.5	6118	3.64	10871	4.78	3616	5.92	1716	7.06	2611	8.2	887	9.34	466		
2.52	6196	3.66	10848	4.8	3503	5.94	1708	7.08	2491	8.22	893	9.36	505		
2.54	6269	3.68	10792	4.82	3503	5.96	1705	7.1	2560	8.24	887	9.38	502		
2.56	6399	3.7	10783	4.84	3467	5.98	1753	7.12	2533	8.26	851	9.4	516		
2.58	6559	3.72	10641	4.86	3364	6	1678	7.14	2588	8.28	837	9.42	497		
2.6	6601	3.74	10535	4.88	3228	6.02	1673	7.16	2537	8.3	842	9.44	502		
2.62	6823	3.76	10491	4.9	3195	6.04	1721	7.18	2548	8.32	835	9.46	477		

Table E.2: X-ray diffraction data for METH1: 4% - Extruded pellets

Deg.	CPS	Deg.	CPS	Deg.	CPS	Deg.	CPS	Deg.	CPS	Deg.	CPS	Deg.	CPS	Deg.	CPS
1.5	2060	2.64	4395	3.78	3044	4.92	1431	6.06	1229	7.2	938	8.34	685	9.48	591
1.52	2091	2.66	4365	3.8	3002	4.94	1429	6.08	1233	7.22	935	8.36	678	9.5	593
1.54	2106	2.68	4404	3.82	2938	4.96	1425	6.1	1227	7.24	917	8.38	690	9.52	593
1.56	2148	2.7	4380	3.84	2868	4.98	1450	6.12	1237	7.26	939	8.4	706	9.54	578
1.58	2187	2.72	4427	3.86	2874	5	1431	6.14	1264	7.28	923	8.42	686	9.56	599
1.6	2241	2.74	4385	3.88	2839	5.02	1390	6.16	1245	7.3	903	8.44	692	9.58	603
1.62	2247	2.76	4419	3.9	2742	5.04	1411	6.18	1241	7.32	887	8.46	658	9.6	597
1.64	2282	2.78	4400	3.92	2746	5.06	1393	6.2	1209	7.34	899	8.48	672	9.62	602
1.66	2295	2.8	4417	3.94	2703	5.08	1374	6.22	1213	7.36	884	8.5	687	9.64	591
1.68	2324	2.82	4388	3.96	2682	5.1	1378	6.24	1232	7.38	867	8.52	650	9.66	588
1.7	2371	2.84	4454	3.98	2627	5.12	1357	6.26	1222	7.4	896	8.54	662	9.68	591
1.72	2329	2.86	4395	4	2561	5.14	1385	6.28	1221	7.42	845	8.56	635	9.7	596
1.74	2431	2.88	4414	4.02	2584	5.16	1364	6.3	1230	7.44	859	8.58	628	9.72	591
1.76	2452	2.9	4380	4.04	2481	5.18	1358	6.32	1250	7.46	833	8.6	634	9.74	593
1.78	2484	2.92	4364	4.06	2473	5.2	1345	6.34	1231	7.48	850	8.62	643	9.76	590
1.8	2500	2.94	4403	4.08	2388	5.22	1363	6.36	1190	7.5	815	8.64	634	9.78	595
1.82	2555	2.96	4377	4.1	2422	5.24	1332	6.38	1185	7.52	811	8.66	621	9.8	599
1.84	2556	2.98	4304	4.12	2351	5.26	1311	6.4	1194	7.54	823	8.68	630	9.82	601
1.86	2586	3	4323	4.14	2320	5.28	1311	6.42	1189	7.56	818	8.7	596	9.84	581
1.88	2657	3.02	4316	4.16	2270	5.3	1305	6.44	1203	7.58	826	8.72	625	9.86	598
1.9	2741	3.04	4240	4.18	2282	5.32	1341	6.46	1162	7.6	823	8.74	608	9.88	597
1.92	2787	3.06	4242	4.2	2177	5.34	1313	6.48	1179	7.62	782	8.76	618	9.9	608
1.94	2792	3.08	4222	4.22	2162	5.36	1299	6.5	1166	7.64	791	8.78	624	9.92	616
1.96	2839	3.1	4205	4.24	2169	5.38	1274	6.52	1146	7.66	776	8.8	610	9.94	608
1.98	2879	3.12	4172	4.26	2102	5.4	1315	6.54	1127	7.68	764	8.82	612	9.96	632
2	2956	3.14	4138	4.28	2099	5.42	1283	6.56	1140	7.7	761	8.84	600	9.98	585
2.02	3001	3.16	4090	4.3	2069	5.44	1302	6.58	1167	7.72	750	8.86	593	10	605
2.04	3026	3.18	4110	4.32	2070	5.46	1301	6.6	1153	7.74	758	8.88	596		
2.06	3041	3.2	4074	4.34	2010	5.48	1290	6.62	1144	7.76	760	8.9	602		
2.08	3180	3.22	4010	4.36	1952	5.5	1281	6.64	1124	7.78	754	8.92	593		
2.1	3166	3.24	4023	4.38	1947	5.52	1286	6.66	1100	7.8	721	8.94	602		
2.12	3221	3.26	3977	4.4	1922	5.54	1251	6.68	1117	7.82	743	8.96	587		
2.14	3287	3.28	3924	4.42	1875	5.56	1293	6.7	1117	7.84	714	8.98	589		
2.16	3327	3.3	3888	4.44	1892	5.58	1253	6.72	1116	7.86	719	9	582		
2.18	3364	3.32	3861	4.46	1874	5.6	1284	6.74	1123	7.88	721	9.02	619		
2.2	3436	3.34	3829	4.48	1844	5.62	1287	6.76	1085	7.9	728	9.04	585		
2.22	3485	3.36	3822	4.5	1773	5.64	1268	6.78	1096	7.92	732	9.06	595		
2.24	3558	3.38	3776	4.52	1795	5.66	1266	6.8	1084	7.94	690	9.08	596		
2.26	3621	3.4	3746	4.54	1755	5.68	1252	6.82	1102	7.96	716	9.1	569		
2.28	3643	3.42	3691	4.56	1746	5.7	1250	6.84	1099	7.98	698	9.12	566		
2.3	3702	3.44	3664	4.58	1701	5.72	1261	6.86	1058	8	671	9.14	575		
2.32	3736	3.46	3678	4.6	1702	5.74	1269	6.88	1073	8.02	679	9.16	595		
2.34	3746	3.48	3558	4.62	1718	5.76	1240	6.9	1031	8.04	679	9.18	587		
2.36	3811	3.5	3606	4.64	1686	5.78	1269	6.92	1050	8.06	712	9.2	596		
2.38	3869	3.52	3550	4.66	1650	5.8	1273	6.94	1040	8.08	705	9.22	598		
2.4	3952	3.54	3466	4.68	1612	5.82	1270	6.96	1021	8.1	698	9.24	579		
2.42	3977	3.56	3456	4.7	1622	5.84	1243	6.98	1040	8.12	675	9.26	567		
2.44	3989	3.58	3425	4.72	1585	5.86	1210	7	1010	8.14	674	9.28	591		
2.46	4049	3.6	3398	4.74	1570	5.88	1263	7.02	1006	8.16	669	9.3	575		
2.48	4081	3.62	3339	4.76	1543	5.9	1249	7.04	1005	8.18	679	9.32	601		
2.5	4147	3.64	3318	4.78	1593	5.92	1268	7.06	1012	8.2	685	9.34	582		
2.52	4121	3.66	3281	4.8	1517	5.94	1233	7.08	971	8.22	681	9.36	573		
2.54	4228	3.68	3267	4.82	1512	5.96	1258	7.1	973	8.24	658	9.38	601		
2.56	4198	3.7	3196	4.84	1512	5.98	1265	7.12	964	8.26	691	9.4	552		
2.58	4284	3.72	3170	4.86	1510	6	1247	7.14	993	8.28	686	9.42	575		
2.6	4276	3.74	3170	4.88	1462	6.02	1239	7.16	961	8.3	668	9.44	605		
2.62	4333	3.76	3043	4.9	1500	6.04	1222	7.18	938	8.32	687	9.46	579		

Table E.3: X-ray diffraction data for METH2: 4% - Extruded pellets

Deg.	CPS	Deg.	CPS	Deg.	CPS	Deg.	CPS	Deg.	CPS	Deg.	CPS	Deg.	CPS	Deg.	CPS
1.5	5647	2.64	4327	3.78	3070	4.92	1521	6.06	1077	7.2	826	8.34	475	9.48	344
1.52	5233	2.66	4383	3.8	2970	4.94	1637	6.08	1065	7.22	856	8.36	426	9.5	345
1.54	5169	2.68	4259	3.82	3031	4.96	1523	6.1	1107	7.24	818	8.38	466	9.52	343
1.56	4868	2.7	4375	3.84	2900	4.98	1540	6.12	1048	7.26	816	8.4	445	9.54	332
1.58	4770	2.72	4206	3.86	2974	5	1469	6.14	1072	7.28	790	8.42	422	9.56	336
1.6	4485	2.74	4348	3.88	2795	5.02	1545	6.16	1053	7.3	801	8.44	413	9.58	349
1.62	4339	2.76	4250	3.9	2972	5.04	1441	6.18	1042	7.32	770	8.46	445	9.6	328
1.64	4098	2.78	4390	3.92	2817	5.06	1475	6.2	1072	7.34	784	8.48	420	9.62	343
1.66	4054	2.8	4288	3.94	2877	5.08	1391	6.22	1080	7.36	738	8.5	440	9.64	348
1.68	3782	2.82	4370	3.96	2765	5.1	1444	6.24	1067	7.38	735	8.52	413	9.66	352
1.7	3883	2.84	4148	3.98	2781	5.12	1363	6.26	1122	7.4	710	8.54	402	9.68	339
1.72	3788	2.86	4273	4	2615	5.14	1389	6.28	1080	7.42	732	8.56	405	9.7	343
1.74	3815	2.88	4109	4.02	2810	5.16	1378	6.3	1058	7.44	655	8.58	410	9.72	340
1.76	3658	2.9	4314	4.04	2614	5.18	1355	6.32	1099	7.46	713	8.6	385	9.74	345
1.78	3793	2.92	4188	4.06	2705	5.2	1370	6.34	1086	7.48	634	8.62	405	9.76	341
1.8	3672	2.94	4159	4.08	2565	5.22	1389	6.36	1072	7.5	688	8.64	400	9.78	341
1.82	3761	2.96	4019	4.1	2637	5.24	1348	6.38	1106	7.52	640	8.66	393	9.8	358
1.84	3650	2.98	4116	4.12	2487	5.26	1322	6.4	1111	7.54	685	8.68	383	9.82	346
1.86	3854	3	3961	4.14	2620	5.28	1275	6.42	1103	7.56	633	8.7	370	9.84	318
1.88	3643	3.02	4072	4.16	2488	5.3	1332	6.44	1077	7.58	659	8.72	400	9.86	340
1.9	3814	3.04	4022	4.18	2481	5.32	1278	6.46	1143	7.6	620	8.74	364	9.88	319
1.92	3794	3.06	3967	4.2	2362	5.34	1298	6.48	1078	7.62	633	8.76	368	9.9	345
1.94	3939	3.08	3855	4.22	2372	5.36	1288	6.5	1108	7.64	600	8.78	361	9.92	336
1.96	3694	3.1	4005	4.24	2324	5.38	1265	6.52	1056	7.66	593	8.8	360	9.94	366
1.98	3828	3.12	3879	4.26	2402	5.4	1200	6.54	1084	7.68	577	8.82	392	9.96	339
2	3800	3.14	3918	4.28	2269	5.42	1293	6.56	1062	7.7	605	8.84	377	9.98	343
2.02	3904	3.16	3786	4.3	2319	5.44	1206	6.58	1062	7.72	554	8.86	359	10	346
2.04	3740	3.18	3827	4.32	2223	5.46	1225	6.6	1048	7.74	571	8.88	377		
2.06	3987	3.2	3702	4.34	2293	5.48	1179	6.62	1090	7.76	592	8.9	378		
2.08	3885	3.22	3880	4.36	2167	5.5	1214	6.64	1062	7.78	586	8.92	355		
2.1	3948	3.24	3670	4.38	2214	5.52	1156	6.66	1097	7.8	569	8.94	375		
2.12	3939	3.26	3764	4.4	2156	5.54	1186	6.68	1030	7.82	563	8.96	331		
2.14	3993	3.28	3528	4.42	2185	5.56	1190	6.7	1092	7.84	494	8.98	339		
2.16	3920	3.3	3666	4.44	2040	5.58	1183	6.72	1044	7.86	540	9	356		
2.18	4104	3.32	3499	4.46	2045	5.6	1150	6.74	1090	7.88	525	9.02	363		
2.2	3953	3.34	3623	4.48	1999	5.62	1184	6.76	1030	7.9	518	9.04	354		
2.22	4125	3.36	3477	4.5	2082	5.64	1130	6.78	1023	7.92	503	9.06	380		
2.24	4047	3.38	3602	4.52	1944	5.66	1161	6.8	1000	7.94	505	9.08	363		
2.26	4178	3.4	3427	4.54	1925	5.68	1135	6.82	1040	7.96	510	9.1	358		
2.28	4085	3.42	3530	4.56	1905	5.7	1147	6.84	1005	7.98	529	9.12	346		
2.3	4318	3.44	3408	4.58	1886	5.72	1145	6.86	1035	8	480	9.14	348		
2.32	4144	3.46	3413	4.6	1847	5.74	1193	6.88	991	8.02	491	9.16	338		
2.34	4290	3.48	3377	4.62	1910	5.76	1111	6.9	1018	8.04	489	9.18	361		
2.36	4129	3.5	3423	4.64	1832	5.78	1137	6.92	990	8.06	479	9.2	343		
2.38	4243	3.52	3299	4.66	1849	5.8	1076	6.94	1001	8.08	460	9.22	358		
2.4	4226	3.54	3411	4.68	1801	5.82	1112	6.96	967	8.1	488	9.24	343		
2.42	4332	3.56	3251	4.7	1830	5.84	1074	6.98	967	8.12	451	9.26	363		
2.44	4262	3.58	3384	4.72	1702	5.86	1140	7	917	8.14	466	9.28	336		
2.46	4404	3.6	3221	4.74	1797	5.88	1057	7.02	964	8.16	445	9.3	342		
2.48	4250	3.62	3298	4.76	1662	5.9	1128	7.04	913	8.18	455	9.32	343		
2.5	4380	3.64	3217	4.78	1649	5.92	1048	7.06	923	8.2	448	9.34	337		
2.52	4301	3.66	3271	4.8	1613	5.94	1096	7.08	890	8.22	467	9.36	342		
2.54	4361	3.68	3081	4.82	1692	5.96	1065	7.1	902	8.24	438	9.38	331		
2.56	4267	3.7	3227	4.84	1587	5.98	1113	7.12	893	8.26	469	9.4	329		
2.58	4537	3.72	3033	4.86	1636	6	1098	7.14	895	8.28	440	9.42	327		
2.6	4362	3.74	3115	4.88	1533	6.02	1115	7.16	842	8.3	448	9.44	319		
2.62	4433	3.76	3074	4.9	1572	6.04	1091	7.18	897	8.32	447	9.46	330		

Table E.4: X-ray diffraction data for METH3: 4% - Extruded pellets

Deg.	CPS	Deg.	CPS	Deg.	CPS	Deg.	CPS	Deg.	CPS	Deg.	CPS	Deg.	CPS	Deg.	CPS
1.5	3705	2.64	2780	3.78	1930	4.92	923	6.06	700	7.2	663	8.34	705	9.48	820
1.52	3587	2.66	2778	3.8	1894	4.94	926	6.08	704	7.22	720	8.36	698	9.5	840
1.54	3542	2.68	2699	3.82	1853	4.96	895	6.1	703	7.24	670	8.38	718	9.52	803
1.56	3476	2.7	2747	3.84	1840	4.98	900	6.12	695	7.26	712	8.4	718	9.54	824
1.58	3500	2.72	2730	3.86	1841	5	839	6.14	728	7.28	701	8.42	720	9.56	818
1.6	3440	2.74	2703	3.88	1813	5.02	848	6.16	724	7.3	672	8.44	729	9.58	875
1.62	3483	2.76	2698	3.9	1841	5.04	812	6.18	705	7.32	695	8.46	700	9.6	856
1.64	3376	2.78	2638	3.92	1850	5.06	829	6.2	680	7.34	690	8.48	681	9.62	842
1.66	3327	2.8	2695	3.94	1768	5.08	839	6.22	719	7.36	693	8.5	722	9.64	841
1.68	3363	2.82	2656	3.96	1737	5.1	828	6.24	723	7.38	700	8.52	693	9.66	807
1.7	3295	2.84	2692	3.98	1721	5.12	832	6.26	723	7.4	703	8.54	729	9.68	853
1.72	3264	2.86	2670	4	1703	5.14	806	6.28	684	7.42	688	8.56	733	9.7	840
1.74	3278	2.88	2602	4.02	1711	5.16	812	6.3	709	7.44	710	8.58	723	9.72	856
1.76	3257	2.9	2654	4.04	1663	5.18	824	6.32	728	7.46	715	8.6	731	9.74	844
1.78	3246	2.92	2613	4.06	1623	5.2	802	6.34	676	7.48	710	8.62	725	9.76	874
1.8	3188	2.94	2622	4.08	1560	5.22	777	6.36	700	7.5	702	8.64	734	9.78	862
1.82	3153	2.96	2619	4.1	1630	5.24	814	6.38	698	7.52	717	8.66	751	9.8	843
1.84	3181	2.98	2634	4.12	1592	5.26	785	6.4	698	7.54	689	8.68	740	9.82	868
1.86	3164	3	2532	4.14	1568	5.28	747	6.42	689	7.56	707	8.7	708	9.84	909
1.88	3168	3.02	2525	4.16	1518	5.3	770	6.44	660	7.58	702	8.72	716	9.86	849
1.9	3169	3.04	2565	4.18	1524	5.32	733	6.46	724	7.6	714	8.74	729	9.88	854
1.92	3067	3.06	2517	4.2	1528	5.34	780	6.48	695	7.62	713	8.76	748	9.9	881
1.94	3090	3.08	2470	4.22	1478	5.36	786	6.5	668	7.64	698	8.78	719	9.92	863
1.96	3025	3.1	2457	4.24	1413	5.38	748	6.52	660	7.66	701	8.8	750	9.94	914
1.98	3078	3.12	2472	4.26	1409	5.4	715	6.54	703	7.68	715	8.82	768	9.96	900
2	3022	3.14	2457	4.28	1344	5.42	743	6.56	708	7.7	691	8.84	742	9.98	867
2.02	3061	3.16	2391	4.3	1414	5.44	748	6.58	687	7.72	693	8.86	722	10	864
2.04	2990	3.18	2453	4.32	1363	5.46	727	6.6	710	7.74	687	8.88	736		
2.06	2968	3.2	2401	4.34	1360	5.48	741	6.62	654	7.76	707	8.9	760		
2.08	2997	3.22	2328	4.36	1333	5.5	719	6.64	706	7.78	717	8.92	725		
2.1	2946	3.24	2376	4.38	1326	5.52	736	6.66	662	7.8	729	8.94	736		
2.12	2952	3.26	2353	4.4	1274	5.54	707	6.68	685	7.82	698	8.96	757		
2.14	2960	3.28	2348	4.42	1250	5.56	703	6.7	693	7.84	695	8.98	738		
2.16	2924	3.3	2324	4.44	1221	5.58	742	6.72	665	7.86	656	9	755		
2.18	2871	3.32	2305	4.46	1260	5.6	703	6.74	667	7.88	729	9.02	733		
2.2	2962	3.34	2305	4.48	1178	5.62	723	6.76	673	7.9	683	9.04	744		
2.22	2910	3.36	2293	4.5	1168	5.64	688	6.78	670	7.92	725	9.06	717		
2.24	2921	3.38	2286	4.52	1186	5.66	713	6.8	648	7.94	697	9.08	744		
2.26	2903	3.4	2255	4.54	1204	5.68	703	6.82	648	7.96	721	9.1	788		
2.28	2892	3.42	2249	4.56	1110	5.7	739	6.84	660	7.98	696	9.12	777		
2.3	2904	3.44	2162	4.58	1113	5.72	705	6.86	662	8	689	9.14	781		
2.32	2920	3.46	2186	4.6	1098	5.74	716	6.88	657	8.02	703	9.16	783		
2.34	2933	3.48	2148	4.62	1097	5.76	714	6.9	679	8.04	749	9.18	778		
2.36	2923	3.5	2103	4.64	1058	5.78	700	6.92	658	8.06	723	9.2	751		
2.38	2895	3.52	2147	4.66	1110	5.8	718	6.94	660	8.08	715	9.22	784		
2.4	2801	3.54	2123	4.68	1079	5.82	723	6.96	650	8.1	695	9.24	798		
2.42	2814	3.56	2155	4.7	1071	5.84	700	6.98	681	8.12	689	9.26	798		
2.44	2872	3.58	2157	4.72	1028	5.86	710	7	675	8.14	706	9.28	835		
2.46	2858	3.6	2064	4.74	1024	5.88	705	7.02	693	8.16	723	9.3	798		
2.48	2756	3.62	2046	4.76	1020	5.9	699	7.04	692	8.18	708	9.32	830		
2.5	2800	3.64	2059	4.78	993	5.92	672	7.06	710	8.2	663	9.34	810		
2.52	2786	3.66	2043	4.8	995	5.94	695	7.08	693	8.22	717	9.36	803		
2.54	2753	3.68	2019	4.82	971	5.96	698	7.1	678	8.24	698	9.38	841		
2.56	2753	3.7	2028	4.84	952	5.98	691	7.12	684	8.26	767	9.4	819		
2.58	2698	3.72	1990	4.86	948	6	717	7.14	690	8.28	704	9.42	798		
2.6	2784	3.74	1982	4.88	930	6.02	674	7.16	693	8.3	728	9.44	828		
2.62	2719	3.76	1926	4.9	904	6.04	723	7.18	679	8.32	680	9.46	805		

Table E.5: X-ray diffraction data for METH3: 6.6% - Extruded pellets

Deg.	CPS	Deg.	CPS	Deg.	CPS	Deg.	CPS	Deg.	CPS	Deg.	CPS	Deg.	CPS	Deg.	CPS
1.5	2738	2.64	654	3.78	725	4.92	393	6.06	335	7.2	331	8.34	350	9.48	385
1.52	2519	2.66	696	3.8	763	4.94	395	6.08	333	7.22	331	8.36	330	9.5	418
1.54	2380	2.68	664	3.82	725	4.96	393	6.1	325	7.24	335	8.38	330	9.52	399
1.56	2165	2.7	665	3.84	688	4.98	404	6.12	310	7.26	349	8.4	333	9.54	405
1.58	1960	2.72	668	3.86	751	5	390	6.14	315	7.28	337	8.42	351	9.56	423
1.6	1736	2.74	685	3.88	694	5.02	394	6.16	320	7.3	353	8.44	350	9.58	408
1.62	1528	2.76	668	3.9	697	5.04	362	6.18	329	7.32	355	8.46	354	9.6	390
1.64	1295	2.78	653	3.92	690	5.06	388	6.2	312	7.34	351	8.48	330	9.62	413
1.66	1160	2.8	657	3.94	695	5.08	371	6.22	297	7.36	329	8.5	347	9.64	421
1.68	1000	2.82	696	3.96	668	5.1	367	6.24	316	7.38	348	8.52	333	9.66	393
1.7	985	2.84	662	3.98	684	5.12	364	6.26	315	7.4	325	8.54	342	9.68	366
1.72	915	2.86	690	4	649	5.14	356	6.28	335	7.42	342	8.56	329	9.7	410
1.74	908	2.88	669	4.02	708	5.16	327	6.3	337	7.44	329	8.58	387	9.72	405
1.76	867	2.9	676	4.04	667	5.18	363	6.32	313	7.46	361	8.6	339	9.74	415
1.78	868	2.92	638	4.06	668	5.2	338	6.34	304	7.48	360	8.62	335	9.76	402
1.8	825	2.94	703	4.08	664	5.22	358	6.36	330	7.5	345	8.64	342	9.78	393
1.82	883	2.96	680	4.1	608	5.24	351	6.38	325	7.52	349	8.66	342	9.8	419
1.84	828	2.98	718	4.12	606	5.26	366	6.4	316	7.54	325	8.68	355	9.82	428
1.86	828	3	690	4.14	610	5.28	348	6.42	331	7.56	352	8.7	375	9.84	440
1.88	801	3.02	713	4.16	587	5.3	350	6.44	340	7.58	332	8.72	339	9.86	416
1.9	793	3.04	661	4.18	635	5.32	340	6.46	315	7.6	342	8.74	349	9.88	417
1.92	742	3.06	699	4.2	588	5.34	343	6.48	318	7.62	345	8.76	380	9.9	419
1.94	767	3.08	683	4.22	587	5.36	327	6.5	339	7.64	341	8.78	365	9.92	409
1.96	757	3.1	693	4.24	580	5.38	350	6.52	322	7.66	348	8.8	338	9.94	445
1.98	773	3.12	691	4.26	583	5.4	327	6.54	328	7.68	344	8.82	358	9.96	405
2	741	3.14	708	4.28	548	5.42	330	6.56	306	7.7	361	8.84	363	9.98	427
2.02	754	3.16	718	4.3	567	5.44	325	6.58	344	7.72	321	8.86	370	10	445
2.04	720	3.18	726	4.32	537	5.46	334	6.6	303	7.74	358	8.88	346		
2.06	795	3.2	722	4.34	569	5.48	320	6.62	328	7.76	328	8.9	376		
2.08	761	3.22	730	4.36	521	5.5	339	6.64	338	7.78	351	8.92	368		
2.1	762	3.24	670	4.38	535	5.52	324	6.66	325	7.8	351	8.94	375		
2.12	738	3.26	709	4.4	505	5.54	351	6.68	323	7.82	343	8.96	364		
2.14	725	3.28	723	4.42	506	5.56	345	6.7	352	7.84	333	8.98	388		
2.16	695	3.3	732	4.44	480	5.58	333	6.72	324	7.86	345	9	369		
2.18	715	3.32	727	4.46	528	5.6	321	6.74	341	7.88	343	9.02	383		
2.2	743	3.34	703	4.48	492	5.62	326	6.76	339	7.9	344	9.04	362		
2.22	721	3.36	716	4.5	489	5.64	330	6.78	343	7.92	318	9.06	364		
2.24	643	3.38	740	4.52	460	5.66	325	6.8	330	7.94	371	9.08	352		
2.26	704	3.4	710	4.54	467	5.68	333	6.82	339	7.96	340	9.1	398		
2.28	680	3.42	755	4.56	459	5.7	341	6.84	318	7.98	316	9.12	391		
2.3	689	3.44	741	4.58	480	5.72	314	6.86	338	8	334	9.14	370		
2.32	662	3.46	761	4.6	458	5.74	330	6.88	319	8.02	353	9.16	362		
2.34	737	3.48	718	4.62	448	5.76	307	6.9	303	8.04	331	9.18	375		
2.36	678	3.5	733	4.64	428	5.78	323	6.92	339	8.06	334	9.2	363		
2.38	675	3.52	779	4.66	455	5.8	308	6.94	336	8.08	325	9.22	394		
2.4	668	3.54	738	4.68	438	5.82	332	6.96	341	8.1	340	9.24	371		
2.42	719	3.56	735	4.7	421	5.84	304	6.98	335	8.12	315	9.26	383		
2.44	659	3.58	735	4.72	424	5.86	354	7	340	8.14	349	9.28	382		
2.46	690	3.6	723	4.74	423	5.88	318	7.02	339	8.16	325	9.3	376		
2.48	653	3.62	763	4.76	417	5.9	308	7.04	350	8.18	335	9.32	388		
2.5	695	3.64	714	4.78	423	5.92	316	7.06	330	8.2	325	9.34	404		
2.52	660	3.66	770	4.8	393	5.94	330	7.08	333	8.22	342	9.36	391		
2.54	679	3.68	735	4.82	416	5.96	313	7.1	323	8.24	323	9.38	392		
2.56	651	3.7	753	4.84	418	5.98	333	7.12	360	8.26	339	9.4	370		
2.58	684	3.72	714	4.86	397	6	314	7.14	354	8.28	323	9.42	407		
2.6	640	3.74	715	4.88	400	6.02	325	7.16	323	8.3	340	9.44	386		
2.62	670	3.76	727	4.9	386	6.04	313	7.18	334	8.32	338	9.46	405		

Table E.6: X-ray diffraction data for METH3: 9.5% - Extruded pellets

Deg.	CPS	Deg.	CPS	Deg.	CPS	Deg.	CPS	Deg.	CPS	Deg.	CPS	Deg.	CPS	Deg.	CPS
1.5	6098	2.64	2378	3.78	3314	4.92	1488	6.06	1099	7.2	917	8.34	683	9.48	513
1.52	5470	2.66	2575	3.8	3267	4.94	1626	6.08	1153	7.22	948	8.36	627	9.5	558
1.54	5323	2.68	2442	3.82	3419	4.96	1508	6.1	1148	7.24	892	8.38	605	9.52	520
1.56	4839	2.7	2499	3.84	3229	4.98	1515	6.12	1077	7.26	895	8.4	639	9.54	567
1.58	4466	2.72	2525	3.86	3349	5	1458	6.14	1140	7.28	906	8.42	623	9.56	525
1.6	3963	2.74	2571	3.88	3132	5.02	1491	6.16	1154	7.3	959	8.44	609	9.58	563
1.62	3694	2.76	2544	3.9	3293	5.04	1429	6.18	1178	7.32	902	8.46	600	9.6	582
1.64	3189	2.78	2669	3.92	3194	5.06	1422	6.2	1145	7.34	947	8.48	588	9.62	546
1.66	2940	2.8	2516	3.94	3301	5.08	1318	6.22	1164	7.36	901	8.5	594	9.64	556
1.68	2728	2.82	2683	3.96	3153	5.1	1383	6.24	1142	7.38	889	8.52	619	9.66	567
1.7	2689	2.84	2500	3.98	3163	5.12	1296	6.26	1098	7.4	836	8.54	595	9.68	523
1.72	2529	2.86	2752	4	3065	5.14	1284	6.28	1105	7.42	901	8.56	557	9.7	574
1.74	2557	2.88	2583	4.02	3168	5.16	1327	6.3	1188	7.44	860	8.58	599	9.72	554
1.76	2424	2.9	2766	4.04	3026	5.18	1344	6.32	1140	7.46	823	8.6	589	9.74	581
1.78	2404	2.92	2664	4.06	3117	5.2	1284	6.34	1205	7.48	857	8.62	578	9.76	547
1.8	2444	2.94	2771	4.08	2915	5.22	1351	6.36	1195	7.5	838	8.64	557	9.78	580
1.82	2390	2.96	2629	4.1	2939	5.24	1311	6.38	1200	7.52	789	8.66	587	9.8	532
1.84	2272	2.98	2818	4.12	2800	5.26	1344	6.4	1160	7.54	830	8.68	547	9.82	547
1.86	2343	3	2733	4.14	2969	5.28	1259	6.42	1213	7.56	817	8.7	568	9.84	546
1.88	2305	3.02	2879	4.16	2764	5.3	1285	6.44	1206	7.58	845	8.72	568	9.86	566
1.9	2357	3.04	2779	4.18	2835	5.32	1262	6.46	1224	7.6	786	8.74	555	9.88	579
1.92	2291	3.06	2900	4.2	2694	5.34	1326	6.48	1181	7.62	827	8.76	573	9.9	580
1.94	2273	3.08	2912	4.22	2730	5.36	1200	6.5	1195	7.64	788	8.78	595	9.92	566
1.96	2291	3.1	2888	4.24	2567	5.38	1234	6.52	1146	7.66	760	8.8	539	9.94	516
1.98	2313	3.12	2812	4.26	2707	5.4	1133	6.54	1202	7.68	792	8.82	560	9.96	560
2	2158	3.14	2926	4.28	2595	5.42	1258	6.56	1199	7.7	795	8.84	536	9.98	590
2.02	2325	3.16	2748	4.3	2566	5.44	1184	6.58	1183	7.72	765	8.86	542	10	577
2.04	2212	3.18	3017	4.32	2570	5.46	1292	6.6	1159	7.74	778	8.88	549		
2.06	2181	3.2	2949	4.34	2394	5.48	1201	6.62	1235	7.76	739	8.9	543		
2.08	2245	3.22	2990	4.36	2330	5.5	1208	6.64	1169	7.78	770	8.92	532		
2.1	2291	3.24	2997	4.38	2365	5.52	1139	6.66	1189	7.8	754	8.94	545		
2.12	2189	3.26	2930	4.4	2316	5.54	1202	6.68	1158	7.82	793	8.96	510		
2.14	2240	3.28	2926	4.42	2349	5.56	1134	6.7	1156	7.84	698	8.98	536		
2.16	2238	3.3	3024	4.44	2216	5.58	1149	6.72	1163	7.86	688	9	509		
2.18	2317	3.32	2990	4.46	2249	5.6	1095	6.74	1181	7.88	721	9.02	552		
2.2	2211	3.34	3128	4.48	2124	5.62	1184	6.76	1107	7.9	727	9.04	515		
2.22	2200	3.36	2975	4.5	2241	5.64	1140	6.78	1167	7.92	710	9.06	530		
2.24	2191	3.38	3170	4.52	2119	5.66	1095	6.8	1072	7.94	697	9.08	528		
2.26	2208	3.4	3079	4.54	2135	5.68	1138	6.82	1156	7.96	664	9.1	532		
2.28	2248	3.42	3232	4.56	2010	5.7	1172	6.84	1084	7.98	696	9.12	535		
2.3	2251	3.44	3114	4.58	2053	5.72	1103	6.86	1163	8	710	9.14	571		
2.32	2245	3.46	3326	4.6	1935	5.74	1122	6.88	1084	8.02	747	9.16	569		
2.34	2290	3.48	3294	4.62	2038	5.76	1139	6.9	1119	8.04	679	9.18	518		
2.36	2300	3.5	3291	4.64	1897	5.78	1158	6.92	1077	8.06	724	9.2	547		
2.38	2259	3.52	3158	4.66	1886	5.8	1138	6.94	1068	8.08	667	9.22	541		
2.4	2292	3.54	3299	4.68	1848	5.82	1116	6.96	1079	8.1	685	9.24	513		
2.42	2349	3.56	3292	4.7	1871	5.84	1103	6.98	1069	8.12	680	9.26	533		
2.44	2279	3.58	3369	4.72	1768	5.86	1159	7	1074	8.14	733	9.28	533		
2.46	2406	3.6	3321	4.74	1757	5.88	1095	7.02	1030	8.16	679	9.3	564		
2.48	2351	3.62	3310	4.76	1737	5.9	1139	7.04	983	8.18	691	9.32	549		
2.5	2418	3.64	3317	4.78	1713	5.92	1096	7.06	999	8.2	697	9.34	557		
2.52	2352	3.66	3308	4.8	1661	5.94	1154	7.08	971	8.22	693	9.36	543		
2.54	2391	3.68	3295	4.82	1633	5.96	1132	7.1	963	8.24	711	9.38	563		
2.56	2474	3.7	3351	4.84	1678	5.98	1204	7.12	997	8.26	716	9.4	494		
2.58	2521	3.72	3299	4.86	1584	6	1105	7.14	1009	8.28	683	9.42	537		
2.6	2393	3.74	3402	4.88	1530	6.02	1141	7.16	938	8.3	676	9.44	508		
2.62	2441	3.76	3301	4.9	1561	6.04	1077	7.18	981	8.32	671	9.46	549		

Table E.7: X-ray diffraction data for RTP: 10% - Extruded pellets

Deg.	CPS	Deg.	CPS	Deg.	CPS	Deg.	CPS	Deg.	CPS	Deg.	CPS	Deg.	CPS	Deg.	CPS
1.5	5738	2.64	2375	3.78	2368	4.92	726	6.06	567	7.2	313	8.34	294	9.48	219
1.52	5272	2.66	2495	3.8	2267	4.94	730	6.08	528	7.22	319	8.36	297	9.5	251
1.54	5226	2.68	2405	3.82	2231	4.96	690	6.1	584	7.24	312	8.38	301	9.52	228
1.56	4749	2.7	2492	3.84	2088	4.98	750	6.12	546	7.26	307	8.4	285	9.54	238
1.58	4591	2.72	2464	3.86	2070	5	695	6.14	555	7.28	325	8.42	313	9.56	228
1.6	4270	2.74	2560	3.88	1949	5.02	725	6.16	560	7.3	314	8.44	311	9.58	218
1.62	4043	2.76	2571	3.9	1893	5.04	713	6.18	555	7.32	298	8.46	310	9.6	242
1.64	3674	2.78	2619	3.92	1773	5.06	730	6.2	526	7.34	316	8.48	305	9.62	233
1.66	3601	2.8	2553	3.94	1741	5.08	752	6.22	553	7.36	314	8.5	303	9.64	227
1.68	3341	2.82	2675	3.96	1680	5.1	713	6.24	542	7.38	318	8.52	283	9.66	218
1.7	3265	2.84	2632	3.98	1663	5.12	693	6.26	540	7.4	301	8.54	282	9.68	235
1.72	3163	2.86	2736	4	1583	5.14	754	6.28	538	7.42	299	8.56	301	9.7	220
1.74	3193	2.88	2665	4.02	1555	5.16	739	6.3	528	7.44	308	8.58	300	9.72	226
1.76	2981	2.9	2802	4.04	1486	5.18	753	6.32	519	7.46	290	8.6	302	9.74	243
1.78	3010	2.92	2723	4.06	1442	5.2	701	6.34	529	7.48	278	8.62	281	9.76	246
1.8	2826	2.94	2870	4.08	1363	5.22	725	6.36	516	7.5	305	8.64	293	9.78	260
1.82	2952	2.96	2773	4.1	1330	5.24	726	6.38	500	7.52	297	8.66	296	9.8	232
1.84	2736	2.98	2889	4.12	1249	5.26	714	6.4	502	7.54	291	8.68	282	9.82	249
1.86	2859	3	2865	4.14	1283	5.28	691	6.42	508	7.56	283	8.7	291	9.84	230
1.88	2733	3.02	3058	4.16	1163	5.3	736	6.44	489	7.58	298	8.72	298	9.86	228
1.9	2656	3.04	2932	4.18	1182	5.32	695	6.46	503	7.6	268	8.74	279	9.88	223
1.92	2650	3.06	3029	4.2	1163	5.34	711	6.48	497	7.62	305	8.76	302	9.9	238
1.94	2677	3.08	2937	4.22	1090	5.36	705	6.5	493	7.64	293	8.78	269	9.92	235
1.96	2545	3.1	3107	4.24	1080	5.38	686	6.52	461	7.66	297	8.8	265	9.94	228
1.98	2639	3.12	3075	4.26	1048	5.4	715	6.54	460	7.68	303	8.82	279	9.96	238
2	2567	3.14	3179	4.28	1063	5.42	712	6.56	458	7.7	274	8.84	255	9.98	261
2.02	2595	3.16	3148	4.3	1018	5.44	693	6.58	467	7.72	294	8.86	281	10	236
2.04	2493	3.18	3267	4.32	964	5.46	705	6.6	439	7.74	276	8.88	265		
2.06	2510	3.2	3143	4.34	941	5.48	693	6.62	493	7.76	257	8.9	269		
2.08	2446	3.22	3361	4.36	920	5.5	696	6.64	446	7.78	295	8.92	265		
2.1	2500	3.24	3284	4.38	897	5.52	688	6.66	446	7.8	278	8.94	258		
2.12	2439	3.26	3423	4.4	900	5.54	700	6.68	443	7.82	286	8.96	263		
2.14	2489	3.28	3330	4.42	865	5.56	656	6.7	460	7.84	278	8.98	283		
2.16	2343	3.3	3418	4.44	869	5.58	666	6.72	440	7.86	298	9	250		
2.18	2451	3.32	3333	4.46	860	5.6	647	6.74	441	7.88	293	9.02	260		
2.2	2361	3.34	3450	4.48	815	5.62	647	6.76	410	7.9	299	9.04	246		
2.22	2374	3.36	3315	4.5	858	5.64	653	6.78	414	7.92	284	9.06	246		
2.24	2360	3.38	3425	4.52	828	5.66	676	6.8	414	7.94	287	9.08	242		
2.26	2413	3.4	3298	4.54	805	5.68	617	6.82	394	7.96	295	9.1	262		
2.28	2328	3.42	3447	4.56	806	5.7	673	6.84	400	7.98	300	9.12	256		
2.3	2358	3.44	3262	4.58	798	5.72	619	6.86	408	8	303	9.14	256		
2.32	2283	3.46	3389	4.6	758	5.74	610	6.88	411	8.02	282	9.16	247		
2.34	2400	3.48	3195	4.62	773	5.76	610	6.9	380	8.04	280	9.18	245		
2.36	2358	3.5	3302	4.64	723	5.78	642	6.92	368	8.06	288	9.2	234		
2.38	2389	3.52	3191	4.66	786	5.8	575	6.94	397	8.08	274	9.22	249		
2.4	2290	3.54	3153	4.68	705	5.82	650	6.96	374	8.1	284	9.24	234		
2.42	2355	3.56	3051	4.7	768	5.84	590	6.98	370	8.12	283	9.26	233		
2.44	2276	3.58	3135	4.72	729	5.86	615	7	363	8.14	280	9.28	241		
2.46	2408	3.6	2921	4.74	728	5.88	570	7.02	370	8.16	290	9.3	232		
2.48	2335	3.62	2931	4.76	713	5.9	589	7.04	352	8.18	299	9.32	235		
2.5	2401	3.64	2849	4.78	748	5.92	565	7.06	340	8.2	308	9.34	235		
2.52	2382	3.66	2796	4.8	718	5.94	620	7.08	354	8.22	283	9.36	233		
2.54	2463	3.68	2634	4.82	736	5.96	581	7.1	340	8.24	290	9.38	229		
2.56	2363	3.7	2760	4.84	729	5.98	597	7.12	347	8.26	293	9.4	238		
2.58	2403	3.72	2559	4.86	738	6	558	7.14	341	8.28	304	9.42	236		
2.6	2353	3.74	2529	4.88	723	6.02	578	7.16	315	8.3	308	9.44	216		
2.62	2503	3.76	2359	4.9	749	6.04	565	7.18	319	8.32	305	9.46	231		

Table E.8: X-ray diffraction data for METH1: 4% - Injection Molded Sample

Deg.	CPS	Deg.	CPS	Deg.	CPS	Deg.	CPS	Deg.	CPS	Deg.	CPS	Deg.	CPS	Deg.	CPS
1.5	4291	2.64	9157	3.78	6341	4.92	2981	6.06	2560	7.2	1955	8.34	1426	9.48	1232
1.52	4356	2.66	9094	3.8	6254	4.94	2978	6.08	2568	7.22	1949	8.36	1412	9.5	1235
1.54	4388	2.68	9175	3.82	6121	4.96	2968	6.1	2556	7.24	1911	8.38	1438	9.52	1235
1.56	4475	2.7	9124	3.84	5976	4.98	3021	6.12	2578	7.26	1956	8.4	1470	9.54	1205
1.58	4556	2.72	9224	3.86	5988	5	2981	6.14	2633	7.28	1923	8.42	1430	9.56	1248
1.6	4668	2.74	9135	3.88	5915	5.02	2895	6.16	2594	7.3	1881	8.44	1442	9.58	1256
1.62	4680	2.76	9205	3.9	5713	5.04	2940	6.18	2585	7.32	1847	8.46	1371	9.6	1244
1.64	4754	2.78	9166	3.92	5722	5.06	2903	6.2	2520	7.34	1873	8.48	1399	9.62	1255
1.66	4781	2.8	9201	3.94	5630	5.08	2863	6.22	2527	7.36	1843	8.5	1432	9.64	1232
1.68	4842	2.82	9141	3.96	5588	5.1	2871	6.24	2566	7.38	1806	8.52	1355	9.66	1225
1.7	4940	2.84	9280	3.98	5472	5.12	2826	6.26	2545	7.4	1867	8.54	1380	9.68	1230
1.72	4852	2.86	9157	4	5335	5.14	2885	6.28	2545	7.42	1760	8.56	1322	9.7	1242
1.74	5065	2.88	9195	4.02	5383	5.16	2841	6.3	2563	7.44	1790	8.58	1308	9.72	1232
1.76	5108	2.9	9124	4.04	5169	5.18	2829	6.32	2603	7.46	1735	8.6	1320	9.74	1236
1.78	5176	2.92	9093	4.06	5152	5.2	2802	6.34	2564	7.48	1770	8.62	1340	9.76	1230
1.8	5209	2.94	9173	4.08	4974	5.22	2840	6.36	2479	7.5	1698	8.64	1321	9.78	1240
1.82	5323	2.96	9119	4.1	5046	5.24	2776	6.38	2470	7.52	1690	8.66	1294	9.8	1247
1.84	5325	2.98	8966	4.12	4898	5.26	2730	6.4	2488	7.54	1714	8.68	1313	9.82	1253
1.86	5388	3	9005	4.14	4833	5.28	2732	6.42	2477	7.56	1705	8.7	1242	9.84	1211
1.88	5535	3.02	8993	4.16	4729	5.3	2718	6.44	2506	7.58	1721	8.72	1303	9.86	1246
1.9	5710	3.04	8833	4.18	4754	5.32	2793	6.46	2421	7.6	1714	8.74	1268	9.88	1244
1.92	5806	3.06	8838	4.2	4535	5.34	2735	6.48	2457	7.62	1630	8.76	1288	9.9	1267
1.94	5817	3.08	8796	4.22	4505	5.36	2707	6.5	2429	7.64	1648	8.78	1299	9.92	1283
1.96	5915	3.1	8761	4.24	4518	5.38	2655	6.52	2388	7.66	1618	8.8	1270	9.94	1267
1.98	5999	3.12	8691	4.26	4380	5.4	2740	6.54	2349	7.68	1591	8.82	1275	9.96	1316
2	6158	3.14	8621	4.28	4372	5.42	2673	6.56	2375	7.7	1586	8.84	1249	9.98	1219
2.02	6251	3.16	8520	4.3	4311	5.44	2712	6.58	2431	7.72	1563	8.86	1235	10	1261
2.04	6304	3.18	8563	4.32	4313	5.46	2711	6.6	2403	7.74	1579	8.88	1241		
2.06	6335	3.2	8488	4.34	4188	5.48	2687	6.62	2384	7.76	1583	8.9	1253		
2.08	6625	3.22	8354	4.36	4068	5.5	2668	6.64	2341	7.78	1571	8.92	1236		
2.1	6595	3.24	8382	4.38	4057	5.52	2679	6.66	2292	7.8	1503	8.94	1255		
2.12	6710	3.26	8286	4.4	4005	5.54	2607	6.68	2326	7.82	1549	8.96	1224		
2.14	6848	3.28	8175	4.42	3907	5.56	2695	6.7	2326	7.84	1488	8.98	1227		
2.16	6931	3.3	8099	4.44	3941	5.58	2611	6.72	2325	7.86	1499	9	1212		
2.18	7008	3.32	8043	4.46	3905	5.6	2675	6.74	2339	7.88	1501	9.02	1289		
2.2	7158	3.34	7976	4.48	3841	5.62	2681	6.76	2261	7.9	1517	9.04	1219		
2.22	7260	3.36	7963	4.5	3694	5.64	2642	6.78	2283	7.92	1525	9.06	1239		
2.24	7413	3.38	7868	4.52	3739	5.66	2637	6.8	2258	7.94	1438	9.08	1242		
2.26	7545	3.4	7804	4.54	3655	5.68	2608	6.82	2296	7.96	1491	9.1	1185		
2.28	7589	3.42	7690	4.56	3637	5.7	2605	6.84	2289	7.98	1455	9.12	1180		
2.3	7713	3.44	7633	4.58	3543	5.72	2628	6.86	2205	8	1399	9.14	1198		
2.32	7783	3.46	7662	4.6	3545	5.74	2643	6.88	2235	8.02	1414	9.16	1240		
2.34	7804	3.48	7413	4.62	3578	5.76	2584	6.9	2148	8.04	1415	9.18	1223		
2.36	7940	3.5	7512	4.64	3513	5.78	2643	6.92	2188	8.06	1483	9.2	1241		
2.38	8061	3.52	7396	4.66	3438	5.8	2653	6.94	2166	8.08	1468	9.22	1246		
2.4	8234	3.54	7222	4.68	3358	5.82	2645	6.96	2127	8.1	1454	9.24	1206		
2.42	8285	3.56	7200	4.7	3380	5.84	2589	6.98	2168	8.12	1407	9.26	1181		
2.44	8311	3.58	7136	4.72	3301	5.86	2521	7	2103	8.14	1403	9.28	1232		
2.46	8436	3.6	7078	4.74	3270	5.88	2630	7.02	2096	8.16	1395	9.3	1198		
2.48	8502	3.62	6955	4.76	3215	5.9	2603	7.04	2093	8.18	1414	9.32	1252		
2.5	8639	3.64	6913	4.78	3320	5.92	2641	7.06	2109	8.2	1427	9.34	1212		
2.52	8585	3.66	6835	4.8	3161	5.94	2569	7.08	2023	8.22	1419	9.36	1193		
2.54	8808	3.68	6805	4.82	3150	5.96	2622	7.1	2027	8.24	1370	9.38	1253		
2.56	8746	3.7	6658	4.84	3151	5.98	2635	7.12	2008	8.26	1440	9.4	1151		
2.58	8925	3.72	6604	4.86	3145	6	2599	7.14	2069	8.28	1429	9.42	1198		
2.6	8909	3.74	6605	4.88	3045	6.02	2581	7.16	2001	8.3	1391	9.44	1260		
2.62	9027	3.76	6340	4.9	3124	6.04	2546	7.18	1955	8.32	1432	9.46	1207		

Table E.9: X-ray diffraction data for METH2: 4% - Injection Molded Sample

Deg.	CPS	Deg.	CPS	Deg.	CPS	Deg.	CPS	Deg.	CPS	Deg.	CPS	Deg.	CPS	Deg.	CPS
1.5	3795	2.64	8281	3.78	5043	4.92	2660	6.06	2505	7.2	2077	8.34	1405	9.48	1209
1.52	3807	2.66	8264	3.8	5013	4.94	2667	6.08	2457	7.22	2033	8.36	1439	9.5	1243
1.54	3877	2.68	8224	3.82	4849	4.96	2641	6.1	2478	7.24	2017	8.38	1426	9.52	1262
1.56	3983	2.7	8247	3.84	4828	4.98	2618	6.12	2533	7.26	2009	8.4	1444	9.54	1261
1.58	4036	2.72	8279	3.86	4790	5	2671	6.14	2535	7.28	1945	8.42	1509	9.56	1255
1.6	4101	2.74	8182	3.88	4744	5.02	2591	6.16	2506	7.3	2007	8.44	1418	9.58	1240
1.62	4121	2.76	8195	3.9	4717	5.04	2569	6.18	2535	7.32	1925	8.46	1442	9.6	1231
1.64	4276	2.78	8178	3.92	4602	5.06	2566	6.2	2518	7.34	1969	8.48	1420	9.62	1234
1.66	4267	2.8	8097	3.94	4483	5.08	2623	6.22	2513	7.36	1882	8.5	1421	9.64	1220
1.68	4336	2.82	8125	3.96	4502	5.1	2576	6.24	2557	7.38	1923	8.52	1418	9.66	1250
1.7	4492	2.84	8031	3.98	4467	5.12	2558	6.26	2579	7.4	1916	8.54	1398	9.68	1191
1.72	4487	2.86	7909	4	4362	5.14	2544	6.28	2480	7.42	1920	8.56	1393	9.7	1255
1.74	4591	2.88	7972	4.02	4325	5.16	2561	6.3	2530	7.44	1841	8.58	1357	9.72	1254
1.76	4728	2.9	7816	4.04	4323	5.18	2477	6.32	2488	7.46	1841	8.6	1418	9.74	1245
1.78	4796	2.92	7878	4.06	4163	5.2	2487	6.34	2493	7.48	1814	8.62	1326	9.76	1265
1.8	4965	2.94	7767	4.08	4193	5.22	2499	6.36	2529	7.5	1801	8.64	1340	9.78	1219
1.82	4972	2.96	7625	4.1	4108	5.24	2465	6.38	2491	7.52	1812	8.66	1311	9.8	1269
1.84	5174	2.98	7519	4.12	4062	5.26	2456	6.4	2508	7.54	1805	8.68	1330	9.82	1242
1.86	5259	3	7565	4.14	3915	5.28	2409	6.42	2497	7.56	1760	8.7	1287	9.84	1223
1.88	5245	3.02	7457	4.16	3954	5.3	2480	6.44	2504	7.58	1763	8.72	1307	9.86	1219
1.9	5439	3.04	7444	4.18	3858	5.32	2469	6.46	2497	7.6	1724	8.74	1293	9.88	1262
1.92	5516	3.06	7354	4.2	3811	5.34	2460	6.48	2525	7.62	1678	8.76	1302	9.9	1262
1.94	5671	3.08	7266	4.22	3810	5.36	2490	6.5	2493	7.64	1684	8.78	1297	9.92	1271
1.96	5690	3.1	7286	4.24	3751	5.38	2402	6.52	2482	7.66	1667	8.8	1293	9.94	1260
1.98	5807	3.12	7092	4.26	3723	5.4	2380	6.54	2453	7.68	1595	8.82	1283	9.96	1249
2	5915	3.14	7063	4.28	3605	5.42	2398	6.56	2441	7.7	1597	8.84	1246	9.98	1275
2.02	6049	3.16	6965	4.3	3626	5.44	2481	6.58	2470	7.72	1653	8.86	1263	10	1273
2.04	6042	3.18	6965	4.32	3701	5.46	2420	6.6	2528	7.74	1625	8.88	1250		
2.06	6309	3.2	6877	4.34	3569	5.48	2387	6.62	2408	7.76	1607	8.9	1296		
2.08	6315	3.22	6683	4.36	3465	5.5	2426	6.64	2449	7.78	1601	8.92	1236		
2.1	6536	3.24	6672	4.38	3458	5.52	2416	6.66	2403	7.8	1553	8.94	1251		
2.12	6622	3.26	6781	4.4	3389	5.54	2471	6.68	2474	7.82	1555	8.96	1265		
2.14	6609	3.28	6654	4.42	3388	5.56	2412	6.7	2449	7.84	1535	8.98	1238		
2.16	6855	3.3	6564	4.44	3363	5.58	2393	6.72	2449	7.86	1532	9	1236		
2.18	6886	3.32	6444	4.46	3284	5.6	2445	6.74	2388	7.88	1526	9.02	1260		
2.2	7099	3.34	6444	4.48	3284	5.62	2418	6.76	2400	7.9	1508	9.04	1208		
2.22	7199	3.36	6255	4.5	3231	5.64	2431	6.78	2359	7.92	1507	9.06	1220		
2.24	7194	3.38	6294	4.52	3239	5.66	2472	6.8	2367	7.94	1482	9.08	1206		
2.26	7346	3.4	6185	4.54	3158	5.68	2450	6.82	2336	7.96	1541	9.1	1275		
2.28	7472	3.42	6160	4.56	3172	5.7	2402	6.84	2389	7.98	1493	9.12	1221		
2.3	7517	3.44	6086	4.58	3092	5.72	2465	6.86	2337	8	1476	9.14	1209		
2.32	7561	3.46	6153	4.6	3048	5.74	2380	6.88	2309	8.02	1510	9.16	1245		
2.34	7723	3.48	5796	4.62	3051	5.76	2360	6.9	2276	8.04	1490	9.18	1252		
2.36	7745	3.5	5863	4.64	2969	5.78	2429	6.92	2298	8.06	1468	9.2	1218		
2.38	7837	3.52	5830	4.66	2951	5.8	2449	6.94	2293	8.08	1461	9.22	1213		
2.4	7953	3.54	5755	4.68	2970	5.82	2461	6.96	2236	8.1	1418	9.24	1229		
2.42	7897	3.56	5732	4.7	2956	5.84	2409	6.98	2312	8.12	1402	9.26	1260		
2.44	8013	3.58	5660	4.72	2893	5.86	2391	7	2267	8.14	1424	9.28	1279		
2.46	8039	3.6	5587	4.74	2846	5.88	2560	7.02	2253	8.16	1489	9.3	1243		
2.48	8131	3.62	5591	4.76	2844	5.9	2509	7.04	2192	8.18	1451	9.32	1187		
2.5	8147	3.64	5516	4.78	2831	5.92	2450	7.06	2205	8.2	1451	9.34	1235		
2.52	8175	3.66	5438	4.8	2811	5.94	2473	7.08	2179	8.22	1448	9.36	1234		
2.54	8236	3.68	5380	4.82	2834	5.96	2488	7.1	2197	8.24	1480	9.38	1221		
2.56	8230	3.7	5344	4.84	2789	5.98	2528	7.12	2171	8.26	1427	9.4	1253		
2.58	8301	3.72	5178	4.86	2706	6	2543	7.14	2103	8.28	1425	9.42	1230		
2.6	8383	3.74	5077	4.88	2702	6.02	2473	7.16	2133	8.3	1390	9.44	1253		
2.62	8313	3.76	5043	4.9	2738	6.04	2549	7.18	2045	8.32	1433	9.46	1236		

Table E.10: X-ray diffraction data for METH3: 4% - Injection Molded Sample

Deg.	CPS	Deg.	CPS	Deg.	CPS	Deg.	CPS	Deg.	CPS	Deg.	CPS	Deg.	CPS	Deg.	CPS
1.5	5233	2.64	8454	3.78	6037	4.92	3806	6.06	2607	7.2	2169	8.34	1757	9.48	1206
1.52	5399	2.66	8416	3.8	5923	4.94	3821	6.08	2550	7.22	2189	8.36	1784	9.5	1229
1.54	5423	2.68	8445	3.82	5964	4.96	3812	6.1	2530	7.24	2192	8.38	1760	9.52	1215
1.56	5440	2.7	8400	3.84	5846	4.98	3698	6.12	2577	7.26	2143	8.4	1708	9.54	1179
1.58	5519	2.72	8343	3.86	5868	5	3664	6.14	2520	7.28	2189	8.42	1748	9.56	1199
1.6	5487	2.74	8271	3.88	5824	5.02	3708	6.16	2562	7.3	2130	8.44	1641	9.58	1216
1.62	5576	2.76	8329	3.9	5786	5.04	3630	6.18	2561	7.32	2169	8.46	1690	9.6	1239
1.64	5649	2.78	8235	3.92	5762	5.06	3573	6.2	2528	7.34	2187	8.48	1673	9.62	1184
1.66	5774	2.8	8326	3.94	5787	5.08	3520	6.22	2488	7.36	2161	8.5	1656	9.64	1203
1.68	5739	2.82	8266	3.96	5657	5.1	3473	6.24	2521	7.38	2112	8.52	1602	9.66	1207
1.7	5840	2.84	8083	3.98	5803	5.12	3503	6.26	2509	7.4	2157	8.54	1607	9.68	1177
1.72	5936	2.86	8162	4	5716	5.14	3466	6.28	2518	7.42	2158	8.56	1575	9.7	1227
1.74	6062	2.88	8164	4.02	5636	5.16	3436	6.3	2484	7.44	2118	8.58	1523	9.72	1226
1.76	6073	2.9	8041	4.04	5593	5.18	3327	6.32	2402	7.46	2116	8.6	1533	9.74	1191
1.78	6101	2.92	7981	4.06	5533	5.2	3300	6.34	2419	7.48	2125	8.62	1510	9.76	1234
1.8	6237	2.94	8019	4.08	5559	5.22	3295	6.36	2534	7.5	2126	8.64	1510	9.78	1259
1.82	6331	2.96	7759	4.1	5578	5.24	3208	6.38	2468	7.52	2088	8.66	1465	9.8	1226
1.84	6443	2.98	7786	4.12	5566	5.26	3236	6.4	2461	7.54	2105	8.68	1456	9.82	1221
1.86	6511	3	7615	4.14	5453	5.28	3189	6.42	2415	7.56	2144	8.7	1426	9.84	1224
1.88	6507	3.02	7577	4.16	5393	5.3	3141	6.44	2351	7.58	2083	8.72	1363	9.86	1213
1.9	6665	3.04	7711	4.18	5360	5.32	3091	6.46	2452	7.6	2082	8.74	1330	9.88	1227
1.92	6723	3.06	7520	4.2	5410	5.34	3132	6.48	2343	7.62	2081	8.76	1397	9.9	1253
1.94	6691	3.08	7513	4.22	5318	5.36	3100	6.5	2396	7.64	2098	8.78	1387	9.92	1235
1.96	6818	3.1	7402	4.24	5261	5.38	3135	6.52	2339	7.66	2020	8.8	1369	9.94	1244
1.98	7038	3.12	7378	4.26	5279	5.4	3086	6.54	2395	7.68	2024	8.82	1356	9.96	1241
2	7155	3.14	7285	4.28	5217	5.42	3053	6.56	2337	7.7	2033	8.84	1353	9.98	1243
2.02	7218	3.16	7223	4.3	5217	5.44	2973	6.58	2330	7.72	1982	8.86	1344	10	1243
2.04	7234	3.18	7188	4.32	5100	5.46	3000	6.6	2261	7.74	2005	8.88	1328		
2.06	7360	3.2	7143	4.34	5126	5.48	3002	6.62	2388	7.76	1998	8.9	1310		
2.08	7352	3.22	7143	4.36	5048	5.5	2925	6.64	2285	7.78	1905	8.92	1273		
2.1	7453	3.24	6968	4.38	4972	5.52	2889	6.66	2311	7.8	1960	8.94	1278		
2.12	7453	3.26	6960	4.4	5030	5.54	2858	6.68	2250	7.82	1965	8.96	1290		
2.14	7572	3.28	6885	4.42	4971	5.56	2885	6.7	2291	7.84	1958	8.98	1313		
2.16	7760	3.3	6772	4.44	4913	5.58	2850	6.72	2289	7.86	1899	9	1278		
2.18	7848	3.32	6854	4.46	4885	5.6	2849	6.74	2249	7.88	1895	9.02	1288		
2.2	7753	3.34	6705	4.48	4884	5.62	2824	6.76	2291	7.9	1914	9.04	1220		
2.22	7926	3.36	6806	4.5	4868	5.64	2770	6.78	2258	7.92	1870	9.06	1279		
2.24	8062	3.38	6669	4.52	4727	5.66	2792	6.8	2300	7.94	1911	9.08	1268		
2.26	8098	3.4	6712	4.54	4648	5.68	2765	6.82	2247	7.96	1878	9.1	1233		
2.28	8125	3.42	6535	4.56	4761	5.7	2774	6.84	2268	7.98	1891	9.12	1249		
2.3	8132	3.44	6586	4.58	4529	5.72	2749	6.86	2240	8	1868	9.14	1241		
2.32	8173	3.46	6445	4.6	4552	5.74	2757	6.88	2238	8.02	1849	9.16	1217		
2.34	8295	3.48	6515	4.62	4533	5.76	2717	6.9	2262	8.04	1788	9.18	1208		
2.36	8382	3.5	6413	4.64	4433	5.78	2656	6.92	2238	8.06	1848	9.2	1247		
2.38	8318	3.52	6409	4.66	4458	5.8	2706	6.94	2213	8.08	1827	9.22	1218		
2.4	8398	3.54	6321	4.68	4388	5.82	2696	6.96	2240	8.1	1818	9.24	1233		
2.42	8315	3.56	6345	4.7	4370	5.84	2611	6.98	2230	8.12	1859	9.26	1213		
2.44	8353	3.58	6287	4.72	4326	5.86	2665	7	2221	8.14	1806	9.28	1197		
2.46	8479	3.6	6199	4.74	4258	5.88	2630	7.02	2188	8.16	1845	9.3	1244		
2.48	8553	3.62	6257	4.76	4214	5.9	2616	7.04	2217	8.18	1767	9.32	1197		
2.5	8600	3.64	6160	4.78	4133	5.92	2612	7.06	2196	8.2	1753	9.34	1176		
2.52	8455	3.66	6206	4.8	4105	5.94	2603	7.08	2200	8.22	1809	9.36	1215		
2.54	8481	3.68	6145	4.82	4106	5.96	2645	7.1	2291	8.24	1807	9.38	1221		
2.56	8436	3.7	6080	4.84	4087	5.98	2634	7.12	2178	8.26	1821	9.4	1190		
2.58	8455	3.72	6104	4.86	3928	6	2596	7.14	2231	8.28	1775	9.42	1223		
2.6	8497	3.74	6013	4.88	3940	6.02	2593	7.16	2222	8.3	1804	9.44	1202		
2.62	8454	3.76	6051	4.9	3861	6.04	2580	7.18	2235	8.32	1775	9.46	1209		

Table E.11: X-ray diffraction data for METH3: 6.6% - Injection Molded Sample

Deg.	CPS	Deg.	CPS	Deg.	CPS	Deg.	CPS	Deg.	CPS	Deg.	CPS	Deg.	CPS	Deg.	CPS
1.5	4416	2.64	4845	3.78	3566	4.92	1628	6.06	1087	7.2	878	8.34	486	9.48	326
1.52	4080	2.66	4983	3.8	3470	4.94	1646	6.08	1063	7.22	942	8.36	487	9.5	369
1.54	4057	2.68	4784	3.82	3454	4.96	1575	6.1	1080	7.24	873	8.38	471	9.52	336
1.56	3766	2.7	5000	3.84	3347	4.98	1588	6.12	1092	7.26	848	8.4	469	9.54	359
1.58	3713	2.72	4803	3.86	3455	5	1586	6.14	1059	7.28	791	8.42	485	9.56	332
1.6	3361	2.74	5021	3.88	3281	5.02	1555	6.16	1070	7.3	844	8.44	483	9.58	362
1.62	3254	2.76	4828	3.9	3351	5.04	1519	6.18	1125	7.32	831	8.46	475	9.6	360
1.64	3099	2.78	4913	3.92	3241	5.06	1520	6.2	1101	7.34	829	8.48	432	9.62	354
1.66	3027	2.8	4782	3.94	3432	5.08	1461	6.22	1124	7.36	797	8.5	476	9.64	340
1.68	2802	2.82	4849	3.96	3226	5.1	1514	6.24	1125	7.38	807	8.52	449	9.66	345
1.7	2958	2.84	4635	3.98	3344	5.12	1417	6.26	1130	7.4	703	8.54	462	9.68	327
1.72	2865	2.86	4879	4	3171	5.14	1421	6.28	1113	7.42	759	8.56	439	9.7	381
1.74	2949	2.88	4612	4.02	3240	5.16	1413	6.3	1143	7.44	732	8.58	434	9.72	332
1.76	2935	2.9	4735	4.04	3097	5.18	1373	6.32	1137	7.46	682	8.6	406	9.74	368
1.78	2913	2.92	4563	4.06	3200	5.2	1333	6.34	1139	7.48	692	8.62	392	9.76	358
1.8	2867	2.94	4673	4.08	3123	5.22	1358	6.36	1128	7.5	746	8.64	418	9.78	363
1.82	2975	2.96	4533	4.1	3190	5.24	1328	6.38	1158	7.52	679	8.66	418	9.8	342
1.84	2928	2.98	4650	4.12	3024	5.26	1314	6.4	1191	7.54	658	8.68	413	9.82	383
1.86	3128	3	4465	4.14	3118	5.28	1255	6.42	1175	7.56	655	8.7	407	9.84	331
1.88	3015	3.02	4521	4.16	2923	5.3	1242	6.44	1145	7.58	669	8.72	398	9.86	368
1.9	3199	3.04	4328	4.18	3065	5.32	1239	6.46	1183	7.6	615	8.74	420	9.88	359
1.92	3122	3.06	4437	4.2	2883	5.34	1258	6.48	1136	7.62	646	8.76	383	9.9	361
1.94	3313	3.08	4324	4.22	2969	5.36	1215	6.5	1206	7.64	618	8.78	414	9.92	356
1.96	3231	3.1	4356	4.24	2805	5.38	1233	6.52	1229	7.66	619	8.8	368	9.94	360
1.98	3313	3.12	4225	4.26	2859	5.4	1185	6.54	1175	7.68	586	8.82	384	9.96	367
2	3284	3.14	4364	4.28	2686	5.42	1219	6.56	1198	7.7	577	8.84	365	9.98	378
2.02	3485	3.16	4180	4.3	2780	5.44	1180	6.58	1252	7.72	576	8.86	386	10	370
2.04	3344	3.18	4216	4.32	2638	5.46	1207	6.6	1238	7.74	582	8.88	385		
2.06	3549	3.2	4118	4.34	2722	5.48	1148	6.62	1245	7.76	572	8.9	378		
2.08	3618	3.22	4144	4.36	2588	5.5	1175	6.64	1185	7.78	565	8.92	389		
2.1	3651	3.24	4105	4.38	2584	5.52	1117	6.66	1215	7.8	527	8.94	380		
2.12	3624	3.26	4107	4.4	2502	5.54	1168	6.68	1170	7.82	535	8.96	369		
2.14	3821	3.28	3924	4.42	2553	5.56	1139	6.7	1251	7.84	517	8.98	406		
2.16	3753	3.3	4127	4.44	2496	5.58	1164	6.72	1180	7.86	540	9	374		
2.18	3943	3.32	3990	4.46	2408	5.6	1080	6.74	1227	7.88	505	9.02	394		
2.2	3977	3.34	4043	4.48	2347	5.62	1142	6.76	1154	7.9	523	9.04	358		
2.22	4017	3.36	3917	4.5	2363	5.64	1078	6.78	1207	7.92	490	9.06	360		
2.24	3938	3.38	4004	4.52	2291	5.66	1107	6.8	1179	7.94	514	9.08	358		
2.26	4209	3.4	3813	4.54	2394	5.68	1085	6.82	1225	7.96	489	9.1	365		
2.28	4187	3.42	3951	4.56	2220	5.7	1095	6.84	1149	7.98	497	9.12	358		
2.3	4334	3.44	3776	4.58	2263	5.72	1061	6.86	1147	8	473	9.14	370		
2.32	4318	3.46	3845	4.6	2130	5.74	1090	6.88	1130	8.02	500	9.16	382		
2.34	4388	3.48	3805	4.62	2150	5.76	1063	6.9	1178	8.04	480	9.18	353		
2.36	4315	3.5	3882	4.64	2063	5.78	1055	6.92	1102	8.06	501	9.2	345		
2.38	4560	3.52	3650	4.66	2060	5.8	1048	6.94	1093	8.08	464	9.22	385		
2.4	4487	3.54	3785	4.68	2000	5.82	1090	6.96	1076	8.1	475	9.24	373		
2.42	4743	3.56	3536	4.7	1969	5.84	1029	6.98	1096	8.12	461	9.26	360		
2.44	4633	3.58	3845	4.72	1896	5.86	1059	7	1053	8.14	496	9.28	353		
2.46	4818	3.6	3643	4.74	1971	5.88	1088	7.02	1047	8.16	423	9.3	355		
2.48	4630	3.62	3694	4.76	1801	5.9	1088	7.04	996	8.18	480	9.32	344		
2.5	4835	3.64	3658	4.78	1825	5.92	1017	7.06	1098	8.2	458	9.34	357		
2.52	4736	3.66	3635	4.8	1750	5.94	1062	7.08	982	8.22	451	9.36	364		
2.54	4851	3.68	3546	4.82	1822	5.96	1022	7.1	1001	8.24	465	9.38	375		
2.56	4775	3.7	3658	4.84	1758	5.98	1092	7.12	979	8.26	468	9.4	340		
2.58	4973	3.72	3477	4.86	1817	6	1064	7.14	969	8.28	443	9.42	345		
2.6	4748	3.74	3592	4.88	1704	6.02	1077	7.16	919	8.3	474	9.44	325		
2.62	5005	3.76	3417	4.9	1667	6.04	1024	7.18	973	8.32	452	9.46	373		

Table E.12: X-ray diffraction data for RTP: 10% - Injection Molded Sample

Deg.	CPS	Deg.	CPS	Deg.	CPS	Deg.	CPS	Deg.	CPS	Deg.	CPS	Deg.	CPS	Deg.	CPS
1.5	3361	2.64	7922	3.78	7144	4.92	4430	6.06	5572	7.2	3066	8.34	2079	9.48	1447
1.52	3418	2.66	7875	3.8	6997	4.94	4384	6.08	5451	7.22	2995	8.36	2108	9.5	1402
1.54	3433	2.68	7926	3.82	6985	4.96	4497	6.1	5461	7.24	2980	8.38	2091	9.52	1413
1.56	3615	2.7	7890	3.84	6725	4.98	4422	6.12	5461	7.26	3041	8.4	2070	9.54	1346
1.58	3707	2.72	7814	3.86	6700	5	4467	6.14	5448	7.28	2928	8.42	2095	9.56	1376
1.6	3767	2.74	7840	3.88	6675	5.02	4390	6.16	5426	7.3	2837	8.44	2045	9.58	1362
1.62	3945	2.76	7738	3.9	6530	5.04	4453	6.18	5411	7.32	2956	8.46	2028	9.6	1334
1.64	3959	2.78	7775	3.92	6272	5.06	4500	6.2	5425	7.34	2880	8.48	1994	9.62	1352
1.66	4018	2.8	7670	3.94	6271	5.08	4469	6.22	5395	7.36	2841	8.5	2002	9.64	1318
1.68	4157	2.82	7692	3.96	6173	5.1	4504	6.24	5450	7.38	2833	8.52	2020	9.66	1296
1.7	4275	2.84	7638	3.98	6086	5.12	4414	6.26	5500	7.4	2848	8.54	2022	9.68	1267
1.72	4385	2.86	7640	4	6156	5.14	4491	6.28	5380	7.42	2791	8.56	1993	9.7	1256
1.74	4493	2.88	7530	4.02	6021	5.16	4546	6.3	5364	7.44	2743	8.58	1984	9.72	1233
1.76	4656	2.9	7615	4.04	5873	5.18	4564	6.32	5299	7.46	2781	8.6	1965	9.74	1288
1.78	4610	2.92	7545	4.06	5891	5.2	4532	6.34	5356	7.48	2642	8.62	1937	9.76	1168
1.8	4834	2.94	7409	4.08	5718	5.22	4559	6.36	5248	7.5	2648	8.64	1933	9.78	1205
1.82	4870	2.96	7451	4.1	5714	5.24	4569	6.38	5285	7.52	2712	8.66	1910	9.8	1156
1.84	4985	2.98	7463	4.12	5434	5.26	4553	6.4	5270	7.54	2588	8.68	1895	9.82	1180
1.86	5078	3	7343	4.14	5406	5.28	4613	6.42	5235	7.56	2567	8.7	1901	9.84	1156
1.88	5193	3.02	7394	4.16	5383	5.3	4660	6.44	5131	7.58	2603	8.72	1847	9.86	1121
1.9	5361	3.04	7394	4.18	5314	5.32	4700	6.46	5083	7.6	2533	8.74	1913	9.88	1142
1.92	5458	3.06	7348	4.2	5308	5.34	4682	6.48	5048	7.62	2526	8.76	1823	9.9	1167
1.94	5518	3.08	7431	4.22	5272	5.36	4697	6.5	4967	7.64	2517	8.78	1833	9.92	1152
1.96	5621	3.1	7440	4.24	5070	5.38	4719	6.52	4985	7.66	2500	8.8	1894	9.94	1113
1.98	5699	3.12	7523	4.26	5058	5.4	4698	6.54	4862	7.68	2439	8.82	1828	9.96	1106
2	5872	3.14	7554	4.28	5183	5.42	4783	6.56	4838	7.7	2476	8.84	1782	9.98	1112
2.02	6023	3.16	7685	4.3	4997	5.44	4773	6.58	4795	7.72	2452	8.86	1830	10	1072
2.04	6071	3.18	7666	4.32	5020	5.46	4825	6.6	4733	7.74	2393	8.88	1778		
2.06	6124	3.2	7712	4.34	5008	5.48	4808	6.62	4625	7.76	2427	8.9	1757		
2.08	6363	3.22	7686	4.36	4885	5.5	4854	6.64	4578	7.78	2393	8.92	1813		
2.1	6340	3.24	7853	4.38	4846	5.52	4849	6.66	4461	7.8	2422	8.94	1728		
2.12	6517	3.26	7938	4.4	4882	5.54	4935	6.68	4598	7.82	2314	8.96	1785		
2.14	6641	3.28	7959	4.42	4813	5.56	4891	6.7	4420	7.84	2364	8.98	1750		
2.16	6674	3.3	7928	4.44	4679	5.58	5006	6.72	4380	7.86	2328	9	1743		
2.18	6857	3.32	7980	4.46	4637	5.6	5036	6.74	4274	7.88	2346	9.02	1736		
2.2	6845	3.34	7995	4.48	4707	5.62	4957	6.76	4226	7.9	2259	9.04	1733		
2.22	6990	3.36	8161	4.5	4749	5.64	5065	6.78	4158	7.92	2263	9.06	1703		
2.24	7195	3.38	8165	4.52	4695	5.66	5049	6.8	4063	7.94	2253	9.08	1678		
2.26	7188	3.4	8087	4.54	4616	5.68	5147	6.82	4012	7.96	2276	9.1	1692		
2.28	7185	3.42	8198	4.56	4663	5.7	5145	6.84	3968	7.98	2251	9.12	1660		
2.3	7332	3.44	8106	4.58	4564	5.72	5231	6.86	3938	8	2211	9.14	1636		
2.32	7397	3.46	8058	4.6	4554	5.74	5139	6.88	3880	8.02	2174	9.16	1585		
2.34	7429	3.48	8069	4.62	4577	5.76	5165	6.9	3736	8.04	2201	9.18	1643		
2.36	7625	3.5	8137	4.64	4553	5.78	5229	6.92	3703	8.06	2191	9.2	1578		
2.38	7698	3.52	8064	4.66	4501	5.8	5190	6.94	3678	8.08	2175	9.22	1630		
2.4	7642	3.54	8016	4.68	4529	5.82	5345	6.96	3619	8.1	2156	9.24	1585		
2.42	7785	3.56	7990	4.7	4429	5.84	5277	6.98	3585	8.12	2144	9.26	1542		
2.44	7879	3.58	7909	4.72	4469	5.86	5277	7	3590	8.14	2137	9.28	1549		
2.46	7816	3.6	7834	4.74	4449	5.88	5347	7.02	3465	8.16	2147	9.3	1525		
2.48	8004	3.62	7739	4.76	4508	5.9	5346	7.04	3417	8.18	2155	9.32	1515		
2.5	7900	3.64	7597	4.78	4574	5.92	5365	7.06	3312	8.2	2073	9.34	1500		
2.52	7837	3.66	7589	4.8	4475	5.94	5425	7.08	3281	8.22	2129	9.36	1459		
2.54	7993	3.68	7550	4.82	4457	5.96	5410	7.1	3323	8.24	2109	9.38	1507		
2.56	7897	3.7	7445	4.84	4390	5.98	5493	7.12	3260	8.26	2060	9.4	1463		
2.58	7862	3.72	7335	4.86	4491	6	5467	7.14	3313	8.28	2070	9.42	1434		
2.6	7975	3.74	7224	4.88	4422	6.02	5441	7.16	3132	8.3	2069	9.44	1472		
2.62	8005	3.76	7255	4.9	4458	6.04	5508	7.18	3130	8.32	2048	9.46	1408		

Vita

Quang Tran Nguyen was born in Vietnam. He and his whole family came to America in 1992 when he was 13. He graduated from Annandale High School in 1997 and subsequently enrolled at the University of Virginia (UVA) to pursue his Bachelor's degree in chemical engineering. The author interned at the National Institute of Standards and Technology for two summers while he was doing his undergraduate study at UVA. Upon graduation from UVA in May 2001, the author attended Virginia Tech in August 2001 to pursue his PhD degree in chemical engineering. He joined the polymer processing group and worked under the guidance of Dr. Donald Baird. The author completed his PhD in the Spring of 2007.